THE EFFECT OF MAGNETITE NANOPARTICLES ON METHANE PRODUCTION FROM THE ANAEROBIC DIGESTION OF ACETATE, PROPIONATE AND GLUCOSE

A thesis submitted in partial fulfilment of the requirements for the

Degree of Doctor of Philosophy

in Civil and Natural Resources Engineering

at the University of Canterbury

By

Ethar Mohammad Al-Essa

Department of Civil and Natural Resources Engineering

University of Canterbury, New Zealand

January 2020

ACKNOWLEDGEMENTS

First and foremost, my deepest appreciation and thanks to my supervisors Dr. Ricardo Bello Mendoza and Dr. David Wareham Associate Professor, Department of Civil and Natural Resources Engineering (CNRE), University of Canterbury, New Zealand. I feel very grateful to have had an opportunity to work under their supervision. Thank you for your valuable time, co-operation, and guidance in carrying out this thesis.

Great pleasure to thank my technical advisors in the Department of CNRE, Mr. Peter McGuigan, Mr. Manjula Premaratne, Aude Thierry and Mr. Dave MacPherson for their extraordinary help and technical assistance through my research work.

This thesis would not have been possible without the support of many people. I am deeply grateful to the College of Engineering and the department of CNRE for helping me during these years of my study both academically and officially. My thanks to all my UC friends for their generous help and suggestions through my thesis writing.

My heartfelt thanks and love to my husband (Khaldoun), my parents, brothers, sisters and my little son (Omar). I would not have got where I am today without their endless love, constant unconditional support and encouragement.

Above all, thanks to almighty God who enabled me to complete my research and get overcome all the challenges that faced me through my thesis journey.

Ethar Al-Essa

ABSTRACT

A series of studies were conducted to explore the effect of different size ranges and concentrations of magnetite nanoparticles on methane production from fresh and degassed anaerobically-digested sludge under different concentrations of acetate, propionate and glucose. Mesophilic digested sludge was used as fresh digested sludge and degassed digested sludge sat for one month at 36 ± 1^{o}C in an incubator. Magnetite was added at three different size ranges of small-sized (50 - 150 nm) purchased from Sigma Aldrich, medium-sized (168 – 490 nm) synthesized via the hydrothermal method, and large-sized (800 nm - 4.5 µm) synthesized via the co-precipitation method at different concentrations of 0, 2, 7, and 20 mM. Initial concentrations of COD:VS ratios of 2:1, 4:1 and 8:1 of acetate, propionate, and glucose; as well further COD:VS ratios of 3:1 and 6:1 of glucose were added. Methane production was monitored periodically over the incubation period and the cumulative maximum methane production was plotted with respect to time. Three replicates were done for each test. Kinetic parameters of lag phase duration and maximum methane production rate were estimated by fitting the modified Gompertz model to experimental methane production curves by nonlinear regression using SPSS software. The statistical analysis was done using a general linear model (GLM) procedure with SAS software.

In the case of the degassed sludge, only the medium magnetite at 2 and 7 mM significantly enhanced the methane production rate by 12 %, as compared to the control (no magnetite). In addition, 2 mM of both small and medium-sized magnetite reduced the lag phase by 17 %, as compared to the control. Conversely, adding magnetite (regardless of the size and the concentration) to fresh sludge significantly increased the methane production rate by 32 % while simultaneously decreasing the lag phase by 15 % - 41 %, as compared to the control. No significant differences in both cumulative methane production and methane yield were observed in the presence of magnetite using either fresh or degassed sludge.

The effect of magnetite is a function of magnetite concentration as well as substrate concentration and type. Increasing acetate and glucose COD:VS ratios from 2:1 to 4:1 in the presence of magnetite significantly increased the maximum methane production rate up to 2 times and 2.5 times respectively; whereas no significant difference was obtained in the control bottles. In

contrast, by increasing the glucose COD:VS ratio from 3 COD: 1 VS to 6 COD: 1 VS, the maximum methane production rate in the presence of magnetite significantly decreased up to 1.9 times; whereas it significantly decreased by 7.6 times in the control bottles. Also, increasing the acetate COD:VS ratio from 4:1 to 8:1 in the presence of magnetite significantly decreased the lag phase duration in the range of 7.7 % to 32.1 %; whereas in the control bottles, the lag phase significantly increased by 35 %. Similarly, increasing the propionate COD:VS ratio from 2:1 to 4:1 and then from 4:1 to 8:1 in the presence of magnetite significantly increased in the lag phase duration around 4.4 days and 6.3 days, respectively; however, in the control bottles the lag phase increased around 6 days and 10 days, respectively. In addition, increasing the glucose concentration from 3 COD: 1 VS to 6 COD: 1 VS in the presence of magnetite significantly extended the lag phase in the range of 2 days to 11 days; whereas in the control bottles the lag phase significantly extended 24 days. On the other hand, the ratios of 4 COD: 1 VS and 8 COD: 1 VS were the most suitable ratios for acetate and propionate when magnetite was added since they achieved a higher methane production rate by (59 % and 32 %) respectively. Magnetite was not able to easily trigger methane production when glucose concentration exceeded the ratio of 4 COD: 1VS, as that increased the VFA production and accumulation rates which cause a pH drop.

Using small-sized, medium-sized and large-sized magnetite, the theoretical calculations revealed that electrons transferred via the magnetite-direct interspecies electron transfer (DIET) method were higher than those transferred via interspecies hydrogen transfer (IET) from acetate degradation at rates 0.0498×10^6 and 0.539×10^6 and 35×10^6, as well from propionate degradation at rates 0.006272×10^6 and 0.0727×10^6 and 4.72×10^6 respectively. This strongly suggests that magnetite serves as electron conduits between electron-donating and electron-accepting microorganisms. In addition, the flux increases with the size of the magnetite particles. However, the size ratio between the particles and the bacterial cells might play a role and affect DIET promotion.

These results confirm that adding magnetite to an anaerobic digester significantly enhances the rate of methane production in anaerobic digestion. However, this positive effect depends on the type and the concentration of substrate as well as the size of magnetite particles.

TABLE OF CONTENTS

LIST OF FIGURES

LIST OF TABLES

CHAPTER 1. INTRODUCTION

The development of renewable energy sources is of increasing interest to many countries seeking clean, affordable and reliable energy. As a renewable energy, biogas provides multiple environmental and economic benefits (Achinas et al., 2017). Biogas is Greenhouse Gas (GHG) neutral because it is produced from plant material. It is a non-toxic, clean-burning, and smoke-free fuel, odorless and colorless and burns with a blue flame similar to that of liquid petroleum gas (Stanley et al., 2013). Biogas can be used as vehicle fuel (Fallde and Eklund, 2015) as well as fuel to produce electricity (Nasir et al., 2012; Hakawati et al., 2017). One petajoule of biogas-derived energy produces 97.2 x 10^6 kWh electricity, equivalent to 22.2 x 10^6 L diesel fuel (Thiele and Mayes, 2008).

Renewable energy is an important and significant part of New Zealand's energy supply (Kelly, 2011). Mainly hydro and other renewable sources (i.e. wind, solar, geothermal, and biogas) generated 81.9% of electricity in 2017 (M.B.I.E., 2018). According to the NZ biogas website (BANZ, 2019), most of the biogas (4.5 PJ) is produced by anaerobic digestion in landfills and wastewater treatment plants. Anaerobic digestion is used in many wastewater treatment plants to produce biogas from residual biological sludge, as is the case for the wastewater treatment plants in Christchurch and Palmerston North. The current estimate of the total energy equivalent of methane collected in New Zealand is around 50 megawatts (mostly used for heat and electricity in industry-scale applications); however, there is potential to increase rural biogas generation from food and animal waste. The NZ vision is to incorporate biogas recovery as the method of choice for future capacity additions at established wastewater treatment plants (Kelly, 2007; BANZ, 2011). It is thought that biogas will become the main, sustainable source of heat, electricity, transport fuel and a future replacement for natural gas (BANZ, 2019).

The underlying theory of anaerobic digestion has been established for decades; however, the technology still has some limitations in terms of application, particularly related to biogas production speed. Consequently, as the interest in biogas production from anaerobic digestion rapidly develops around the world, a significant research interest has arisen recently about improving the ability of anaerobic microorganisms to produce biogas from different substrate types by adding conductive materials such as magnetite particles.

CHAPTER 2. LITERATURE REVIEW

2.1 Anaerobic Digestion

Anaerobic digestion (AD) is a typical method used for biological waste treatment where the population of microorganisms works in an interactive manner to break down and convert biodegradable organic matter into carbon dioxide and methane via two phases (Parkin and Owen, 1986; Ariunbaatar et al., 2014). In the first phase (hydrolysis/acetogenesis) complex organic matter (carbohydrates, fats, and proteins) is hydrolyzed into dissolved smaller molecules (sugars such as glucose, fatty acids, and amino acids). These smaller molecules are then assimilated by fermentative bacteria into volatile acids (propionic, butyric, and acetic acid), hydrogen, and carbon dioxide. Long chain volatile acids are further degraded by obligate hydrogen- producing acetogens mainly into acetic acid, as well as hydrogen and carbon dioxide (Kleinstreuer and Poweigha, 1982; Holm-Nielsen and Esbensen, 2011). In the second phase (methanogenesis), acetic acid, hydrogen and carbon dioxide are the precursors used directly by methanogenic microorganisms during methane production (Speece, 1983; Stams et al., 2006).

The AD metabolic pathway is illustrated schematically in Figure 2.1. Complete degradation of volatile fatty acids (i.e. acetic and propionic acids) into methane is a key step in the anaerobic degradation of organic compounds where the communities have to grow in conditions that are close to thermodynamic equilibrium (Mawson et al., 1991). Propionate and acetate degradation into methane require syntrophic association between propionate-oxidizing bacteria that form acetate, H_2, and CO_2 from propionate and hydrogenotrophic methanogens that utilize the hydrogen and acetate to form methane (Boone and Bryant, 1980; Müller et al., 2010). It has often been reported that the slow syntrophic degradation of propionate is a critical limiting factor in anaerobic digestion (Stams and Plugge, 2009).

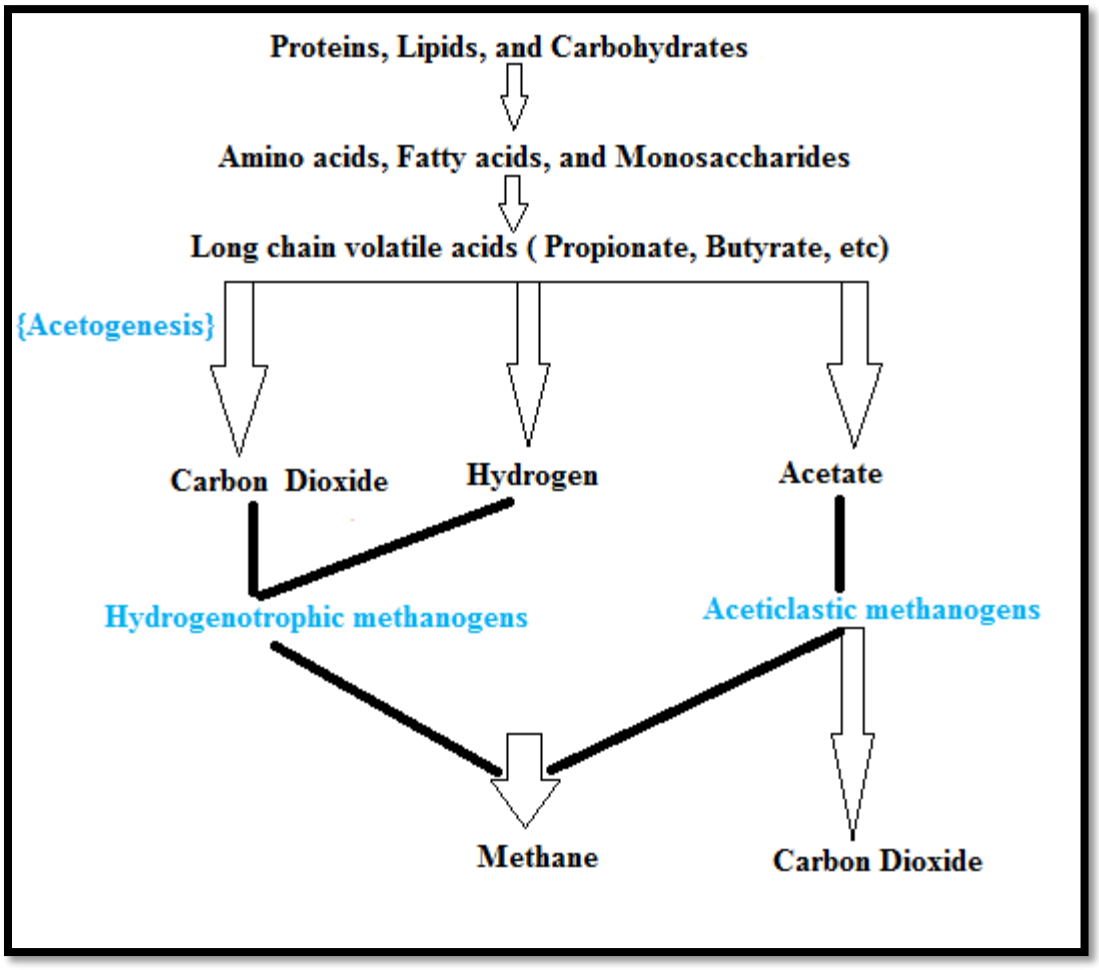

Figure 2.1. Schematic of anaerobic degradation process (adapted from George et al. (2003) and de Lemos Chernicharo (2007).

According to the reactions shown in equation 1 to 4 (Angelidaki et al., 2011), approximately 72 % of the methane produced originates from acetate (McDonald, 2007; Khanal, 2008). However, the values of the change in free energy shown below indicate that more free energy is released in reaction 4, so thermodynamically it is more favourable. Reaction 1 is only energetically favorable (i.e. $\Delta Go' < 0$) if the acetate and partial pressure of hydrogen are kept at low levels ($< 10^{-6}$ to 10^{-4} atm) by H_2- utilizing hydrogenotrophic methanogens.

$$4\ \text{Propionate}^- + 12\ H_2O \rightarrow 4\ \text{Acetate}^- + 4\ HCO_3^- + 28H^+ + 24e^- \quad \Delta Go' = +304.4\ \text{kJ} \quad (1)$$

$$27H^+ + 3\ HCO_3^- + 24e^- \rightarrow 3\ CH_4 + 9\ H_2O \quad \Delta Go' = -136\ \text{kJ} \quad (2)$$

$$\text{Acetate}^- + H_2O \rightarrow CH_4 + HCO_3^- \quad \Delta Go' = -31\ \text{kJ} \quad (3)$$

$$CO_2 + 4H_2 \rightarrow CH_4 + 2H_2O \quad \Delta Go' = -139.1\ \text{kJ} \quad (4)$$

Accumulation of acetate and H_2 lead to a pH drop, upsetting the methanogenic bacteria and reducing the production of methane. Hydrogen can also inhibit hydrogenotrophic methanogenesis if its concentration is higher than 100 ppm (Speece, 1996). Therefore, the complete degradation of soluble organic matter to methane requires a balanced population of obligate H_2-producing acetogenic bacteria and H_2-consuming methanogens, as well as an uninterrupted transfer of hydrogen between these two groups. This transfer is known as interspecies electron transfer (IET) (Bryant et al., 1977; Phelps et al., 1985; Whitman et al., 1992; Marchaim and Krause, 1993; Wu et al., 1993).

2.2 Factors Affecting AD Process for Methane Production

Anaerobic digestion efficiency depends on a number of factors. These include, sludge age, organic loading, temperature, pH, carbon/nitrogen ratio, and retention time. These factors play a key role in methanogenesis and greatly influence metabolic conditions for the microorganisms' growth.

2.2.1 Sludge Age

As noted before, methane production is performed by a consortium of interdependent microorganisms including hydrolytic, acid forming, acetogenic, and methanogenic bacteria. Angelidaki et al. (2009) suggested that fresh anaerobic sludge in particular has a wide microbial diversity which ensures a sufficient level of hydrolytic and methanogenic activity. Fresh sludge also has enough food to ensure a healthy food-microorganism (F/M) ratio (0.04-0.10 kg BOD/ kg MLVSS-d) which helps in achieving optimal production of biogas (De Vrieze et al., 2015; Hadiyarto et al., 2015). In a typical anaerobic digester, the food/microorganism ratio is a safety

factor to meet target effluent standards (Speece, 1983). The balance between the mass of substrate consumption and the mass of biomass generation helps in achieving optimal production of biogas (Hadiyarto et al., 2015). However, when the sludge is aged (i.e. degassed) the F/M ratio becomes low, and as such, bacteria metabolism may be impaired (Manure, 2001; Hadiyarto et al., 2015).

2.2.2 Organic Load

Organic load (OL) is a parameter commonly used to keep digestion balance. Organic load represents the amount of organic matter, often measured as volatile solids, fed into a digester (Mao et al., 2015). It affects the performance of anaerobic digestion in terms of volatile solids (VS) removal efficiency and methane yield (Gou et al., 2014). With increasing levels of OL above the optimum range (0.04 – 0.10 kg BOD/ kg MLVSS-d), the balance between the rate of hydrolysis/acidogenesis and methanogenesis can be greatly disturbed (Luste and Luostarinen, 2010). As result of extremely high OL, the hydrolysis/acidogenesis bacteria are likely to have higher activity than the methanogens. This increases the concentration of VFAs and correspondingly causes a pH drop which leads to irreversible acidification and finally results in the inhibition of VFA conversion to methane gas (Nagao et al., 2012). Previous studies have stated that methane production depends on substrate concentration. For example, Sanchez et al. (2001) reported that an increase in the initial concentration of organic matter (3.3, 7.0, 12.0, 19.3 and 26.3 g COD/L) caused an increase methane production yield. Chae et al. (2008) anaerobically digested swine manure at different feed loads (5 %, 10 %, 20 % and 40 % (feed volume/ digester volume)) at different temperatures within the mesophilic range (from 25 to 35^{o}C). Results showed that feeding loads up to 20 % were the upper limit of applicable feed load of swine manure within mesophilic digestion ranges (from 25 to 35^{o}C). In addition, regardless of the digestion temperature, increasing the feed load from 5 % to 40 % decreased the biogas yield (CH_4 L/g VS added) with approximately 54 % reduction in the methane yields at 40 % feed load. Similarly, Zhang et al. (2014) conducted batch experiments at four feed loadings (40, 50, 65 and 80 g VS/L) under mesophilic conditions. Their results showed that the cumulative methane production decreased by 32.4 %, 26.4 %, 60.1 %, and 32.4 % respectively, as feed loading increased from 40 g VS/L to 80

g VS/L. Furthermore, Tanimu et al. (2014) conducted batch experiments under mesophilic conditions (37^{o}C) at feed loading of 0.5, 1.5, 3.5 and 5.5 g VS/L. Their results showed that methane production increased with increasing the feed loading up to 3.5 g VS/L in the digester and then decreased at 5.5 g VS /L. In addition, the gas production continued up to day 30 (except at 0.5 and 5.5 g VS/L) where biogas production stopped on day 26 and 28 respectively. Adding low substrate concentration (0.5 g VS/L, i.e. limited feed loading) caused interruption in the gas production. However, the pH decreased rapidly with increasing the feed loading due to significant volatile fatty acids (VFA) production and accumulation.

The effect of volatile fatty acids on methanogenesis has been widely studied (Hanaki et al., 1981; Van Lier et al., 1993; Ahring et al., 1995; Wong et al., 2013), and it is widely accepted that propionic acid inhibits methanogenesis more strongly than acetic or butyric acid. Siegert and Banks (2005) investigated the effect of VFA in batch anaerobic digestion. A synthetic mixture of volatile fatty acids (18 % acetic acid, 50 % propionic acid, 5 % butyric acid, 27 % other VFA) was added as a substrate at the concentrations of 0, 1, 2, 4, 6, 8, 10, 12, 16 and 20 g /L. The results of daily biogas production showed that by increasing the VFA concentration; the methane percentage in the biogas decreased (as compared to the carbon dioxide percentage). The methane to carbon dioxide ratio in the biogas for the VFA concentrations of 1, 2, 4 and 6 g were 1:1.25, 1:1.5, 1:1.9 and 1:33, respectively. In addition, no biogas production was observed above a VFA concentration of 6 g/L. These results suggest that an increase in the concentration of VFA causes inhibition in the methane production.

2.2.3 Temperature

Microorganisms' activity, especially that of methanogens, is very sensitive to temperature changes, which directly affect the methane production. Many studies have examined the effect of temperature on methane yield in the anaerobic digestion process (Angelidaki and Ahring, 1994; Hansen et al., 1999; Lee et al., 2009; Zhang et al., 2009; Jiang et al., 2013; Bowen et al., 2014 ; Gou et al., 2014). These studies suggest that temperature and microbial activity act in tandem; that is anaerobic digestion becomes increasingly impaired as the temperature drops below 20 °C. It has

been reported that as temperature decreases, the VFA production rate, substrate utilization rate, and the methanogenic activity all decrease, resulting in increased lag periods for the onset of methanogenesis ('start-up' times); thus methane yields also decrease (Bowen et al., 2014). In the temperature range of 20 to 40 °C, methane production at 40 °C was 2.49 times higher than that at 20 °C (Gou et al., 2014). Lee et al. (2009) examined the effect of temperature on methane yield in the anaerobic digestion process of food waste leachate (FWL). Four different temperatures, 25, 35, 45 and 55 °C, at a pH of 7.8, were investigated for a period of 20 days. The highest cumulative methane yield (CMY) obtained was found at 35 °C, while the CMY at 25, 45 and 55 °C were lower by 8%, 13% and 32%, respectively, than the value obtained at 35 °C. Similar observations were also reported by Zhang et al. (2009) demonstrating that higher methane production was achieved at 35 ± 2 °C in comparison to 55 ± 2 °C at any pH (4.0- 11.0). Jiang et al. (2013) have also reported that better VFA production was observed at 35 °C compared to 45 and 55 °C. Another study confirmed these results and concluded that with the increase of operating temperature from 37 °C to 60 °C, biogas yield continuously decreased (Angelidaki and Ahring, 1994; Hansen et al., 1999). In general, it has been reported that the optimum reaction temperatures for microbial growth and activity under mesophilic and thermophilic conditions are 35 – 37 °C and 55 – 60 °C, respectively (Nguyen et al., 2007; Bowen et al., 2014).

2.2.4 pH

As defined by Trussell et al. (1989), pH is the intensity of the acidic or basic character of a solution or hydrogen ion activity at a given temperature. pH changes have a significant effect on the microbial community and substrate degradation and therefore on methane production. It has been observed that when fermentative bacteria convert glucose to hydrogen at a pH range of 4.0 – 7.0, the growth rate of microorganisms increases as pH increases to 7.0. This was accompanied by an increased degradation of glucose where the maximum degradation was achieved for pH ranging 5.5 – 7.0. In addition, at low pH (4.0 – 5.5) methane production was not observed; however, it increased drastically to be 3 ± 1 % at pH 6.0 and 9 ± 1 % at pH 7.0 (Fang and Liu, 2002). Methane generation was greatly reduced at acidic and alkaline conditions while the highest methane

production was observed in most cases at pH 7.0 (Zhang et al., 2009). The degradation of total suspended solids (TSS) and volatile suspended solids (VSS) is also significantly affected by pH. In a previous study, four reactors for the treatment of urban solid waste were set up at 37 °C, three were controlled at pH 6.0, 7.0, and 8.0, and one was run without pH control (Dinamarca et al., 2003). The best results for organic degradation rate were achieved at pH 7.0 and 8.0 where TSS degradation reached near 75% and VSS degradation near 80%. In addition, it has been shown that volatile fatty acids (VFA) composition and soluble chemical oxygen demand (SCOD) are affected by the level of pH (Fang and Liu, 2002; Zhang et al., 2009; Jiang et al., 2013). For example, the effect of pH was investigated by operating four reactors at pH 5.0, 6.0, 7.0, and without pH control, all of them at 35 °C (Jiang et al., 2013). The greatest VFA and SCOD concentrations occurred at pH 6.0. A similar trend was observed for the VFA/SCOD ratio, which shows how much soluble substance is converted into VFA. In any anaerobic digestion process, a stable pH and optimal biological activity is required to make methanogenesis more efficient. The methanogens' activity is greatly reduced at acidic (lower pH level) and alkaline (higher pH level) conditions (Zhang et al., 2009). Methanogens prefer almost neutral pH conditions with a general range between 6.5 and 8.2 and the optimal pH is 7.0 (Ağdağ and Sponza, 2005; Lee et al., 2009).

2.2.5 Carbon - Nitrogen Ratio (C/N)

Methane production is sensitive to the carbon and nitrogen content of organic materials (Mao et al., 2015). A higher carbon content supplies more carbon for methane production, whereas a considerable amount of nitrogen is needed to maintain microbial activity and growth (Wu et al., 2010). The C/N ratio is important to control biological treatment systems (Wang et al., 2012). On one hand, as the C/N ratio becomes too low, ammonia starts to accumulate, the pH value increases and this inhibits methanogenic bacteria. On the other hand, if the C/N ratio becomes too high, methanogens consume nitrogen rapidly resulting in decreasing gas production (Wang et al., 2012; Jiang et al., 2013).

Biogas production is greatly increased when there is a good balance between carbon and nitrogen (El-Mashad and Zhang, 2010). This was observed in experiments operated for 55 days under

mesophilic condition (35 ± 1 °C) with different C/N ratios of 21.9, 26.23, and 35.61. The highest biogas yield was obtained with the C/N ratio of 21.19 (Jiang et al., 2013). In another study, C/N ratios of 15, 20, 25, 30, and 35 were tested at a temperature of 35°C, while C/N ratios of 20, 25, 30, 35, and 40 were tested at a temperature of 55°C. The highest methane potentials were observed with C/N ratios of 25 and 30 at 35 °C and 50 °C respectively (Gou et al., 2014). Previous studies show that the ideal C/N ratio ranges from 20 to 35 for anaerobic digestion with a ratio of 25 being the most commonly used (Punal et al., 2000; Nguyen et al., 2007; Wu et al., 2010; Zhang et al., 2013; Gou et al., 2014; Wang et al., 2014).

2.2.6 Retention Time

Retention time (RT) is the number of days which are required to complete organic matter degradation (Villain and Marrot, 2013). Two major types of retention time, hydraulic retention time (HRT) and solid retention time (SRT), affect biogas production (Bolzonella et al., 2005; Kim et al., 2006; Nges and Liu, 2010; Aslanzadeh et al., 2013; Gou et al., 2014; Kwietniewska and Tys, 2014; Mao et al., 2015). Hydraulic retention time (HRT) is the time the liquid spends in the anaerobic digester and is equal to the biological digester volume (V) divided by the influent flow rate (Q). Too short HRTs usually result in VFA accumulation, whereas longer than optimum HRT causes ineffective utilization of digester components (Nagamani and Ramasamy, 1999). The solid retention time can be defined as the average time that microorganisms (solids) spend in the anaerobic digester (Ogejo et al., 2009; Kwietniewska and Tys, 2014). Effective retention time depends on temperature, organic load and substrate composition (Mao et al., 2015). There is a clear relationship between the applied HRT, SRT and biogas production; in particular, too low or too high SRT values result in low biogas production (Manure, 2001; Bolzonella et al., 2005; Nges and Liu, 2010). Bacteria need sufficient time (SRT) to grow and restore accidental loss via the effluent. Once bacteria loss exceeds their growth rate, wash-out occurs and the digestion process can fail (Manure, 2001; Ogejo et al., 2009).

2.3 Direct Electron Transfer (DIET) Mechanism

Some anaerobic microorganisms transfer electrons between them using hydrogen and formate as electron carriers in what is known as interspecies electron transfer mechanism (IET) (Bryant et al., 1977; Phelps et al., 1985; Marchaim and Krause, 1993). In recent years, it has been hypothesized that the electron transfer in anaerobic digestion proceeds also by direct electric current between electron-donating and electron-accepting microorganisms (DIET) via membrane-associated cytochromes or conductive pili for electron exchange (Morita et al., 2011; Liu et al., 2012a; Shrestha et al., 2013; Rotaru et al., 2014a). This hypothesis was firstly put forward by Summers et al. (2010) in defined co-cultures of *G. metallireducens* and *G. sulfurreducens* where ethanol was the electron donor and fumarate was the electron acceptor. Although, *G. metallireducens* cannot use fumarate as an electron acceptor and *G. sulfurreducens* cannot oxidize ethanol, it was found that a co-culture of *G. metallireducens* and *G. sulfurreducens* stimulated the release of electrons during the oxidation of ethanol and the acceptance of the electrons during the reduction of fumarate to succinate. They observed that *Geobacter* species were able to create electrically conductive aggregates that facilitated the transfer of electrons. They concluded that DIET was the predominant electron transfer mechanism under certain conditions for effective electron transfer. Some methanogens, either *Methanosarcina barkeri* (Rotaru et al., 2014a) or *Methanosaeta harundinacea* (Rotaru et al., 2014b), have also been observed to create direct electrical connections with a *G. metallireducens* co-culture thus allowing electrons to be transferred directly in the conversion of carbon dioxide to methane. Table 2.1 summarizes observational and experimental evidence for DIET in anaerobic digestion where ethanol oxidation under conditions occurred, even though IET via hydrogen or formate was not feasible.

Table 2.1. Evidence for DIET in defined co-cultures

Reference	Electron donating	Electron accepting	Observation
Summers et al. (2010)	*G. metallireducens*	*G. sulfurreducens*	Formation of electrically conductive aggregates
Rotaru et al. (2014a)	*G. metallireducens*	*Methanosarcina barkeri*	Formation of close aggregates
Rotaru et al. (2014b)	*G. metallireducens*	*Methanosaeta harundinacea*	Formation of close aggregates

Compared with IET, DIET does not require complex and multiple enzymatic steps for electron transfer. Storck et al. (2016) found that the external electron transfer rate for DIET (44.9×10^3 e^-/cell pair/sec) was higher than for IET (5.24×10^3 e^-/cell pair/sec). Furthermore, Jing et al. (2017) found that the Gibbs free energy was more negative and a higher propionate degradation rate was achieved for DIET as compared to IET.

2.4 Conductive Materials to Sustain DIET

Growing evidence shows that the supplementation of conductive materials and minerals, such as carbon cloth (Chen et al., 2014), biochar (Zhao et al., 2015), activated carbon (Liu et al., 2012a), hematite (Kato et al., 2010; Kato et al., 2012a) and nanoscale zero-valent iron (Carpenter et al., 2015; Suanon et al., 2016), can facilitate the DIET mechanism. The microorganisms seem to tightly attach to the surface of the conductive materials and form electrical currents, which enhance microorganisms to get involved in DIET thereby increasing methane production (Lovley, 2011; Kato et al., 2012b; Cruz Viggi et al., 2014; Park et al., 2018). For example, Luo et al. (2015) conducted mesophilic anaerobic batch tests in 500 mL serum bottles which were inoculated with 1 g VS/L of crushed anaerobic granular biomass, fed with 4, 6 and 8 g/L of glucose in the absence (control bottles) and presence of biochar (treatment bottles). The results showed that the lag phase was reduced significantly by 11 %, 30 % and 22 % and the maximum methane production rate increased significantly by 87 %, 22 % and 5 %, by the addition of glucose at 4, 6 and 8 g/L

respectively in the treatment bottles as compared to the control bottles. In addition, Tian et al. (2017) conducted batch experiments in 250 mL serum bottles that contained 0 mg/L (control), 30 mg/L and 120 mg/L of nano-graphene and glucose as carbon source with a concentration of 2 g COD/L for two weeks. They found that the relative methane production rate was accelerated by 17.0 % and 51.4 % with 30 mg/L and 120 mg/L of nano-graphene respectively as compared to the control. These results confirm that adding conductive materials triggers DIET and consequently enhances methane production. The interspecies electron transfer mechanisms involved in methanogenesis are illustrated in Figure 2.2.

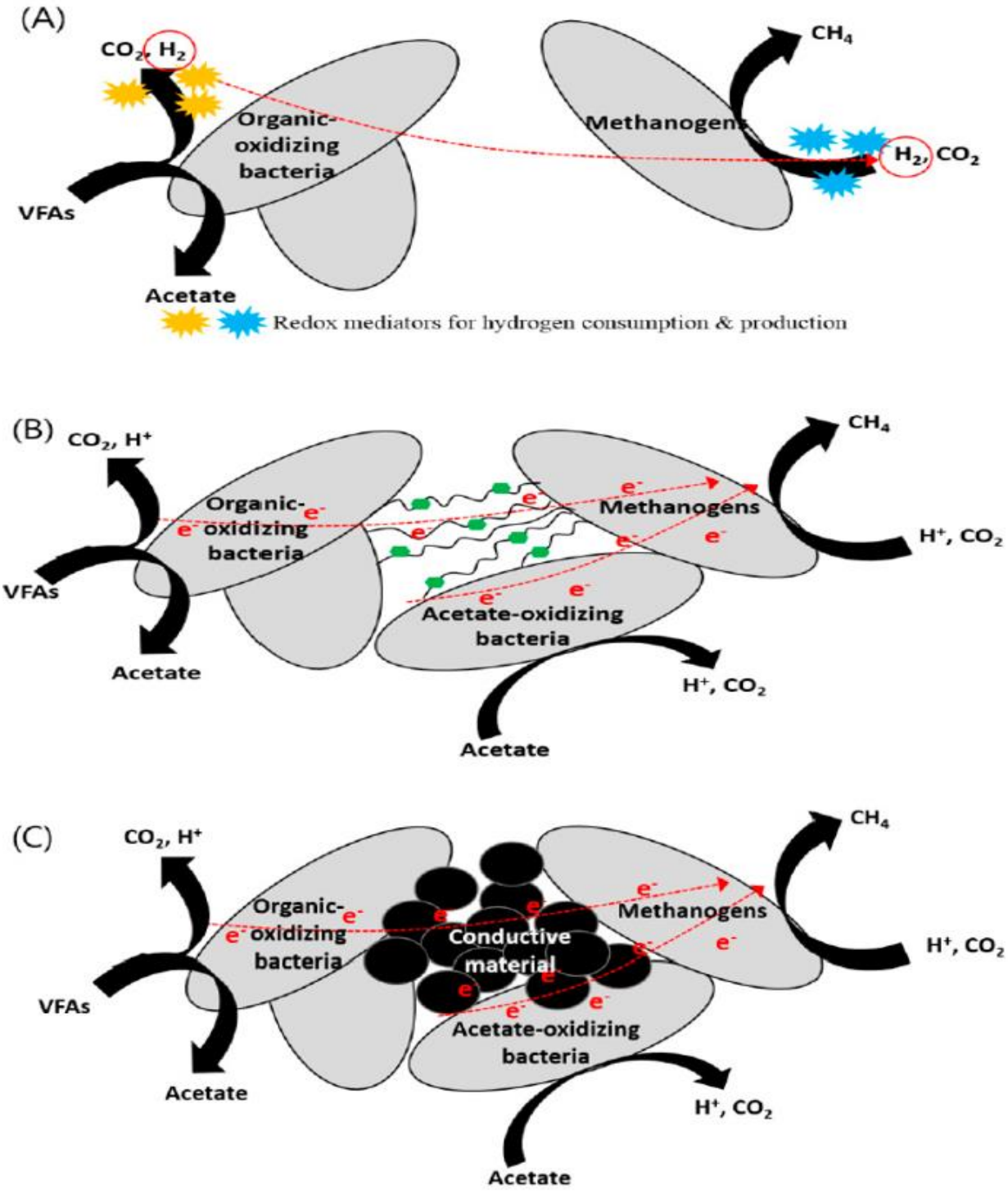

Figure 2.2. Mechanisms of (A) indirect interspecies electron transfer (IIET) via hydrogen, (B) Direct interspecies electron transfer (DIET), and (C) conductive material-mediated DIET (Adapted from Baek et al. (2018)).

2.4.1 Magnetite Particles (MNP) to Promote DIET

Magnetite is one of the most promising conductive minerals that boosts and sustains DIET. Magnetite can be synthesized easily by the addition of stoichiometric amounts of Fe^{2+} and Fe^{3+} in a basic solution with particle size control possible (Kang et al., 1996). Furthermore, their superparamagnetic properties allow for easy and rapid separation from a bioreactor effluent via a magnetic field (Keyhanian et al., 2011). In addition, the most important characteristic of magnetite as a promoter for DIET is its conductivity. The distinctive electrical conductivity properties of magnetite particles (Cruz Viggi et al., 2014) enable them to serve as conduits for electron exchange (Nakamura et al., 2009). These properties make magnetite suitable for use in experiments to test whether conductive materials stimulate DIET mechanism.

It has been documented that *Geobacter* and *Methanosarcina* species exchange electrons via MNP accelerating the conversion of intermediates of organic substrate into methane (Kato et al., 2012a; Yamada et al., 2015). Kato et al. (2010) suggested that magnetite is used by some bacteria (particularly *Geobacter* species) for transporting electrons to distant terminal acceptors. This suggestion has been supported later by Kato et al. (2012b) who found that electric currents were generated from *G. sulfurreducens* to *Thiobacillus denitrificans* through acetate oxidation and nitrate reduction in the presence of MNP. Additionally, Aulenta et al. (2013) confirmed that MNP stimulated the reductive dechlorination of trichloroethene (TCE), a groundwater pollutant, by allowing electrons to be transferred extracellularly from acetate-oxidizing to TCE-dechlorinating microorganisms.

Adding magnetite to promote DIET has been studied with several intermediates of organic substrate in mixed cultures. Cruz Viggi et al. (2014) first studied the effect of adding magnetite on propionate degradation with rice paddy soil as inoculum. They found that the methane production rate was 33 % higher as compared to the control; they suggested that this enhancement resulted from magnetite mediated DIET working as an electron conduit between microorganisms. In addition, Yamada et al. (2015) revealed that faster degradation of acetate and propionate occurred successfully by adding magnetite under thermophilic conditions. Zhuang et al. (2015a) used

benzoate as a substrate and found that its degradation rate in the presence of magnetite was increased by 53 % as compared to a control.

On the other hand, there are some limitations of magnetite being promoting DIET. It has been reported that DIET was only detected in cocultures of *Geobacter* species, and in cocultures of *G. metallireducens* with *Methanosaeta harundinacea* (Stams and Plugge, 2009) or *Methanosarcina barkeri* (Rotaru et al., 2014a); however, in some studies *Geobacter* species are existing in low percentages or even absent. In addition, DIET requires outer membrane c-type cytochromes and pili (Lovley, 2017) but syntrophic fatty acid-degrading bacteria (e.g., *Syntrophomonas wolfei* and *Syntrophus aciditrophicus*) (Sieber et al., 2014) and most methanogens (i.e. *Methanopyrales, Methanococcales, Methanobacteriales* and *Methanomicrobiales*) (Thauer et al., 2008) does not have the genes. Moreover, not all microorganisms are able to perform direct interspecies electron transfer as a known syntrophic ethanol oxidizing bacterium (*Pelobacter carbinolicus*), that could only establish syntrophic interactions with *Geobacter sulfurreducens* via IET (Rotaru et al., 2012) although it contains c-type cytochromes (Haveman et al., 2006).

2.5 Influence of Magnetite Nanoparticles on Methane Production

Cruz Viggi et al. (2014) reported that, during the first of two feeding cycles, a mesophilic methanogenic culture amended with nanometre-sized (100–150 nm) magnetite particles started the degradation of propionate after 6 days of initial incubation and completed it after 48 days; compared to 16 and 55 days, respectively, in the absence of MNP. This translates to a reduction of 62.5 % in the lag-phase time and 12.7 % in the length for methane production, and a 33 % increase in the methane production rate. Similarly, in the second feeding cycle, the maximum rate of methane formation in magnetite-amended bottles was 31 % higher than that in unamended bottles. It is worth mentioning that complete degradation of propionate took approximately 16 days regardless of whether MNP were added or not. Also, acetate was the only organic acid derived from propionate which reached a peak concentration at day 34 and was depleted at day 55 in MNP-supplemented bottles compared to 42 and 58 days, respectively, in the non-supplemented bottles, meaning a faster production and conversion into methane.

Similarly, Yamada et al. (2015) investigated the enhancement of methanogenic degradation of volatile fatty acids (i.e. 20 mM acetate and 25 mM propionate) by supplementation of magnetite (anaerobic stock solution 5 and 10 mM). The results showed that the acetate decomposition rate was significantly enhanced by the supplementation of 5 and 10 mM magnetite (15 vs 23 days), as compared to the control. The supplementation of 5 mM magnetite also significantly enhanced the degradation rate of propionate, which was completely degraded within 50 days, as compared to 150 days in the control. This indicates that the methane production rate was accelerated by 60 % and 30 % from propionate and acetate, respectively, by the addition of magnetite.

Magnetite nanoparticles also have the capability of enhancing methane production in paddy-soil enrichment. For example, it has been reported that in a semi–continuous paddy-soil enrichment, the time period of methane production from acetate in 8-10 nm of magnetite-amended bottles was, on average 35.8 % shorter and the methane production rate was 60 % higher than in the unamended bottles (Yang et al., 2015b). Consistent with these results, previous studies on batch incubation of paddy-soil enrichments with acetate revealed that a significant increase of more than 30 % in the methane production rate was achieved by adding magnetite (10-50 nm) (Kato et al., 2012a; Zhou et al., 2014).

Furthermore, another study on paddy-soil conducted by semi–continuous enrichment with propionate and magnetite supplement showed that the length of the lag-phase and the methane production period were on average 43.3 % and 31.7% shorter, respectively, than in a non-magnetite-supplemented control. Apparently, propionate was depleted sooner with magnetite supplementation even though the lag-phase time was prolonged. Consequently, the rate of methane production was higher, on average 93 %, compared to that in the non-supplemented control (Yang et al., 2016).

A recent investigation about the effect of adding magnetite (8-10 nm) to a paddy-soil enrichment using ethanol as a substrate revealed that in the magnetite-amended bottles the rate of methane production was on average 17 times higher and the lag-phase time was on average 60 % shorter than that of the unamended bottles (Yang et al., 2015a). The results reported by Kato et al. (2012a) confirmed the positive effect of magnetite (20 mM as Fe atom) since the time period for methane

production was reduced (on average 18 %) and the rate of methane production was increased (on average 45 %) as a result of adding magnetite compared to control bottles (without magnetite). Moreover, the use of magnetite 6.4 mM Fe ion and 25mM as Fe atoms also enhanced and stimulated butyrate and benzoate degradation as well as methane production rates respectively (Li et al., 2015; Zhuang et al., 2015a).

Jing et al. (2017) conducted an experiment in which the control reactor contained 30 mM of propionate only, while the second reactor contained 30 mM propionate and 10 mg/L nano magnetite. The results showed that 10 mg/L conductive magnetite enhanced the methane production rate from propionate by around 44 % in batch experiments. Additionally, Abdelsalam et al. (2017) examined methane production from slurry digestion with the addition of 20 mg/L of synthesized magnetite nanopowder (7 ± 0.2 nm). Their results showed that the highest methane percentage (79.3 %) was produced by the addition of 20 mg/L of magnetite (as compared to the control).

Recently, Zhuang et al. (2018) confirmed the ability of magnetite to enhance methane production even under high ammonia levels (which is considered a toxic environment for syntrophic acetate oxidization). The authors used fresh mesophilic anaerobic sludge as an inoculum, magnetite (25 mM as Fe atoms, 50–100 nm) as an additive, and acetate as a substrate. Their results showed that magnetite nanoparticles increased the methane production rate from acetate by 36 – 58 %, as compared with the anaerobic reactors (without magnetite) under the same ammonia level (5.0 g/L NH_4^+–N).

More recently, Beiki and Keramati (2019) conducted an experiment to measure biogas production from sugar beet waste. Magnetite nanoparticles, chitosan, and titanium dioxide were used separately as additives. The results showed that adding magnetite nanoparticles led to a slight increase in methane production as well as volatile solid and total solid reduction in the anaerobic reactors as compared to the control and the chitosan, and titanium dioxide anaerobic reactors.

Namal (2019) showed that DIET through conductive materials cannot however be easily stimulated for complex organics. They investigated the effects of 1 g/L dose of four different conductive materials on anaerobic degradation by using batch anaerobic reactors. Commercial magnetite (0 –75 μm), graphite (0–50 μm), granular activated carbon (15–75 μm) and iron sulfate were added as a conductive material and 50 % glucose solution (concentration of 4000 mg soluble COD/L) was used as a substrate. Their results showed that there was no significant difference in total methane production between treatments (averaged 769.4 mL) except for the granular activated carbon reactor that had the lowest methane production (540.1 mL). In addition, the methane production rates reached a maximum for all reactors at day 5. After that, methane production rates decreased for all reactors, which indicates that after day 5 further decomposition of substrates into organic acids is limited. They also observed a significant decrease in the lag time in the magnetite reactor, as compared to the control reactor (0.65 vs 1.28 days) followed by the graphite (1.03 days) and iron sulfate (1.17 days) reactors, respectively. However, the longest lag phase time was observed by adding granular activated carbon (1.62 days).

From the above research, it is clear that the addition of magnetite nanoparticles results in a significant increase in the methane production rate and a decrease of the lag phase. This was corroborated theoretically by Cruz Viggi et al. (2014) who estimated the maximum electron flux from acetogenic to methanogenic microorganisms during the oxidation of propionate and the reduction of CO_2 to be around 10^6 times higher via electronic conduction with magnetite (i.e. direct interspecies electron transfer) than via hydrogen diffusion (i.e. interspecies hydrogen transfer). Therefore, methane production rate seems to be enhanced by a greater electron transfer when magnetite is present in the medium. In contrast, it has been shown that the addition of magnetite nanoparticles do not change the total methane yield (Yamada et al., 2015; Yang et al., 2015b; Yang et al., 2016). That is, the total amount of methane produced was approximately in the expected range regardless of the presence or absence of MNP. On the other hand, the amount of methane eventually produced from VFA (e.g. propionate, acetate) was either lower or higher than the predicted value from the stoichiometry of the classical degradation pathway (Kato et al., 2012a; Cruz Viggi et al., 2014; Yamada et al., 2015; Yang et al., 2015b). If magnetite nanoparticles do improve the methane yield, this would suggest that these nanoparticles are used as a nutrient

(source of iron) by the microorganisms. In line with that, one would also expect an increase in methane yield when ferrihydrite (which is also a source of iron) is used. However, this suggestion has been disproved by Kato et al. (2012), Li et al. (2015) and Yamda et al. (2015) who showed that the methane yield was higher in the control bottles (without ferrihydrite) than that in the supplemented bottles (with ferrihydrite) indicating that the use of ferrihydrite either suppressed or inhibited methanogenesis. As such, ferrihydrite could not be used as a nutrient (source of iron ions).

Physical and chemical characteristics of nanoparticles such as the surface area, the electrical conductivity, and the purity can potentially influence biological reactions (Martins et al., 2018). In addition, during the synthesis process, some nanoparticle metals may combine, causing an inhibitory or even a toxic environment to microbial communities (Faisal et al., 2019). In particular, there are some reports that directly indicate that nanoparticles can inhibit methanogenic activity. For example, high concentration of magnesium oxide and silver nanoparticles (up to 500 mg/g TSS) were shown to inhibit methane production (Martins et al., 2018). There is little evidence in the literature however that magnetite particles have an inhibitory effect on the production of methane. For example, Kato et al. (2012a) reported that magnetite may change the microbial community in that *Methanobacterium* was only observed in a control culture during the addition of magnetite to anaerobic digesters which means that they experienced inhibition in the presence of magnetite.

2.6 Factors Affecting Magnetite Performance

Many factors influence the performance of magnetite nanoparticles including their size and dose, substrate type and dose, and the sludge type and microbial community dynamics. Therefore, gaining a better understanding of how these factors affect MNP performance would allow for optimising the maximum substrate degradation and the maximum methane production rate.

2.6.1 Magnetite Nanoparticles Size and Concentration

The stimulatory effect of magnetite nanoparticles on methane production seems to be dose and size dependent (Jiang et al., 2008; Verma and Stellacci, 2010; Abdelsalam et al., 2017). Casals et al. (2014) found that biogas production was 66.6 % higher when using 7 nm MNP than when using a size of 24 nm. Besides that, the released free iron ions when using 7 nm particles was 23 mg/L while the concentration was 0 mg/L at the 24 nm size. This suggests that using a small size (8-10 nm) increases the activity of methanogens and boosts the methane production rate. Furthermore, recent studies indicated that, when using a nanoparticle size of 8-10 nm, the rate of methane production was 60 % higher than that of the control (no MNP), but only 30 % higher when using a larger nanoparticle size of 10-50 nm (Kato et al., 2012a; Yang et al., 2015b).

Li et al. (2015) showed that with different MNP concentrations (0.0213, 0.213 and 2.13 mM) methane production increased with the concentration of MNP. In addition, Casals et al. (2014) showed that methane formation increased when the MNP concentration was increased from 0 to 1.166 mM and then decreased when the MNP concentration was increased above 1.166 mM. Similarly, the result of testing MNP at increasing concentrations above 20 mM (80, 160 and 320 mM) showed that the methane production (rate and amount) was not improved (Yang et al., 2015b; Yang et al., 2016). This suggests that there is a MNP concentration limit for a positive effect on methane formation and above that limit methanogenesis decreases or is inhibited.

These observations indicate how magnetite concentration and size critically affect the methane production rate. In short, much higher or much lower concentrations and very small or very large sizes inhibit the methane production process. Overall, however, it is difficult to compare studies as many factors besides magnetite size and concentration play a role in methanogenesis. Therefore, within the parameters of any experiment, it is important to monitor the MNP size and concentration to form the necessary level of aggregation.

2.6.2 Substrate Type and Dose

The effect of MNP on anaerobic digestion performance seems also to be related to the substrate type and dose. The result of testing MNP without an external substrate showed that the methane production rate was higher in the absence of MNP than in their presence (Cruz Viggi et al., 2014). This suggests that a minimum concentration of substrate is required for magnetite nanoparticles to serve as electrical conduits. Most studies have focused on using either acetate (Kato et al., 2012a; Zhou et al., 2014; Yamada et al., 2015; Yang et al., 2015b) or propionate as a substrate (Cruz Viggi et al., 2014; Yamada et al., 2015; Yang et al., 2016). Fewer studies have tested butyrate, ethanol or cellulose (Casals et al., 2014; Li et al., 2015; Yang et al., 2015a).

In addition, further studies showed that the methane production rate increased with increasing the concentration of acetate and propionate up to 50 and 20 mM respectively; whereas no significant enhancement in methane production rate was observed when substrate concentrations were increased above those limits (Yang et al., 2015b; Yang et al., 2016). These results suggest that in the presence of MNP, a substrate would give a good performance for methane production if it is provided within a suitable concentration range.

2.6.3 Sludge and Microbial Community Composition

The efficiency of MNP also seems to be linked to the sludge type and the structure of the microbial community. Yang, Shi, et al. (2015) tested the effect of MNP on soils from three different rice fields, each of them with a different microbial composition. The result showed different response to MNP since different values of methane rate production (2.0, 4.5, 4.5 mmole/d) were obtained.

So far, most experiments on the effect of MNP have been conducted using fresh bacterial enrichments from paddy soil samples (Kato et al., 2012a; Zhou et al., 2014; Li et al., 2015; Yang et al., 2015a; Yang et al., 2015b; Yang et al., 2016). Fewer studies have used fresh anaerobic methanogenic cultures from municipal wastewater treatment plants (Cruz Viggi et al., 2014; Yamada et al., 2015; Suanon et al., 2016). Considering these experiments, since magnetite showed the ability to enhance methane production from fresh sludge, adding magnetite to aged (i.e.

degassed) sludge may also produce positive results in terms of methane production. Challenges still exist, however, as there is insufficient research reviewing the impact of adding magnetite nanoparticles on methane production on different ages of sludge.

The evidence above suggests that magnetite enhances the methane production and many factors affect the performance of magnetite on methane production. To date, most studies investigate the effect of a specific size and concentration of magnetite on methane production from a specific substrate type and concentration in fresh co-cultures. However, there is a need to have a greater understanding of the effect of magnetite on methane production when more complex substrates are used, especially under different community metabolic conditions. Thus, the interest of this research is to systematically study the effect of magnetite concentration and size on methane production from different substrate concentrations in different sludge cultures. As well for the first time, investigate the effect of magnetite on methane production from glucose at different concentrations.

2.7 Research Objectives

The main goal of this research was to identify the conditions that favor maximum methane production rate in the presence of magnetite. More specifically, the objectives were first to study the effect of magnetite particles on methane production using fresh and aged (i.e. degassed) sludge and secondly to study the effect of magnetite concentration on methane production in the presence of different concentrations of propionate, acetate, and glucose. These objectives were accomplished in three phases:

Phase I explored the conditions that enhance or inhibit methane production in magnetite-amended anaerobic digestion. For that objective, preliminary batch test experiments were conducted to explore the conditions that improve methane production in the presence of magnetite. First, batch test calibration experiments were carried out to examine the stability of an anaerobic batch bottle and identify suitable concentration of VS. Batch tests were also carried out to explore the effect of magnetite dose on methane production from acetate and propionate, the effect on methane production of using magnetite synthesized in the lab or sourced from a commercial manufacturer, and finally the effect of using magnetite from a suspension.

Phase II explored the effect of magnetite on methane production using two different sludge ages. Fresh and degassed sludge were tested with 2 and 7 mM of small, medium and large sized magnetite.

Phase III explored the effect of using propionate, acetate and glucose under different concentrations on methane production. Acetate, propionate (with three different concentrations) and glucose (with five different concentrations) were added separately as a substrate into the serum bottles in the presence of different magnetite concentrations (i.e. 2, 7 and 20 mM).

CHAPTER 3. MATERIALS AND METHODS

3.1 Overview

As mentioned, this research has two overall objectives: the first is to investigate and compare the effect of conductive magnetite on methane production when using a fresh digested sludge and when using a degassed digested sludge. The second is to evaluate the effect of the concentration of propionate, acetate and glucose on methane production in the presence of different magnetite concentrations. To achieve these objectives experiments were conducted with the following goals:

- Synthesize magnetite by the co-precipitation and hydrothermal methods.
- Examine the stability of an anaerobic batch bottle (i.e. identify suitable concentrations of VS and sufficient COD:VS ratios) (Run1).
- Conduct preliminary experiments to see the effect of adding magnetite on methane production (Run 2, Run 3, Run 4 and Run 5).
- Investigate the effect of using different size ranges and concentrations of magnetite using fresh vs degassed digested sludge.
- Measure the total organic carbon of the digested sludge liquor for up to a month to find out how it changes from fresh to degassed sludge with time.
- Analyze the concentration of dissolved iron in the anaerobic batch medium over time to assess the dissolution of magnetite.
- Evaluate the effect of adding propionate and acetate with three different COD:VS ratios (2 COD: 1 VS, 4 COD: 1 VS and 8 COD: 1 VS).
- Evaluate the effect of adding of glucose with five different COD:VS ratios (2 COD: 1 VS, 3 COD: 1 VS, 4 COD: 1 VS, 6 COD: 1 VS and 8 COD: 1 VS).
- Measure the volatile fatty acid, the glucose concentration and pH to see how they affect the production of methane.

3.2 General Materials and Methods

3.2.1 Source of Biomass

The seed digested sludge samples were collected from a mesophilic anaerobic digester fed with sludge from the primary sedimentation tanks and final clarifiers at the wastewater treatment plant (WWTP) located in the Bromley suburb of Christchurch, New Zealand. The WWTP receives mostly domestic wastewater with a small portion of industrial effluents. The samples were either used fresh (i.e. immediately after collection) or degassed (i.e. after incubation for up to one month) under anaerobic conditions at 36 ± 2^{o}C.

3.2.2 Substrate Stock Solutions

Several stock solutions of acetate, propionate, and glucose were prepared at different concentrations. The pH was measured using a pH meter and adjusted if necessary by sodium bicarbonate to around 7-7.8.

3.2.3 Magnetite Nanoparticle Preparation

Magnetite nanoparticles (MNP) were prepared by either the co-precipitation or the hydrothermal methods (Kang et al., 1996; Du et al., 2012).

The co-precipitation method is simple and effective; however, the prepared particles are not very stable under ambient conditions and easily adsorb oxygen to form maghemite (Lu et al., 2007; Ali et al., 2016). Different factors affect the stability of the prepared nanoparticles such as preparation temperature, mixing speed, and presence of oxygen (Lu et al., 2007; Mascolo et al., 2013). As such, MNP were prepared via the co-precipitation method described by Kang et al. (1996) under high temperature of 80-100^{o}C (Ozkaya et al., 2009) and under a flow of nitrogen gas (Kim et al., 2001) to prevent uncontrollable oxidation of Fe^{+2} into Fe^{+3}.

For co-precipitation synthesis, a sodium hydroxide (1000 mL, 1.5 M) solution was deoxygenated by purging with nitrogen gas for 30 min and heating to 80^{o}C. At the same time, 8.0 g of $FeCl_2$ and 20.8 g of $FeCl_3$ were dissolved in a combined volume of 3.4 mL of 12.1 N HCl and 100 mL of deoxygenated water (i.e. nitrogen sparging for 30 min). Following that, the resulting solution of iron oxides was slowly dribbled into the sodium hydroxide solution using a dropping funnel under vigorous stirring (i.e. 1300 rpm) (Figure 3.1). During this preparation step, the reaction medium was kept under a flow of nitrogen gas and the temperature was controlled at 80 – 100^{o}C to prevent the introduction of oxygen to the solution. An instant black precipitate of magnetite (Fe_3O_4) was generated which was separated from the liquid with an external magnetic field to check the paramagneticity. After that, the black precipitate was washed by adding deoxygenated water and the solution decanted after centrifugation at 4000 rpm. This was done several times. Finally, the magnetite precipitate sample was dried in an oven at 36^{o}C overnight. The generated MNP were measured to be about 15.0 g.

Magnetite nanoparticles were also prepared via a hydrothermal method as described by Du et al. (2012) and shown in Figure 3.2. Briefly, 8.1 g of $FeCl_3.6H_2O$ and 21.6 g of sodium acetate were dissolved in 240 mL ethylene glycol with stirring and heating simultaneously. The temperature was then increased to 80 – 100^{o}C. After stirring for 2 h, the yellow-brown color solution was transferred to a Teflon-lined stainless-steel autoclave and heated in an oven at 200^{o}C for 18 h. Then, the autoclave was left to cool to room temperature. The obtained black magnetite particles were washed with acetone and water for several times and then dried in an oven at 36^{o}C. The generated MNP were measured to be about 3.0 g.

Obtaining stable, spherical, homogenous composition and narrow size ranges of these particles was the goal of synthesis methods, which was successfully achieved after many preparation attempts. Finally, commercial MNP were purchased from Sigma-Aldrich China with 50-100 nm particle size and 97 % trace metals.

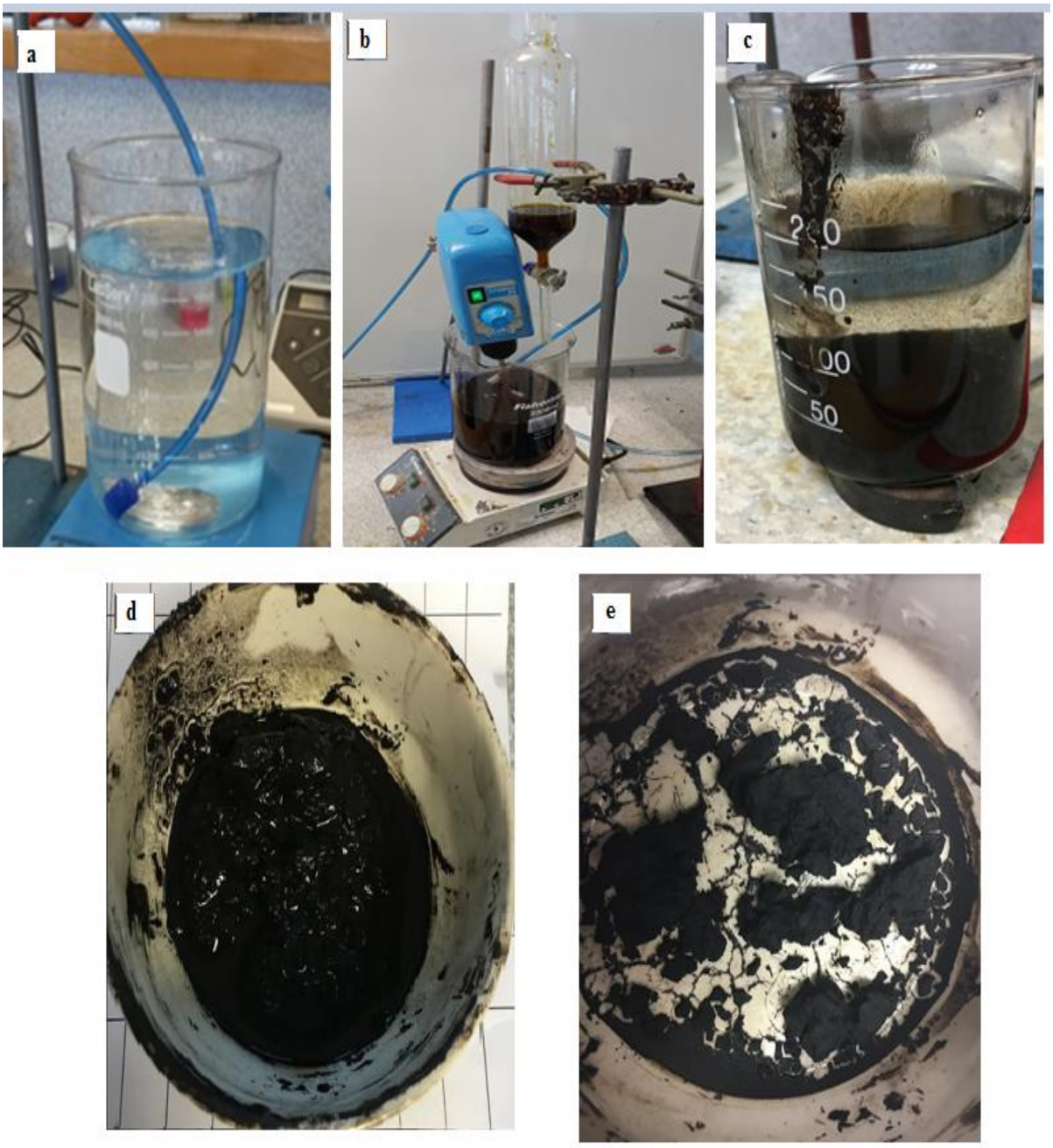

Figure 3.1. Formation of magnetite nanoparticles via the co-precipitation method (Kang et al., 1996). (a) Deoxygenation of deionized water, (b) Adding the aqueous solution of ferrous and ferric into degassed and heated NaOH, (c) Generation of the black precipitate, (d) Obtaining the black precipitate by washing several time with deionized water, (e) nanopowder dried at 36ºC.

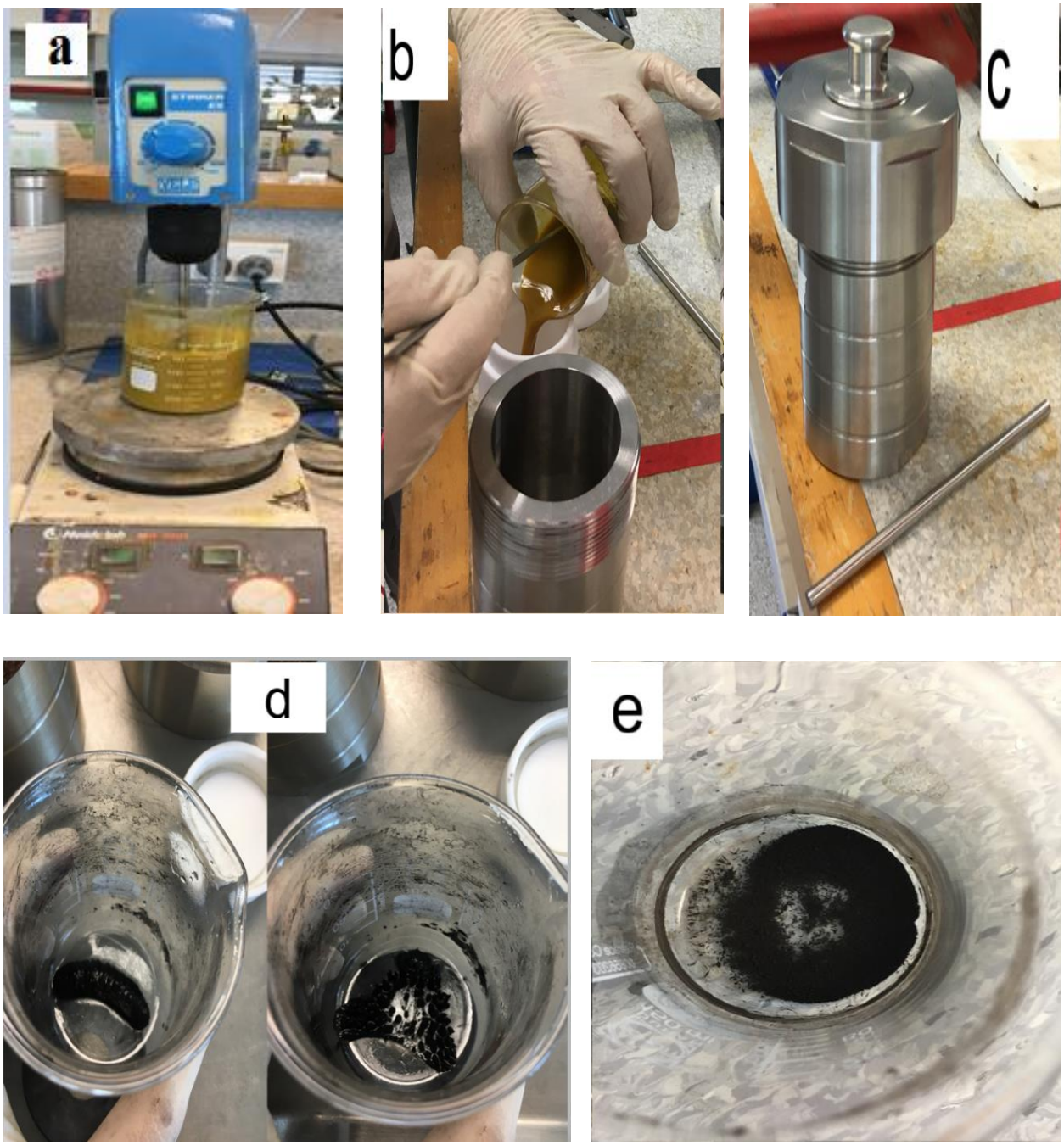

Figure 3.2. Preparation of magnetite nanoparticles via the hydrothermal method (Du et al., 2012). (a) Mixing the chemicals together under vigorous stirring and heating for 2 hr, (b) Transferring the produced solution to the autoclave, (c) Closing the autoclave tightly then heating it in an oven at 200 ^{o}C. (d) Checking the paramagneticity of the obtained black magnetite particles, (e) nanopowder dried at 36^{o}C.

3.2.4 Anaerobic Medium

The synthetic anaerobic medium containing macronutrients, micronutrient and vitamins was prepared as described by Angelidaki and Sanders (2004). Different volumes of stock solutions A, B, C, D and E (as shown in Table 3.1) were added to 974 mL of distilled water to prepare 1 liter of anaerobic medium. Then the mixture was bubbled with nitrogen gas. After that, 0.5 g of cysteine hydrochloride, 2.6 g of sodium bicarbonate and 0.25 g/L of $Na_2S.9H_2O$ were added. The medium was kept in the fridge at 4℃ until dispensed to serum bottles.

Table 3.1. Composition of stock solutions used to prepare one liter of anaerobic medium (Angelidaki and Sanders, 2004)

Stock solution, mL	Chemical and their final concentration (g/L), in distilled water
(A) 10	NH_4Cl, 100; NaCl, 10; $MgCl_2.6H_2O$, 10; $CaCl_2.2H_2O$, 5
(B) 2	$K_2HPO_4.3H_2O$, 200
(C) 1	Resazurin 0.5
(D) 1	$FeCl_2.4H_2O$, 2; H_3BO_3, 0.05; $ZnCl_2$, 0.05; $CuCl_2.2H_2O$, 0.038; $MnCl_2.4H_2O$, 0.05; $(NH_4)_6Mo_7O_{24}.4H_2O$, 0.05; $AlCl_3$, 0.05; $CoCl_2.6H_2O$, 0.05; $NiCl_2.6H_2O$, 0.092;ethylenediaminetetraacetate, 0.5; concentrated HCl, 1 mL; $Na_2SeO_4.10H_2O$, 0.1.
(E) 1	Biotin, 0.002; folic acid, 0.002; pyridoxine acid, 0.01; riboflavin, 0.005; thiamine hydrochloride, 0.005; cyanocobalamine, 0.0001; nicotinic acid, 0.005; P-aminobenzoic acid, 0.005; lipoic acid, 0.005; DL-pantothenic acid, 0.005.

3.2.5 Batch Experiments

Batch experiments were conducted using 165 mL serum bottles as described by Cruz Viggi et al. (2014). Three different groups (i.e. control, magnetite-supplemented, and blank) were used to explore the effect of magnetite addition on methane production. Control bottles were spiked with either acetate, propionate or glucose as a substrate and inoculated with anaerobic digested sludge. The volumes of the substrate solution and the inoculum were adjusted to give an initial COD:VS ratio of 2:1, 4:1 or 8:1. The inoculum was kept under anaerobic conditions during the process of transfer to the bottles. No magnetite was added to the control bottles. Magnetite-supplemented bottles were prepared with the same type and amount of substrate and inoculum in the control bottles. Magnetite (i.e. synthesized or commercial) was introduced into the bottles to a final concentration of 2, 5, 7, 10, 12 .5, 15, 20, 30 or 40 mmole/L. In order to determine the methane production from the inoculum itself, blank bottles were simultaneously prepared with anaerobic medium and methanogenic culture (i.e. digested sludge) but without substrate and without magnetite.

Anaerobic medium was added to achieve 120 mL as the final working volume in all test bottles. The initial pH value was adjusted in the range of 7.5−7.8 by adding a few drops of 20 M sodium hydroxide were necessary. All test bottles were flushed with nitrogen gas and sealed with rubber stoppers and aluminum crimps to keep anaerobic conditions. Resazurin was used as an indicator of anaerobic conditions. If a bottle's color changed to pink, that meant the bottle had sufficient oxygen to be considered aerobic and in this case, the essay had to be repeated. The component description of the different batch tests is shown in Figure 3.3. All tests (i.e. blank, control and magnetite amended) were performed in triplicate.

Once prepared, the test bottles were incubated at 36 ± 2^{o}C and methane production was periodically monitored by sampling and analysis of biogas from the headspace.

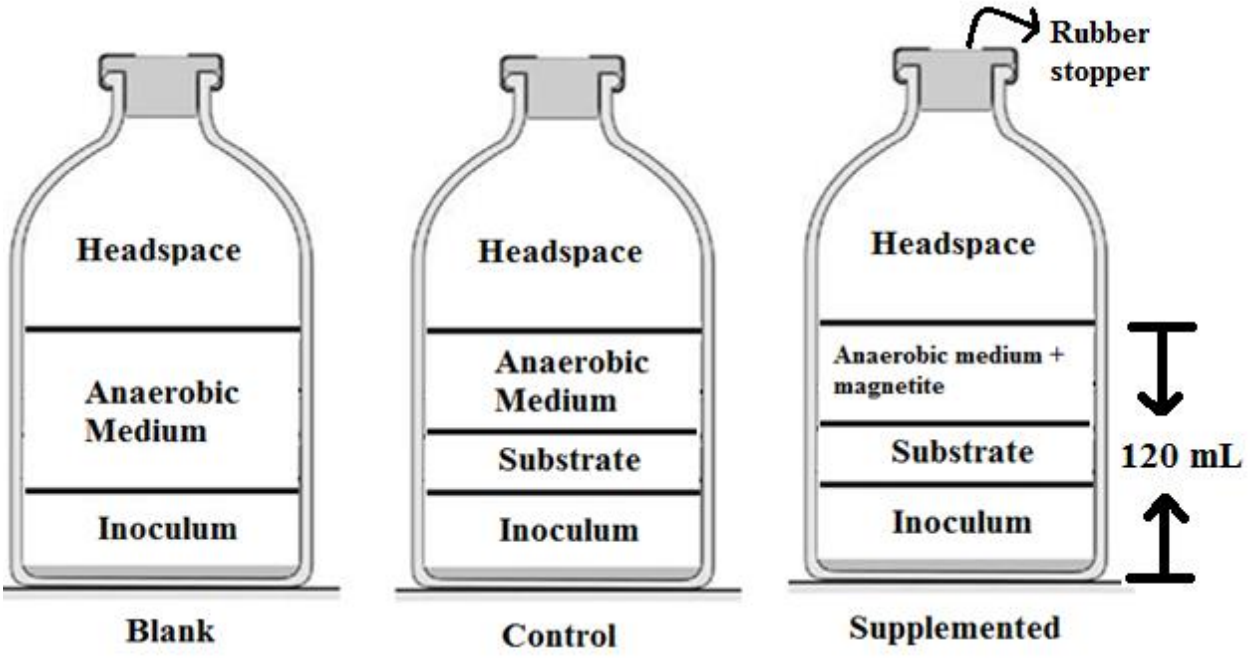

Figure 3.3. Schematic representation of experimental setup to assess methane production in anaerobic batch treatment bottles.

3.3 Analytical Methods

The anaerobic digestion performance was evaluated through biogas production. The following sections describe the analytical methods used in the research.

3.3.1 Magnetite Nanoparticles Characterization

Three MNP samples were characterized (i.e. hydrothermal, co-precipitation and commercial) at the University of Auckland using X-ray diffraction (XPS) and scanning electron microscopy (SEM). The commercial magnetite was analyzed for validation purposes.

X-ray diffraction analysis was carried out to characterize the phase composition. Data was collected on a Kratos Axis UltraDLD (Kratos Analytical, Manchester, UK) using monochromated Al Ka X-rays, operating at 150W with a pass energy of 160 for the survey and 20 for the core level

scans. The data was fitted with CasaXPS because it is very sensitive to $Fe^{3+}$and Fe^{2+} cations (Ma et al., 2013). Relative sensitivity factors provided by Kratos and adapted to the instrument were used. These were based on the Wagner basis set. A Shirley baseline was fitted and GL (30) synthetic peaks were used to record each spectrum.

The results from X-ray diffraction showed each oxidation state as a main peak and satellited for both the Fe2$p_{3/2}$ and Fe2$p_{1/2}$ regions. Comparing the synthesized magnetite with the commercial sample, the XPS patterns show identical diffraction peaks (Figure A.1, Appendix A). The reference sample indicates that the levels of Fe2$p_{3/2}$ and Fe2$p_{1/2}$ were 710.4 eV and 723.9 eV, respectively. For the synthesized sample (co-precipitation), they were 710.5 eV and 724.0 eV for both the Fe2$p_{3/2}$ and Fe2$p_{1/2}$ peaks respectively. These results are in agreement with the literature in that the core-levels spectra of Fe2p3/2 and Fe2p1/2 are 711.28 and 724.64 eV (Ma et al., 2013), 710.9 and 724.9 eV (Teng et al., 2003).

Scanning electron microscope analysis was performed on the MNP samples for morphology and particle size characterization. SEM images (Figure A.2, Appendix A) showed that the co-precipitation and hydrothermal samples consisted of homogenous particles with nearly spherical shapes. The average particle diameter was calculated from SEM images using an image analysis programme FEG Quanta 200 F (FEG = Field Emission Gun). The EDS detector was SiLi (Lithium drifted) with a Super Ultra-Thin Window, Peltier stage (2°C – 50°C), high temp stage (70°C – 1400°C). The diameters of the synthesized magnetite particles ranged from 800 nm to 4.5 µm and from 168 to 490 nm for the co-precipitation and hydrothermal methods respectively (Appendix A, Figure A.3).

3.3.2 Physical-Chemical Characterization

Seed sludge was characterized before incubation by physico-chemical analysis such as total solids (TS), total volatile solids (VS), pH and total organic carbon. All analyzes were done in duplicate to ensure statistically representative results. All analyzes were undertaken according to Standard Methods for the Examination of Water and Wastewater (Association, 2005).

All TS and VS analyzes were completed within 48 hours. Well-mixed sludge samples (50 mL) were evaporated to dryness in pre-weighed dried dishes at 105℃ for 24 h. After an additional 30 minutes of cooling in a desiccator, the combined TS and standard dish were weighed [$Mass_{(solids+dish)}$] and the increase in weight was converted to a concentration (mg/L) by accounting for the volume of sample used. The concentration of VS was subsequently measured by weighing the combined ashes and evaporating dish after ignition for 4 h at 550℃. All the equations are shown in Appendix B. A pH meter was used for pH measurement (see Appendix B, Figure B.1 and Figure B.2 for details). Total organic carbon (TOC) to measure the level of organics in the liquid phase of anaerobic batch test was analyzed with a Shimadzu TOC-L CSH analyzer with TOC-control L v1.01 software. In order to calibrate the results, reference solutions were used containing 1000 ppm standard stock (KHP) and deionized water (blank, TOC= zero). Each TOC measurement was run in duplicate. TOC was measured for the same digested sludge sample over a month from the first collection day.

3.3.3 Ferrous Ion Measurement

Ferrous ion was measured following HACH method 8146 using a spectrophotometer according to Standard Methods for the Examination of Water and Wastewater (Association, 2005). A clean, round sample cell was filled with 25 mL of sample, and then ferrous iron reagent powder was added to the sample cell and mixed up to three minutes. For the blank, a second round sample cell was filled with 25 mL of a sample (no ferrous iron reagent powder). For analysis, the blank was run first to zero the spectrophotometer, then the sample was run to obtain the ferrous ion concentration.

3.3.4 Biogas Analysis

3.3.4.1 Manometric Biogas Measurement

The measurement of biogas volume produced at room temperature and pressure (RTP) was done manometrically following a water displacement method as described by Procházka et al. (2012)

(Figure 3.4). Saturated NaCl solution was used as a barrier liquid in the water displacement device to avoid dissolution of carbon dioxide (Rozzi and Remigi, 2004).

A fixed 4 mL volume of biogas was sampled from the bottle's headspace using a gas tight syringe (Hamilton, USA). The syringe was then connected to a plastic tube via a two-way valve. After the proper connection was done, the two-way valve was opened and the saturated-salt solution moved up (negative) or down (positive) in the graduated glass tube due to the pressure difference. The reading of displacement was recorded. Calculations were done to convert the headspace biogas volume to biogas volume at RTP. For example, if the headspace volume in the bottle was 63 mL, the gas sample was 4 mL and water displacement was 0.1 mL, then the headspace biogas volume at RTP was:

$$Headspace\ biogas\ volume\ at\ RTP = \left(\frac{4\ mL + 0.1\ mL}{4\ mL}\right) * \ (63\ mL + 4\ mL)$$

$$= 68.675\ mL$$

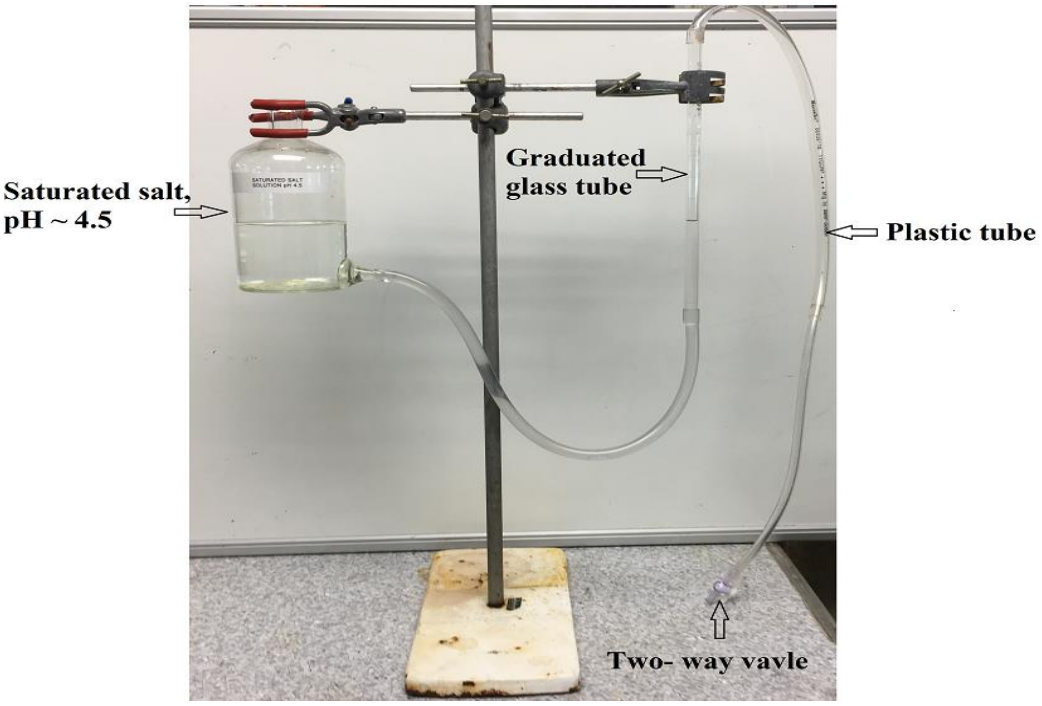

Figure 3.4. Water displacement technique used to measure the volume of biogas at RTP (Procházka et al., 2012). If the atmospheric pressure was greater than the pressure inside anaerobic bottle (negative pressure), the saturated-salt water will move up. While if the pressure inside anaerobic bottle was greater than the atmospheric pressure (positive pressure), then it will move down.

3.3.4.2 Biogas Composition

Gas chromatography (GC) is a well-known method to determine biogas (methane and carbon dioxide) composition (Figure 3.5). Generally, chromatographic data are presented as a chromatogram (i.e. a plot of retention time (x-axis) against detector response (y-axis). This plot provides the retention time and the peak area that is proportional to the amount of compound that has passed the detector (Figure 3.6).

For a batch bottle, after measuring the biogas volume using the water displacement device, the same 4 mL volume sample was injected directly into an Agilent 7820A gas chromatograph. The setup of the GC gas composition method was as follows:

Agilent 19095P-Q04 stainless steel column with 30 m × 530 µm × 40 µm; helium carrier gas 10 mL/min with pressure 10.6 psi; oven temperature 30°C; injector temperature 70°C; TCD temperature 155°C . All analyzes were undertaken in triplicate for more reliable results. The retention times of 1.591 and 2.123 min for standard methane (60 %) and carbon dioxide (30 %) respectively are shown in Figure 3.6.

Figure 3.5. Biogas composition measured by injecting a gas sample into GC.

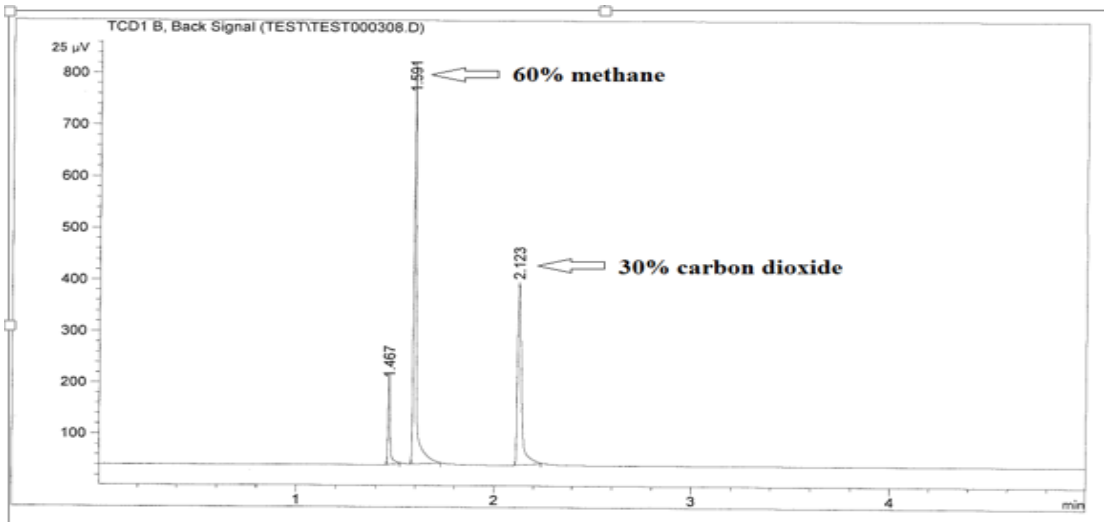

Figure 3.6. Gas chromotograph plot for a standard methane gas analysing sample. The retention times of 1.591 for standard methane (60 %) and and 2.123 min for standard carbon dioxide (30 %).

To calculate the methane percentage in a sample the gas chromatograph was calibrated. For GC calibration, three samples (4 mL each) of different volume percent 0.25, 0.5, and 0.75 of 10 mL standard gas (60 % methane, 30 % CO_2, and 10 % nitrogen) were mixed with air using a gas tight Hamilton syringe. Each sample was then injected into the GC. The calibration curves (methane and carbon dioxide) are shown in Appendix C (Table C.1, Figure C.1 and Figure C.2). The obtained equation from calibration curve was used to calculate the percentage of methane. For example; after injecting the gas sample, if the GC reading for methane area was 921; using the equation of calibration curve $\% CH_4 = \frac{methane\ AREA}{63.204}$,

$$\% CH_4 = \frac{921}{63.204} = 14.5719\ \%$$

After calculating the percentage of methane in a sample, further calculations were done to convert methane % to mmole/g VS. See Appendix D for a sample calculation.

3.3.5 Volatile Fatty Acid Analysis

For the analysis of volatile fatty acids (VFA), 2 mL of the liquid medium was taken periodically over the incubation period. This was filtered to 0.22 µm, adjusted to reduce the pH lower than 2 and then placed in the GC-FID. The GC conditions were as follows. Agilent Technologies 7280A Column: HP 19091N-133I, HP INNOWax Polyethlene Glycol with 30 m x 250 µm x 0.25 µm. Gas: Nitrogen with flowrate of 2.2 ml/min, pressure 60 psi, Hydrogen 50 psi, Air 60 psi and Helium 82 psi. The initial Oven temperature 80ºC increase at 10ºC/min to 250ºC, was held at 260ºC for 2 min, with FID detector at 300ºC. The volatile fatty acids (acetic, propionic and butyric) were identified by comparing the retention time against known standards. The retention times of 4.886, 5.368, and 5.871 minutes for standard acetic, propionic and butyric acids respectively are shown in Figure 3.7.

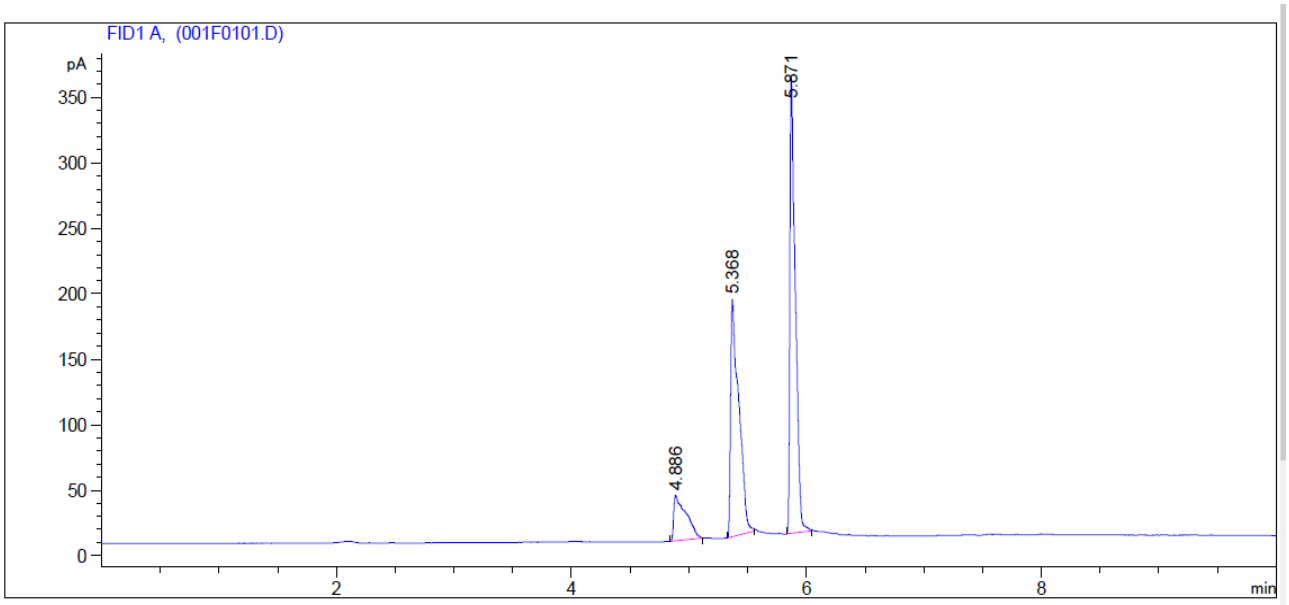

Figure 3.7. Gas chromatograph plot for VFA standards. The retention times of 4.886, 5.368 and 5.871 min for standard acetic, propionic and butyric respectively.

3.3.6 Glucose Concentration

Glucose concentrations were measured according to the phenol- sulfuric acid method as described by Dubois et al. (1956) and Albalasmeh et al. (2013). A fixed volume of 2 mL of the liquid medium was taken after 7 days of incubation, filtered to 0.22 µm, then pipetted into a colorimetric tube and mixed with 1 mL of 5 % aqueous solution of phenol. Subsequently, 5 mL of concentrated sulfuric acid was added rapidly to the mixture. After allowing the test tubes to stand for 10 min, they were vortexed for 30 sec then placed for 20 min in a water bath at 30^{o}C for color development. Finally, UV light absorption at 490 nm was read using a UV spectrophotometer. Standard curves of glucose concentration were prepared by reading UV light absorption at 490 nm at known concentrations of 0.01, 0.03, 0.05, 0.07 g/L.

3.3.7 Microbial Analysis

Genomic DNA extraction and purification was conducted in the Laboratory of Molecular Biology of the Bio-Prospection Research Centre, Lincoln University, New Zealand. About 20 mL of sludge were centrifuged at 5000 rpm (20^{o}C) for 10 min. The supernatant was decanted and the sediment pellet put in liquid nitrogen and stored in an ultra-freezer at - 80^{o}C until further processing. For genomic DNA (gDNA) extraction, the sludge pellet was transferred to a sterile mortar and crushed with a pestle. About 250-500 mg of the crushed sample material was then collected for DNA extraction and purification using a NucleoSpin kit (Macherey-Nagel) for gDNA from soil and sediment. The manufacture's protocol for DNA purification was followed with the following changes: 700 µL of SL1 lysis buffer without Enhancer SX was used in the first extraction step, a FastPrep instrument (MP Biomedicals) at 5.5. M/s for 60 s was used for cell lysis instead of a vortex, and 60 µL of SE buffer was used for final DNA elusion. The DNA in the final extract was quantified with a NanoDrop spectrophotometers (ThermoFisher Scientific) with scanning in the 220 to 350 nm wavelength range. All extracted samples showed high enough DNA concentrations with minimum contamination (see example in Fig. 3.8). In addition, an agarose gel (0.8% in 1x TAE buffer with RedSafe nuclic acid staining solution) was run to verify yield and DNA quality. Four µL of Invitrogen high DNA mass ladder (ThermoFisher Scientifc) was used for sizing and approximate quantification of double-stranded DNA in the range of 1,000 bp to 10,000 bp. The electrophoresis was run at 90 V and maximum Amp for 25 minutes. The obtained agarose gel showed minimum band smearing suggestion the RNA contamination was not a significant issue (Fig. 3.9). Individual gDNA samples from independent cultures were combined, based on equal mass, to produce a single composite gDNA sample for sequencing.

16S rDNA sequencing was done by Macrogen Oceania PL on an Illumina platform with Herculase II fusion DNA polymerase Nextera XT index V2 library kit and 16S Metagenomic Sequencing Library Preparation Part #15044223 Rev. B. The Illumina NGS workflow included 4 basic steps: (1) Sample preparation: quality control was run on the provided samples before proceeding to library construction. (2) Library construction: the sequencing library was prepared by random fragmentation of the DNA or cDNA sample, followed by 5' and 3' adapter ligation. Adapter-ligated

fragments were then PCR amplified and gel purified. PCR amplification was conducted with Bakt_341F (CCTACGGGNGGCWGCAG) and Bakt_805R (GACTACHVGGGTATCTAATCC) primers for Bacteria and 27F (TCCGGTTGATCCYGCCGG) and 516R (GGTDTTACCGCGGCKGCTG) primers for Archaea. (3) Sequencing: for cluster generation, the library was loaded into a flow cell where fragments were captured on a lawn of surface-bound oligos complementary to the library adapters. Each fragment was then amplified into distinct, clonal clusters through bridge amplification. When cluster generation was complete, the templates were ready for sequencing using Illumina platform. (4): Raw data: finally, sequencing data was converted into raw data for the operational taxonomic unit (OTU) analysis.

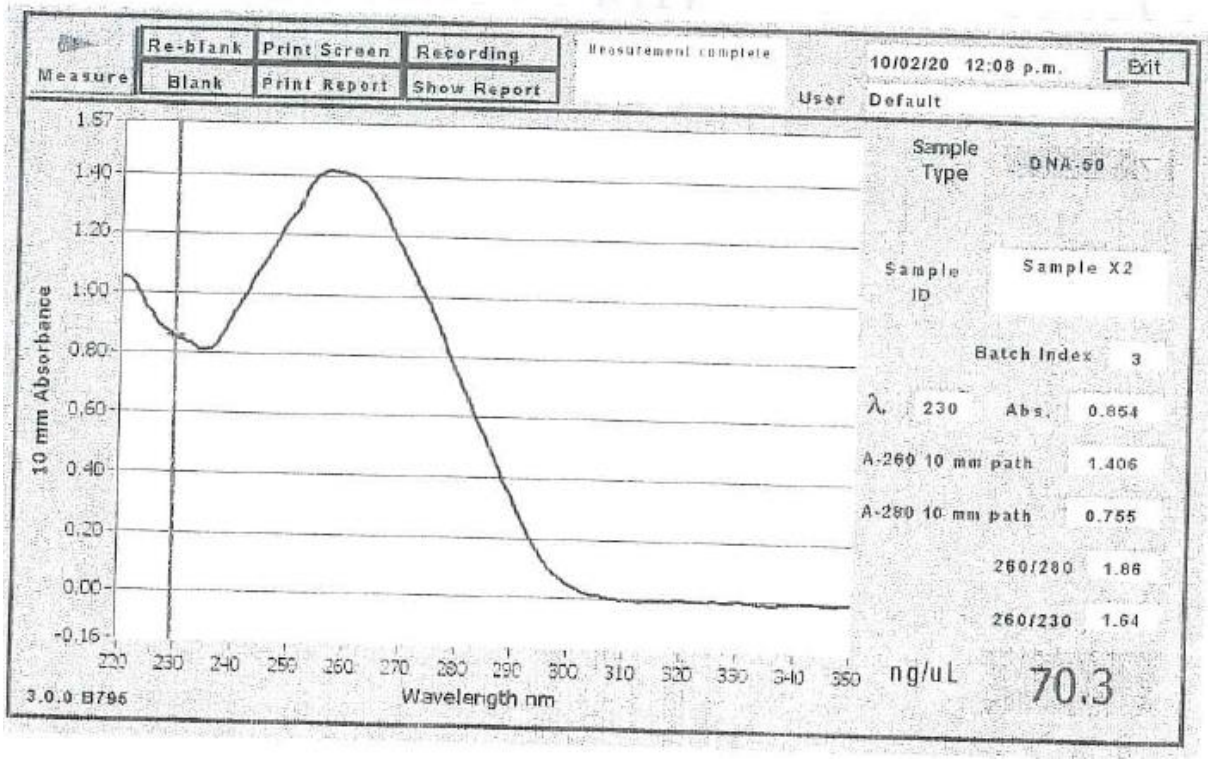

Figure 3.8. Example of a spectrogram showing the concentration of DNA in a sample at 260 nm wavelength. A good yield was obtained (70.3 ng/µL). The ratio A_{260}/A_{230} (1.64) was above the minimum acceptable value of 1.5 indicating a good level of DNA purity. Similarly, the ratio A_{260}/A_{280} (1.86) was within the expected range of 1.8 – 1.9 suggesting that protein and/or RNA contamination was not present. This was the case for most samples.

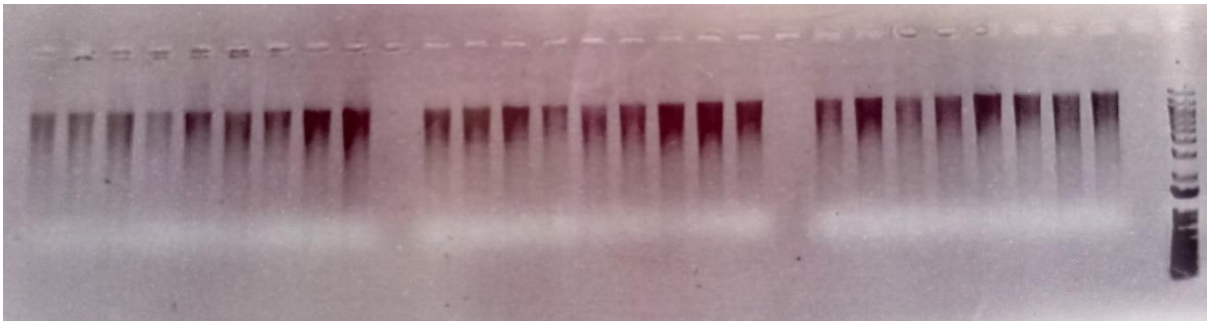

Figure 3.9. Agarose gel showing little band smearing that suggests good-quality DNA samples (i.e. low RNA contamination).

3.3.8 Estimation of Methane Production Kinetic Parameters

The cumulative methane volume produced from the experiment was plotted as a function of time and then the modified Gompertz model (Eq.1) was fitted to the experimental data using SPSS software. This allowed the estimation of the lag phase time (λ, d) and the maximum methane production rate (R, mmole/g VS/d).

$$M_p = CMP * EXP\left(-EXP\left(\frac{R * (\lambda - t) * 2.7183}{CMP} + 1\right)\right) \quad \ldots\ldots\ldots\ldots\ldots\ldots\ldots\ldots\ldots\ldots\ldots\ldots\ldots\ldots Eq.1$$

Where Mp is the predicted methane production (mmole/g VS), CMP is the cumulative methane at the end of incubation (mmole/g VS) and t is the time of methane production (Nielfa et al., 2015). The steps of evaluation of the experimental cumulative methane production and the theoretical values obtained by the simulation of the modified Gompertz model are shown in Appendix E.

Figure 3.10 shows an example of experimental cumulative methane production and the modeled methane value obtained with the modified Gompertz model. It seems that the obtained results from the modified Gompertz fitted adequately the experimental results (confidence intervals (R^2) of 99 %). The coefficient of determination (R^2) is a guideline to evaluate the accuracy of the model and how well it predicts future outcomes. The closer the value of R^2 is to 1, the better the non-linear regression fits the data.

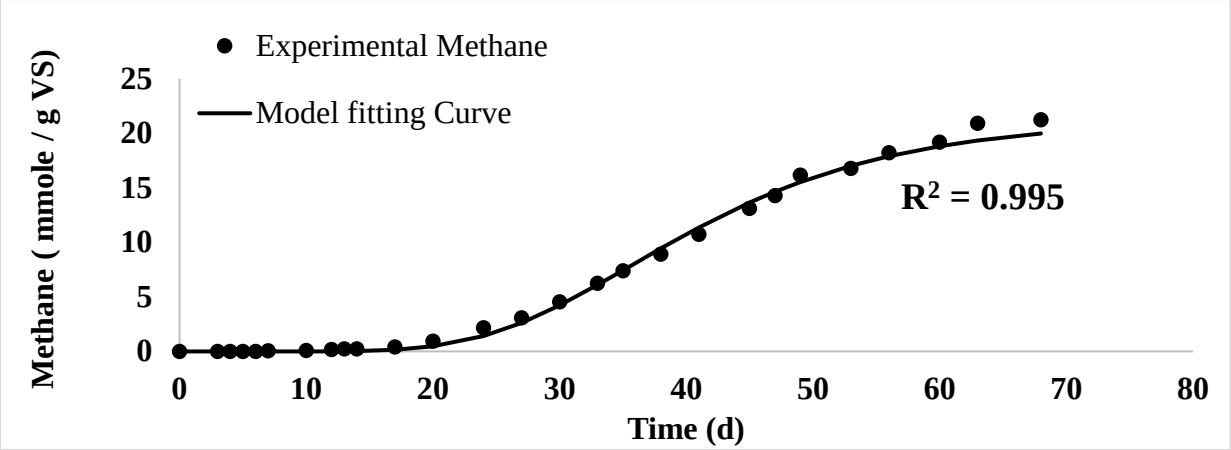

Figure 3.10. Evolution of experimental and predicted methane production by modified Gompertz model.

3.3.9 Statistical analysis of Data

The effect of magnetite nanoparticles on methane production with different supplement conditions (in terms of repeated measurements of lag phase, maximum methane production, cumulative methane production, and methane yield) was evaluated using general linear model (GLM) procedure of SAS (2015). Significance was given when $P < 0.05$, and significant differences between means were separated by the Least Significant Difference (LSD).

Furthermore, the standard error was calculated (i.e. the approximate standard deviation of a statistical sample population). The standard error is a statistical term that measures the accuracy with which a sample represents a population. In statistics, a sample mean deviates from the actual mean of a population; this deviation is the standard error. Standard deviation (SD) and the standard error (SE) are calculated by the following equations

$\left(SD = \sqrt{\frac{\sum_{i=1}^{N}(X_i - \overline{X})^2}{N-1}}\right)$ and $\left(SE = \frac{SD}{\sqrt{N}}\right)$, where N is the number of observation, X_i is each of the values of the data, $\overline{X}$ is the mean of X_i.

CHAPTER 4. EXPLORING THE EFFECT OF MAGNETITE NANOPARTICLES ON METHANE PRODUCTION

To explore the conditions that enhance methane production in magnetite-supplemented anaerobic digestion, batch tests were carried out using different types and concentrations of magnetite nanoparticles, different types and concentrations of substrate, and fresh and degassed biomass culture. The experimental conditions evaluated are summarized as follows:

1. **Run (1): Batch test calibration**

Experiments were conducted using acetate as a substrate to examine the stability of an anaerobic batch bottle, as well as to identify suitable concentrations of VS and sufficient COD:VS ratios. Blanks (with no acetate) were run using digested sludge as well as activated sludge under different ranges of VS (0.2, 0.5 and 1.5 g/L). Control bottles had acetate at COD:VS ratios of 2:1, 3:1 and 4.5:1. Table 4.1 shows the details of the treatment conditions.

2. **Run (2)**: **Effect of magnetite dose on methane production from acetate-cultivated cultures**

Experiments were conducted to study the effect of adding commercial magnetite nanoparticles with different concentrations (i.e. 5, 10, 15, 20, 30, or 40 mmole/L) on methane production from acetate that was added at a COD:VS ratio of 2:1. This was done to verify that (i) the experimental methods were reliable and (ii) to identify a suitable range of magnetite concentration for further tests.

3. **Run (3)**: **Effect of magnetite type on methane production from propionate-cultivated cultures**

Experiments were conducted using magnetite nanoparticles at a concentration of 20 mM to evaluate the effect of magnetite type on methane production from propionate-cultivated cultures. Two magnetite nanopowders (one commercial and one prepared via the hydrothermal method) were tested. Propionate was loaded into the bottles corresponding to a final COD:VS ratio of 2:1.

4. **Run (4): Effect of magnetite dose on methane production from propionate-cultivated cultures**

Magnetite prepared via the hydrothermal method was tested with different concentrations (i.e. 0.07, 0.7, or 7 mmole/L) using propionate as a substrate to assess the effect of magnetite dose on methane production from propionate-cultivated cultures. After methane production reached a plateau, all bottles were flushed with nitrogen gas (in order to remove the methane gas) and then re-fed with propionate.

5. **Run (5)**: **Effect of using magnetite as suspension on methane production**

In the previous runs (run 2, run 3, and run 4), magnetite was supplemented as a nanopowder. In Run 5 however magnetite was supplemented as suspension under different concentrations (7, 12.5, or 20 mM) to investigate the effect of using magnetite as suspension on methane production, as compared to using it as nanopowder. The propionate was loaded into the bottles corresponding to a final COD:VS ratio of 2:1

4.1 Run (1): Batch Test Calibration

Seed sludge was collected and characterized as described previously (Sections 3.2.1 and 3.3.2). After measuring the VS of the seed sludge and calculating the COD equivalent of acetate (Appendix F), the activity and stability of seed digested sludge to produce methane under anaerobic condition was examined following the methodology presented by Angelidaki and Sanders (2004) and Hussain and Dubey (2017). Three experimental groups were conducted to confirm the activity of methanogens (experiment 1) to minimize the organic load of inoculum as much as possible (experiment 2), and establish the maximum appropriate anaerobic sludge loading (VS) and inoculum to substrate ratio (experiment 3). The details are shown in Table 4.1. Blank and control bottles were carried out as mentioned previously in Section 3.2.5. Upon preparation, all bottles had nitrogen gas bubbled in to purge oxygen before being sealed with rubber stoppers of an appropriate size (held in place with an aluminum crimp). The batch bottle's headspace was

continuously monitored and any biogas generated was periodically sampled for analysis. All experiments were carried out in triplicate. The initial pH throughout all experiments was measured to be 7 -8.

Table 4.1. Run (1): The details of batch test calibration under various conditions.

Experiment purpose	Experimental run	Experimental condition	Experimental group	Number of bottles
Biomass activity	Experiment (1)	Different sludge types (Digested vs Activated)	Blank	3 for each sludge type
Minimum allowable VS concentration	Experiment (2)	Variable rang of VS (0.2, 0.5 and 1.5 g/L)	Blank	3 for each VS Concentration
Appropriate COD:VS ratio	Experiment (3)	Different COD:VS of acetate ratios (2:1, 3:1 and 4.5:1)	Control	3 for each COD:VS concentration

In experiment (1), the biomass activity was examined for both digested sludge and activated sludge. Blank bottles were run with no substrate and with volatile solid concentration of 1.5 g/L. Figure 4.1 shows the results from experiment (1) which confirmed that the digested sludge had efficient, viable, and active methanogens to produce methane with the methane production (mmole/g VS) over the period of incubation for digested sludge around three times higher than that at the activated sludge.

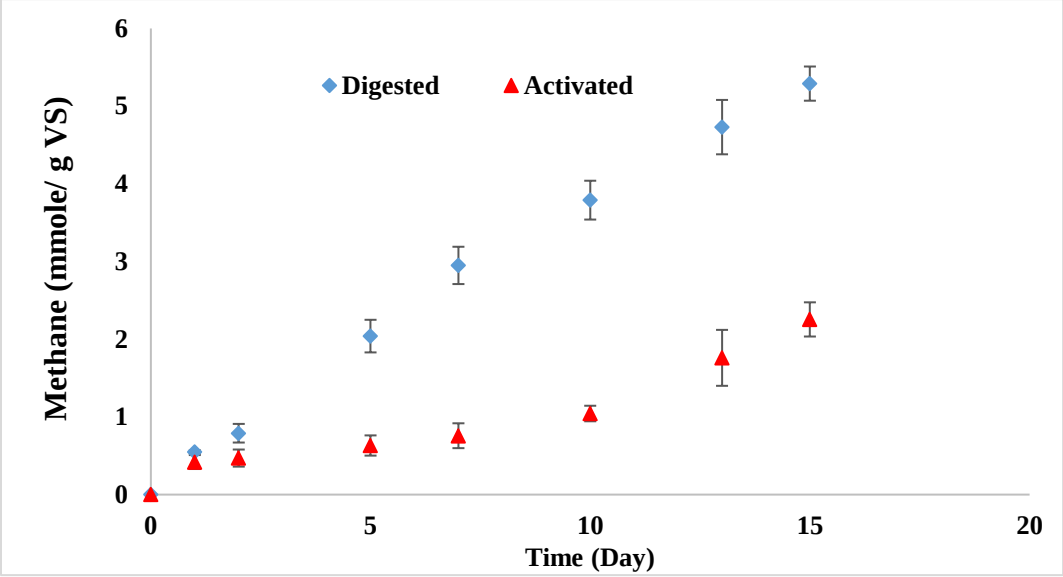

Figure 4.1. Time course of methane production testing digested and activated sludge inocula. Error bars represent the standard deviation of triplicate experiments.

In experiment (2), blank bottles were run in order to determine the minimum allowable VS concentration. Variable volatile solids concentrations of mesophilic-digested sludge of 0.2, 0.5 and 1.5 g/L were tested (Figure 4.2).

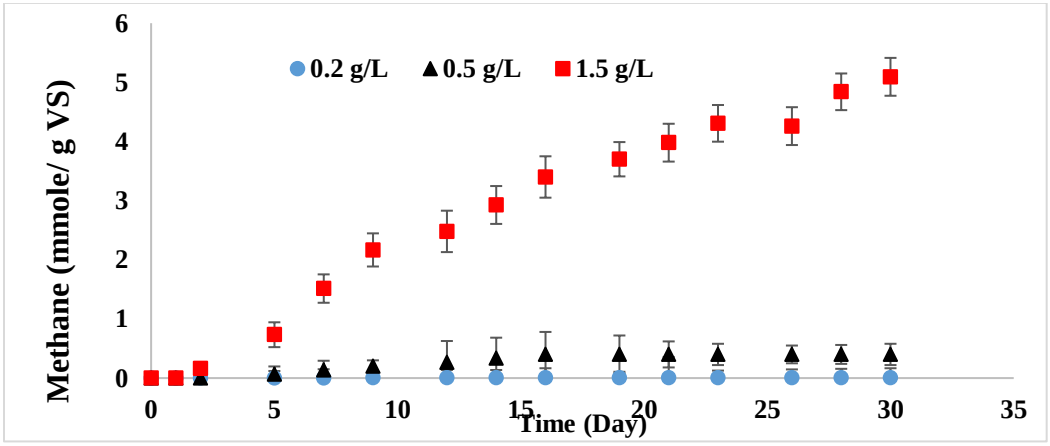

Figure 4.2. Time course of methane production testing different VS concentrations. Error bars represent the standard deviation of triplicate experiments.

The results of experiment (2) showed that the better concentration (VS) of mesophilic sludge was 1.5 g/L.

In experiment (3), batch bottles determined the appropriate COD:VS ratio that produced the maximum methane rate. The final concentration of VS was 1.5 g/L in all control bottles. All bottles were independently spiked with final concentrations of 3, 4.5, and 6.8 g/L of acetate to achieve COD:VS ratio of 2:1, 3:1 or 4.5:1 respectively (Figure 4.3).

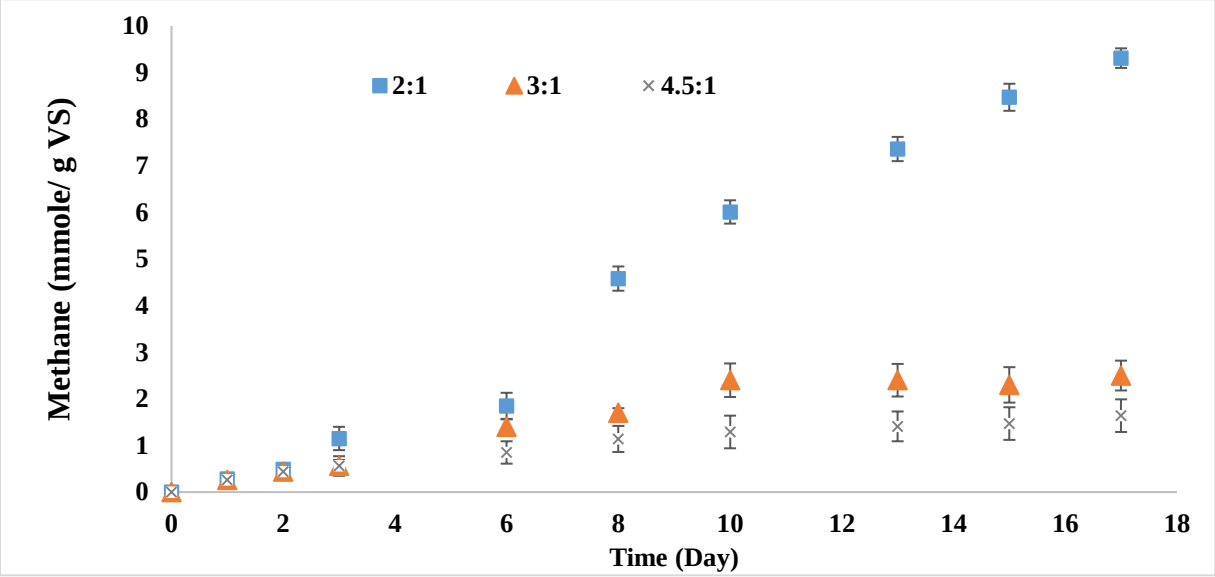

Figure 4.3. Time course of methane production testing different COD:VS ratios of 2:1, 3:1 and 4.5:1. Error bars represent the standard deviation of triplicate experiments.

The results from experiment (3) showed that the appropriate amount of inoculum and substrate to achieve the maximum production of biogas was 2:1.

4.2 Run (2): Effect of Magnetite Nanoparticles Concentration on Methane Production from Acetate-Cultivated/Supplemented Cultures

An experiment was conducted to explore the effect of MNP on methane production. Commercial MNP were purchased from sigma Aldrich with 50-100 nm particle size and 97 % trace metals. Batch experiments were carried out as described in Section 3.2.5. The inoculum (i.e. 1.5 g/L of VS) and substrate (i.e. 1.5 g/L of acetate) were loaded into the control bottles corresponding to a final COD:VS of 2:1. Commercial MNP were introduced into the treatment bottles with different concentrations (i.e. 5, 10, 15, 20, 30, and 40 mmole/L) in addition to 1.5 g/L of VS and 1.5 g/L of acetate. Finally, all bottles were flushed with nitrogen and closed with rubber stoppers. After the cumulative methane production curve reached a plateau, a fresh dose of acetate was added (1.5 g/L) in both the control and magnetite-amended bottles to achieve the same working volume (i.e. 120 mL). Table 4.2 summarizes the details of each experimental treatment. Each treatment was performed in triplicate.

Table 4.2. Run (2): The details of each treatment group exploring the effect of commercial MNP on methane production.

Experimental group	Substrate		Magnetite		Number of bottles
	Type	Dose; g/L	Type	Dose; mmole/L	
Control	Acetate	1.5	------	------	3
Supplemented	Acetate	1.5	Commercial	5	3
				10	3
				15	3
				20	3
				30	3
				40	3

All results of methane production over the incubation period are presented as mmole CH_4/g VS vs time as shown in Figure 4.4. No observable enhancement in the methane rate was observed by adding the magnetite nanoparticles over two feeding cycles (Figure 4.4 – a, and b). However, over the second feeding cycle; magnetite-supplemented bottles of 20 mM produced more methane from day 1 to day 8, as compared to the other bottles. After that, all bottles produced the same amount of methane which indicates that magnetite had some ability to enhance the methane production. However, further investigations were still needed using different substrate and/ or magnetite type to determine the full scope of adding magnetite.

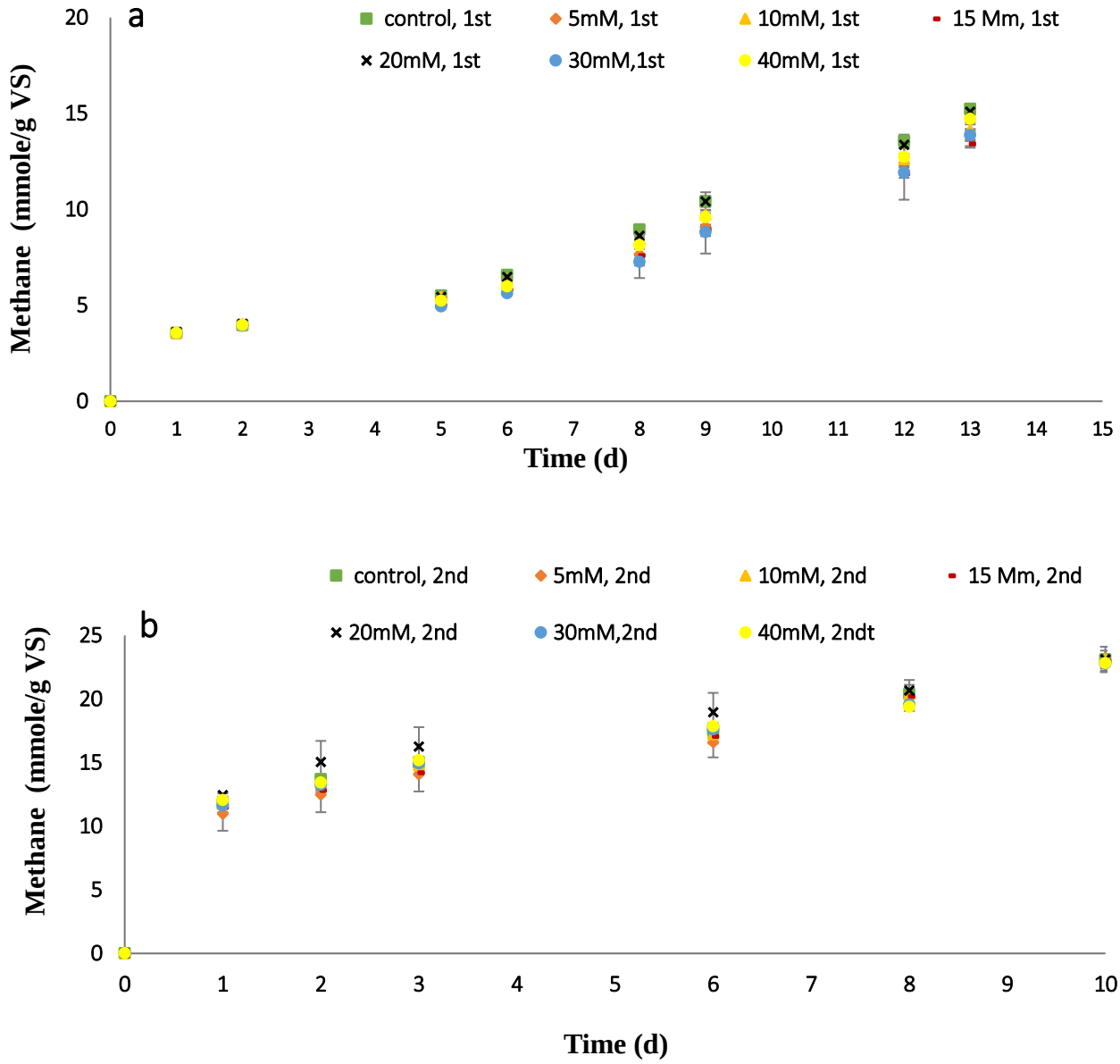

Figure 4.4. Average methane produced in commercial magnetite-amended bottles and control bottles in two feeding cycles of acetate (1.5 g/L). (a) Average methane produced in magnetite-amended bottles vs controls in first feeding cycle of acetate. (b) Average methane produced in magnetite amended- bottles vs controls in second feeding cycle of acetate. Error bars represent the standard deviation of triplicate experiments.

4.3 Run (3): Effect of Magnetite Types on Methane Production from Propionate-Cultivated Cultures

In order to find appropriate conditions for adding magnetite, propionate was used instead of acetate as a substrate and two types of magnetite were investigated. The first type of nanoparticles was commercial magnetite purchased from Sigma Aldrich (50-100 nm particle size, 97 % trace metals). The second type was dried nanopowders prepared in the lab via the hydrothermal method described previously (Section 3.2.3). Anaerobic serum bottles were incubated as discussed previously in Section 3.2.5. The inoculum (1.5 g/L) and 2 g/L of propionate were added to the bottles corresponding to a final COD:VS ratio of 2:1. Twenty mmole/L of magnetite nanopowder was then introduced into the treatment bottles as shown in Table 4.3. Two feeding cycles were done for all treatments except the blank bottles, while the third feeding cycle was done for the control and hydrothermal MNP-amended bottles.

Table 4.3. Run (3): The details of each treatment group exploring the effect of the commercial and hydrothermal magnetite on methane production.

Experimental group	Substrate		Magnetite		Number of bottles
	Type	Dose; g/L	Type	Dose; mmole/L	
Control	Propionate	2	------	------	3
Supplemented	Propionate	2	Commercial	20	3
			Hydrothermal	20	3

The two types of magnetite produced different responses in term of methane production but the effect also depended on the stage in the feeding cycle. That is to say, on whether methane evolved from the first, second or third feeding (Fig 4.5). During the first feeding cycle (the first 20 days in Fig 4.5), the methane production in the control bottles was higher than that of the magnetite-amended bottles regardless of the type of particles. However, during the second and the third

feeding cycles, the presence of magnetite nanoparticles prepared via the hydrothermal method slightly enhanced the methane production, as compared to the control bottles. This suggest that an acclimation period is necessary for the microorganisms to respond to magnetite amendment. Conversely, the commercial magnetite nanopowder did not improve the methane production during the first and the second feeding cycles. As such, the third feeding cycle was not carried out. The variation in methane production between the two types of magnetite may be attributed to the variation in magnetite properties such as particle size distribution.

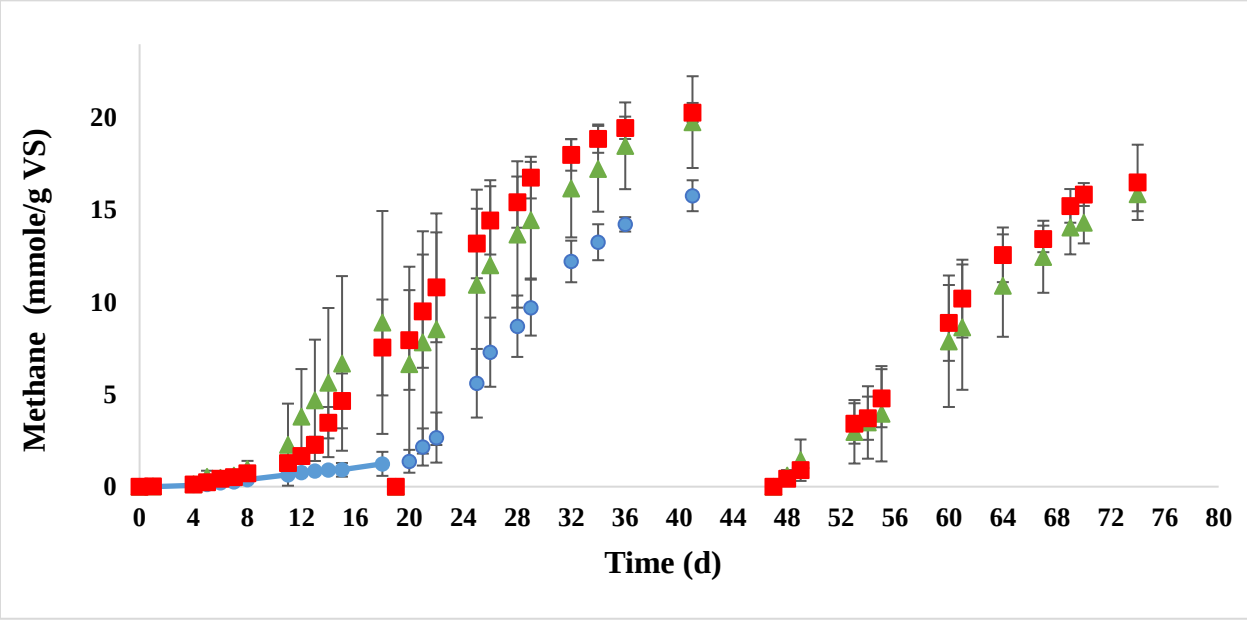

Figure 4.5. Average methane production (mmole/g VS). The symbols ▲, ■, and ● represent the control, 20 mM of hydrothermal magnetite and 20 mM of commercial magnetite respectively in three feeding cycles of propionate (2 g/L). The second feeding cycle of propionate started at day 19 and the third feeding cycle started at day 47. Error bars represent the standard deviation of triplicate experiments.

4.4 Run (4): Effect of Magnetite Doses on Methane Production from Propionate-Cultivated Culture

The results of the previous run (Run 3) indicated that adding 20 mM of hydrothermal magnetite enhanced the methane production from propionate. As such, this run was further investigated to find the effect of adding 7, 0.7 and 0.07 mmole/L of hydrothermal magnetite (i.e. prepared as described in Section 3.2.3) on methane production from 2 g/L of propionate corresponding to a final COD:VS of 2:1 (Table 4.4). After the produced methane reached a plateau in the controls and magnetite amended-bottles, they were flushed with nitrogen gas in order to remove the methane gas and then re-fed (replaced) with a fresh dose of propionate to yield the same working volume (i.e. 120 mL).

Table 4.4. Run (4): The details of each treatment group exploring the effect of different magnetite nanopowders on methane production.

Experimental group	Substrate		Magnetite		Number of bottles
	Type	Dose; g/L	Type	Dose; mmole/L	
Control	Propionate	2	------	------	3
Supplemented	Propionate	2	Hydrothermal	0.07	3
				0.7	3
				7	3

All results are shown in Figure 4.6. During the first 20 days of incubation, the production of methane was similar in all bottles. However, by day 27, the maximum production of methane in the 7 mM-supplemented bottles (8 mmole/g VS) was twice that of the control, 0.7 mM-supplemented and 0.07 mM- supplemented bottles (4 mmole/g VS) Moreover, methane production reached 17 mmole/g in 7 mM magnetite and control bottles at day 45. All bottles produced a similar amount of methane during the second feeding cycle (day 46 to day 60). These results indicate that one feeding cycle is enough to study the effect of magnetite on methane production. In addition, adding 7 mM of medium size range of magnetite is a suitable concentration that enhances the

methane production. On the other hand, Baek et al. (2016) studied the effect of magnetite supplementation in continuous anaerobic digestion of dairy effluent over 250 days. They found that the applied magnetite recycling method effectively supported enhanced DIET activity and biomethanation performance over a long period (>250 days) without adding extra magnetite.

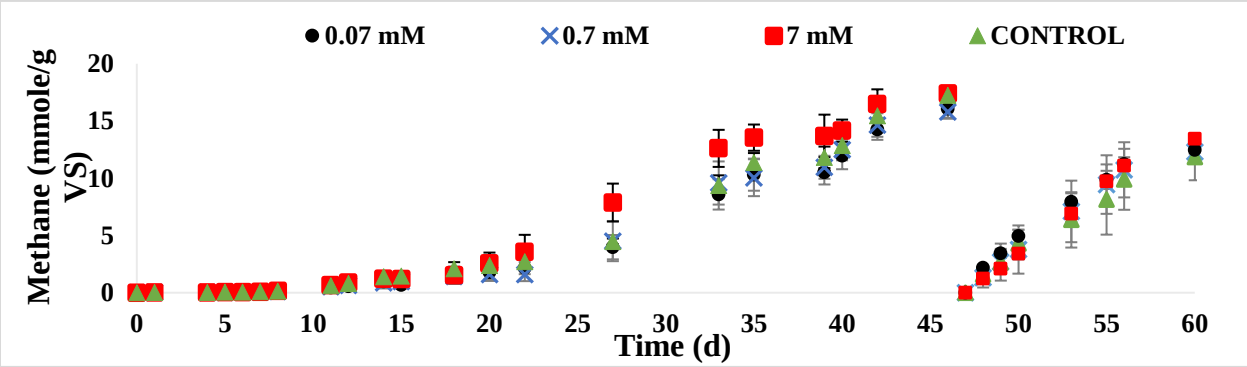

Figure 4.6. Average methane production (mmole/g VS) in two feeding cycles of propionate (2 g/L). The symbols ■, x, ●, and ▲ represent the average methane production in 7, 0.7 and 0.07 mM of magnetite amended- bottles and control bottles respectively. Error bars represent the standard deviation of triplicate experiments.

4.5 Run (5): Effect of Using Magnetite as Suspension on Methane Production

Magnetite was added as powders through all the previous runs (Run 2, 3 and 4). Therefore, an experiment was conducted to explore the effect of using magnetite as a suspension (stock solution) on methane production (Table 4.5). The magnetite suspension was prepared as described by Wang et al. (2016). The MNP black precipitate formed via the hydrothermal method was suspended in deoxygenated water (30 min nitrogen gas bubbling) via ultra-sonication for 1 h at 40 kHz and 250W. This suspension was then added to the bottles by weight to reach specific final concentrations of 7, 12.5 and 20 mM, respectively. Anaerobic serum bottles using propionate as a substrate, with a final concentration of 2 g/L corresponding to a final COD:VS ratio of 2:1 were used. After the methane produced reached a plateau in the controls and magnetite-supplemented bottles, they were then re-fed (replaced) with a fresh dose of the substrate to achieve the same working volume (i.e. 120 mL). The results from Run 5 (Figure 4.7) show that methane production in two feeding cycles was similar in all bottles. These results indicate that using a suspension of

magnetite did not show a substantial difference compared to the nanopowders supplement; therefore, it was not investigated further.

Table 4.5. Run (5): The details of each treatment group exploring the effect of different magnetite doses on methane production. Magnetite was used as a suspension.

Experimental group	Substrate		Magnetite		Number of bottles
	Type	Dose; g/L	Type	Dose; mmole/L	
Control	Propionate	2	------	------	3
Supplemented	Propionate	2	Hydrothermal	7	3
				12.5	3
				20	3

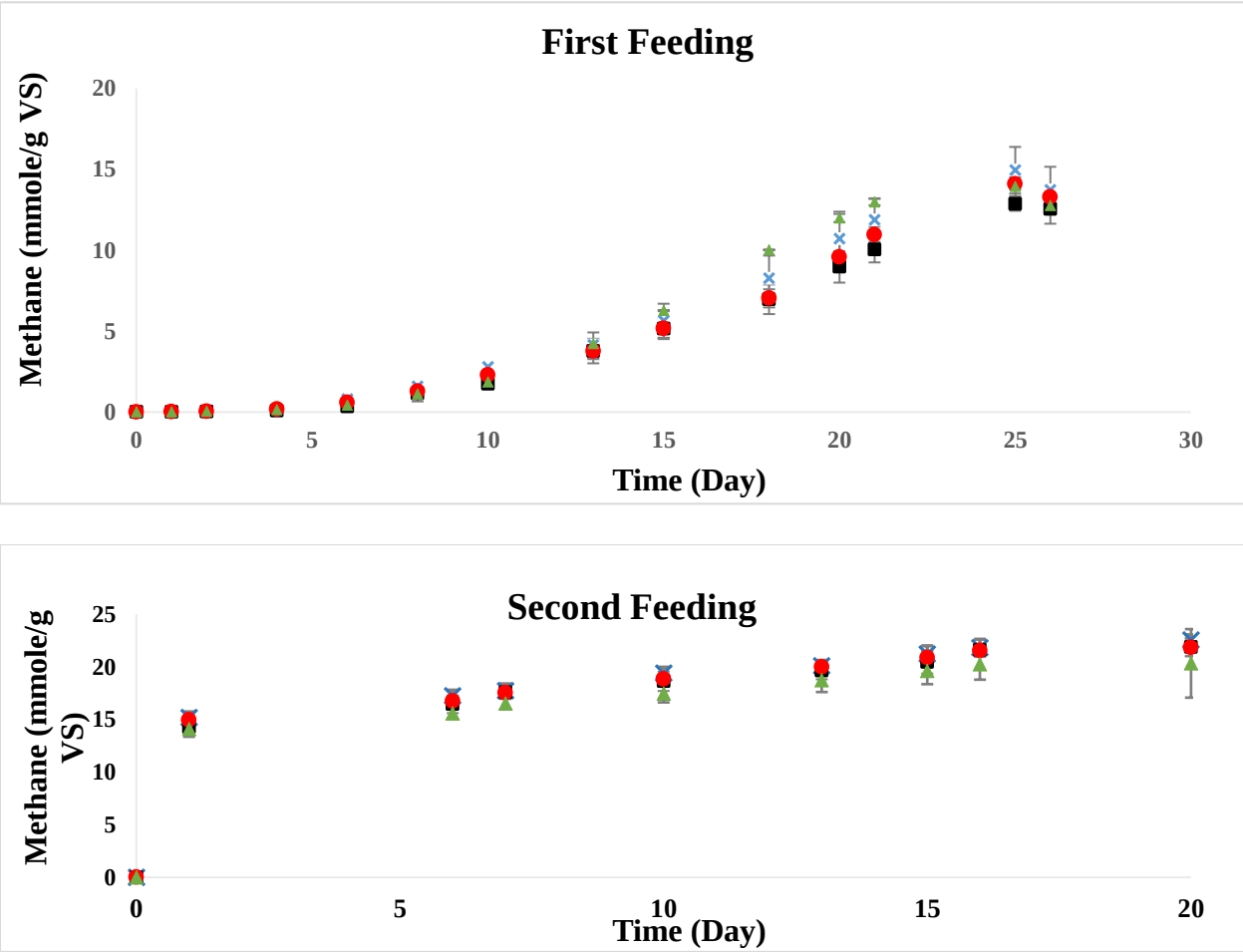

Figure 4.7. Average methane production as mmole/g VS in two feeding cycles of propionate (2 g/L). The symbols ●, ■, x and ▲ represent the methane production in the 7 mM, 12.5 mM, 20 mM and control respectively. Error bars represent the standard deviation of triplicate experiments.

4.6 Summary of Preliminary Experiments

The previous set of experiments investigated magnetite under conditions that enhanced and/or inhibited methane production. The results confirm the ability of the anaerobic batch system to produce methane from digested sludge at a level three times as compared to activated sludge. In addition, the minimum allowable concentration (VS) of mesophilic sludge was 1.5 g/L with the appropriate COD:VS ratio of 2:1.

The preliminarily experiments confirm a positive effect of adding magnetite nanopowder on methane production from acetate and propionate right from the first feeding cycle, therefore, obviating the need to test further. Magnetite nanopowder of medium size at concentrations of 7 and 20 mM showed a positive effect on methane production; however, using magnetite as a suspension did not show any difference compared to nanopowder, therefore, further investigation into suspended nanoparticles was abandoned. The standard deviation for some of the treatments was relatively high and only decreased with repeating experiments. This may be attributed to the sample size and standardization of the preparation procedures. The size and the concentration of magnetite seems to have an effect on methane production. These results also indicate that the stimulatory effect of MNP on methane production could be dependent on the substrate type and concentration.

CHAPTER 5. THE EFFECT OF MAGNETITE SIZE AND CONCENTRATION ON METHANE PRODUCTION FROM FRESH AND DEGASSED ANAEROBIC SLUDGE

5.1 Objectives and Experimental Setup

The first objective was to identify what sort of inoculum (fresh or degassed) is the best for assessing the effect of magnetite on methane production. To achieve this objective, batch experiments were conducted (as described in Section 3.2.5) using digested sludge with biomass at two different growth phases. The inoculum used was fresh mesophilic digested sludge (i.e. sludge with microbial community ongoing exponential growth phase) and degassed mesophilic-digested sludge, left to age for one month at 36 ± 1^{o}C (i.e. sludge with microbial community with low activity at the stationary or death stage). The second objective of this chapter was to study the effect of both size and concentration on methane production. To this end, the magnetite concentrations used are 2 and 7 Mm based on previous results (i.e. preliminary experiments) and research (Barua and Dhar, 2017). Batch assays using small (50 to 150 nm), medium (168 to 490 nm) and large-size (800 nm to 4.5 µm) magnetite particles were conducted to assess the effect of particle size on methane production.

Figure 5.1 shows a schematic representation of the experimental design to assess methane production in anaerobic batch treatment bottles. Propionate (27 mM) was used as a substrate except in blank bottles. No magnetite was added into the control and blank bottles. Data was presented as mean ± standard deviations of triplicates. As the experiment had two levels of magnetite concentrations (2 and 7 mM) and three levels of magnetite size (small, medium and large), plus one control group (Figure 5.1), the data was statistically analyzed using a Factorial + control model (augmented factorial design), with SAS 2015 software (Marini, 2003). The experimental data was analyzed by two-way ANOVA (SAS, 2015) with a factorial orthogonal contrast arrangement of treatments (two levels of magnetite concentrations × three levels of magnetite size plus control treatment). These contrasts were formed in order to compare the main effects of adding magnetite

(control vs. magnetite addition), magnetite concentration (2 vs. 7 mM) and magnetite size (small vs. medium, medium vs. high, small vs. high).

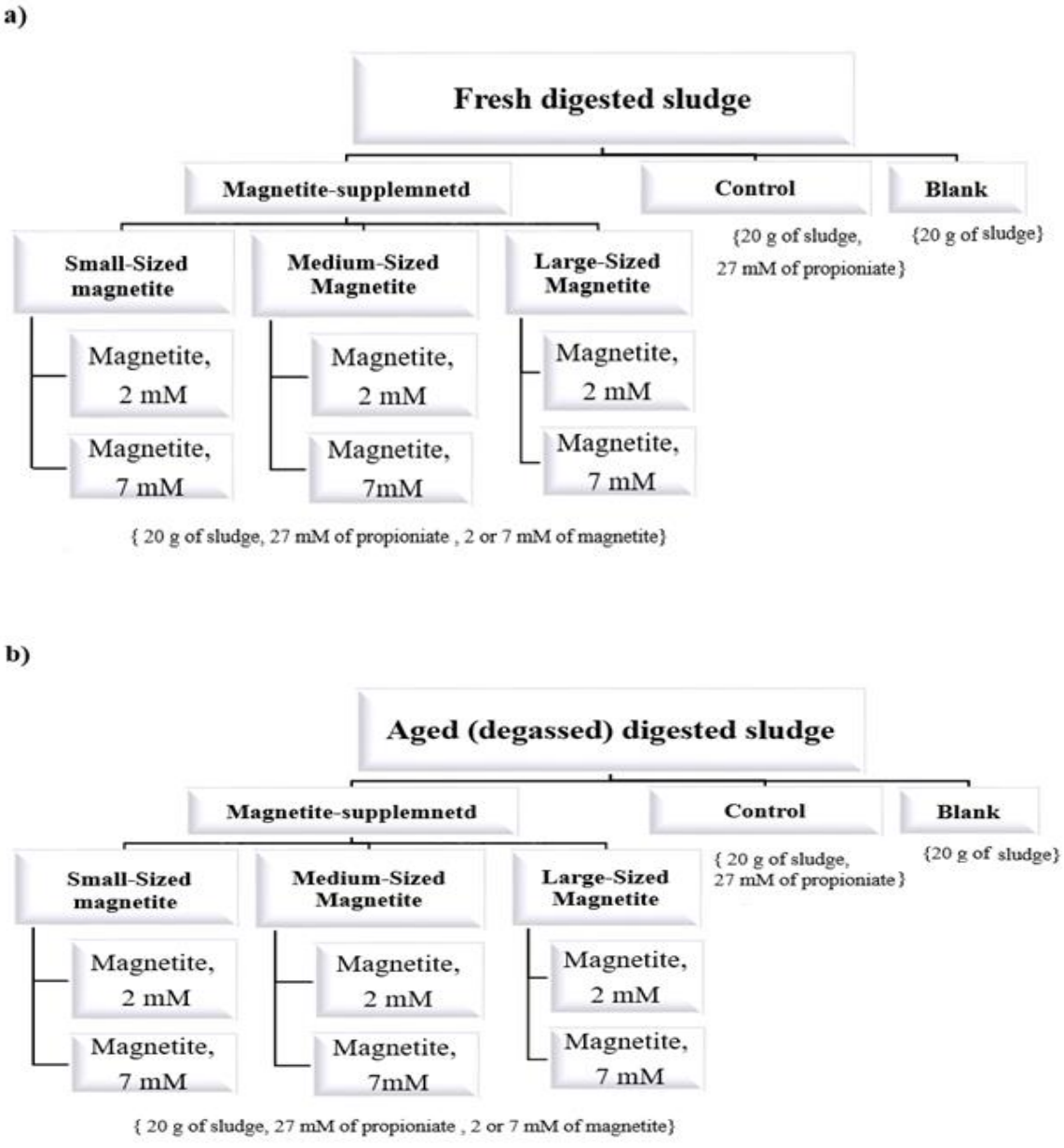

Figure 5.1. Schematic representation of experimental setup to assess methane production in anaerobic batch treatment bottles.

The third objective was to study the effect of magnetite on methane production under substrate-limited condition. For this, an additional batch experiment was run consisting of (1) blank bottles with no magnetite and no propionate, (2) blank bottles with 7 mM of magnetite and no substrate, (3) control bottles with 27 mM of propionate and no magnetite, and (4) magnetite-supplemented bottles with both 27 mM of propionate and 7 mM of medium magnetite. As the experiment had two levels of propionate (0 and 27 mM) and two levels of magnetite concentrations (0 and 7 mM), the data were evaluated in a 2 × 2 factorial arrangement treatments through statistical analysis of two-way of variance (ANOVA) using general linear model (GLM) procedure of SAS (2015).

Finally, in order to investigate the possibility of using magnetite as a nutrient (source of iron), the ferrous ion concentration was measured. For this purpose, a set of batch experiments were conducted with the liquid medium of both the control and the medium-size 2 mM of magnetite-supplemented bottles being analyzed every 5 days during the incubation. The ferrous ion was determined using a spectrophotometer.

5.2 Results and Discussion

5.2.1 Methane Production from Fresh Sludge and Degassed Sludge

The methane production (mmole/g VS) from fresh digested sludge was analyzed throughout 35 days of incubation with the most active period occurring between day 4 and day 20 (Figure 5.2 (a-c)) before a plateau was reached. For degassed digested sludge, the methane production was analyzed for 68 days with the most active time being between day 25 and day 50 (Figure 5.2 (d-f)) before its corresponding plateau was reached at approximately day 60.

As mentioned previously, blank bottles were used to examine the sludge's baseline (or endogenous) activity without any substrate or magnetite. Figure 5.2 indicates that the maximum methane production in the blank bottles was 3.4 mmole/g VS in the case of the fresh sludge (Fig 5.2 (a-c)) and 2 mmole/g VS in the case of the degassed sludge (Fig 5.2 (d-f)). This shows that the digested sludge had viable, active methanogens that produced methane regardless of whether the

sludge was fresh or degassed. However, the blank bottles produced a very low amount of methane and therefore they were neglected.

Figure 5.2 also shows that the maximum methane production in the control bottles (substrate but no magnetite) was around 20.56 ± 0.96 mmole/g VS (Fig 5.2 (a-c)) and 18.79 ± 0.23 mmole/g VS (Fig 5.2 (d-f)) in the fresh and degassed sludge, respectively. Figure 5.2 indicates that, in general, the substrate concentration (i.e. 27 mM of propionate) was a suitable amount of food for methanogens to produce methane from fresh and degassed digested sludge. Figure 5.2 also clearly shows that adding magnetite particle resulted in accelerated methane production (i.e. effectively reducing the incubation period). This could have implications on anaerobic digester size. The use of fresh sludge with different MNP concentrations (2 and 7 mmole/L), resulted in similar maximum methane production across all particle sizes (20.24 ± 0.06 mmole/g VS).

On the other hand, the methane production from degassed sludge was similar in the beginning but over the length of the experiment, the maximum methane production was slightly lower in all 7 mM supplemented bottles, with the most difference occurring in the large particle size bottles (which had only 16.24 mmole/g VS), as compared to the other magnetite-supplemented bottles at 20.38 mmole/g VS. In this latter case, the amount of methane was even less than the control bottle which was at 18.8 mmole/g VS.

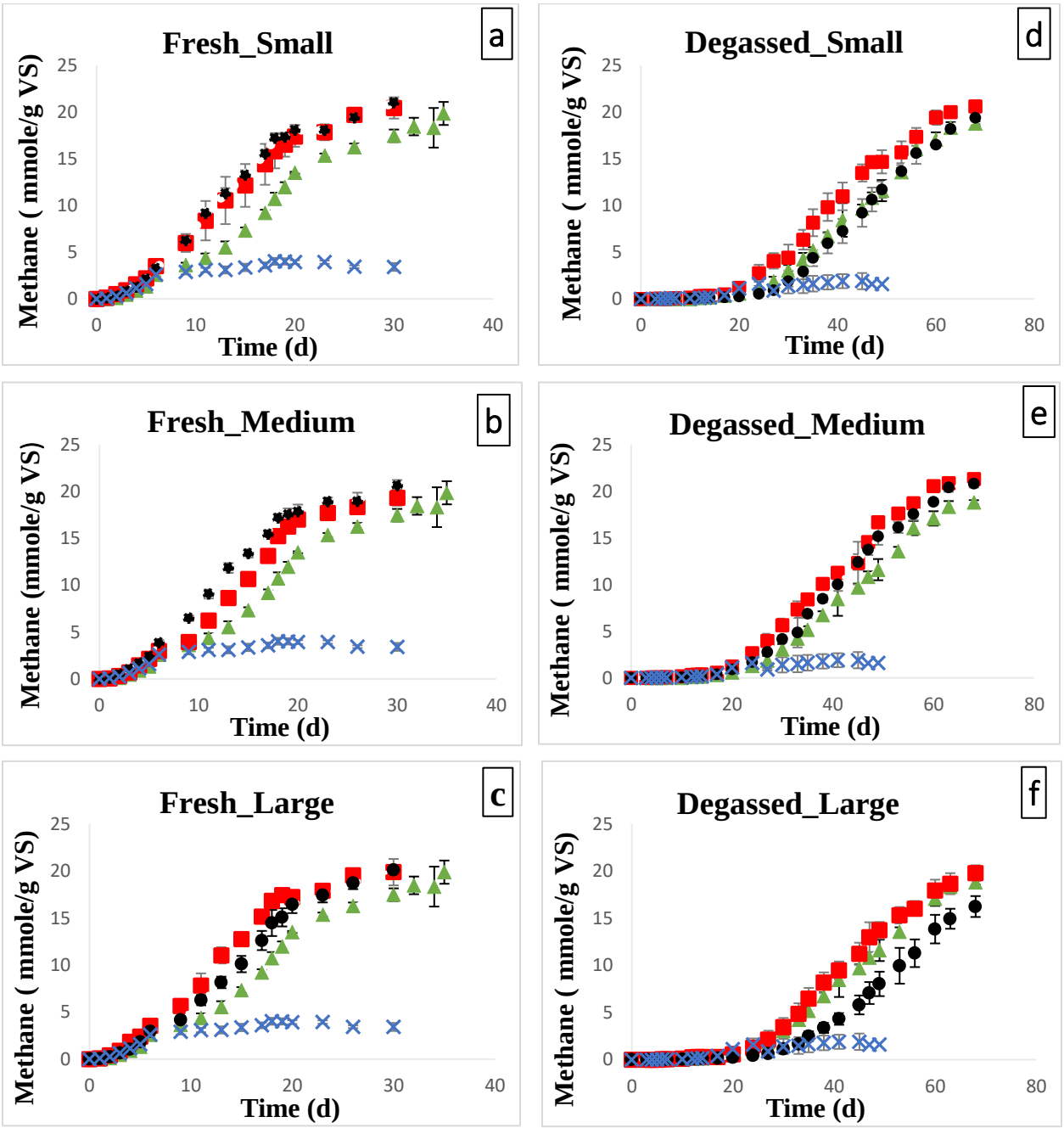

Figure 5.2. Methane production as a function of incubation time. The Figures a, b and c represent the methane production as a result of the effect of small, medium and large-sized magnetite on fresh sludge. Figures d, e and f represent the methane production as a result of the effect of small, medium and large-sized magnetite on degassed sludge. The symbols ▲, ■, ●, and x represent the control, 2 mM of magnetite, 7 mM of magnetite, and blank respectively. Error bars represent the standard deviation of triplicate experiments.

5.2.2 Effect of Magnetite on Methane Production Kinetic Parameters

Table 5.1 and Table 5.2 show the kinetic parameters for methane production from fresh and degassed digested sludge. The coefficient of determination (R^2) was discussed in Section 3.3.7.

The results of Table 5.1 indicate that magnetite significantly enhanced the methane production rate and reduced the lag phase as compared to the control. In particular, the addition of magnetite into fresh sludge results in an increase in methane production rate (by 32 %) as compared to the control ($P < 0.05$). The lag phase time in all the magnetite-supplemented bottles was on average 1 - 3 days (15 % - 41 %) shorter than that in the control bottles.

On the other hand, adding two different concentration of magnetite (2 and 7 mM) did not produce any significant difference in methane production rate and lag phase. Similarly, adding three magnetite size ranges (small, medium and large) did not significantly change the methane production rate and lag phase; however, the only exception, was large magnetite particles, which significantly extended the lag phase as compared to the small magnetite particles (contrast p – value = 0.022; < 0.05). In addition, it seems that the effect of the concentration of magnetite did not relate to the size of magnetite as the contrast P-value of the interaction was greater than 0.05. However, the only significant interaction between the concentration of magnetite and the size of magnetite was found for the lag phase (contrast P-value =0.022). These results indicate that the effect of magnetite on the reduction of the lag phase depends on an interrelationship between size and concentration.

Table 5.1. Influence of magnetite concentration and size on methane production kinetic parameters from fresh sludge

Item			Methane Parameters				
Magnetite Concertation (mM)	**Magnetite Size**	**N**	**Rate (mmole/g VS/d)**	**Lag (day)**	**CMP (mL CH_4)**	**Yield**	**R^2**
Control	Non	3	0.98 ± 0.04^b	6.48 ± 0.7^a	72.75 ± 3.38	1.14	0.97
2 mM	Small	3	1.30 ± 0.18^a	4.32 ± 0.7^c	73.35 ± 3.34	1.14	0.99
	Medium	3	1.28 ± 0.05^a	5.56 ± 0.4^b	69.33 ± 1.48	1.08	0.98
	Large	3	1.33 ± 0.03^a	4.29 ± 0.4^c	71.43 ± 3.93	1.11	0.98
7 mM	Small	3	1.33 ± 0.03^a	4.15 ± 0.2^c	74.39 ± 1.05	1.17	0.99
	Medium	3	1.32 ± 0.06^a	3.81 ± 0.1^c	73.04 ± 2.08	1.15	0.99
	Large	3	1.20 ± 0.12^a	5.48 ± 0.2^b	71.11 ± 0.64	1.12	0.99
Standard Error			0.05	0.26	1.48	0.03	
P-value			0.005	0.0001	0.32	0.39	
Contrast P-value							
Control vs adding magnetite			0.0001	0.0001	0.694	0.56	
Magnetite Concertation							
2 vs 7			0.610	0.280	0.244	0.12	
Magnetite Size							
Small vs medium			0.44	0.450	0.96	0.95	
Medium vs large			0.83	0.110	0.092	0.17	
Large vs small			0.32	0.026	0.101	0.19	
Interaction of Magnetite							
(Concentration x Size)			0.16	0.022	0.65	0.77	

^{a,b,c} means in the same column with different superscripts are significantly different ($P < 0.05$). N: is the number of observation. Rate: The maximum methane production rate (mmole/g VS/d), The lag phase time (days), CMP: Maximum cumulative methane produced (mL CH_4), Methane yield: calculated at day 43 by dividing the cumulative mole of CH_4 with the total mole glucose added, R^2: 1- (residual sum of squares) / (corrected sum of squares).

Table 5.1 also indicates that the average maximum cumulative methane produced and the methane yield were 72.20 ± 1.69 mL CH_4 and 1.13 ± 0.03 mole of methane per mole of propionate respectively, in all bottles. There was also no significant difference between the magnetite-supplemented and the control bottles. In addition, there was no significant difference in the CMP and methane yield observed between the small, medium and large-supplemented bottles; as well as between the magnetite concentrations of 2 and 7 mM. Consequently, no interaction existed between the magnetite concentration and the magnetite size for the CMP and the methane yield ($P > 0.05$).

Table 5.2 shows the methane production kinetic parameters from the degassed digested sludge without and with magnetite at different concentrations and sizes. The results show no consistency in the methane production rate by adding magnetite. Only the medium-size magnetite at 2 and 7 mM significantly increased the methane production rate (0.665 vs 0.593 mmole/g VS/d; (12 %)), as compared to the control. However, the contrast P –value indicates that no significant difference was obtained in the methane production rate by adding magnetite (control vs addition of magnetite).

On the other hand, the contrast P – value shows that the maximum methane production rate was similar in all magnetite bottles under different concentrations. The results also show that the maximum methane production rate was different in all magnetite bottles under different supplementation of size ranges. That is, small- size versus medium-size was significantly different (contrast $P = 0.002$). As well, large-size versus small-size was significantly different (contrast $P = 0.041$). However, medium-size versus large-size was not significantly different (contrast $P = 0.127$). Significant interaction existed between the magnetite concentration and magnetite size for the methane production rate ($P < 0.05$).

Table 5.2. Influence of magnetite concentration and size on methane production kinetic parameters from degassed sludge

Item			Methane Parameters				
Magnetite Concertation (mM)	**Magnetite Size**	**N**	**Rate (mmole/g VS/d)**	**Lag (day)**	**CMP (mL CH_4)**	**Yield**	**R^2**
Control	Non	3	0.59 ± 0.04^{bc}	26.5 ± 1.6^{c}	76.64 ± 1.05^{ab}	1.16^{ab}	0.98
2 mM	Small	3	0.62 ± 0.02^{ab}	22.2 ± 1.9^{d}	75.94 ± 1.99^{ab}	1.15^{ab}	0.98
	Medium	3	0.66 ± 0.05^{a}	22.0 ± 1.5^{d}	78.41 ± 0.40^{a}	1.18^{a}	0.98
	Large	3	0.63 ± 0.02^{ab}	25.2 ± 1.9^{c}	72.88 ± 3.05^{bc}	1.10^{bc}	0.99
7 mM	Small	3	0.65 ± 0.00^{ab}	29.4 ± 1.9^{b}	71.42 ± 2.39^{c}	1.08^{c}	0.99
	Medium	3	0.67 ± 0.02^{a}	25.0 ± 1.1^{c}	76.56 ± 1.46^{ab}	1.16^{ab}	0.99
	Large	3	0.56 ± 0.05^{c}	33.2 ± 1.1^{a}	59.81 ± 4.08^{d}	0.90^{d}	0.97
Standard Error			0.018	0.93	1.36	0.020	
P-value			0.009	0.0001	0.0001	.0001	
Contrast P-value							
Control vs adding magnetite			0.079	0.751	0.014	0.014	
Magnetite Concertation							
2 vs 7			0.474	0.0001	0.0001	.0001	
Magnetite Size							
Small vs medium			0.002	0.0001	0.0001	.0001	
Medium vs large			0.127	0.029	0.015	0.017	
Large vs small			0.041	0.026	0.0001	.0001	
Interaction of Magnetite (Concentration x Size)			0.021	0.721	0.007	0.006	

^{a,b,c,d} means in the same column with different superscripts are significantly different ($P < 0.05$). N: is the number of observation. Rate: The maximum methane production rate (mmole/g VS/d), The lag phase time (days), CMP: Maximum cumulative methane produced (mL CH_4), Methane yield: calculated at day 43 by dividing the cumulative mole of CH_4 with the total mole glucose added, R^2: 1- (residual sum of squares) / (corrected sum of squares).

In the degassed batch experiment, the most significant reduction in the lag phase (4 days; i.e. 17 % shorter) was observed by adding 2 mM of both small and medium sized magnetite compared to the control ($P < 0.05$). On the other hand, the lag phase time was 25 days in both the 7 mM of medium and 2 mM of large-size supplemented bottles. This time was similar to the 26 days in the control bottles ($P > 0.05$). Furthermore, the lag phase was 3 days longer in the 7 mM of small-size supplemented bottles as well as 7 days longer when large-sized magnetite at 7 mM was added into the bottles, as compared to the control bottles ($P > 0.05$). However, the contrast P value indicates that by adding magnetite, the lag phase was not significantly different, as compared to the control ($P > 0.05$).

On the other hand, the lag phase was significantly increased (22 -25 vs 25-33 days) by increasing the magnetite concentration from 2 mM to 7 mM (contrast $P < 0.05$). Similarly, there was a statistically significant difference in the lag phase observed between the small, medium and large-supplemented bottles ($P < 0.05$); however, the lag phase was the longest in the large –supplemented bottles. No interaction ($P < 0.05$) was observed between magnetite concentration and magnetite particle size for the lag phase.

Table 5.2 shows that cumulative methane production and methane yield in the 2 mM of small, medium and large magnetite were not significantly different, as compared to the control. However, cumulative methane production and methane yield in the 7 mM of small and large magnetite were significantly lower, as compared to the control. In addition, the contrast P – value indicates there was a statistically significant difference in the CMP and yield observed between the small, medium and large-supplemented bottles, as well as between 2 mM of magnetite and 7 mM of magnetite ($P <0.05$). Furthermore, there was significant interaction between the magnetite concentration and the magnetite size for both CMP and yield.

The results shown in Table 5.1 and 5.2 indicate that adding magnetite significantly increases the methane production rate up to 32 % and reduces the lag phase up to 41 % as compared to the control. These results are in agreement with previous findings. For example, Dalla Vecchiaa et al. (2016), Cruz Viggi et al. (2014), and Jing et al. (2017) all demonstrated that magnetite-particle supplementation to a methanogenic sludge enhanced the rate of methane generation (when propionate was the substrate) up to 22 %, 33 % and 44 % respectively. In addition, Cruz Viggi et al. (2014) reported that adding 25 mM of magnetite resulted in a 10 % reduction in the lag-phase time as compared to their control. Furthermore, as mentioned by Yamada et al. (2015), magnetite supplementation accelerated methanogenesis by reducing the time required for complete degradation of propionate by 67 % (50 vs 150 days) as compared to the control. Variation in the enhancement percentages may result from using different propionate concentrations and/or different sludge types. These results suggest that electrically conductive magnetite possibly served as electrical conduit between propionate-oxidizing acetogens and carbon dioxide-reducing methanogens. This suggestion was supported by Cruz Viggi et al. (2014) who found that in the presence of magnetite the theoretical electrical current was 10^6 times higher (3×10^{-5} A) as compared to that in the absence of magnetite (4×10^{-12} A). Yang et al. (2016) suggested that magnetite accelerated the propionate oxidation by acting as an electron acceptor, rather than stimulating DIET. In addition, it has been suggested that magnetite acting as electron donor in the direct reduction of CO_2 to CH_4 by hydrogentrophic methanogens (Su et al., 2013; Abdelsalam et al., 2017). Other possible action of magnetite in anaerobic digestion is heavy metals removal due to their adsorption capacity and thereby reducing the inhibitory effect and the toxicity of the excessive amounts of the heavy metals on microorganisms activity (Carlos et al., 2013). During the anaerobic digestion the released ferrous ion (Fe^{2+}) could combine with sulfide (S^{2-}) which dismissed the inhibitory effects of S^{2-} on microbial communities (Li et al., 2007) and correspondingly reduced hydrogen sulfide H_2S in biogas and significantly stimulated methane production in certain cases (Wang et al., 2016).

However, magnetite does not have a significant effect on CMP and yield. Jing et al. (2017) reported that the maximum methane production (CMP) and methane yield were not significantly different when using different magnetite concentrations ranging from 0.04 – 4 mM. This may suggest that

magnetite is not used as a nutrient (i.e. source of iron) by the microorganisms. This was supported by measurements of ferrous ion concentrations in a separate test that indicated no change in the ferrous ion concentration occurred over time in both the magnetite-supplemented and control bottles; thereby excluding the possibility of iron acting as a nutrient. Previous studies also support these results in that the methane yield in the control bottles (without ferrihydrite) was higher than that in the supplemented bottles (with ferrihydrite) indicating that ferrihydrite could not be used as a source of iron (Kato et al., 2012a; Li et al., 2015; Yamada et al., 2015; Zhuang et al., 2015b).

In the present research, it is also noted that the average methane yield was slightly lower (1.12 mole of methane per total mole of propionate added) than the theoretical methane yield predicted (1.75 mole of methane per total mole of propionate added) from the stoichiometry of the propionate degradation pathway ($4C_3H_5O_2^- + 4H^+ + 2H_2O \rightarrow 7CH_4 + 5CO_2$). This is possibly due to the incubation was stopped before the substrate was completely utilized by the microorganisms and converted to methane. Another possibility is the presence of alternative electron acceptors in the mesophilic digested sludge inoculum. Cruz Viggi et al. (2014) assumed that their low methane yield was due to the presence of sulfate and nitrate that consumed part of the propionate, via sulfate reduction or denitrification. Another reason is that the microorganisms consumed part of the supplied propionate to maintain cell growth (Yang et al., 2016).

Table 5.1 also indicates that both the magnetite concentration and the magnetite size using fresh digested sludge does not affect the maximum methane production rate, nor CMP nor yield. However, the effect of magnetite supplementation on the reduction of the lag phase depends on an interrelationship between size and concentration. On the other hand, using degassed sludge, both magnetite concentration as well as magnetite size significantly affects the lag phase, CMP and yield; however, both magnetite size and concentration have an independent effect on the maximum methane production rate. Previous studies have shown that magnetite has a positive effect on methane production only when a suitable particle size and concentration are used. For example, Casals et al. (2014) found that biogas production was 66.6 % less when using 24 nm magnetite than when using a size of 7 nm. In addition, they showed that methane production increased when the magnetite concentration was raised from 0 to 1.166 mM; however, thereafter it decreased when

the magnetite concentration increased. Similarly, the results of testing magnetite at concentrations above 20 mM (80, 160 and 320 mM) revealed that both the methane production rate and amount was not improved (Yang et al., 2015b; Yang et al., 2016); nor was there any significant change in the lag-phase time or the yield or methane production rate using acetate (Yang et al., 2015b). In a different study; however, as the magnetite was added at concentrations of 20, 80, 160, and 320 mM, the methane production rate and the lag phase were similar 0.066, 0.067, 0.064, and 0.063 mmole/d and 1.9, 1.88, 2.41, and 3.15 d respectively (Yang et al., 2016). Finally, in a recent study, a batch experiment conducted with 30 mM sodium propionate at different concentrations of magnetite nanoparticles resulted in methane production rates of 4.11, 4.33, and 4.06 mL/d and lag phase times of 9.5, 9.6, and 9.1 d; when magnetite was added at concentrations of 0.04, 0.4, and 4 mM respectively (Jing et al., 2017).

All these observations suggest that magnetite characteristics play a significant role in methane production with much higher concentrations and very large sizes inhibiting the methane production process. This can be explained by nanoparticles aggregation; that is to say, an increase in magnetite concentration and size leads to a higher frequency of collision and particle-particle interactions, which increases the possibility of aggregation (Maximova and Dahl, 2006; Baalousha, 2009). Ultimately, excessive aggregation results in a decrease in specific surface area and; correspondingly, a decrease in reactivity, thereby undermining the performance of magnetite (Tang and Lo, 2013). Another reason for the occasional inhibitory effect of magnetite could be impurities (i.e. other metals in the magnetite composition can inhibit or be toxic to the microbial community). For example, in this research, the large-sized magnetite particles had other metals (i.e. Na, Cl, Si, and Cr) not present in the medium- and small-sized magnetite (Appendix A, Figures A.4, A.5, and A.6). In addition, it has been reported that magnetite can lead to microbial community changes (i.e. Methanobacterium was not detected in the magnetite cultures but was detected in the control (Kato et al., 2012a)). Furthermore, Kassab et al. (2020) reported high dosages of zero valent iron can extensively damage bacterial cell membranes through decomposition of protein groups. This could lead to accumulation of hydrogen and VFAs causing an inhibitory effect on methane production.

Overall, however, it is difficult to compare studies as many factors besides magnetite size and concentration play a role in methanogenesis and further investigation is needed to examine the microbial community before and after adding magnetite nanoparticles. Therefore, within the parameters of any experiment, it is important to monitor the magnetite size and concentration to identify the necessary level of aggregation that improves methane production. In the present study, the results suggest that magnetite characteristics (size and concentration) affect the methane production kinetic parameters; however, they depend on the sludge age.

5.2.3 Effect of Magnetite and Sludge Age on Methane Production

To study the effect of sludge age and magnetite on methane production kinetic parameters; the data of all magnetite-supplemented bottles (2, 7 and 20 mM of small, medium and large) in both fresh and degassed batch experiments was analyzed. The statistical analysis was done using a 2 × 3 × 3 factorial arrangement treatment (two levels of sludge ages, three levels of magnetite concentrations and three levels of magnetite size ranges) through statistical analysis of two-way analysis of variance (ANOVA) using a general linear model (GLM) procedure of SAS (2015).

Table 5.3 indicates that sludge age had a strong effect on methane production kinetic parameters in the presence of magnetite. For example, fresh sludge significantly enhanced the maximum methane production rate (1.2933 vs 0.6311 mmole/g Vs) and reduced the lag phase (4.6011 vs 26.1668 days), as compared to degassed sludge. However, the sludge age (fresh vs degassed), did not have a significant effect on both CMP and yield. Magnetite supplementation (different size ranges and different concentration levels) also did not have a significant effect on the methane production rate by using different sludge ages, with no significant interaction observed between magnetite and sludge ages. However, the lag phase time was significantly affected by different magnetite size ranges, as well as by different magnetite concentration and this was dependent on the sludge's age. The cumulative methane production and yield were significantly affected by different magnetite size ranges, with significant interactions between magnetite and sludge age ($P < 0.05$).

Table 5.3. The effect of sludge age on methane production kinetic parameters in the presence of magnetite.

Main effect	**Rate (mmole/g VS/d)**	**Lag (day)**	**CMP (mL CH_4)**	**Yield**
Sludge type				
Fresh	1.2933[a]	4.6011[b]	72.1078[a]	1.1278[a]
Degassed	0.6311[b]	26.1668[a]	72.5028[a]	1.0950[a]
Standard error	0.024	0.629	1.293	0.021
P- value				
Magnetite size	0.137	0.002	0.025	0.003
Magnetite concentration	0.494	0.0001	0.062	0.148
Sludge age	0.0001	0.0001	0.762	0.148
Interaction				
Magnetite Size x Sludge age	0.7724	0.0223	0.0036	0.008
Magnetite concentration x Sludge age	0.819	0.0001	0.0045	0.002

[a,b] means in the same column with different superscripts are significantly different ($P < 0.05$).

The reason for the lower methane production rate and the extension to the lag phase in the degassed sludge may be that as the sludge ages in the incubator (i.e. degasses), the microorganisms consume most of the available nutrients (i.e. food) and; after a period with no food, the microorganisms starve. As such, this may disturb the microbial growth rate sufficiently such that a high concentration of large-sized magnetite may have a negative impact on the lag phase, reflected in an increase in time that microbial communities need to adjust to a new environment. Regueiro et al. (2012) reported a relation between microbial activity and microbial community structure and this activity depended upon the type of biomass and the operational conditions that determined the growth of specific populations. It has been suggested that the inoculum should be fresh and have an active microbial population, with an adequate balance between all the microbial communities to ensure that the anaerobic digestion process does not face any limitations (Amann et al., 1995; McMahon et al., 2004; Angelidaki et al., 2009). In addition, when the sludge is fresh, the quick growth of microorganisms shortens the lag phase time (Grant and Long, 1985; Madigan et al.,

2008). However, in the present research, the digested sludge was left in the incubator for a month; thus, the microorganisms were facing a food shortage meaning the growth slowed as the exhausted microbes took time to adjust to the new anaerobic environment and proceed with methane production (Manure, 2001; Hadiyarto et al., 2015). These observations are confirmed by the total organic carbon data (Figure 5.3). That is, when the sludge was fresh, it contained abundant food and the microorganisms were therefore highly active, consuming the organic matter at a high rate as denoted by a sharp decrease in the concentration of TOC (day 0 to day 17). By day 20, the reducing food availability lowered the growth rate of the microorganisms and the cells started to release total organic carbon which is most likely due to cell lysis/endogenous respiration (Van Loosdrecht and Henze, 1999). A similar pattern for TOC increase and explanation was observed and offered by Yates and Smotzer (2007) and Rolfe et al. (2012).

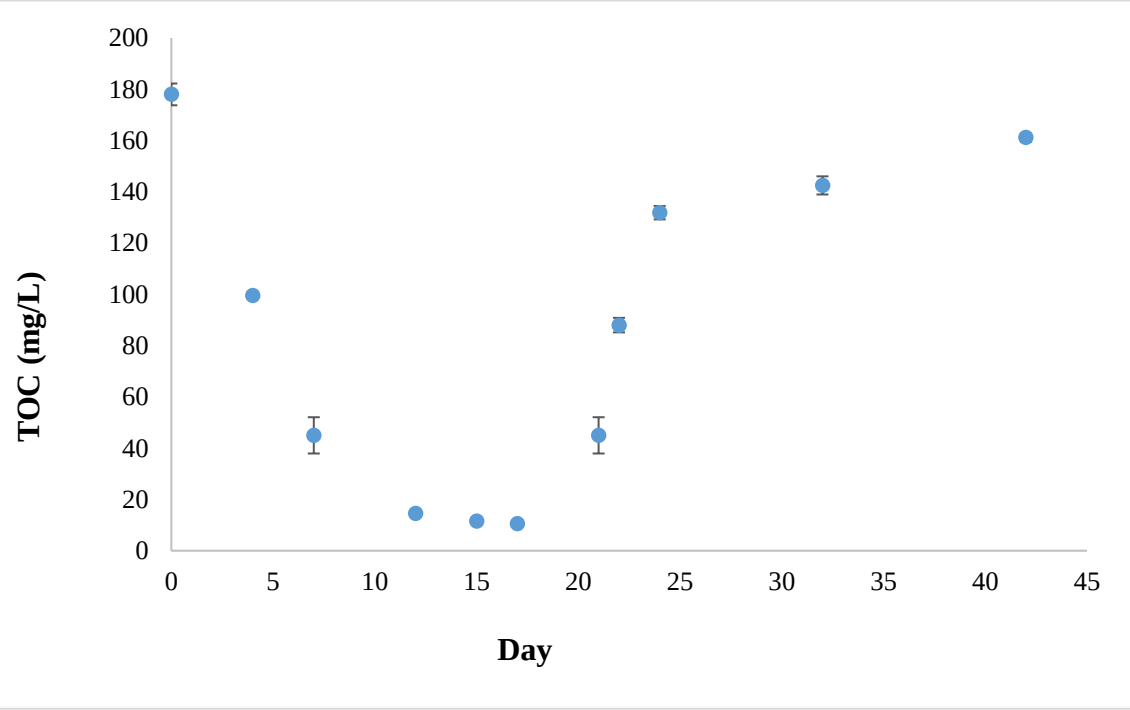

Figure 5.3. Total organic carbon for digested sludge over a period of settling at 36°C.

The overall results showed that magnetite had a different effect on methane production depending on whether from fresh and aged sludge was used. That is to say, magnetite did enhance the methane production when microorganisms are in the exponential growth phase as compared when they are in the decay phase. This indicate that the effect of magnetite on the methane production kinetic parameters depends on the sludge age; with the general recommendation being to add magnetite to the fresh sludge to maximize the rate of methane production and reduce the lag phase.

5.2.4 Effect of Magnetite on Methane Production under Substrate-Limited Condition

The previous results revealed the favourable conditions for the production of methane by adding both magnetite and substrate in anaerobic digestion. In order to assess whether endogenous (blank) methane production is affected by the presence of magnetite, an experiment was conducted under substrate-limited condition as shown in Figure 5.4 and Table 5.4.

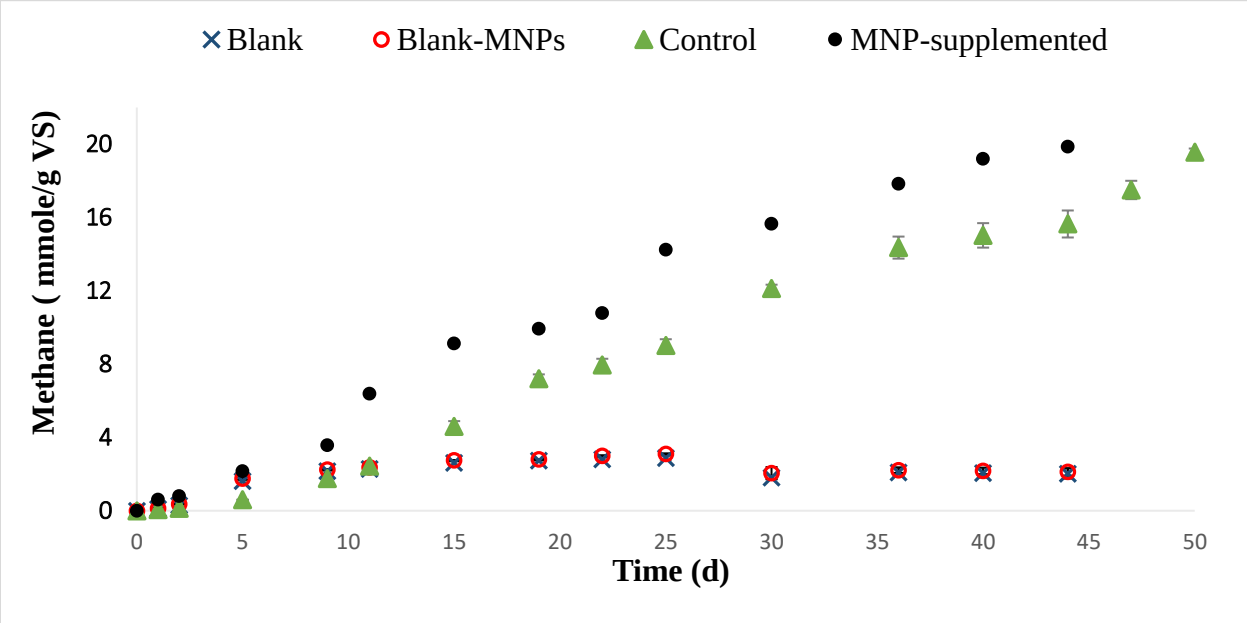

Figure 5.4. Methane production as a function of incubation time. The symbols ●, ▲, x and o represent the magnetite-supplemented bottles, control bottles, blank bottles and blank with magnetite-supplemented bottles respectively.

Figure 5.4 shows the methane production from the blank bottles (with no magnetite and no propionate) and the blank bottles with 7 mM of medium magnetite and no propionate. The results indicate that methane production was quite similar for both groups of blank and blank with magnetite.

Table 5.4. The effect of magnetite and propionate presence on methane production

Treatment	Item			Methane production P		
	Propionate (mM)	Magnetite (mM)	N	Rate (mmole/g VS/d)	Lag (day)	CMP (mL CH_4)
Blank	0	0	3	0.58 ± 0.06^{c}	1.07 ± 0.04^{c}	8.73 ± 1.21
Blank with magnetite	0	7	3	0.60 ± 0.06^{c}	1.07 ± 0.06^{c}	9.20 ± 0.88
Control	27	0	3	0.87 ± 0.04^{b}	7.48 ± 0.58^{a}	80.8 ± 2.76
Magnetite supplemented	27	7	3	1.18 ± 0.01^{a}	3.91 ± 0.10^{b}	82.13 ± 2.07
Standard error				0.028	0.129	0.801
Main effect						
Magnetite concentration						
	0		6	0.724	4.2750	44.567^{A}
	7		6	0.9829	2.4882	45.667^{A}
Propionate concentration						
	0		6	0.591	1.0687	8.967^{Y}
	27		6	1.025	5.6945	81.27^{X}
P - value						
Magnetite concentration				0.0003	0.0001	0.2069
Propionate concentration				0.0001	0.0001	0.0001
Interaction of concentration (magnetite x propionate)				0.0009	0.0001	0.4519

^{a,b,c} or ^{X,Y,Z} means in the same column with different superscripts are significantly different ($P < 0.05$).

Table 5.4 shows that no significant difference in maximum methane production rate or lag phase were observed by adding magnetite to the biomass (blank bottles). Although the lag phase was extended to a great extent in the magnetite-supplemented bottles (as compared to the blank with magnetite bottles), apparently, the maximum methane production rate in magnetite-supplemented bottles (containing both 7 mM of magnetite and 27 mM of propionate) was 1.5 times the blank with magnetite (containing 7 mM of magnetite and no substrate).

In addition, Table 5.4 indicate that the interaction between propionate and magnetite was significant for both maximum methane production rate and the lag phase. On the other hand, it is obvious that adding propionate (27 mM) resulted in an increase in the cumulative methane production (CMP) as compared to the absence of propionate (0 mM). This because the substrate provides plenty of food for microorganisms; however, adding magnetite did not significantly increase the cumulative methane produced in the treatments trials.

These results indicate that adding magnetite to enhance the methane production rate depended on the presence of an external substrate. Cruz Viggi et al. (2014) showed that the methane production rate was 20 % lower when magnetite was present (but no external substrate), as compared to when magnetite was not present, and again no external substrate. These results indicate that the stimulatory effect of magnetite to enhance the methane production rate is substrate dependent. This also implies that there might be a minimum concentration of substrate required for magnetite nanoparticles to serve as electrical conduits. This minimum concentration could be a function of number of factors including substrate type, community structure, etc. Cruz Viggi et al. (2014) observed that without an external substrate, magnetite had a negative effect on methanogenic activity.

5.2.5 Conclusion

Both magnetite characteristics (size and concentration) play a role in methane production. Overall, using large (800 nm to 4.5 µm) size does not enhance methane production, as compared to small (50-150 nm) and medium (168 to 490 nm) size ranges. Both magnetite concentrations 2 mM and 7 mM enhance the methane production; while, the stimulatory effect of magnetite on methane production requires the presence of a substrate.

In addition, adding magnetite to enhance the methane production is related to the growth phase of microorganisms. The findings indicate that magnetite has a positive effect on methane production when the digested sludge is fresh (i.e. in the exponential growth phase), as compared to aged (i.e. in the decay phase). Adding magnetite enhanced the methane production rate by 32 % and 12 % in the fresh and degassed sludge, respectively, as compared to the control. In addition, the lag phase was 41 % shorter and 17 % shorter in the fresh and degassed sludge, respectively, as compared to the control. However, no improvement in methane yield was observed, as compared to the control. These results could have a broad impact influencing the maximum methane production given that there are thousands of full-scale plants worldwide.

CHAPTER 6. EFFECT OF MAGNETITE ON METHANE PRODUCTION FROM MESOPHILIC SLUDGE THAT IS CULTIVATED WITH ACETATE, PROPIONATE, AND GLUCOSE

6.1 Objectives and Experimental Setup

This chapter investigates the effect of magnetite (medium-sized at 0, 2, 7 and 20 Mm) on methane production from different substrates (acetate, propionate and glucose). Each substrate was tested separately at three different concentrations corresponding to initial COD:VS ratios of 2:1, 4:1 and 8:1. The volatile solids (VS) concentration was fixed in all bottles to be 1.5 g/L. All bottles were run in triplicate.

Blank bottles were tested to examine the sludge's baseline (or endogenous) activity (no substrate and no magnetite). Control bottles had substrate and no magnetite. Magnetite-supplemented bottles had both substrate and magnetite. Figure 6.1 shows the experimental design to investigate the effect of different concentration of magnetite (MNP) on methane production using acetate, propionate, and glucose as a substrates.

Data was presented as mean ± standard deviation of triplicate. As the experiment had three levels of substrate concentrations (COD:VS of 2:1, 4:1 and 8:1) and four levels of magnetite concentrations (0, 2, 7, and 20 mM), the data was evaluated by 3 × 4 factorial arrangement treatments through statistical analysis of two-way of variance (ANOVA) using the general linear model (GLM) procedure of SAS (2015). The data was analyzed by two-way ANOVA to determine the main effects and their interaction. Differences were considered to be significant at $P < 0.05$ and significant differences between means were separated by Least Significant Difference tests.

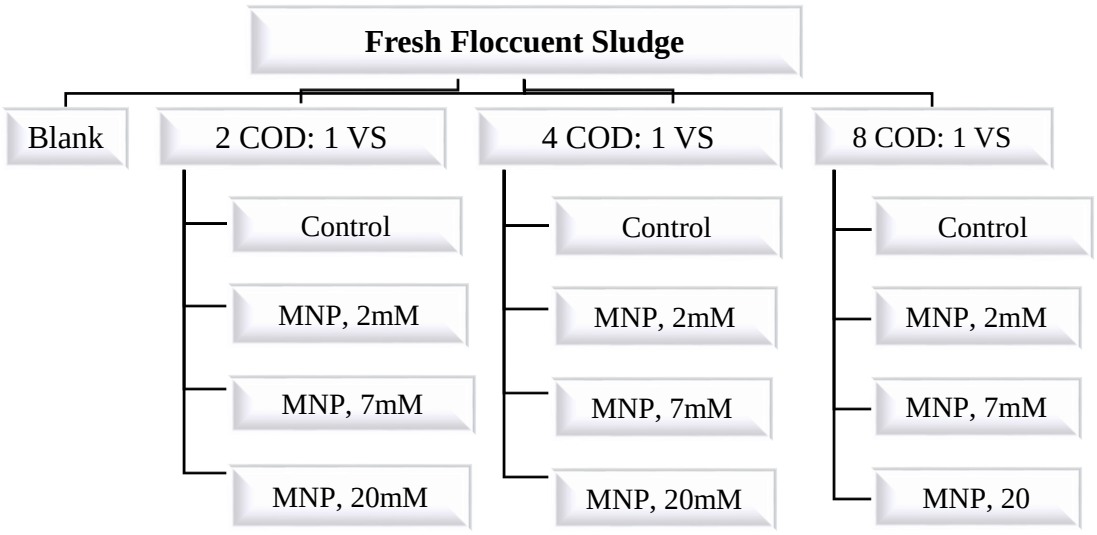

Figure 6.1. Experimental design to investigate separately the effect of different concentration of acetate, propionate and glucose in the presence of magnetite (MNP) on methane. Volatile solid (VS) in all batch experiments was 1.5 g/L.

6.2 Results and Discussion

Methane from the blank bottles (no substrate and no magnetite) reached a maximum of 4.84 mmole/g VS and since this amount was very small it was neglected (Figure 6.2).

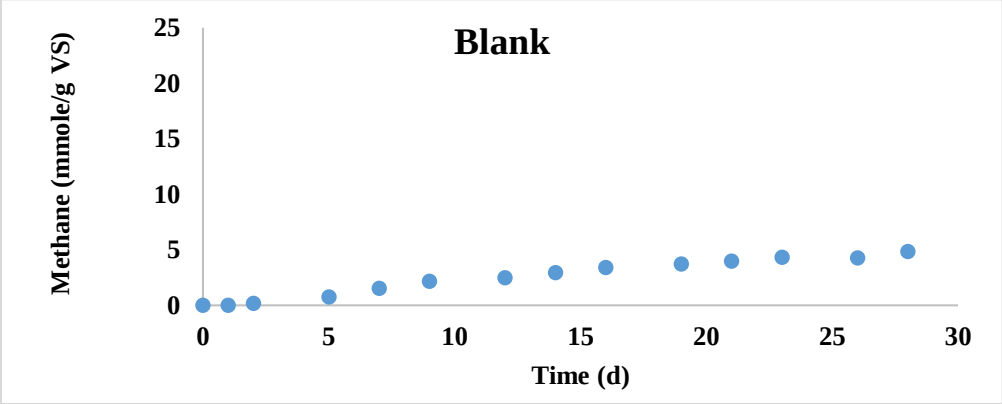

Figure 6.2. Methane production from blank bottles.

6.2.1 The Effect of Magnetite on Methane Production Profiles

The methane production profiles from different substrates (i.e. acetate, propionate and glucose) are shown in Figures 6.3, 6.4 and 6.5. Each figure presents the methane production from specific substrate at three different concentrations (2 COD: 1 VS, 4 COD: 1 VS, and 8 COD: 1 VS) with the addition of different magnetite concentrations (2, 7 and 20 mM) as well as in the absence of magnetite (control bottles).

Figure 6.3 shows that methane production from acetate at 2 COD: 1 VS ratio was clearly observed at day 3 and produced at approximately the same speed in the bottles until day 14. After that (from day 15 to day 30), a large amount of methane was produced in the magnetite-supplemented bottles (13 versus 9.56 mmole/g VS at day 30), as compared to the control. At a COD:VS ratio of 4:1, the methane production started at day 3 in all bottles but reached a plateau faster in the magnetite-supplemented bottles (after 11 vs 14 days) as compared to the control. However, around 14.77 mmole/g VS was produced in all bottles at day 30. The methane production at 8 COD: 1 VS ratio was produced at similar speed in all bottles and reached a plateau at day 20; however, the amount of methane at day 30 was higher in the magnetite-supplemented bottles (21.8 vs 19.8 mmole/g VS) as compared to the control. It is obvious that by increasing the acetate concentration from 2 COD: 1 VS to 8 COD: 1 VS the amount of methane produced increased.

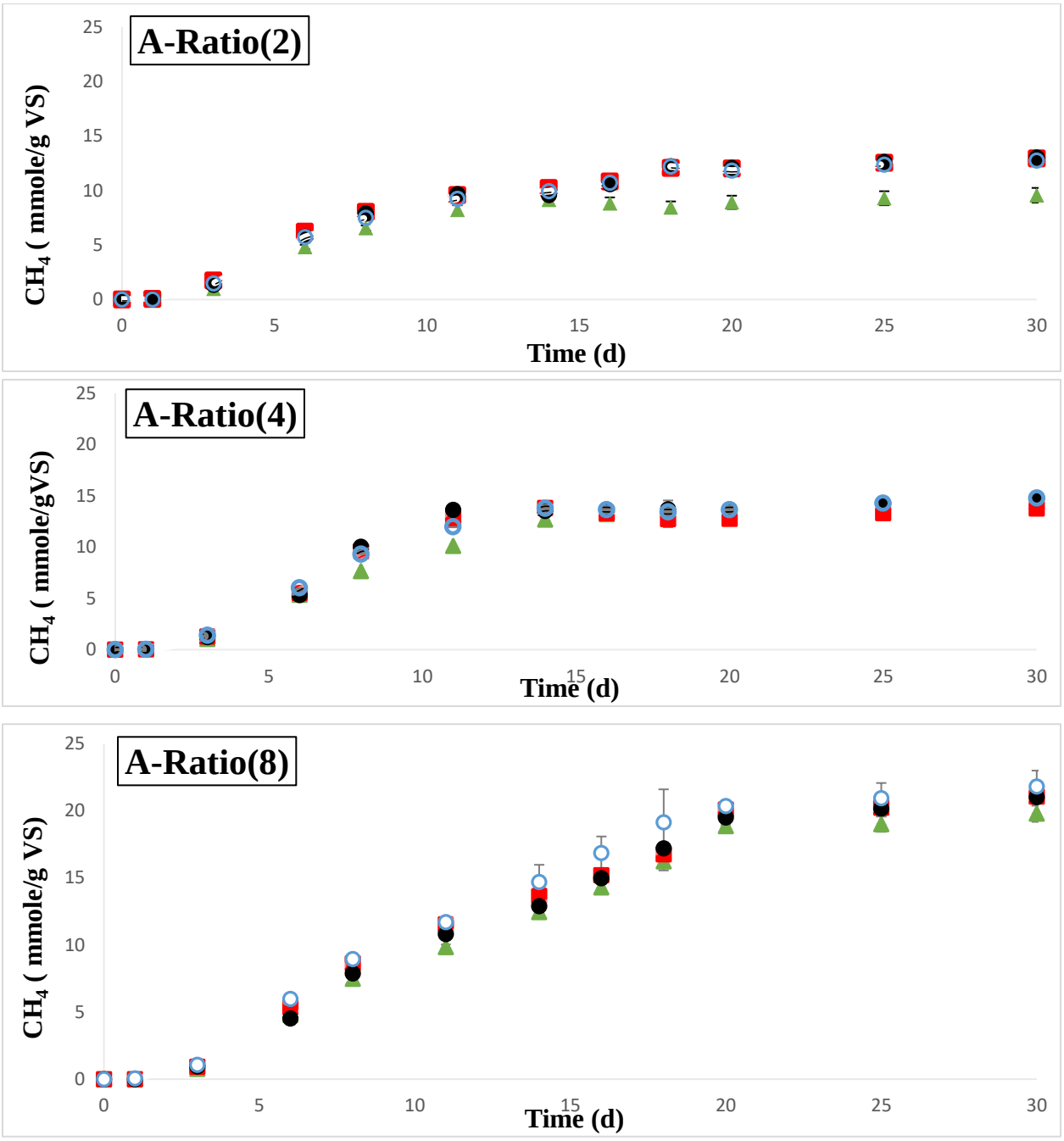

Figure 6.3. Methane production (mmole/g VS) over 30 days of incubation. Figures A-Ratio(2), A-Ratio(4) and A-Ratio(8) represent methane production from acetate at 2 COD: 1 VS, 4 COD: 1 VS and 8 COD: 1 VS ratios respectively. The symbols ▲, ■, ●, and o represent the control, 2 mM of magnetite, 7 mM of magnetite, and 20 mM of magnetite respectively. Error bars represent the standard deviation of triplicate experiments.

Figure 6.4 shows that at a propionate ratio of 2 COD: 1 VS; methane production started at day 5 and continued until day 25. After that, the amount of methane produced in the magnetite-supplemented bottles was larger than the control bottles reaching 16 mmole/g VS at day 55 as compared to 14.06 mmole/g VS.

At a propionate ratio of 4 COD: 1 VS, the methane was produced after 7 - 9 days in all bottles and then was produced more rapidly in the magnetite-supplemented bottles to reach around 16.5 mmole/g VS at day 55 as compared to 14.37 mmole/g VS the control bottles.

By increasing the propionate ratio up to 8:1, the methane began to be produced after 12-14 days in all bottles and was then produced more rapidly in the magnetite-supplemented bottles, as compared to control bottles. At day 30 and day 41, the methane amount in the magnetite-supplemented bottles (9.46 and 13.23 mmole/g VS respectively), doubled that of the control (4.51 and 7.95 mmole/g VS respectively). At day 55, the produced methane reached 15.38 mmole/g VS in magnetite-supplemented bottles versus 12.32 mmole/g VS in the control bottles.

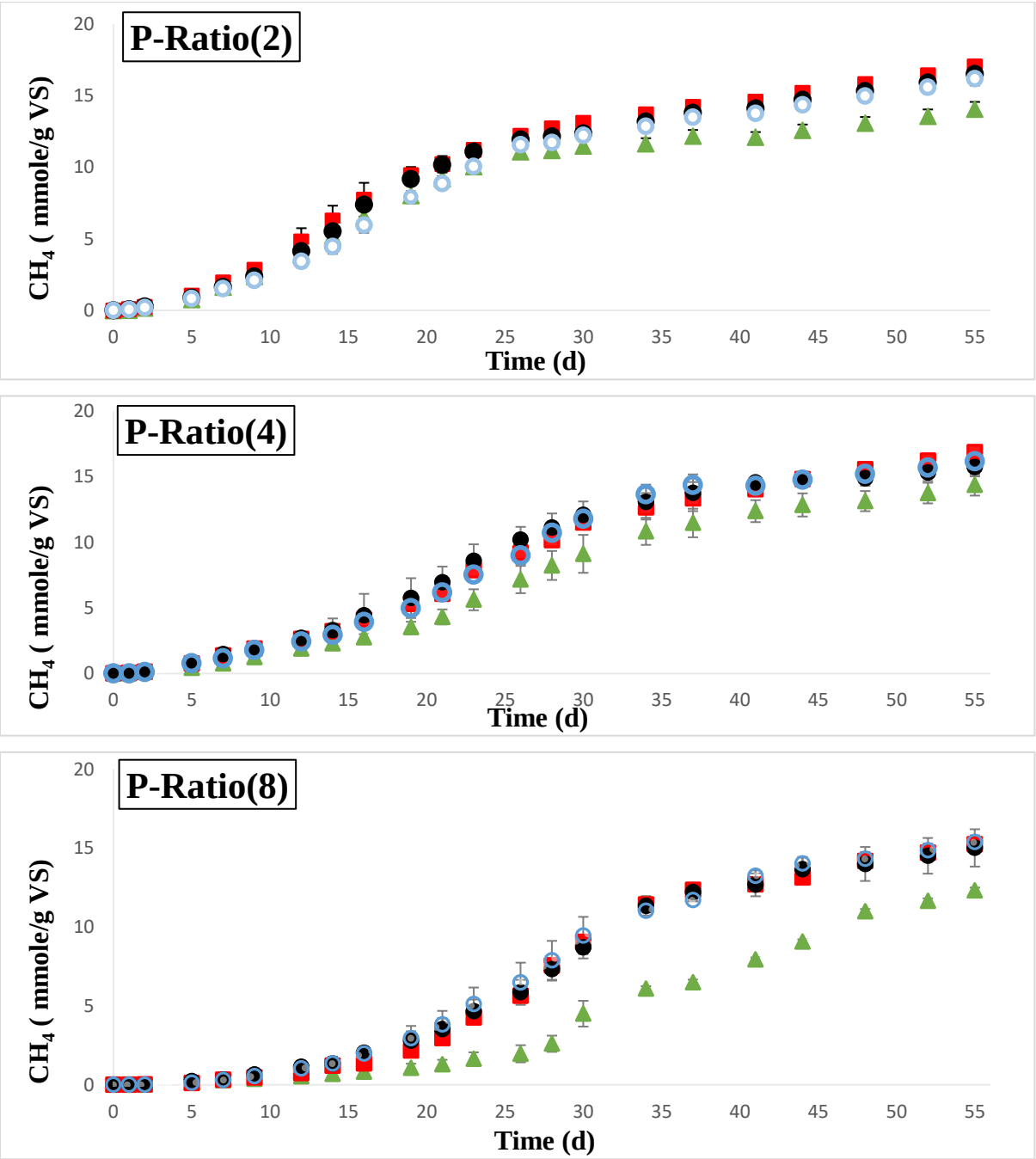

Figure 6.4. Methane production from propionate over the incubation time. P-Ratio(2), P-Ratio(4) and P-Ratio(8) represent methane production from propionate at 2 COD: 1 VS, 4 COD: 1 VS and 8 COD: 1 VS ratios respectively. The symbols ▲, ■, ●, and o represent the control, 2 mM of magnetite, 7 mM of magnetite, and 20 mM of magnetite respectively. Error bars represent the standard deviation of triplicate experiments.

At the glucose ratio of 2:1 (Figure 6.5), although all bottles produced methane at a similar speed from day 0 to day 18, a lower amount of methane was produced in the control bottles from day 22 to day 36 as compared to the magnetite-supplemented bottles. However, all bottles produced 11 mmole/g VS of methane at day 44.

At the glucose ratio of 4 COD: 1 VS, the control bottles produced methane earlier (18 vs 22 days), as compared to the magnetite-supplemented bottles; however, at day 30 magnetite-supplemented bottles of 7 and 20 mM started to produce methane more rapidly as compared to the control. At day 44, the magnetite-supplemented bottles had methane amounts of 11.35 mmole/g VS as compared to 8.66 mmole/g VS in the control bottles.

Figure 6.5 shows that by increasing the glucose concentration to 8 COD: 1 VS no methane production was observed in all bottles until day 26. After that, the 7 mM, 20 mM and 2 mM magnetite-supplemented bottles produced methane more rapidly to reach 3.19, 1.73 and 1.04 mmole/g VS, respectively, as compared to 0.06 mmole/g VS in the control bottles.

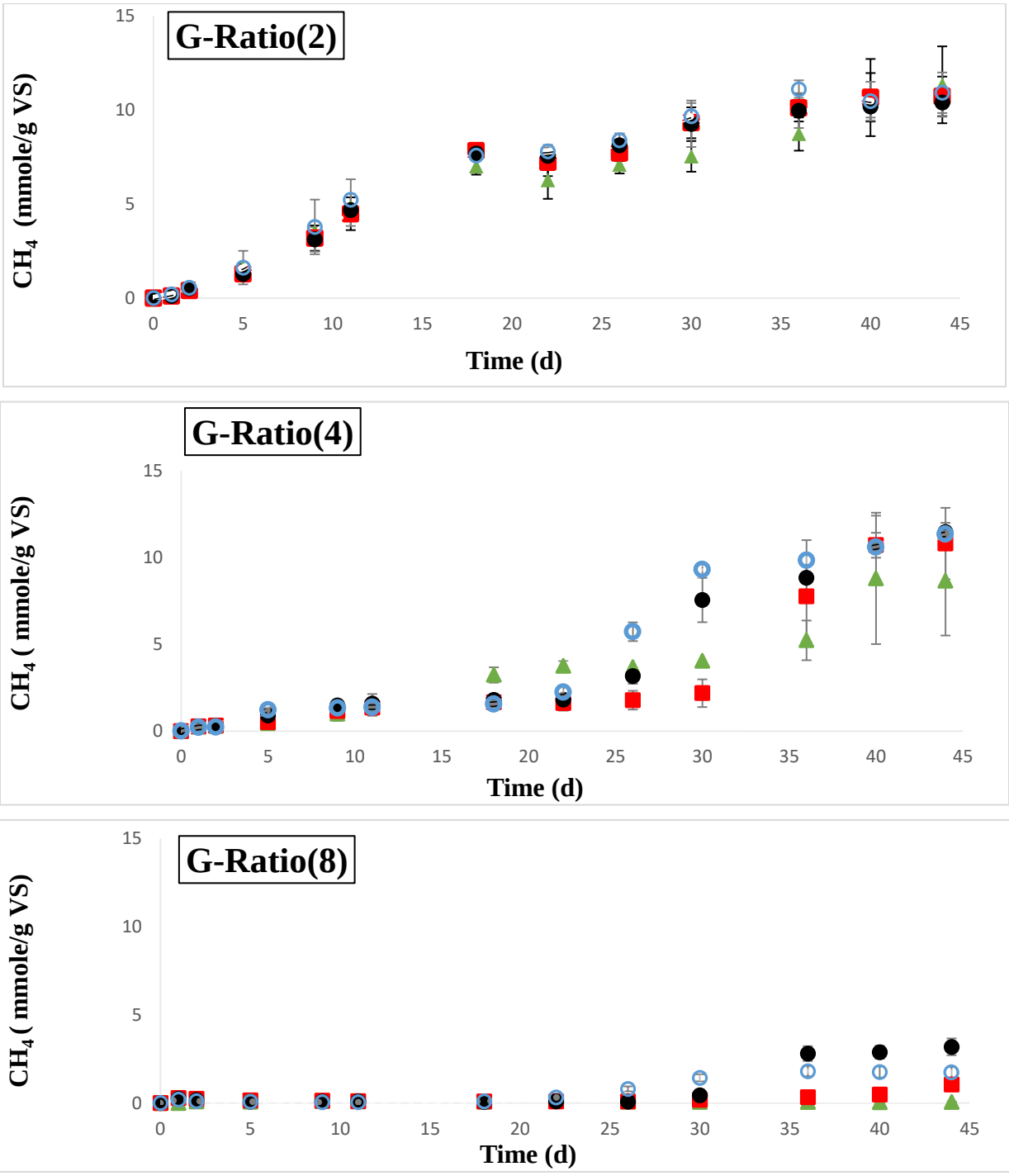

Figure 6.5. Methane production from glucose over the incubation time. G-Ratio (2), G-Ratio (4) and G-Ratio (8) represent methane production from glucose at 2 COD: 1 VS, 4 COD: 1 VS and 8 COD: 1 VS ratios respectively. The symbols ▲, ■, ●, and o represent the control, 2 mM of magnetite, 7 mM of magnetite, and 20 mM of magnetite respectively. Error bars represent the standard deviation of triplicate experiments.

6.2.2 Potential of Adding Magnetite to Enhance the Methane Production at Different Substrate Concentrations

Tables 6.1, 6.2 and 6.3 present the methane production kinetic parameters in terms of maximum methane production rate (mmole/g VS/ d), lag phase duration (day), maximum cumulative methane production (mL) and methane yield (mole methane produced per mole substrate added) from acetate, propionate and glucose, respectively. Tables 6.1, 6.2 and 6.3 show that the coefficient of determination (R^2) values (obtained by fitting a modified Gompertz model to the experimental methane-accumulation curves by non-linear regression using SPSS software) were between 0.95 – 0.99. This indicates that the modified Gompertz model adequately describes the experimental data. Tables 6.1, 6.2 and 6.3 also show the standard deviation (SD) and standard error (SE) for each methane parameter (rate, lag phase, cumulative methane produced and yield).

Table 6.1. The effect of magnetite addition on methane production kinetic parameters at three different concentrations of acetate.

Item			Methane parameters				
COD: VS	**Magnetite concentration (mM)**	**N**	**Rate (mmole/g VS/d)**	**Lag (day)**	**CMP (mL CH_4)**	**Yield**	**R^2**
2	0	3	$1.152 \pm 0.07^{c,d}$	2.059 ± 0.13^{c}	41.43 ± 2.91^{e}	0.574^{b}	0.99
	2	3	1.049 ± 0.06^{d}	0.961 ± 0.12^{d}	56.05 ± 0.88^{d}	0.776^{a}	0.99
	7	3	1.013 ± 0.02^{d}	1.106 ± 0.06^{d}	56.39 ± 1.40^{d}	0.781^{a}	0.99
	20	3	1.027 ± 0.07^{d}	1.223 ± 0.11^{d}	55.28 ± 0.21^{d}	0.765^{a}	0.99
4	0	3	1.32 ± 0.08^{c}	2.288 ± 0.25^{b}	62.43 ± 1.62^{c}	$0.432^{d,c}$	0.99
	2	3	2.104 ± 0.20^{a}	3.166 ± 0.26^{a}	$59.58 \pm 2.36^{d,c}$	0.412^{d}	0.98
	7	3	2.043 ± 0.11^{a}	3.099 ± 0.15^{a}	63.96 ± 0.59^{c}	0.443^{c}	0.98
	20	3	1.59 ± 0.04^{b}	$2.24 \pm 0.17^{c,b}$	64.00 ± 0.60^{c}	0.443^{c}	0.99
8	0	3	1.268 ± 0.03^{c}	3.098 ± 0.04^{a}	85.67 ± 2.62^{b}	0.296^{f}	0.99
	2	3	$1.336 \pm 0.04^{c,b}$	2.396 ± 0.04^{b}	91.23 ± 2.86^{a}	$0.316^{f,e}$	0.99
	7	3	$1.334 \pm 0.02^{c,b}$	2.875 ± 0.07^{a}	91.04 ± 5.34^{a}	$0.315^{f,e}$	0.99
	20	3	1.483 ± 0.14^{b}	2.532 ± 0.37^{b}	94.42 ± 5.17^{a}	0.327^{e}	0.98
Standard error			0.052	0.101	1.58	0.0098	
Main effect							
Magnetite concentration							
	0	9	1.248	2.391	63.18	0.434	
	2	9	1.496	2.174	68.95	0.502	
	7	9	1.464	2.360	70.46	0.513	
	20	9	1.367	1.998	71.24	0.512	
COD:VS							
	2	12	1.060	1.338	52.29	0.724	
	4	12	1.765	2.698	62.50	0.433	
	8	12	1.355	2.657	90.59	0.314	
P- value							
Magnetite concentration			0.0001	0.0002	0.0001	0.0001	
Acetate concentration			0.0001	0.0001	0.0001	0.0001	
Interaction							
(Magnetite x Acetate)			0.0001	0.0001	0.0006	0.0001	

^{a,b,c,d,e,f} means in the same column with different superscripts are significantly different ($P < 0.05$). N: is the number of observation. The lag phase time (days), Rate: The maximum methane production rate (mmole/g VS/d), CMP: Maximum cumulative methane produced (mL CH_4), Methane yield: calculated at day 30 by dividing the cumulative mole of CH_4 with the total mole acetate added, R^2: 1- (residual sum of squares) / (corrected sum of squares).

Table 6.2. The effect of magnetite addition on methane production kinetic parameters at three different concentrations of propionate.

Item			Methane parameters				
COD: VS	**Magnetite concentration (mM)**	**N**	**Rate (mmole/g VS/d)**	**Lag (day)**	**CMP (mL CH_4)**	**Yield**	**R^2**
2	0	3	0.542± 0.03^{ba}	4.42± 0.35^{f}	60.90± 2.20	0.781^{c}	0.99
	2	3	0.576± 0.01^{ba}	3.70± 1.04^{f}	73.87± 1.09	0.947^{a}	0.99
	7	3	0.568± 0.01^{ba}	4.16± 0.10^{f}	71.58±0.75	0.918^{b}	0.99
	20	3	0.555± 0.01^{ba}	5.40± 0.10^{f}	70.15±2.10	0.899^{b}	0.99
4	0	3	0.493± 0.06^{cb}	10.88± 0.77^{d}	62.26± 3.49	0.399^{f}	0.99
	2	3	0.531± 0.02^{b}	8.22± 0.61^{e}	73.09± 0.83	0.469^{d}	0.98
	7	3	0.613± 0.07^{a}	8.65± 1.33^{e}	68.24± 3.14	0.437^{e}	0.99
	20	3	0.596± 0.02^{a}	9.52± 0.47^{ed}	70.05± 1.41	0.449^{ed}	0.99
8	0	3	0.455± 0.03^{c}	20.92± 1.30^{a}	53.35± 0.78	0.171^{h}	0.99
	2	3	0.644± 0.01^{a}	16.11± 0.63^{b}	66.01± 0.20	0.212^{g}	0.99
	7	3	0.595± 0.02^{a}	14.78± 1.62^{cb}	65.03± 5.33	0.209^{g}	0.99
	20	3	0.597± 0.02^{a}	14.28± 2.01^{c}	66.63± 1.85	0.213^{g}	0.99
Standard error			0.018	0.611	1.38	0.0094	
Main effect							
Magnetite concentration							
0		9	0.496	12.07	58.84^{Z}	0.450	
2		9	0.584	9.34	70.99^{X}	0.543	
7		9	0.592	9.20	68.28^{X}	0.521	
20		9	0.583	9.73	68.94^{X}	0.521	
COD:VS							
2		12	0.560	4.42	69.12^{A}	0.886	
4		12	0.558	9.32	68.41^{A}	0.438	
8		12	0.573	16.52	62.76^{B}	0.201	
P- value							
Magnetite concentration			0.0001	0.0001	0.0001	0.0001	
Propionate concentration			0.4907	0.0001	0.0001	0.0001	
Interaction (Magnetite x Propionate)			0.0009	0.0001	0.265	0.0001	

^{a,b,c,d,e,f,g} or ^{A,B} or ^{X,Y,Z} means in the same column with different superscripts are significantly different ($P < 0.05$). N: is the number of observation. Rate: The maximum methane production rate (mmole/g VS/d), The lag phase time (days), CMP: Maximum cumulative methane produced (mL CH_4), Methane yield: calculated at day 54 by dividing the cumulative mole of CH_4 with the total mole propionate added, R^2: 1- (residual sum of squares) / (corrected sum of squares).

Table 6.3. The effect of magnetite addition on methane production kinetic parameters at three different concentrations of glucose

Item			Methane parameters				
COD: VS	**Magnetite concentration (mM)**	**N**	**Rate (mmole/g VS/d)**	**Lag (day)**	**CMP (mL CH_4)**	**Yield**	**R^2**
2	0	3	$0.35 \pm 0.01^{c,d}$	2.67 ± 0.58^{f}	49.09± 8.85	1.093	0.97
	2	3	0.44 ± 0.03^{c}	2.04 ± 0.93^{f}	46.43± 4.56	1.033	0.95
	7	3	0.46 ± 0.04^{c}	2.18 ± 1.34^{f}	45.03 ± 3.26	1.003	0.96
	20	3	0.49 ± 0.06^{c}	1.85 ± 1.23^{f}	47.26 ± 4.66	1.053	0.97
4	0	3	$0.32 \pm 0.02^{c,d}$	11.00 ± 1.00^{e}	37.53 ± 13.66	0.418	0.98
	2	3	1.08 ± 0.16^{a}	27.67 ± 2.31^{b}	46.87 ± 8.91	0.522	0.99
	7	3	0.69 ± 0.09^{b}	$20.00 \pm 1.73^{c,d}$	49.67 ± 2.35	0.553	0.98
	20	3	0.83 ± 0.14^{b}	18.67 ± 1.15^{d}	49.18± 1.41	0.548	0.99
8	0	3	-------	-----	--------	------	
	2	3	0.11 ± 0.01^{d}	24.00 ± 1.00^{c}	1.10 ± 0.10	0.06	0.98
	7	3	$0.53 \pm 0.21^{b,c}$	30.33 ± 0.58^{a}	15.15 ± 1.57	0.080	0.98
	20	3	0.21 ± 0.06^{d}	21.67 ± 3.21^{c}	7.50 ± 1.34	0.043	0.97
Standard error			0.055	0.863	3.371	0.053	
Main effect							
Magnetite concentration							
	0	9	0.223	4.556	28.88^{Y}	0.51^{X}	
	2	9	0.541	17.91	31.469^{XY}	0.54^{X}	
	7	9	0.561	17.50	36.617^{X}	0.55^{X}	
	20	9	0.512	14.063	34.65^{XY}	0.55^{X}	
COD:VS							
	2	12	0.438	2.19	46.950^{A}	1.05^{A}	
	4	12	0.727	19.33	45.81^{A}	0.51^{B}	
	8	12	0.213	19.00	5.943^{B}	0.05^{C}	
P- value							
Magnetite concentration			0.0001	0.0001	0.0463	0.75	
Glucose concentration			0.0001	0.0001	0.0001	.0001	
Interaction							
(Magnetite x Glucose)			0.0001	0.0001	0.0872	0.48	

^{a,b,c,d,e,f} or ^{A,B,C} or ^{X,Y,Z} means in the same column with different superscripts are significantly different ($P < 0.05$). N: is the number of observation. Rate: The maximum methane production rate (mmole/g VS/d), The lag phase time (days), CMP: Maximum cumulative methane produced (mL CH_4), Methane yield: calculated at day 45 by dividing the cumulative mole of CH_4 with the total mole glucose added, R^2: 1- (residual sum of squares) / (corrected sum of squares).

The maximum methane production rate is related to both of the substrate concentration and the presence of magnetite. Increasing the substrate concentration of acetate and glucose up to 4 COD: 1 VS with the presence of magnetite enhanced the methane production rate as compared to increasing the substrate concentration in the absence of magnetite. Table 6.1 shows that the maximum methane production rate in the control bottles did not change significantly by increasing the concentration of acetate (1.152 and 1.32 mmole/g VS at COD:VS ratios of 2:1 and 4:1 respectively). Contrary to that, adding 2, 7 and 20 mM of magnetite at the acetate ratio of 4 COD: 1 VS significantly increased the maximum methane production rate 2 times, 2 times and 1.5 times, respectively, as compared to that at an acetate ratio of 2 COD: 1 VS. Table 6.3 shows that the maximum methane production rate in the control bottles did not change significantly by increasing the concentration of glucose (0.35 and 0.32 mmole/g VS at COD:VS ratios of 2:1 and 4:1 respectively). However, adding 2, 7 and 20 mM of magnetite at the glucose ratio of 4 COD: 1 VS significantly increased the maximum methane production rate 2.5 times, 1.5 times and 1.7 times, respectively, as compared to that at a glucose ratio of 2 COD: 1 VS.

The lag phase duration strongly depends on the substrate concentration; as the substrate concentration increases the lag phase increases. However, increasing the substrate concentration of acetate, propionate and glucose with the presence of magnetite did not increase the lag phase as much as that in the absence of magnetite. Table 6.1 shows that increasing the acetate COD:VS ratio from 4:1 to 8:1 resulted in a significant increase in the lag phase duration in the control bottles by 35 %. Furthermore, adding 2, 7 and 20 mM of magnetite at the acetate ratio of 4 COD: 1 VS significantly decreased the lag phase duration by 32.1 %, 7.7 % and 11.5 %, respectively, as compared to that at an acetate ratio of 8 COD: 1 VS. Table 6.2 indicates that increasing the propionate COD:VS ratio from 2:1 to 4:1 and then from 4:1 to 8:1 resulted in a significant increase in the lag phase duration from around 6 days and 10 days in the control bottles as compared to around 4.4 days and 6.3 in the magnetite-supplemented bottles respectively. Table 6.3 shows that increasing the concentration of glucose to 8 COD: 1 VS in the absence of magnetite increased the lag phase beyond the incubation period (i.e. no methane production was observed), as compared to that in presence of magnetite (methane was observed between 21 days and 30 days).

On the other hand, the overall results of the present study show that under a specific substrate concentration, magnetite has the ability to enhance the methane production rate (up to 59 % from acetate at 4 COD: 1 VS and 41.5 % from propionate at 8 COD: 1 VS) and reduce the lag phase duration (up to 59 % and 32 % in the acetate and propionate fed cultures respectively) as compared to the control. The positive effect of adding magnetite on enhancing the maximum methane production rate and reducing the lag phase in glucose-cultivated culture is also clear at ratio of 8 COD: 1 VS.

Increasing the concentration of acetate, propionate and glucose with the presence of magnetite enhanced the CMP as compared to increasing the concentration in the absence of magnetite. Table 6.1 also shows that increasing the concentration of acetate from 4 COD: 1 VS to 8 COD: 1 VS significantly increased the CMP by 47.2 % and 37.2 % in the magnetite supplemented and control bottles respectively. Table 6.2 shows that increasing the concentration of propionate from 4 COD: 1 VS to 8 COD: 1 VS significantly decreased the CMP by 7.2 % and 17 % in the magnetite supplemented and control bottles respectively. Table 6.3 shows that increasing the concentration of glucose from 2 COD: 1 VS to 4 COD: 1 VS significantly decreased the CMP by 30.8 % in the control bottles whereas no significant change in the CMP was observed in the magnetite-supplemented bottles. In addition, increasing the concentration of glucose from 4 COD: 1 VS to 8 COD: 1 VS the control bottles did not produce methane as compared to magnetite-supplemented bottles.

Furthermore, increasing the concentration of acetate, propionate and glucose decreased the methane yield in all bottles with and without the presence of magnetite.

On the other hand, the present results indicate that adding magnetite under a specific concentration of acetate and propionate increased the CMP and yield productions as compared to the control. This can be explained because in the acetate and propionate experiments, the analysis was stopped prematurely. It could be possible to produce more methane from the control bottles (no magnetite) to reach the same amount of methane in the magnetite-supplemented bottles.

The effect of increasing the substrate concentration on methane production is related to the magnetite concentration. Adding magnetite at concentrations of 2 mM, 7 mM and 20 mM was within a suitable concentration limit to have a positive effect on methane production. The main effect indicates that increasing the magnetite concentration from 2 mM to 7 mM and 20 mM did not show a significant difference in the maximum methane production rate, CMP and yield from acetate, propionate and glucose. On the other hand, adding 20 mM significantly shorted the lag phase as compared to 2 and 7 mM in acetate and glucose cultivated cultures. Table 6.1, Table 6.2 and Table 6.3 also show that a significant interaction between magnetite concentration and substrate (acetate, propionate and glucose) concentration ($P = 0.0001 < 0.05$) was relevant for the maximum methane production rate and lag phase duration. In addition, a significant interaction between magnetite concentration and substrate (acetate but not glucose) concentration was relevant for the CMP and yield. No significant interaction between magnetite concentration and propionate concentration was found for the CMP; however, a significant interaction for the yield was observed.

The results from this research are in agreement with several studies that have reported that adding conductive materials (such as magnetite, granular activated carbon, biochar and graphene) increase the methane production rate. For example, the maximum methane production rate from propionate was increased by~44 % (Jing et al., 2017) and 33 % (Cruz Viggi et al., 2014) with the addition of 4.5 mM and 25 mM of magnetite respectively. In addition, adding 20 mM of magnetite to enriched paddy soil (with 20 mM of acetate) led to a 33 % - 40 % acceleration in the methane production rate (Kato et al., 2012a). Furthermore, adding granular activated carbon to an anaerobic digester sludge fed by acetate produced a 1.8-fold methane rate higher than that of control (Lee et al., 2016). Similarly, an anaerobic digester sludge fed with glucose showed an increase of 51.4 % in the methane production rate when graphene was added to the medium (Tian et al., 2017) and of 21 % when the medium was supplemented with biochar (Luo et al., 2015) supplementations respectively. Cruz Viggi et al. (2014) supported the present findings, when they observed that adding magnetite resulted in a reduction of lag phase (10 %), as compared to the control. Furthermore, Yamada et al. (2015) reported that the time required for complete degradation of propionate was 67 % shorter in the presence of magnetite, as compared to the control. Enhancing

the methane production rate and reducing the lag phase in the presence of magnetite suggest that magnetite can serve as electrical conduits, which enable electrons to transfer between electron-donating and electron-accepting organisms more rapidly than in the absence of magnetite. Cruz Viggi et al. (2014) and Lin et al. (2018) confirmed this when they stated that magnetite and biochar in anaerobic digestion served as electrical conduits resulting in the highest maximum methane production rate and the shortest lag phase time. They supported that assertion by calculation of the theoretical electron carrier fluxes values for magnetite and graphene were 7.5×10^6 and 0.0004×10^6, respectively, higher than that via IET.

The results also indicate that the main observed effects of the substrate (acetate, propionate and glucose) concentration are an increase in the duration of the lag phase, an increase in CMP and a decrease in methane yield. However, increasing the COD:VS ratio of acetate and glucose up to 4:1 and of propionate up to 8:1 enhances the maximum methane production rate. This can be explained in that compared to low substrate concentrations, when high substrate concentrations are added, microorganisms need more time to adjust to the high substrate concentration and produce methane. This results in extension of the lag phase. Once the microorganisms adjusted to the new environment, they start to produce methane rapidly (a higher methane production rate) and as a result large amounts of methane are produced at the end of the incubation time (CMP). However, the total amount of methane was lower than the predicted value (thermodynamically) and this result in a decrease in the methane yield (mmole methane per mmole substrate).

Cruz Viggi et al. (2014) revealed that testing magnetite without an external substrate showed that the methane production rate was higher in the absence of magnetite than in their presence. Other studies have shown that in the presence of magnetite, the methane production rate increased with increasing the concentration of acetate and propionate up to 50 and 20 mM respectively; whereas when substrate concentrations were increased above those limits, no significant enhancement in methane production rate was observed (Yang et al., 2015b; Yang et al., 2016).

The above results suggest that in the presence of magnetite, a substrate would enhance performance of methane production by serving as electrical conduits if the substrate was provided within a suitable concentration range (minimum concentration – maximum concentration).

On the other hand, it has been reported that excessively increasing the substrate concentration can cause a rapid pH drop and inhibit methanogen activity thus reducing methane production (Fang and Liu, 2002; Jiang et al., 2012). This was clearly seen in Figure 6.6, which presented the measured pH values at day 45 of the liquid medium in the serum bottles that contained glucose as a substrate. It also shows that increasing the concentration of glucose from 2:1 to 4:1 resulted in a pH drop from 6.9 to 6.5 in the magnetite-supplemented bottles, as compared to a pH drop from 6.88 to 5.53 in the control bottles. In addition, increasing the concentration of glucose to 8:1 resulted in a pH drop to an average of 4.7 and 4.44 in the magnetite supplemented and control bottles respectively. This indicates that when increasing the glucose concentration up to 4 COD: 1 VS, adding magnetite keeps the pH close to 7. However, the glucose concentration of 8 COD: 1 VS is a critical concentration (too high), even in the presence of magnetite, to produce methane.

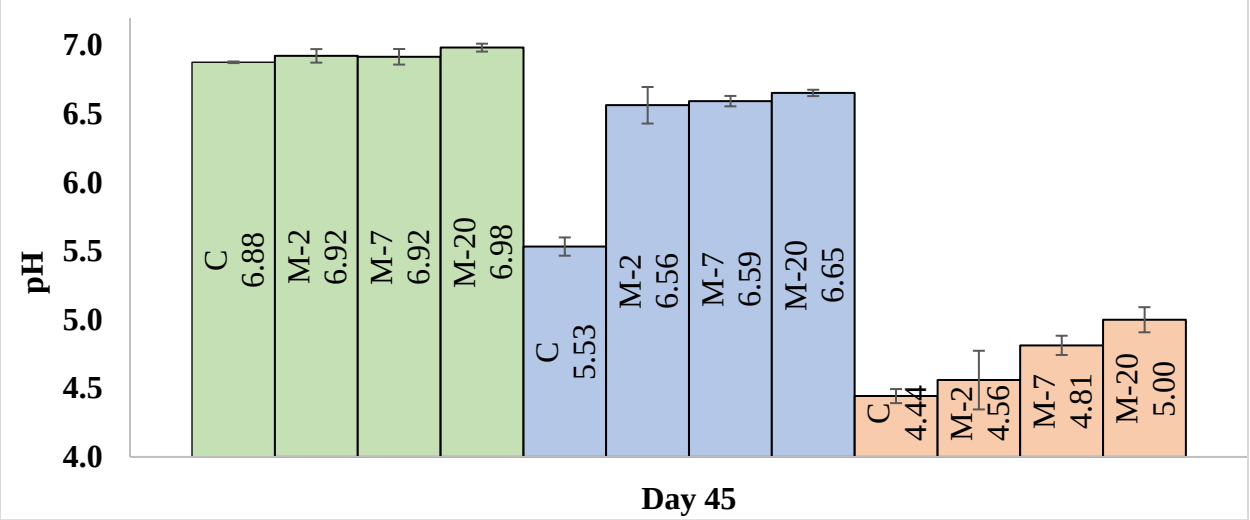

Figure 6.6. The pH value of liquid medium in the serum bottles that contained glucose as a substrate. pH was measured at day 45 (the end of incubation). C, M-2, M-7 and M-20 present the pH value in the control, magnetite of 2 mM, magnetite of 7 mM and magnetite of 20 mM bottles respectively. The green, blue and pink columns present the COD:VS ratios of 2:1, 4:1 and 8:1 respectively.

6.2.3 Potential of Adding Magnetite to Enhance the Methane Production from Different Substrate Types

To study the effect of substrate type on methane production in the presence of magnetite, the substrate ratio of 4 COD: 1 VS was selected as a case study. Data was presented as mean ± standard deviations (of triplicates). As the experiment had three levels of substrate types (acetate, propionate, and glucose) and three levels of magnetite concentrations (2, 7, and 20 mM), the data was evaluated by 2 × 3 factorial arrangement through statistical analysis of two-way of variance (ANOVA) using the general linear model (GLM) procedure of SAS (2015). The data was analyzed by two-way ANOVA to determine the main effects and their interaction. Differences were considered to be significant at $P < 0.05$ and significant differences between means were separated by Least Significant Difference tests.

The methane production kinetic parameters in the magnetite-supplemented bottles (2, 7 and 20 mM) using 4 COD: 1 VS of acetate (50 mmole/L), 4 COD: 1 VS of propionate (54 mmole/L) and 4 COD: 1 VS of glucose (31 mmole/L) were statistically analyzed.

Table 6.4 shows that the substrate type had a significant effect on the maximum methane production rate, the lag phase, the CMP and the yield ($P < 0.05$). In addition, a significant interaction between magnetite concentration and substrate type was relevant for the maximum methane production rate and the lag phase.

Table 6.4. The effect of substrate type on methane production kinetic parameters.

Main effect	**Rate (mmole/g VS/d)**	**Lag (day)**	**CMP (mL CH_4)**	**Yield**
Substrate type				
Acetate	1.9122^{a}	2.8848^{a}	62.5167^{b}	0.4333^{b}
Propionate	0.5800^{c}	8.7962^{b}	70.4604^{a}	0.4518^{b}
Glucose	0.8633^{b}	22.111^{c}	48.5756^{c}	0.5411^{a}
Standard error	0.065	0.671	1.979	0.021
P- value				
Magnetite concentration	0.0014	0.0001	0.7482	0.779
Substrate type	0.0001	0.0001	0.0001	0.0001
Interaction Magnetite concentration x Substrate type	0.003	0.0001	0.1881	0.513

^{a,b,c} means in the same column with different superscripts are significantly different ($P < 0.05$).

The highest value of the maximum methane production rate in the presence of magnetite was observed when acetate was used (1.9122 mmole/g VS), as compared to propionate and glucose. In addition, Table 6.4 shows that the time needed to observe the production of methane (the lag phase time) increased from 2.88 days to 8.79 and 22.11 days when acetate ($C_2H_3O_2$), propionate ($C_3H_6O_2$) and glucose ($C_6H_{12}O_6$) were used respectively. These results indicate that organic material with a low number of carbon atoms produce methane more quickly than substrates containing a greater number of carbon atoms. More specifically, acetate and propionate can be directly used by methanogens whereas glucose needs to be transformed through metabolic pathways into acetate and propionate before being used as a substrate by methanogens. Yamada et al. (2015) support this observation since their results show that under the same conditions of magnetite supplementation, the degradation of acetate was completed after 15 days, compared to 50 days for propionate. Methane production when magnetite was introduced with acetate was 70 % faster than with propionate. Guo-Qin et al. (2016) stated that; since acetate changes relatively quickly to acetic acid; the hydrogen-producing acetogenic microorganisms are very active providing lots of extracellular matrix for methanogens to use acetic acid to produce methane. This

makes methane production in acetate-cultivated cultures easier than that in propionate and glucose cultivated cultures.

Table 6.4 shows that the cumulative methane production was significantly higher for propionate as compared to acetate and glucose. In addition, the methane yield was calculated as mmole methane at the end of the incubation period per mmole of initial substrate added. The theoretical methane yield is derived from the equations for acetate degradation $CH_3COO^- + H_2O \rightarrow CH_4 + HCO_3^-$, $\Delta Go' = -31\,KJ/mol$ (Yang et al., 2015b), propionate degradation $4CH_3CH_2COO^- + 4H^+ + 2H_2O \rightarrow 7CH_4 + 5CO_2$, $\Delta Go' = 76\,KJ/mol$ (Cruz Viggi et al., 2014) and glucose degradation $C_6H_{12}O_6 + 3H_2O \rightarrow 3HCO_3^- + 3CH_4 + 3H^+$, $\Delta Go' = -16.8\ KJ/mol$ (Nakano and Zuber, 2004). As shown on Table 6.4, the methane yield from acetate was twice as low as the theoretical (0.433 vs 1), 4 times lower than the theoretical value for propionate (0.4518 vs 1.75), and 6 times lower than the theoretical value for glucose (0.5411 vs 3). The theoretical value is generally calculated according to the assumption that the substrate is totally consumed; whereas, the actual value was calculated at specific time (days) (for acetate at day 30, propionate at day 54 and glucose at day 45). This means that not all the substrate had been degraded by the time the incubations periods were stopped.

6.3 Theoretical Calculation of Interspecies Electron Transfer via H_2 Diffusion and via Magnetite-DIET

In the present study, acetate and propionate were investigated for establishing DIET via magnetite in AD. For the calculations using acetate as a substrate, the following reactions apply (Fotidis et al., 2014):

$\text{Acetate}^- + 4H_2O \rightarrow 2HCO_3^- + 9\,H^+ + 8\,e^-$ $\qquad \Delta G_O' = +104.6\,kJ$

$8\,e^- + HCO_3^- + 9\,H^+ \rightarrow CH_4 + 3H_2O$ $\qquad \Delta G_O' = -135.6\,kJ$

For the calculations using propionate as a substrate, the following reactions apply:

$4\ \text{Propionate}^- + 12H_2O \rightarrow 4\ \text{Acetate}^- + 4\ HCO_3^- + 24e^- + 28\ H^+$ $\qquad \Delta Go' = +304.4$ kJ

$27\ H^+ + 3\ HCO_3^- + 24e^- \rightarrow 3\ CH_4 + 9\ H_2O$ $\qquad \Delta Go' = -408$ kJ

Table 6.5 shows the values of theoretical calculation of interspecies electron transfer via H_2 diffusion and via Magnetite-DIET based on Fick's diffusion law and the Nernst equation as reported by Cruz Viggi et al. (2014) and Lin et al. (2018). These calculations were done under several assumptions. Namely, an inter bacterial distance of 5 $x10^{-7}$ m, an average cell diameter of 2 x 10^{-6} m for both acetogens and methanogens, spherical shape for both types of bacteria, the electrons released are transferred to methanogens via an electron conduit consisting of magnetite particles, the electrical conduit was assumed to be a wire, and the concentration of the reactants and products were used as reported in the literature.

The maximum electron transfer via H_2 was calculated based on Fick's diffusion law

$$i = D_f * \frac{S_{cell}}{d} * \left([H_2]_{Highest} - [H_2]_{Lowest}\right) * n * F$$

where D_f : Diffusion coefficient of H_2 in water; 4.5 $x10^{-9}$ m^2/s, S_{cell} : Surface area of the cell; (spherical with diameter of 2 x 10^{-6} m) 1.268 $x10^{-11}$ m^2, d : Distance between cells; 5 $x10^{-7}$ m, n : Mol of electron per mole of H_2, F : Faraday's constant; 96485 s*A/mol, $\Delta G^{ó}$: Standard Gibbs free energy change per reaction, R: 0.00831451 kJ/mol/K, and T: 308.15 K.

The maximum electron transfer via magnetite - DIET was calculated based on the Nernst equation;

$$i = \sigma * \frac{S_{conduit}}{d} * (E_{met} - E_{ace})$$

$$(E_{met} - E_{ace}) = {-\Delta G'}/{n * F}$$

where σ : Electrical conductivity of magnetite; 2.5 x 10^6 Ω/m^2, $S_{conduit}$: Cross-sectional area of the conductive material; (a wire with diameter of 168 – 490 $x10^{-9}$ m), d : Distance between cells; 5 $x10^{-7}$ m, n : mol of electron per reaction, F : Faraday's constant ; 96.485 kJ/mol.V, $\Delta G^{ó}$: Standard Gibbs free energy change per reaction, R: 0.00831451 kJ/mol/K, and T: 308.15 K.

A sample of the theoretical calculation of interspecies electron transfer via H_2 diffusion and via magnetite-DIET is illustrated in Appendix G.

Table 6.5. Theoretical calculation of DIET/IET

Parameters	Substrate	
	Acetate	Propionate
$\Delta G^{O'}_{Oxidation}$	+104.6	+304.4
$\Delta G^{O'}_{Reduction}$	-136	- 408
$\Delta G^{O'}_{Overall}$	-31.4	- 103.6
$[HCO^-_3]$	0.03 M	0.03 M
$[C_2H_3O_2^-]$	0.0005 M	0.0005 M
$[C_3H_5O_2^-]$	X	0.005 M
$[CH_4]$	2.04×10^{-5} M	2.04×10^{-5} M
$[H_2]_{Highest}$	0.0226 mol/m^3	0.2494 mol/m^3
$[H_2]_{Lowest}$	0.00018 mol/m^3	0.00018 mol/m^3
Mole of electron per reaction	8	24
Mole of H_2	4	12
ΔE	0.0622 V	0.09 V
Flux via IET	49.5×10^{-11} A	549×10^{-11} A
Flux via $DIET_{(small\ magnetite\ size)}$	2.47×10^{-5} A	3.69×10^{-5} A
Flux via $DIET_{(medium\ magnetite\ size)}$	26.7×10^{-5} A	39.9×10^{-5} A
Flux via $DIET_{(large\ magnetite\ size)}$	1730×10^{-5} A	2950×10^{-5} A
$DIET_{(small\ magnetite\ size)}$/ IET	0.0498×10^6	0.00672×10^6
$DIET_{(medium\ magnetite\ size)}$/ IET	0.539×10^6	0.0727×10^6
$DIET_{(large\ magnetite\ size)}$/ IET	35×10^6	4.72×10^6

The ratio between electrons transfer via DIET and via H_2 diffusion for acetate and propionate were 0.539×10^6 and 0.0727×10^6 respectively. On one hand, this indicates that magnetite can serve as electrical conduits and enable the electrons to transfer faster. On the other hand, these results are in agreement with the results of the main effect of acetate and propionate (Table 6.4). The maximum methane production rate in acetate cultivated culture was 4 times, as compared to the maximum methane production rate in propionate cultivated culture. This confirms that acetate degrades more quickly as compared to propionate (Section 6.2.3). In addition, as the size of magnetite increaded the DIET flux increase, however that was not in agreement with the obtained results (Section 5.2.2). This may be due to the size ratio between the particles and the bacterial

cells, which might play a role and put a limit to the particle size that promotes DIET. These results suggest that adding magnetite to an anaerobic digester may significantly enhance the ability of anaerobic digestion to produce methane at a faster rate than conventional methods.

6.4 Conclusion

The magnetite performance depends on the substrate types and concentrations as well as the magnetite concentration. The COD:VS ratio of 4:1 was the best to produce the maximum methane production rate in the presence of magnetite from acetate (on average 2.0735 mmole/g VS/d) and glucose (1.08 mmole/g VS/d). Whereas the COD:VS ratio of 8:1 was the best to produce the maximum methane production rate from propionate (on average 0.612 mmole/g VS/d). The findings of this chapter indicate that increasing the acetate COD:VS ratio from 4:1 to 8:1 in the presence of 2, 7 and 20 mM of magnetite resulted in shortening the lag phase by a significant amount (32.1 %, 7.7 % and 11.5 % respectively). In addition, increasing the propionate COD:VS ratio from 2:1 to 4:1 and then from 4:1 to 8:1 resulted in a significant increase in the lag phase duration around 4.4 days and 6.3 days, respectively, in the magnetite-supplemented bottles.

Acetate produced the highest value of the maximum methane production rate in the presence of magnetite as compared to that from propionate and glucose. The theoretical calculations of electrons flux indicate that magnetite can serve as electrical conduits and enable the electrons to transfer faster by at least 10^6 for both acetate and propionate, as compared to electron transfer in the control.

Finally, the results indicate that methane production from glucose at 8 COD: 1 VS is critical even in the presence of magnetite, as compared to glucose COD:VS ratios of 4:1 and 2:1. This relates to a pH drop to an average 4.7 – 4.4 by increasing the glucose concentration up to 8 COD: 1 VS. It is concluded that magnetite cannot easily stimulate methane production from glucose at a high concentration. As such, the potential for using magnetite for enhancing glucose degradation is still unclear and needs further investigation.

CHAPTER 7. EFFECT OF MAGNETITE ON METHANE PRODUCTION FROM GLUCOSE AT DIFFERENT CONCENTRATIONS

7.1 Objectives and Experimental Setup

Although glucose has been used as a substrate to study the methane potential associated with adding several conductive materials, magnetite has not been used to enhance the methane production in the present of glucose. The previous experimental results indicated that magnetite did not stimulate methane production from glucose at 8 COD: 1 VS (as compared to COD:VS ratios of 2:1 and 4:1). To further investigate the potential of adding magnetite to enhance methane production from glucose, however, batch tests were conducted by adding 0, 2, 7 and 20 mM of medium-magnetite at two different concentrations of glucose corresponding to initial COD:VS ratios of 3:1 and 6:1 while the volatile solids (VS) concentration was fixed in all bottles at 1.5 g/L. All anaerobic batch tests were run in triplicate. The experimental design is shown in Figure 7.1.

Data was presented as mean ± standard deviation of triplicates. As the experiment had two levels of glucose concentrations (COD:VS of 3:1 and 6:1) and four levels of magnetite concentrations (0, 2, 7, and 20 mM), the data was evaluated in a 2 × 4 factorial arrangement through statistical analysis of two-way of variance (ANOVA) using a general linear model (GLM) procedure of SAS (2015). The data was analyzed by two-way ANOVA to determine the main effects and their interaction. Differences were considered to be significant at $P < 0.05$ and significant differences between means were separated by Least Significant Difference tests.

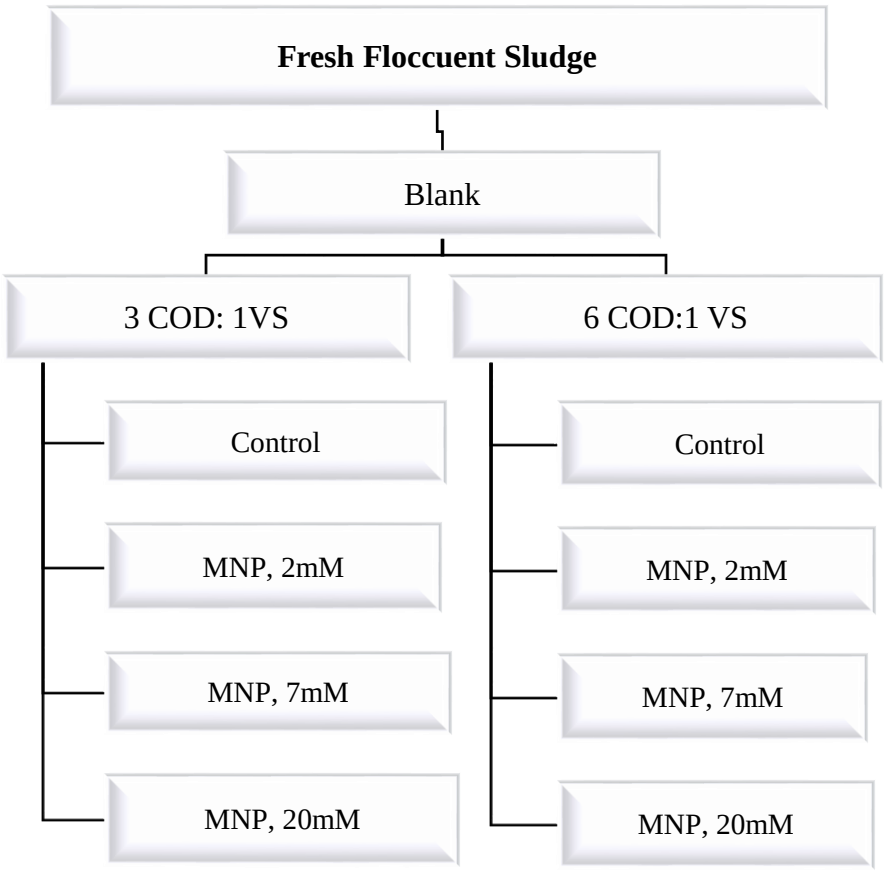

Figure 7.1. Experiment design to investigate the potential of adding magnetite to enhance the glucose degradation. The volatile solid (VS) in all batch experiments was 1.5 g/L. Blank bottles did not have magnetite or glucose, Control bottles had glucose and no magnetite and finally MNP bottles had both magnetite and glucose.

7.2 Results and Discussion

Blank bottles (no magnetite and no substrate) produced methane and reached a maximum of 3.26 ± 0.09 mmole/g VS. This amount was too low so it was neglected (Figure 7.2).

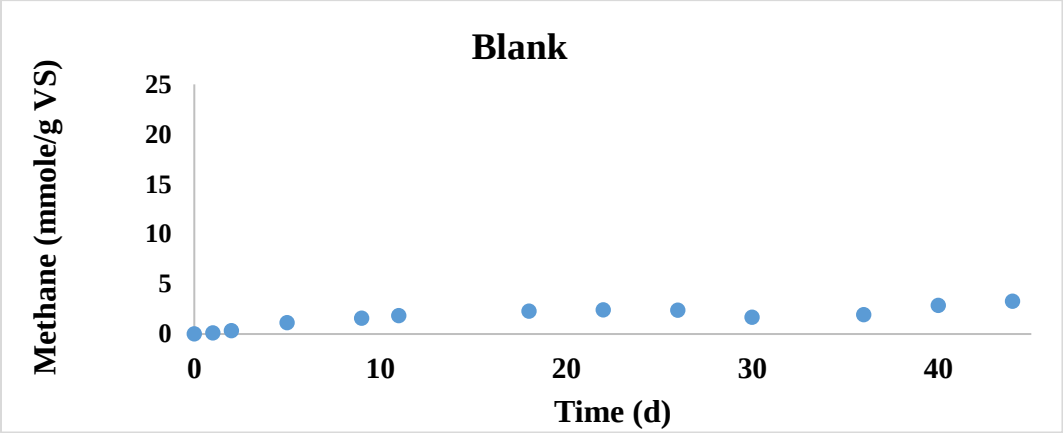

Figure 7.2. Methane production profile from blank bottles where no magnetite and no glucose were added to the bottles.

7.2.1 Methane Production Profile from Glucose

The methane production profiles from glucose at different concentrations is shown in Figure 7.3. The profiles (mmole CH_4/g VS) indicate that the methane production in all bottles started at day 25 and reached a plateau at day 40 at 2.8 g/L of glucose concentration (3 COD: 1 VS) whereas it started after 28 days in all bottles at 5.8 g/L of glucose concentration (6 COD: 1 VS). However, at the different glucose concentrations, the highest production of methane was observed in the 7 mM and 20 mM magnetite-supplemented bottles. On the other hand, Figure 7.3 shows that an increase in the glucose concentration up to a 6:1 COD:VS ratio, inhibited the methane production in all bottles as compared to 3 COD: 1 VS. This indicates that both the concentration of glucose as well as the magnetite concentration have a direct effect on methane production.

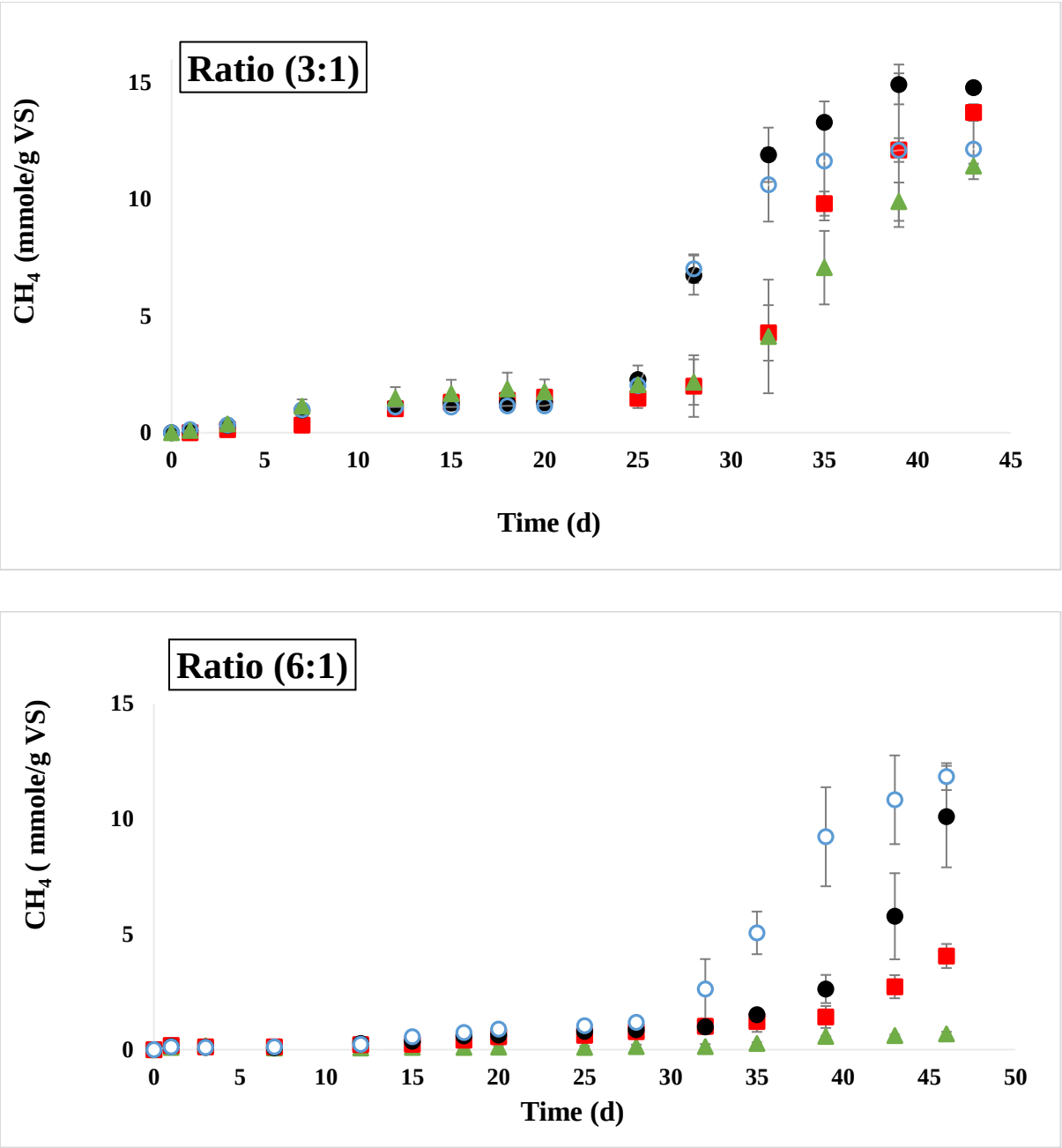

Figure 7.3. Methane production from glucose over the incubation time. Ratio (3:1) and Ratio (6:1) represent methane production from glucose at 3 COD: 1 VS and 6 COD: 10 VS ratios respectively. The symbols ▲, ■, ●, and o represent the control, 2 mM of magnetite, 7 mM of magnetite, and 20 mM of magnetite respectively. Error bars represent the standard deviation of triplicate experiments.

7.2.2 Potential of Adding Magnetite to Enhance the Methane Production at Different Glucose Concentrations

Table 7.1 presents the methane production kinetic parameters in terms of maximum methane production rate (mmole/g VS/ d), lag phase duration (day), maximum cumulative methane production (mL) and methane yield (mole methane produced per mole substrate added). Table 7.1 shows that the coefficient of determination (R^2) values (obtained by fitting a modified Gompertz model to the experimental methane-accumulation curves by non-linear regression using SPSS software) were between 0.95 – 0.99. This indicates that a non-linear regression fits the data in comparison to the simple average. Table 7.1 also shows the standard deviation (SD) and standard error (SE) for each methane parameter (rate, lag phase, cumulative methane produced and yield).

The maximum methane production rate decreased when the glucose concentration was increased from 3 COD: 1 VS to 6 COD: 1 VS; however, the reduction in the maximum methane production rate in the presence of magnetite was less than that in the absence of magnetite. Table 7.1 indicates that the interaction between magnetite concentration and glucose concentration for the maximum methane production rate is 0.680 (higher than 0.05) and in this case the superscripts (a,b) are shown at the main effect values. Table 7.1 shows that by increasing the glucose COD:VS ratio, the maximum methane production rate significantly decreased by 1.7 times and 1.9 times in the 7 and 20 mM of magnetite-supplemented bottles, respectively; whereas it significantly decreased by 7.6 times in the control bottles.

The lag phase duration strongly depends on the substrate concentration; as the substrate concentration increases the lag phase increases. However, the increase in the lag phase duration with the presence of magnetite was less than that in the absence of magnetite. Table 7.1 shows that increasing the glucose concentration from 3 COD: 1 VS to 6 COD: 1 VS significantly extended the lag phase in the range of 2 to 11 days in the magnetite-supplemented bottles; whereas the lag phase was significantly extended by 24 days in the controls.

On the other hand, the present results indicate that magnetite under a specific glucose concentration, significantly increases the maximum methane production rate and reduces the lag phase as compared to the control. Table 7.1 shows that in the magnetite-supplemented bottles (at 7 and 20 mM), the methane production rate from glucose at a COD:VS ratio of 3:1 was 1.5-fold and 2-fold respectively as compared to the control. In addition, it was 9.2-fold and 9.5-fold respectively at 6 COD: 1 VS, as compared to the control. However, 2 mM of magnetite did not show any enhancement at both COD:VS ratios, as compared to the control. In addition, Table 7.1 shows that the lag phase time in all the magnetite-supplemented bottles was significantly shorter (on average 4 days at 3 COD: 1 VS and (16.8 - 25.5 days) at 6 COD: 1 VS), as compared to the control bottles.

Table 7.1. The effect of magnetite addition on methane production kinetic parameters from glucose at two different concentrations

Item			Methane Parameters				
COD: VS	**Magnetite concentration (mM)**	**N**	**Rate mmole /g VS /d**	**Lag (day)**	**CMP (mL)**	**Yield**	**R^2**
3:1							
	0	3	0.91 ± 0.43	28.33 ± 1.53^{c}	62.93 ± 5.81^{a,b}	0.93 ± 0.09^{a}	0.98
	2	3	1.31 ± 0.07	24.00 ± 1.00^{d}	66.75 ± 1.43^{a,b}	0.99 ± 0.02^{a}	0.97
	7	3	1.79 ± 0.07	24.00 ± 0.00^{d}	61.74 ± 2.11^{a,b}	0.92 ± 0.03^{a}	0.99
	20	3	2.10 ± 0.18	24.00 ± 0.00^{d}	60.17 ± 5.56^{a,b}	0.89 ± 0.08^{a}	0.99
6:1							
	0	3	0.12 ± 0.04	52.12 ± 3.35^{a}	2.96 ± 0.38^{e}	0.02 ± 0.00^{c}	0.95
	2	3	0.18 ± 0.03	26.59 ± 1.82^{c,d}	17.29 ± 2.49^{d}	0.13 ± 0.02^{c}	0.97
	7	3	1.08 ± 0.73	35.30 ± 2.55^{b}	43.76 ± 17.46^{c}	0.32 ±0.13^{b}	0.98
	20	3	1.12 ± 0.25	29.92 ± 1.04^{c}	51.27 ± 2.53^{b,c}	0.38 ±0.02^{b}	0.98
Standard Error			0.185	1.030	4.024	0.037	
Main effect							
Magnetite concentration							
	0	6	0.516^{b}	40.23	32.95	0.478	
	2	6	0.741^{b}	24.96	42.02	0.561	
	7	6	1.434^{a}	29.65	52.75	0.621	
	20	6	1.612^{a}	26.95	55.72	0.637	
Glucose concentration							
	3:1	12	1.528^{a}	25.08	62.9	0.93	
	6:1	12	0.624^{b}	35.98	28.82	0.215	
P- value							
Magnetite concentration			0.0001	0.0001	0.0001	0.0001	
Glucose concentration			0.0001	0.0001	0.0001	0.024	
Interaction (Magnetite x Glucose)			0.680	0.0001	0.0001	0.0001	

^{a,b,c,d,e} means in the same column with different superscripts are significantly different ($P < 0.05$). N: is the number of observation. Rate: The maximum methane production rate (mmole/g VS/d), The lag phase time (days), CMP: Maximum cumulative methane produced (mL CH_4), Methane yield: calculated at day 43 by dividing the cumulative mole of CH_4 with the total mole glucose added, R^2: 1-(residual sum of squares) / (corrected sum of squares).

Others have reported that the addition of magnetite increased the maximum methane production rate by 15.4 % and reduced the lag phase by 13.9 % (Yin et al., 2017). Similarly, Luo et al. (2015) found that biochar addition significantly increased the maximum methane production rate by 87 %, 21 %, and 5.2 % and reduced the lag phase by 11 %, 30 % and 22 % at 4, 6 and 8 g/L glucose concentrations, respectively. In addition, Tian et al. (2017) revealed that the relative methane production rate from glucose was enhanced by up to 51.4 % with adding nano-graphene, as compared to the control. It has also been reported that the methane conversion efficiency increases by adding conductive materials to anaerobic digesters (Dang et al., 2016). For example, Namal (2019) calculated methane conversion efficiencies and found that the methane conversion efficiency using magnetite was higher (94 % vs 85 %) as compared to a control which is indicative of increased DIET mechanism by magnetite addition. Cruz Viggi et al. (2014) confirmed that higher electron transfer efficiency occurs when magnetite is added. Lin et al. (2018) stated that by adding biochar, electrons are transferred between electron-donating and electron-accepting organisms more rapidly (10^6 faster as compared to the control). These observations are in agreement with the results Section 6.2 where the ratio between electrons transfer via DIET and via H_2 diffusion for propionate and acetate were 0.208 x 10^6 and 0.5 x 10^6 respectively.

Increasing the concentration of glucose decreased the CMP and the methane yield; however, the reduction was less with magnetite addition as compared to the control. Table 7.1 shows that the reduction in CMP and methane yield were17.98 mL and 0.6 mole methane produced per mole glucose added in the 7 mM and 20 mM of magnetite-supplemented bottles; whereas the reduction in CMP and methane yield were 59.97 mL and 0.91 mole methane produced per mole glucose added in the control bottles. This agrees with a recent study showing that a low concentration of glucose (20 %) was more efficient for methane production; while increasing the glucose concentration up to 80 % resulted in a methane yield reduction by 42 % (Guo-Qin, Fang et al. 2016). At the same time, the calculated values for the main effect were 0.934 and 0.215 mole methane / mole glucose added for 3 COD: 1 VS and 6 COD: 1 VS, respectively, which are less than the theoretical value (3 mole methane / mole glucose consumed). This difference relates to the methane yield at day 43, which may not be enough time to degrade the glucose completely into methane, as compared to the theoretical value which assumes all the glucose is degraded.

On the other hand, Table 7.1 indicates that under a specific glucose concentration of 3 COD: 1VS, no statistical difference in the CMP (on average 62.92 ± 2.73 mL CH_4) and methane yield (on average 0.93 ± 0.04) between magnetite and control was observed ($p > 0.05$). At 6 COD: 1 VS, the cumulative production of methane and yield were significantly lower in the control, as compared to the magnetite-supplemented bottles. Chapter 6 agrees with these results, as discussed previously in Section 6.2.2.

Table 7.1 indicates that the effect of magnetite on methane production from glucose depends not only on the glucose concentration but also on the magnetite concentration. The overall results of Table 7.1 indicate that adding 7 mM and 20 mM of magnetite significantly enhanced the maximum methane production rate, CMP and methane yield as compared with adding 2 mM of magnetite. In addition, a significant interaction between magnetite concentration and glucose concentration was relevant for the lag phase, CMP and methane yield.

To study the effect the of adding magnetite (7 mM) and glucose concentration (3 COD: 1VS and 6 COD:1 VS) on the methane production, the glucose concentration over the incubation time, the volatile fatty acid and pH were measured in the control that was conducted without magnetite and the magnetite-supplemented bottles that had 7 mM of medium-sized magnetite.

7.2.2.1 Glucose Concentration over Time

The results of the glucose concentration in the anaerobic serum bottles after 7 and 14 days of the incubation are shown in Figure 7.4. It is apparent that the glucose was fermented after a week into simple molecules in the presence of magnetite and that fermentation was 23.64 % faster at 3 COD: 1 VS and 55.32 % faster at 6 COD: 1 VS, as compared to the control. Fig 7.4 (a) also shows that the glucose amount was completely fermented after 14 days in all the bottles except the control bottles which still had 0.006 mg/L of glucose at ratio of 3 COD: 1 VS.

These results indicate that magnetite has the ability to enhance the degradation of glucose over a two week period agreeing with the hypothesis of faster degradation of glucose to smaller organic compounds as observed by Liu et al. (2012b).

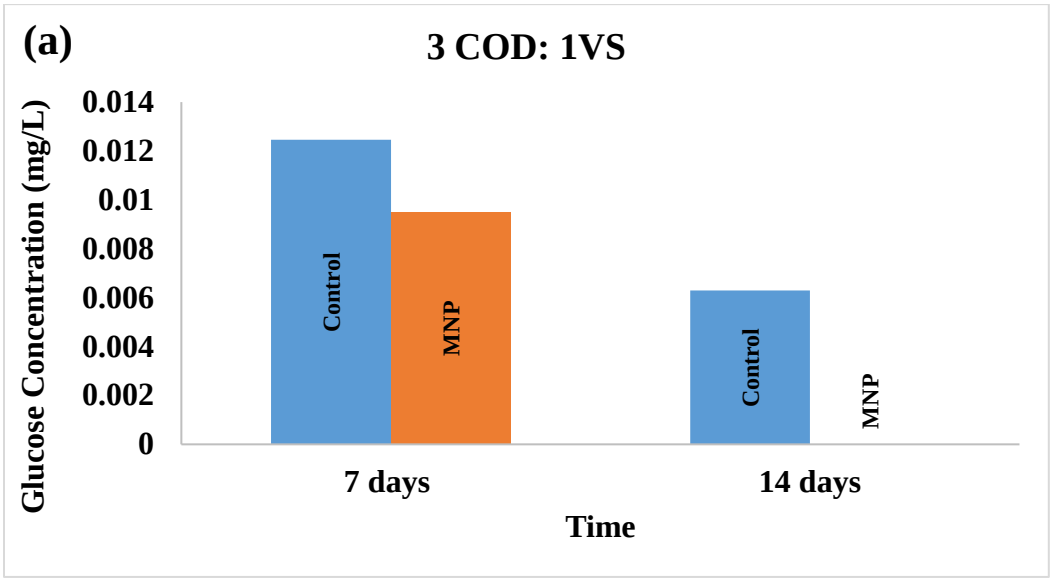

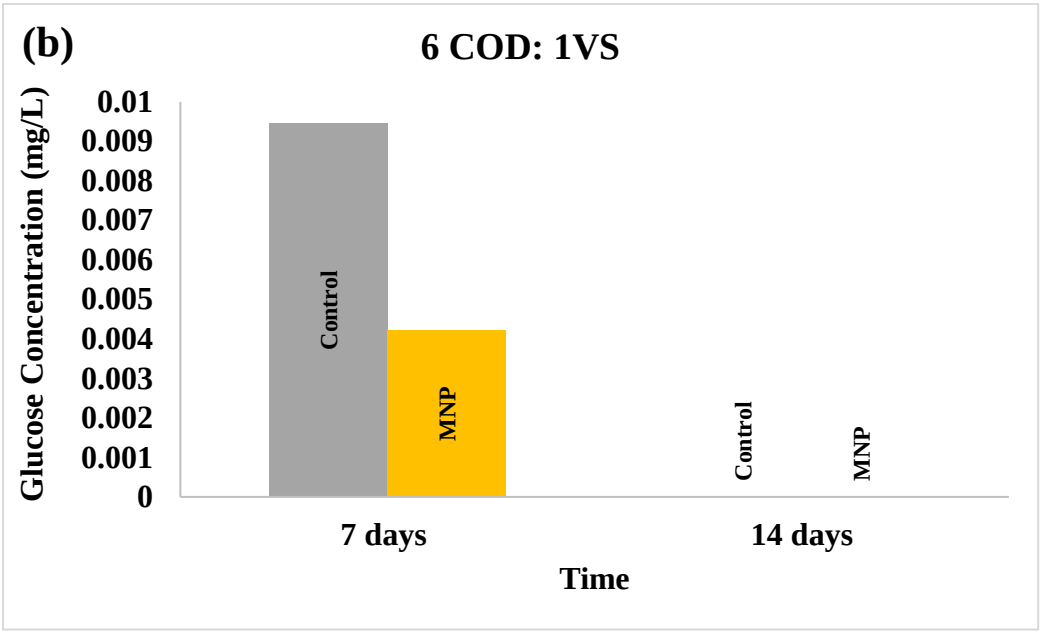

Figure 7.4. Glucose concentration in the anaerobic serum bottles. (a) and (b) represent the glucose at 3 COD: 1 VS and 6 COD: 1 VS respectively. The control was run without magnetite while the magnetite-supplemented bottles had 7 mM of medium-sized magnetite.

7.2.2.2 VFA Production

Figures 7.5 and 7.6 indicate that propionate and acetate were the major VFAs, accumulated during the glucose degradation over 52 days of incubation. Butyrate, however, was observed only in the control bottles at day 45 as shown in Figure 7.7.

Volatile fatty acid accumulation was substantially less in the presence of magnetite; however, the amount of accumulation was also directly related to the glucose concentration. As shown in Figure 7.5, in the presence of magnetite, propionate reached a peak concentration higher and earlier (4660 mg/L after 25 days vs 2700 mg/L after 28 days) before being completely degraded (day 45 vs day 52), as compared to the control. As well, acetate reached a peak concentration higher and earlier (322 mg/L after 25 days vs 259 mg/L after 28 days) indicative of faster production from glucose. The acetate was depleted sooner (day 39 vs day 45), as compared to the control ,indicative of faster conversion into methane.

In contrast, when the glucose concentration was increased to 6 COD: 1 VS (Figure 7.6); the propionate concentration was similar in all bottles reaching a peak at day 28. After that, it was degraded faster in the magnetite-supplemented bottles, as compared to the control. The acetate concentration was higher in the control (until day 28) and after that the acetate concentration peak was similar in all bottles (700 mg/L) and then was depleted faster in the magnetite-supplemented bottles, as compared to the control. Although increasing the glucose concentration resulted in VFA accumulation (Figure 7.6), the propionate concentration in the magnetite-supplemented bottles was around 66.7 % lower (600 vs 1802 mg/L at day 52), as compared to the control. In addition to all these results, butyrate (Figure 7.7) was observed at day 45 in the control bottles (28.6 mg/L at 3COD: 1 VS and 406.2 mg/L at 6 COD: 1 VS).

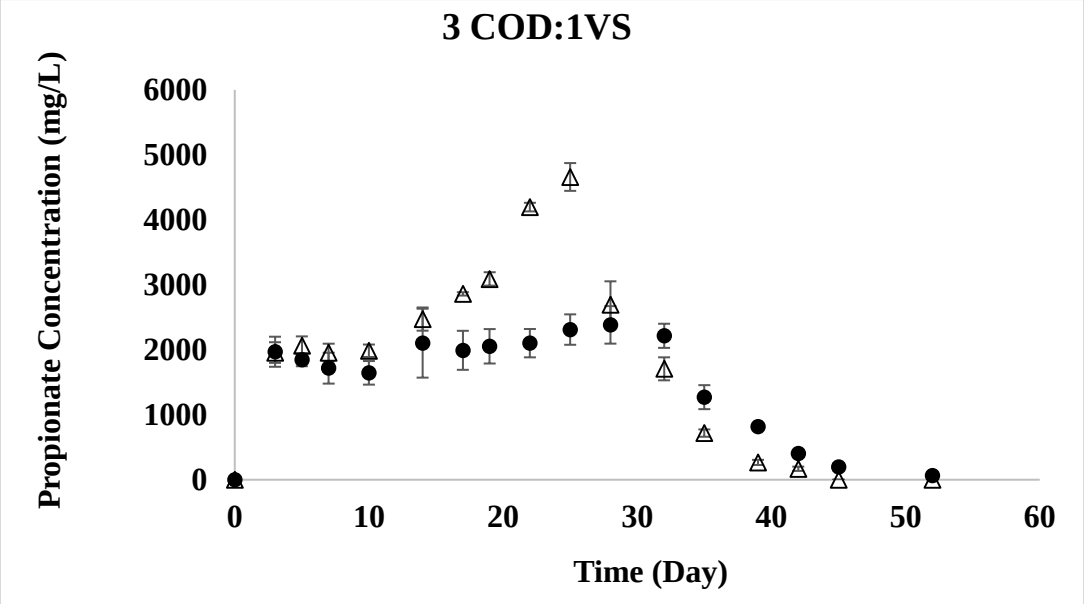

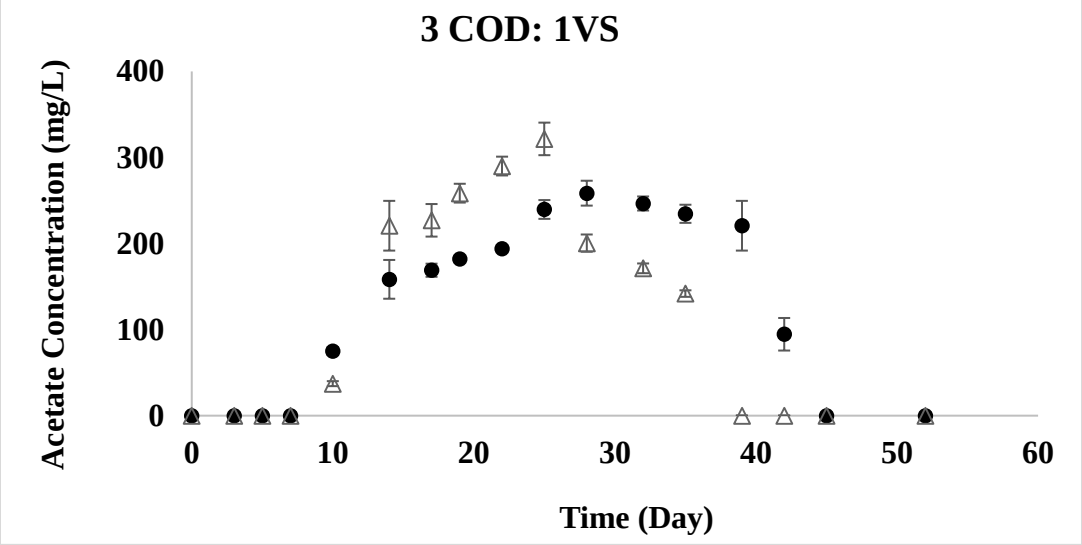

Figure 7.5. Propionate and acetate concentrations as mg/L over 60 days of anaerobic serum bottles cultivated by glucose at 3 COD: 1 VS. The symbols ● and Δ represent the control and 7 mM of magnetite respectively.

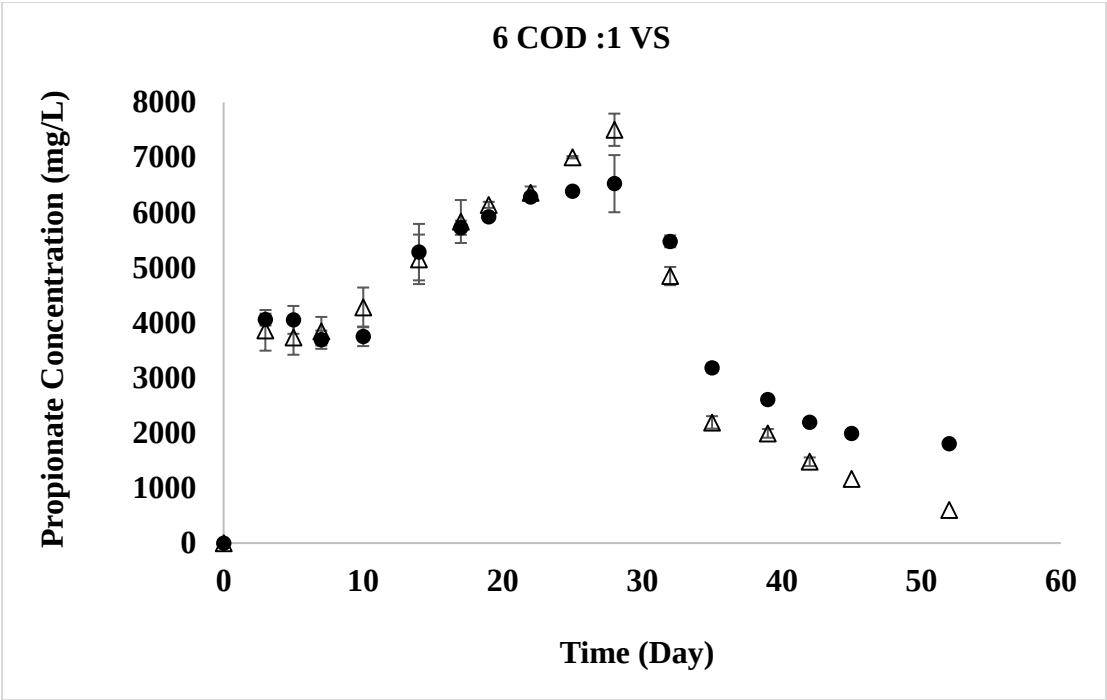

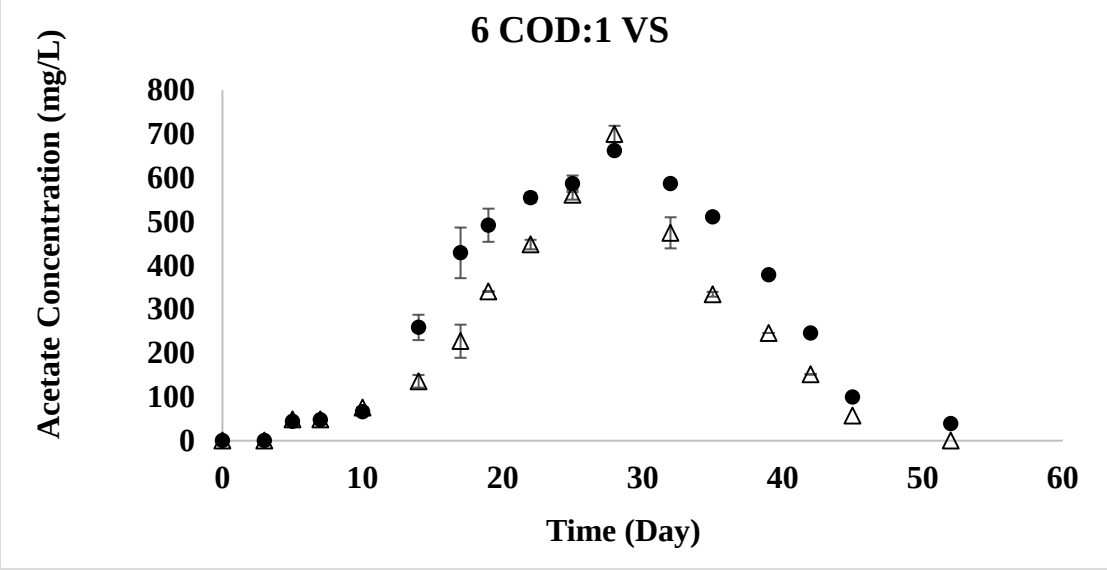

Figure 7.6. Propionate and acetate concentrations as mg/L over 60 days of anaerobic serum bottles cultivated by glucose at 6 COD: 1 VS. The symbols ● and Δ represent the control and 7 mM of magnetite respectively.

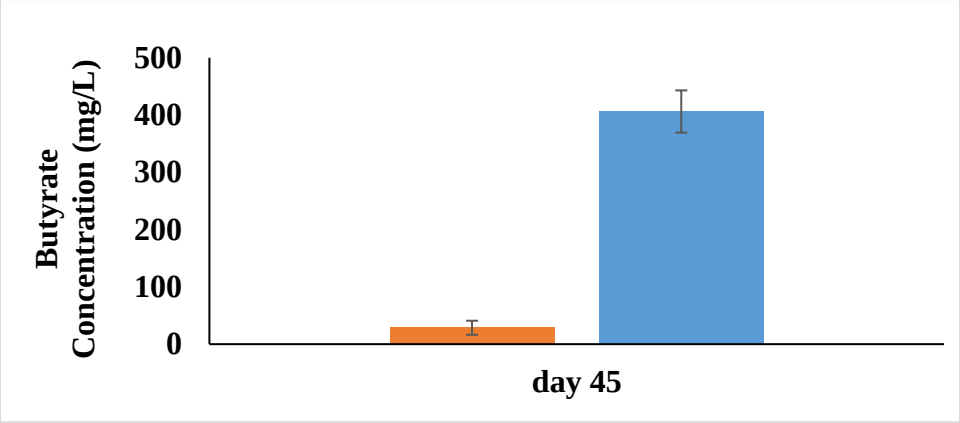

Figure 7.7. Butyrate concentration as mg/L at day 45 of control bottles cultivated by glucose. The orange and blue columns represent the butyrate concentration 3 COD: 1 VS and 6 COD: 1 VS of glucose respectively.

Finally, Figure 7.8 shows the pH value at day 45 in all bottles. At a glucose concentration of 3 COD: 1 VS, all the bottles had almost neutral pH (~ 7). By increasing the glucose concentration to 6 COD: 1 VS, the pH dropped in all bottles with the lowest pH in the control bottles.

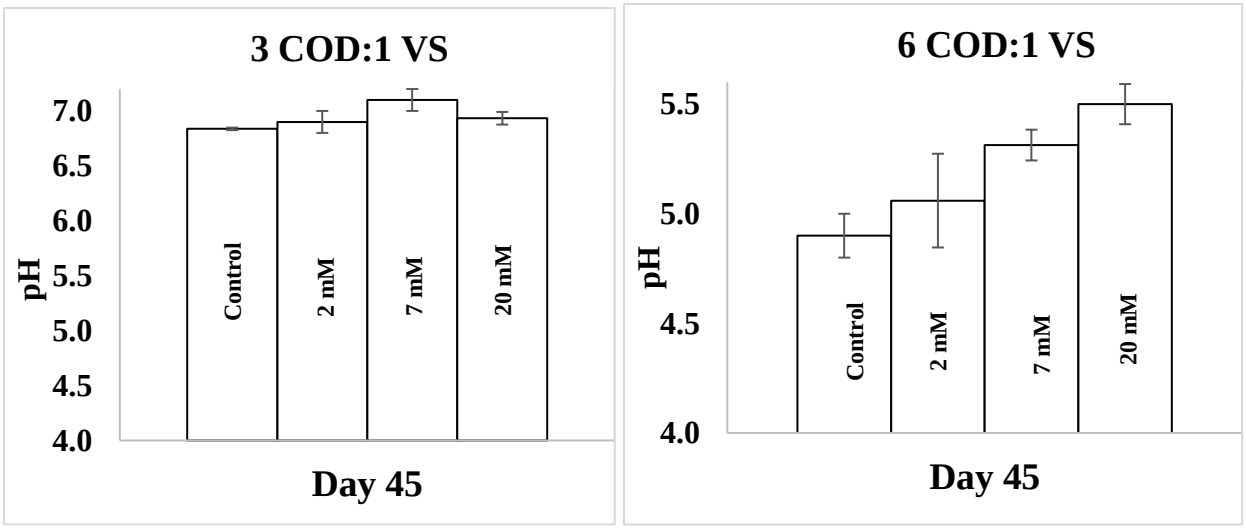

Figure 7.8. The pH value of liquid medium in the serum bottles that contained glucose as a substrate. The pH value was measured at day 45 (the end of incubation) for the control and magnetite-supplemented bottles (2 mM, 7 mM and 20 mM).

The previous results indicate that faster production and consumption of VFA occurs in the presence of magnetite and this consequently enhances the stability of the anaerobic process by preventing rapid pH drop. Yin et al. (2017) reported that magnetite enhanced VFA production (the propionic concentration was 244.9 ± 11.9 mg/L at hour 3 in the magnetite bottles whereas it was just 219.9 ± 10.8 mg/L at hour 5 in the control bottles). In addition, VFA consumption was faster (at hour 9, the propionic acid concentration was 56.2 ± 7.9 mg/L and 134.5 ± 23.4 mg/L in the magnetite and control bottles respectively). Luo et al. (2015) also showed that increasing the concentration of glucose from 2 - 8 g/L increased the VFA accumulation; however, they reported that the VFA formation and degradation were simultaneously stimulated by adding biochar (1.3–1.6 times for acetic acid and 2.6 times for propionic acid), as compared to the control. Furthermore, adding graphene caused a significant decrease in the acetate concentration (88.9 % of the control) (Tian et al., 2017). These results indicate that VFA production and consumption depend on glucose concentration and the presence of magnetite. In addition, these results suggest that magnetite supplementation facilitates not only DIET but also affects the hydrolysis/acidification process.

In contrast, Yan et al. (2017) studied the effect of conductive materials (i.e. carbon nano-tube (CNT) and granular activated carbon (GAC)) on mesophilic anaerobic batch reactors fed with an initial glucose concentration of 1100 mg/L. There was no significant difference in methane production and glucose consumption rates in the control and conductive materials reactors. As well, no VFA accumulation was observed in either reactors. These findings are similar to the findings of Zhao et al. (2017) who ran semi-continuous reactors using glucose as a substrate with the supplementation of a conductive carbon cloth. Namal (2019) also showed that there was no significant difference in the total methane production rate from glucose between reactors using commercial magnetite (0 –75 μm) and a control reactors. There was, however, a significant decrease in the lag time in the magnetite reactor (0.65 vs 1.28 days), as compared to the control reactor. These observations are very likely due to glucose being a more complex substrate than acetate and propionate for anaerobic communities. Table (7.2) shows that glucose is metabolized in more than one reaction.Therefore, conductive materials do not have a direct effect on glucose metabolism.

Table 7.2. Main reactions presented in methanogenesis (adapted from (Liu et al., 2016)).

Substrate	Reaction
Acetate	$CH_3COOH \rightarrow CH_4 + CO_2$
Propionate	$CH_3CH_2COOH + 2H_2O \rightarrow CH_3COOH + CO_2 + 3H_2$
Glucose	$C_6H_{12}O_6 \rightarrow CH_3CH_2CH_2COOH + 2CO_2 + 2H_2$ $C_6H_{12}O_6 + 2H_2O \rightarrow 2CH_3COOH + 2CO_2 + 4H_2$ $C_6H_{12}O_6 + 2H_2 \rightarrow 2CH_3CH_2COOH + 2H_2O$

7.2.3 Microbial Analysis

The microbial community analysis was based on taxonomic composition obtained by sequencing the 16S rRNA genes (See Appendix I for details). The initial seed sludge as well as sludge from the incubated bottles under glucose ratios of 3 COD: 1 VS and 6 COD:1 VS were analysed after two and eight weeks of incubation.

Figure 7.9 and Figure 7.10 show the operational taxonomic unit (OTUs) and community diversity respectively. The OTUs in the magnetite treatments after 2 weeks and 8 weeks at 3 COD: 1VS ratio was higher by 7 % and 3 % respectively than that in the control. When the glucose concentration was raised (at 6 COD: 1 VS) there was a corresponding increase in the OTUs in the control after 2 weeks however in this case magnetite had no effect. This indicates that the driving factor for growth of the microorganisms is the glucose concentration. That is to say, the microorganisms that feed on glucose benefited by the higher concentration of glucose and grew more. In addition, Figure 7.10 shows the microbial diversity in each batch test bottle. Both, the Shannon index and the inverse Simpson showed a similar trend. The value of the Shannon diversity index was initially around 4.8 and then there was an increase with time in the control at 3 COD: 1 VS ratio. This is likely due to the microorganisms having more time to grow as well as glucose to feed. In this case, magnetite did not seem to increase the diversity. When the glucose concentration increased from 3 COD: 1 VS to 6 COD: VS ratio, the diversity slightly decreased in the control

but increased in the magnetite additions. Furthermore, the diversity of micro-organisms as indicated by the Shannon Index in magnetite-treated samples after 2 weeks and 8 weeks was higher by 2 % and 10.6 % respectively, than the diversity compared to the control and even the diversity compared to the glucose at 3 COD: 1 VS ratio. It is worth noting that this is not actually reflecting a specific change in methanogen cultures; but more a reflection on the change in the whole community including also fermentative bacteria which grow faster than methanogens in additions to being able to use glucose as a source of carbon. The results indicate therefore that the supplementation of magnetite to digested sludge increased the diversity of bacterial communities. In addition, the microbial population increased as soon as glucose became available (Figure 7.4); however, once glucose became unavailable (after two weeks) the population started to decrease. This correlated to a change in VFA concentration (Figure 7.5) (i.e. the concentration of VFA started to accumulate from day 14).

The archaeal and bacterial community composition is shown in Figure 7.11 and Figure 7.12 respectively. The results indicate that *Methanothermobacter* (i.e. a typical hydrogenotrophic methanogen) and *Methanosarcina* (i.e. a methanogen that produces methane using all three metabolic pathways of methanogenesis) were the predominant methanogens in all bottles. The initial relative ratio of Archaea did not change after two weeks of incubation due to the slow growth rate of Archaea. After eight weeks of incubation, the abundance of total *Methanothermobacter* in the magnetite bottles was 1.4 times at 3 COD:1VS and 2 times at 6 COD: 1VS higher than that in the control. The abundance of *Methanosarcina* was 3 times at 3 COD: 1 VS and 10.5 times at 6 COD: 1 VS higher than that in the control. The total ratio of *Methanothrix* at glucose ratio of 3 COD: 1 VS increased in the magnetite bottles by 1.7 times as compared to the control bottles. This data seems to reflect a more stabilized anaerobic environment in the magnetite bottles. However, the total ratio of *Methanothrix* at 6 COD: 1 VS in the magnetite bottles decreased by 3.2 times as compared to the control bottles. *Mathanospirillum* was enriched in both controls after eight weeks but not in the magnetite treatments, probably as a result of being outnumbered by *Methanosarcina* and *Methanothermobacter*. On the other hand, after eight weeks (as shown in Appendix I, Table I.1), increasing the glucose concentration from 3 COD: 1 VS to 6 COD: 1 VS resulted in an increase of the total ratio of *Methanothermobacter* up to 1.3 times and *Methanosarcina* up to 7

times in the magnetite supplemented bottles as compared with control bottles. These observations suggest that magnetite likely offers an appropriate environment for *Methanosarcina* and *Methanothermobacter* to flourish in an anaerobic digester. In addition, these results show that increasing the glucose concentration in the presence of magnetite enriched the *Methanothermobacter* and *Methanosarcina* community. Most studies have shown that adding magnetite improved the presence of *Methanosarcina* (Kato et al., 2012; Cruz Viggi et al., 2014; Yamada et al., 2015; Zhuang et al., 2015; Baek et al., 2016; Yang et al., 2016; Jing et al., 2017). In addition, Yan et al. (2017) reported that in a glucose co-culture, *Methanothermobacter* was the most abundant in all reactors. They also reported that *Methanosarcina* in granular activated carbon (GAC) and carbon nanotube (CNT) groups were almost two times more abundant than that in control groups. The authors attributed the enhanced methanogenesis mainly to electric syntrophy rather than the electron shuttling of soluble iron.

Coprothermobacter, Lutaonella and *Rectinema* genus were the dominant bacterial genera (i.e. > 2.7%) and quite similar in all bottles. Gagliano et al. (2015) revealed that *Coprothermobacter* spp. can establish a syntrophy with hydrogenotrophic archaea to improve protein degradation, or they play as a source of thermostable enzymes. In this study the total ratio of *Bacteroidales, Defluviitoga, and Thauera* were less than 0.8 % whereas Yamada et al. (2015) and Yang et al. (2016) observed that these genera were the dominant sequences in the magnetite supplement in an anaerobic culture. This difference is likely due to using different sludge in which these genera were present in a lower proportion.

In this study, a relative higher abundance of *Acetomicrobium* (i.e. an acetic acid producing bacteria) was observed in the magnetite bottles as compared to the control. It is worth noting that *Clostridia* (i.e. a glucose fermentative anaerobic bacteria) was less than 1 % (see Appendix I for details) in all bottles except in the magnetite bottles after eight weeks at glucose ratio of 3 COD: 1 VS. In addition, the relative abundance of *Clostridia* was not changed by increasing the glucose concentration from 3 COD:1 VS to 6 COD:1VS. These results suggested that *Clostridia* was not enriched at high concentration of glucose regardless of the addition of magnetite. Moreover, it has also been reported that the electroactive bacteria *Geobacter* species can create direct electrical

connection with *Methanosarcina barkeri* in the conversion of CO_2 to methane (Rotaru et al., 2014). However, *Geobacter* species were absent or present in low percentages (< 0.2 % in the magnetite bottles after 2 weeks). This may suggest that other microorganisms participated in DIET. Also, it is possible that magnetite acts as an electron acceptor (i.e. in the propionate oxidation) or an electron donor (i.e. in the direct reduction of CO_2 to CH_4) rather than promoting DIET (Su et al., 2013; Yang et al., 2016; Abdelsalam et al., 2017).

The above results indicate that an increase in the glucose concentration sustains a higher microbial growth. However, in the present of magnetite, increasing the glucose concentration from 3 COD: 1 VS to 6 COD: 1VS resulted in improved the activity of methanogens with the highest enrichment of Methanosarcina (i.e. a methanogen that produces methane using all three metabolic pathways of methanogenesis) and some bacteria such as *Cryptanaerobacter, Thermoclostridium, Pelotomaculum, Acetomicrobium, Thauera, Sedimentibacter*, and *Desulfofundulus*. These results indicate that magnetite particles in combination with the concentration of glucose had a clear effect on the structure of the microbial community probably by facilitating the DIET pathway. Akarsubasi et al. (2005) mentioned that changes in the microbial community structure can lead to changes in metabolic functioning in a bioreactor as the functional attributes of a biological process depend on the activity of the microbes working in the system.

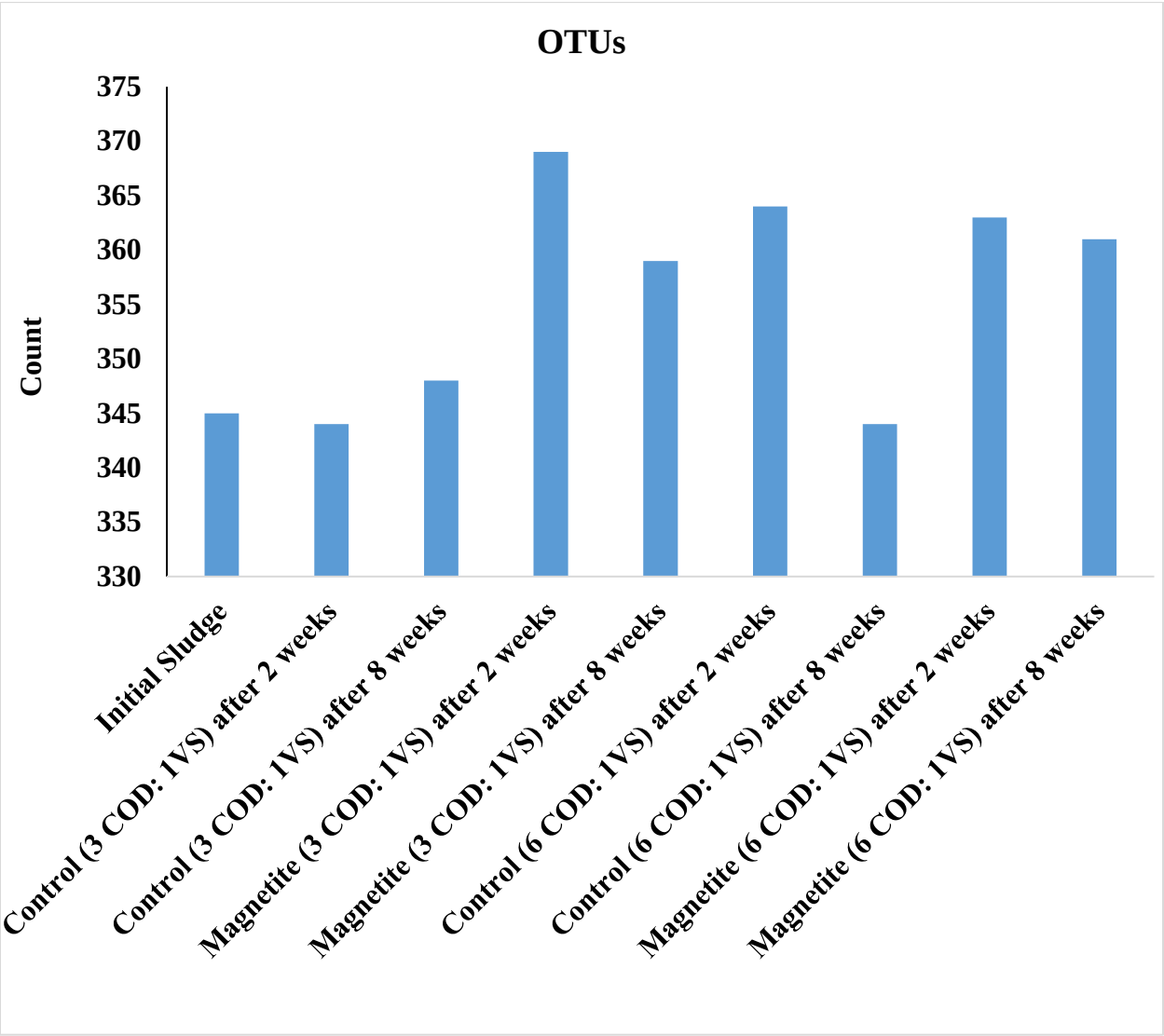

Figure 7.9. The operational taxonomic unit (OTUs).

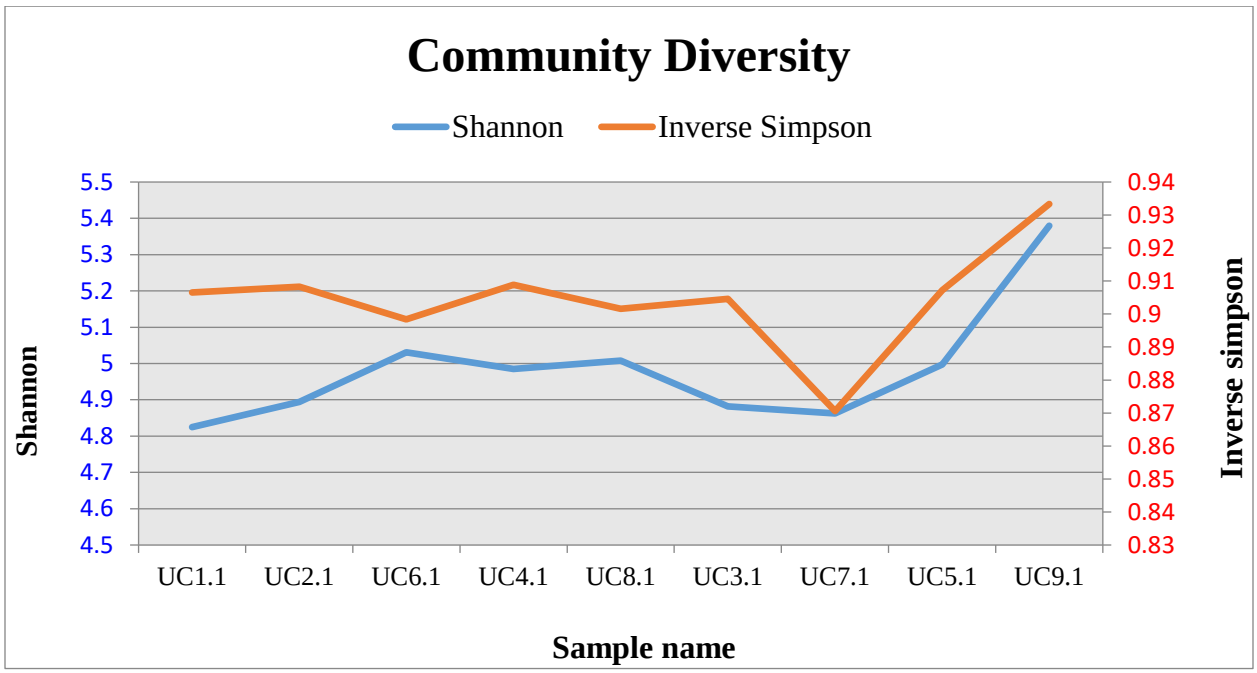

Figure 7.10. Shannon Community Diversity and Inverse Simpson results

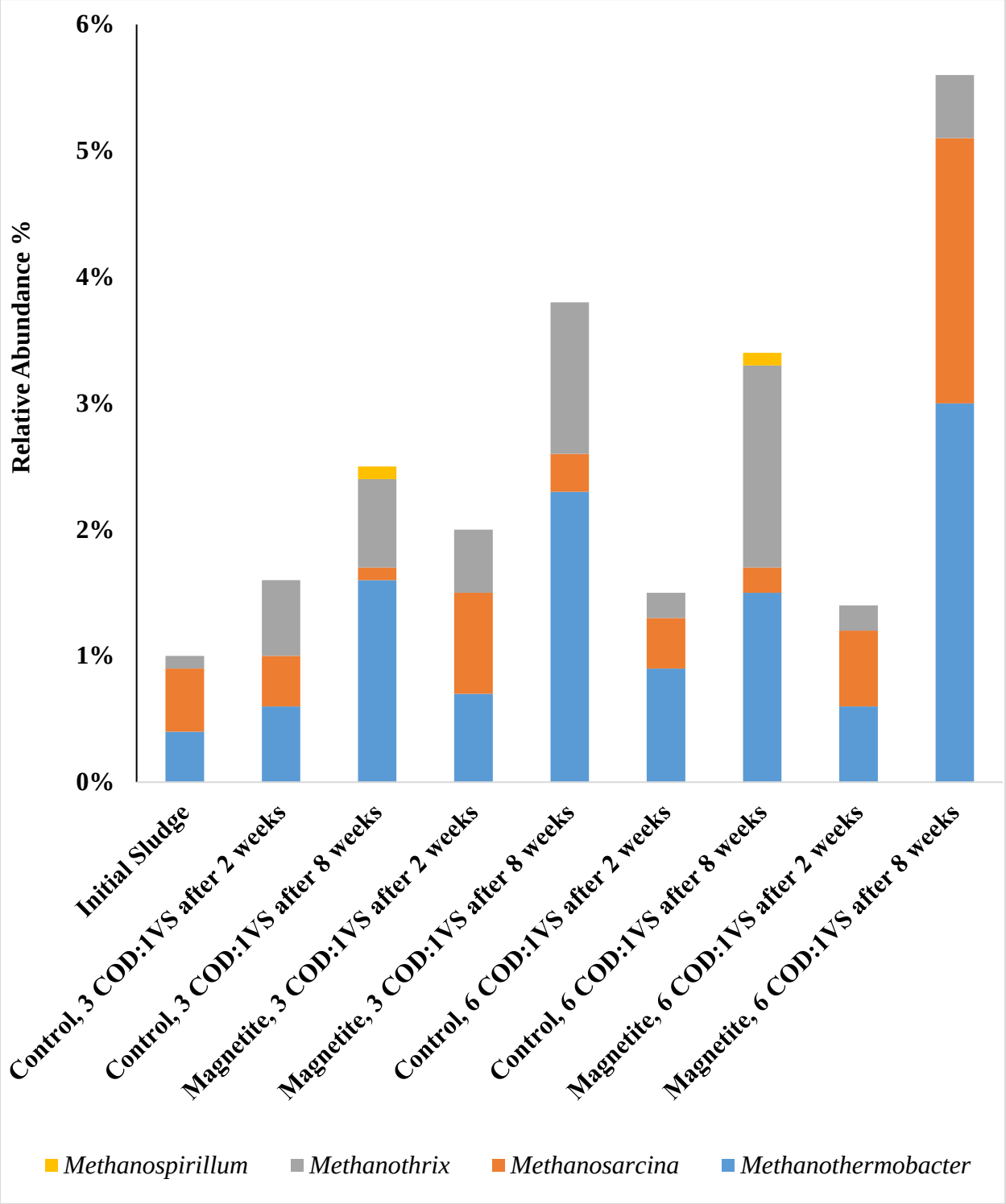

Figure 7.11. Archaeal community structure at genus level associated with different conditions.

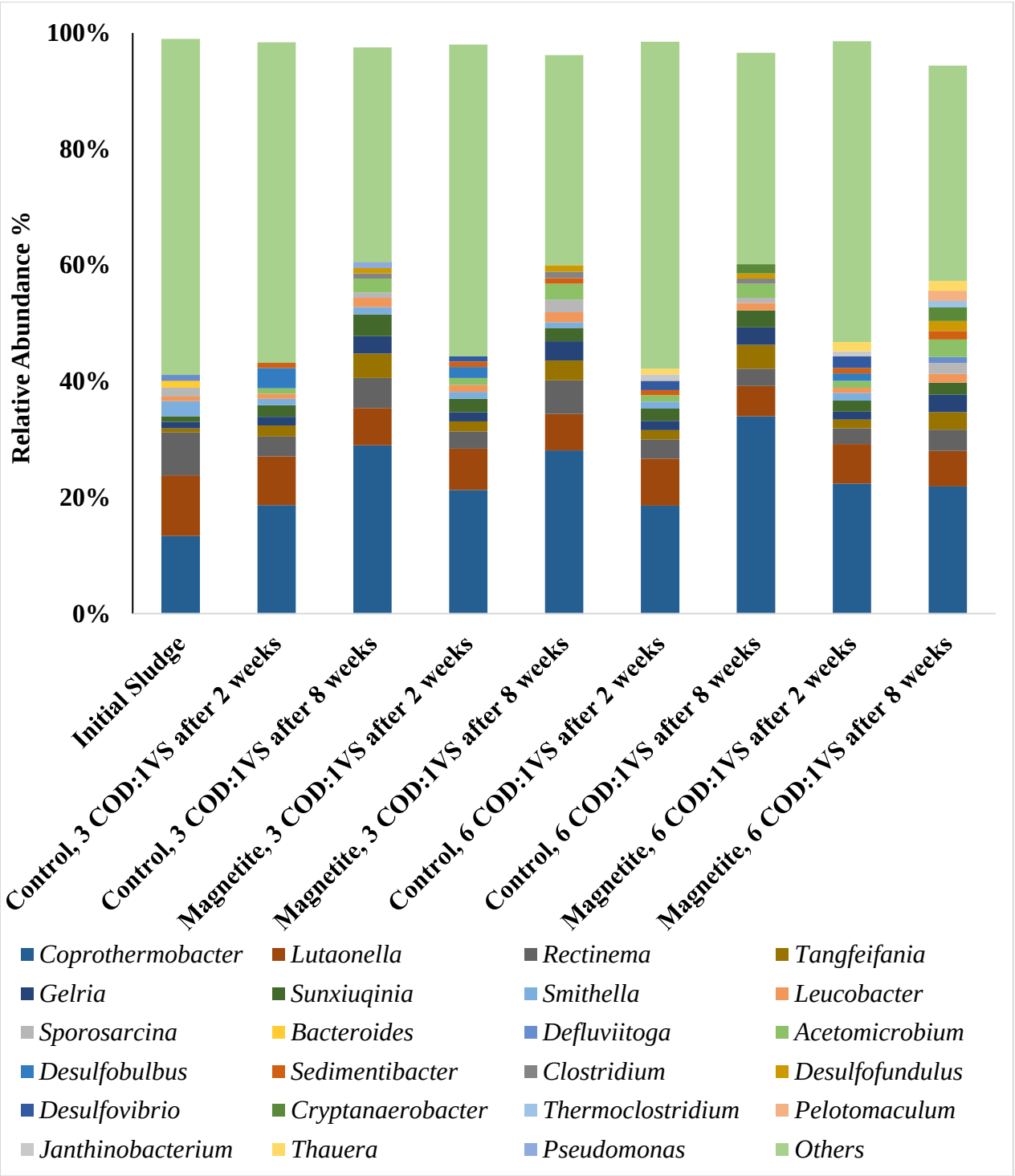

Figure 7.12. Bacterial community structure at genus level. Genus level with relative abundance lower than 0.8 % were classified into group ‘others’.

7.3 Conclusion

There is the potential for adding magnetite to enhance methane production from glucose at high concentrations.

The overall results indicate that increasing the glucose concentration from 3 COD: 1 VS to 6 COD: 1 VS, results in a decrease in the maximum methane production rate and an increase in the lag phase duration in all bottles. The reduction in the maximum methane production was on the average 1.8 times in the magnetite-supplemented bottles and 7.6 times in the control bottles; in addition, the increase in the lag phase duration was in the range of 2 days to 11 days in the magnetite-supplemented bottles and was 24 days in the control bottles. The results also show the ability of magnetite to enhance the fermentation of glucose (23.64 % faster at 3 COD: 1 VS and 55.23 % faster at 6 COD: 1VS), as compared to the control. These results indicate that adding magnetite enhances the methane production rate and decreases the lag phase duration as compared to the control.

Both cumulative methane production and methane yield depend on the incubation time. It appears that a large amount of methane was produced within a short period in the magnetite-supplemented bottles as compared to the control; however, should the control bottles had been left incubating for longer, they might had produced as much methane as in the magnetite-supplemented bottles did.

Acetate and propionate were the main volatile fatty acids produced from glucose fermentation. The accumulation of VFA increased by increasing the glucose concentration; however, it was less in the magnetite-supplemented bottles as compared to the control. In addition, increasing the glucose concentration resulted in a pH drop, with the lowest pH in the control bottles.

The overall results indicate that magnetite performance depends on the concentration of glucose which plays an essential role in anaerobic digestion stability because it affects the VFA production and accumulation rates and the pH level. Glucose as a substrate seems to be a complex organic and therefor requires a suitable environment to be converted into methane. As such, it is important to provide a suitable concentration of glucose (3 COD: 1 VS) to achieve the maximum methane production in the presence of magnetite.

CHAPTER 8. CONCLUSIONS AND RECOMMENDATIONS

8.1 General Conclusions

This research has examined the potential for magnetite to enhance methane production by serving as electrical conduits in the anaerobic digestion process. Results indicate that to achieve the highest methane production possible, attention should be paid to the magnetite characteristics (i.e. particle size and concentration), the sludge age (i.e. condition of inoculum) and the substrate concentration and type. More specifically, the following conclusions arise from this research:

Adding magnetite of small (50-150 nm) and medium (168 to 490 nm) size ranges seem to increase the methane production rate and shorten the lag phase. Conversely, large particle sizes (800 nm to 4.5 µm) should be avoided. Magnetite concentrations of 2 mM, 7 mM, and 20 mM showed a positive effect on methane production. However, the effect of both magnetite size and concentration is related to the inoculum age. To enhance methane production in the presence of magnetite, the sludge should be used fresh where the microoganisms would be expected in exponential growth. Magnetite exerts the highest effect on the maximum methane production rate from the fresh sludge (P- value of control versus adding magnetite was $0.0001 < 0.05$) as compared to that from degassed sludge (P- value of control versus adding magnetite was $0.079 > 0.05$).

In addition, the stimulatory effect of magnetite on methane production requires the presence of substrate. By increasing the substrate COD:VS ratio from 2:1 to 4:1 in the presence of magnetite, the maxium methane production from acetate and glucose (but not propionate) increased as compared to when magnetite was absent. In addition, by increasing the acetate COD:VS ratio from 4:1 to 8:1 and by increasing the propionate COD:VS ratio from 2:1 to 4:1 and then to 8:1, in the presence of magnetite, the lag phase duration decreased as compared to that when magnetite was absent.

The maximum methane production rate decreases, and the lag phase duration increases when the glucose concentration is increased from 3 COD: 1 VS to 6 COD: 1 VS in all bottles (with and without magnetite). However, the reduction in the maximum methane production and the increase in the lag phase duration were less in the magnetite-supplemented bottles (on the average 1.8 times and in the range of 2 days to 11 days) as compared to the control (7.6 times and 24 days) in the control bottles. In addition, in the presence of magnetite, the fermentation of glucose was 23.64 % faster at 3 COD: 1 VS and 55.23 % faster at 6 COD: 1VS, as compared to the control. Moreover, adding magnetite results in decrease both the VFA accumulation and a pH drop. That is, magnetite seems to ameliorate the negative effects of overloading the anaerobic digester with readily fermentable substrate such as glucose.

The highest value of the maximum methane production rate in the presence of magnetite was produced from acetate as compared to that from propionate and glucose. However, The results suggest using acetate with the concentration up to 4 COD: 1 VS or propionate with the concentration up to 8 COD : 1 VS. Further study is needed on the effect of glucose concentration on methane production when it is 6 COD: 1 VS or more.

Overall, the highest maximum methane production rate (1.33 - 3.4 times) and the shortest lag time (15.38 % - 53 %) were obtained in the magnetite-supplemented bottles. This suggests that DIET via magnetite is faster than IET via hydrogen for methane formation. This was supported by theoretical calculations of the maximum electron carrier fluxes via magnetite through acetate and propionate degradation. These were at least 10^6 higher than that via IET. The application of magnetite appears as a good strategy to turn anaerobic digester more resilient to disturbance caused by high substrate concentration, VFAs accumulation and pH dropping. These finding may have a broad impact on the operation of a full-scale anaerobic digester operations (i.e. minimizing the lag phase, increasing the methane production rate, and reducing the impact of VFA accumulation) as well as on renewable energy biotechnology given that there are thousands of full-scale plants worldwide.

8.2 Recommendations

Although the theoretical calculations show that electron transfer in the presence of magnetite was higher than that in the absence, these calculations were done under several assumptions (i.e. interbacterial distance, the average diameter and the spherical shape of both acetogen and methanogen, the electrons released are transferred to a methanogen via an electron conduit consisting of magnetite particles, and the electrical conduit was assumed to be a wire). Further experiments using an electrolytic cell (i.e. two electrodes, the anode and the cathode, which are solid metals connected to an external circuit that provides an electrical connection between the two parts of the system) could measure the electrical currents in the presence and in the absence of magnetite (Figure 8.1) to confirm these assumptions.

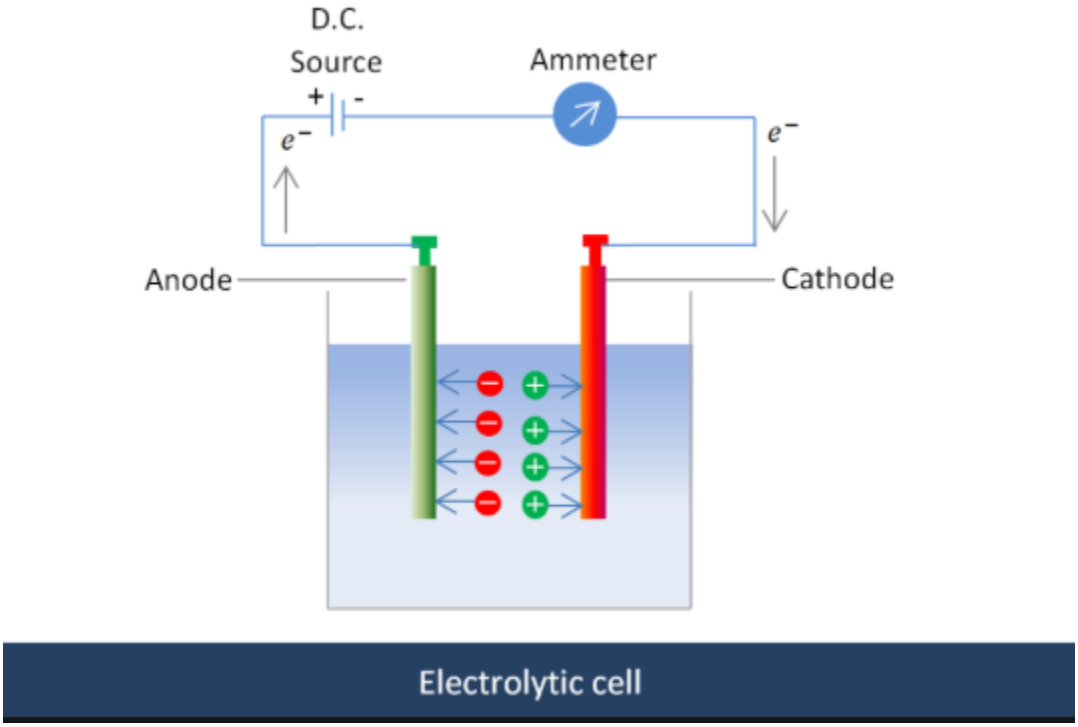

Figure 8.1. Experimental set up to measure the electrical currents.

Using either acetate or propionate as substrates has a positive effect on methane production in the presence of magnetite. However, the results indicate that the potential for adding magnetite to enhance methane production from glucose still needs further investigation. For example, it still unclear whether magnetite (as is the case of semi-conductive Fe (III) oxide) can help to decompose complex organics. Thus, further investigations should be conducted using glucose under conductive Fe (III) oxide-supplemented and magnetite conditions to examine the factors that affect glucose degradation.

To address the hypothesis that suggests "in the presence of magnetite the more robust methanogenic degradation of substrate is ultimately due to the presence of a more abundant and/or active methanogenic population", further investigations are needed to study the relative amount of bacteria and maximum hydrogenophilic methane production rate in the presence and absence of magnetite.

Soluble microbial products (SMP) and extracellular polymeric substances (EPS) produced by microorganisms have the potential to act as the electron shuttle between microorganisms and conductive materials (Zhu et al., 2017). Further investigations are needed to study the production of EPS or SMP by anaerobic microorganisms exposed to magnetite.

In addition, so far, most experiments on the effect of magnetite have been conducted using bacterial enrichments from paddy soil samples and anaerobic methanogenic cultures from municipal wastewater treatment plants. Granular activated carbon has been shown to have the ability to enhance methane production from up-flow anaerobic sludge blanket reactors (UASB), thus, adding magnetite to UASB could produce positive results in terms of methane production. There is also a need for addressing the practical aspects of using magnetite in industrial scale anaerobic digesters. For example, the optimal dosage and application frequency of magnetite in a specific situations should be identified. Similarly, the recovery of magnetite nanoparticles to avoid iron accumulation in a system especially with repeated applications, should be investigated. In addition, the costs versus benefits of using magnetite at industrial scale requires further research.

Appendix A. The Characterization of Magnetite Nanoparticles

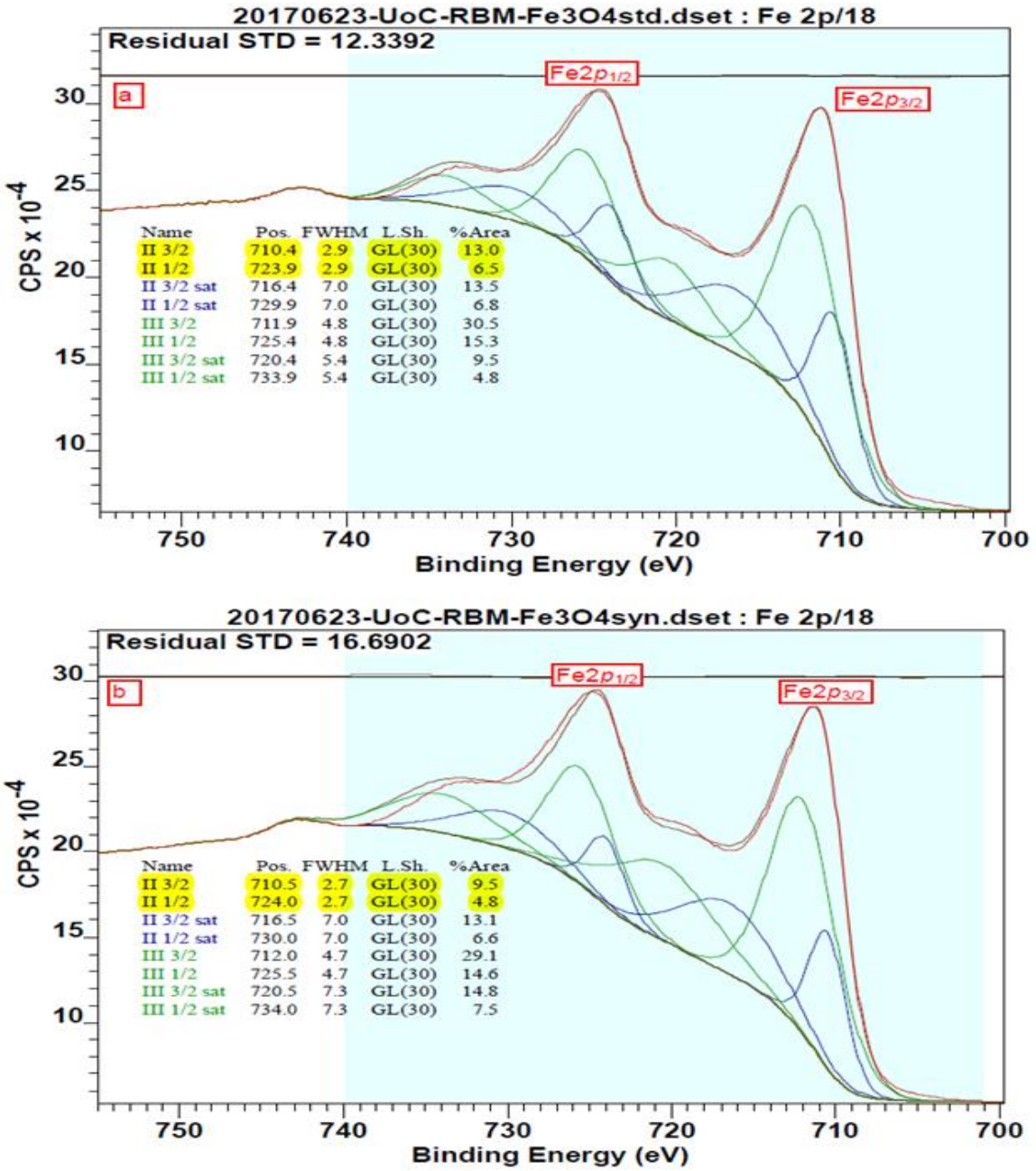

Figure A.1. Fe2p XPS patterns for the reference sample (a), and the prepared sample (b). $Fe2p_{3/2}$ and $Fe2p_{1/2}$ are II 3/2 and II 1/2 respectively.

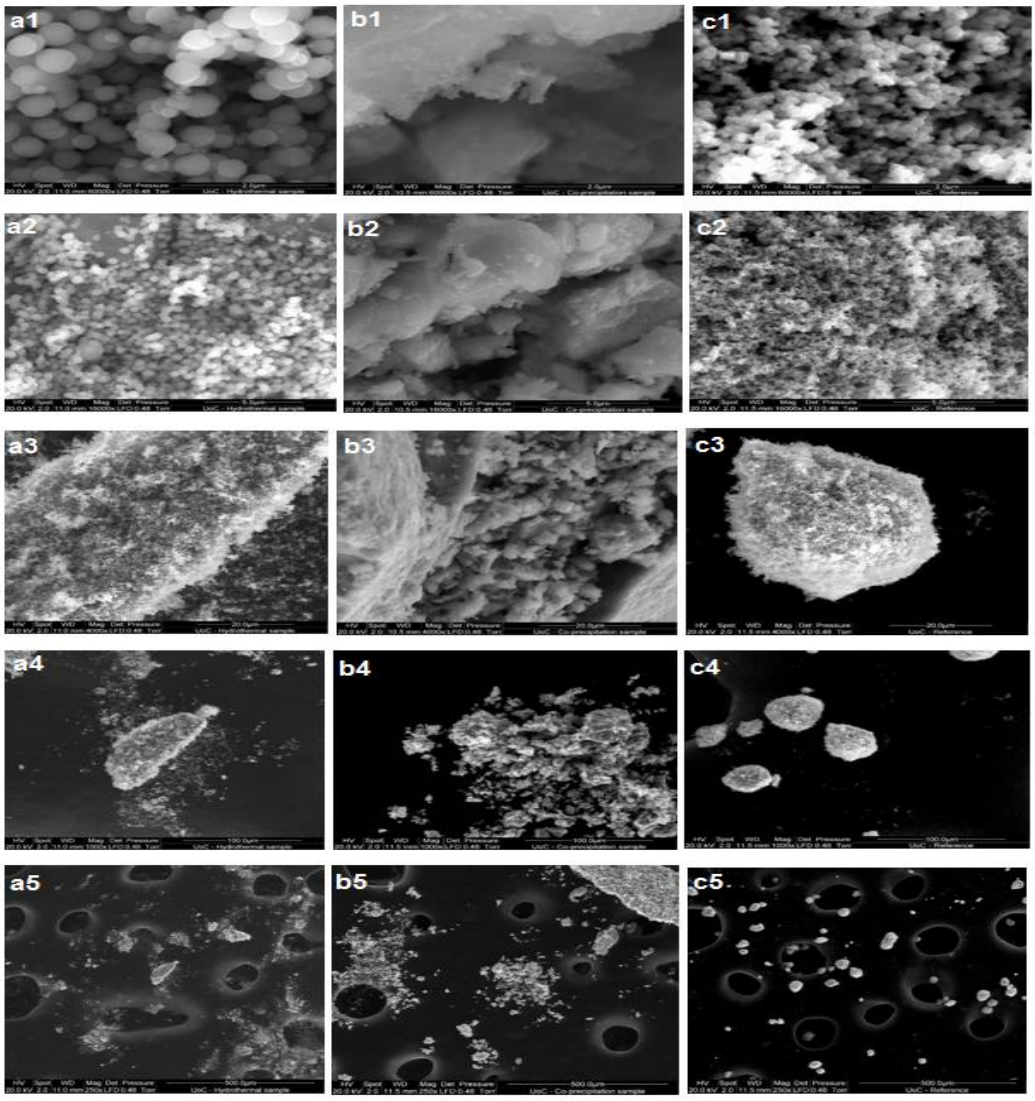

Figure A. 2. SEM images of the reference sample (a), and the prepared sample (b) at different bar scales. SEM images of (a1 and b1) at 100 µm, (a2 and b2) at 20 µm and (a3 and b3) at 2 µm

Size diameter (FEI ESEM Details): Model: FEI Quanta 200 F (FEG = Field Emission Gun). Manufactured in The USA. The EDS detector was SiLi (Lithium drifted) with a Super Ultra Thin Window, Peltier stage (2°C – 50°C), High temp stage (70°C – 1400°C). EDS Detector: The following conditions may all be recorded on the data bar of your images at the time you take them: Voltage, Spot Size, Magnification, Detector type, Working Distance, Pressure, Temperature, Time/Date, Scale bar, Sample name. Attachments: EBSD Detector Peltier stage (2°C – 50°C) High temp stage (70°C – 1400°C).

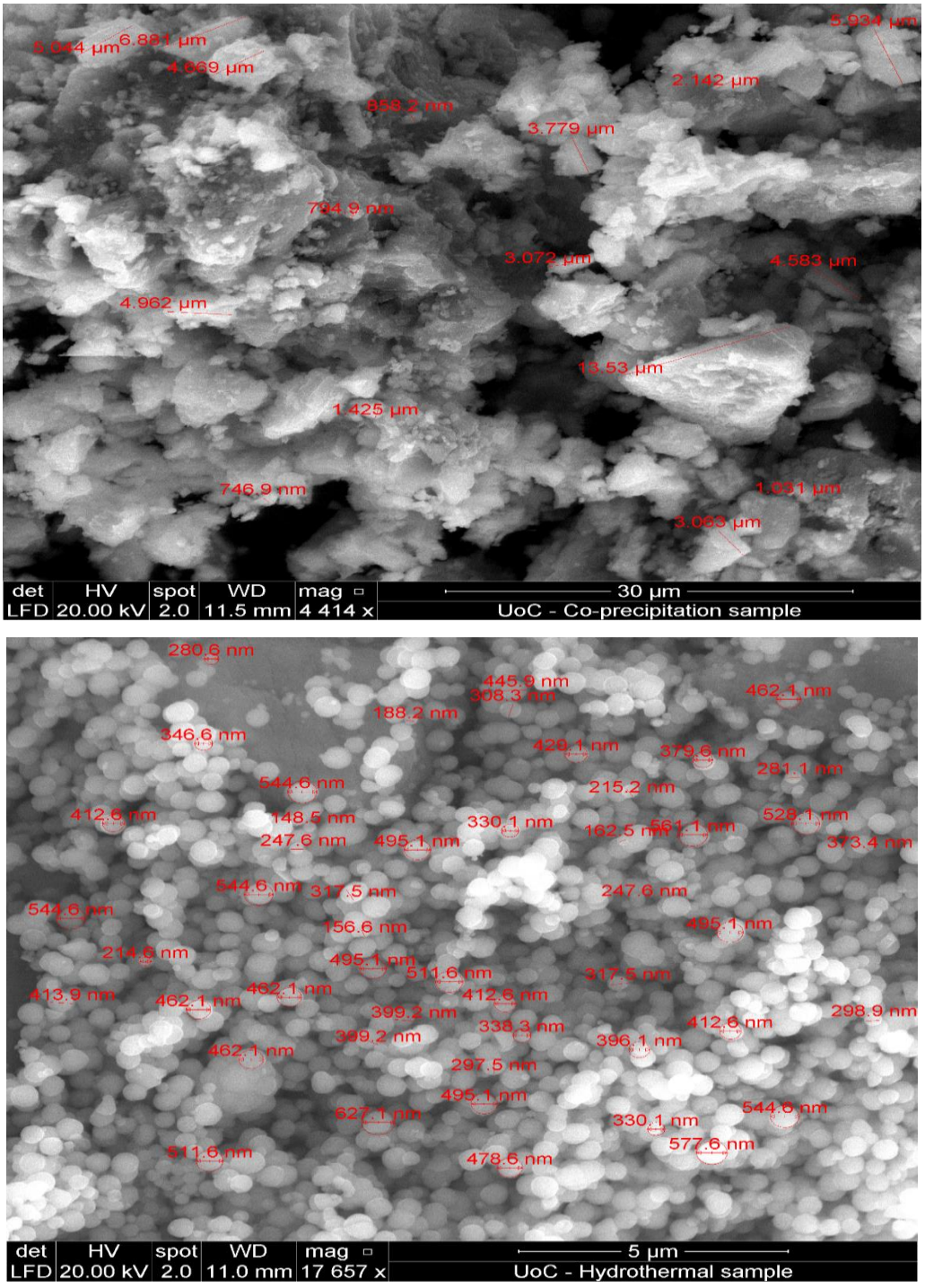

Figure A.3. Size diameters for both co-precipitation and hydrothermal samples

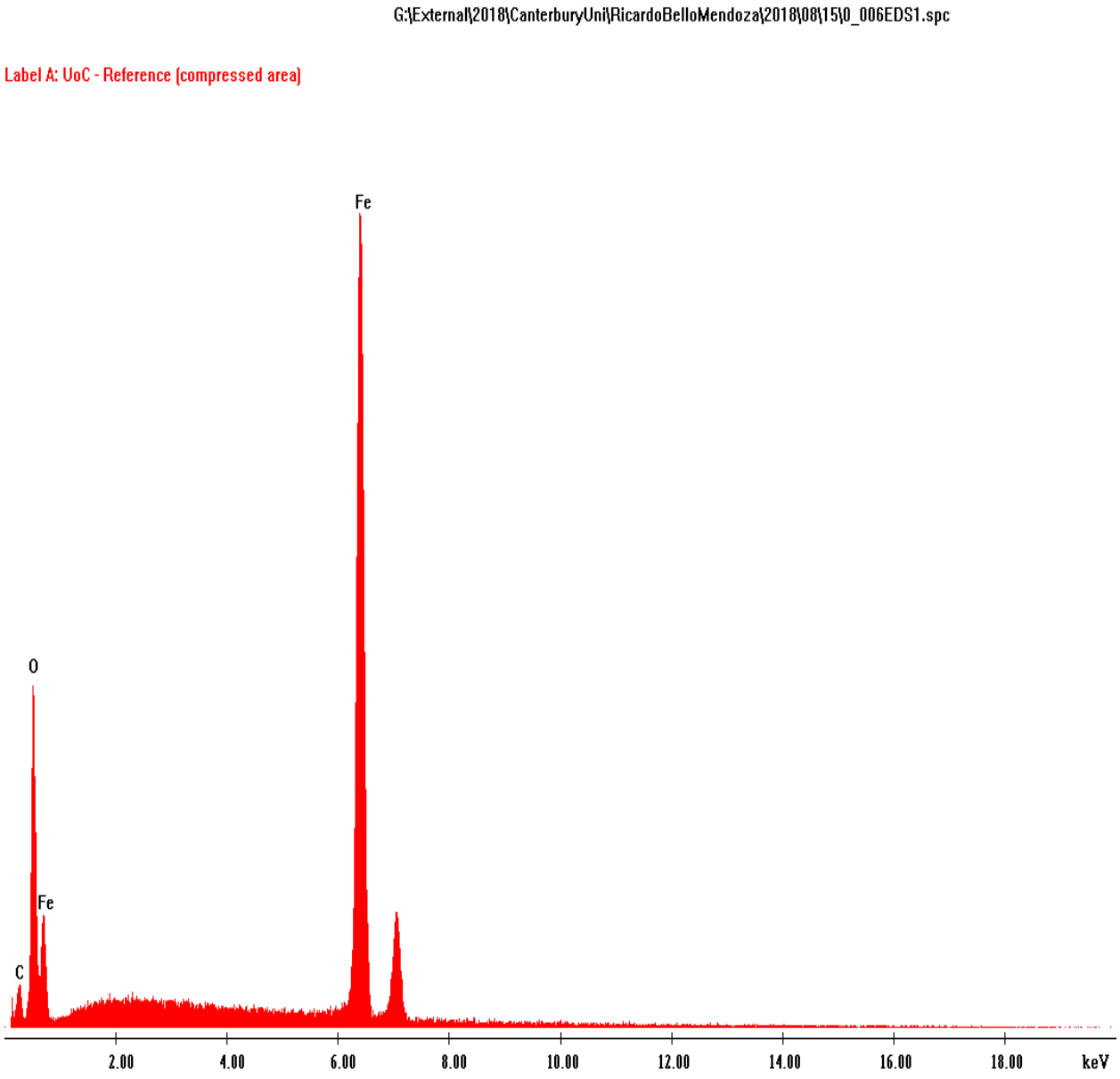

Figure A.4. EDS results for small sized of magnetite

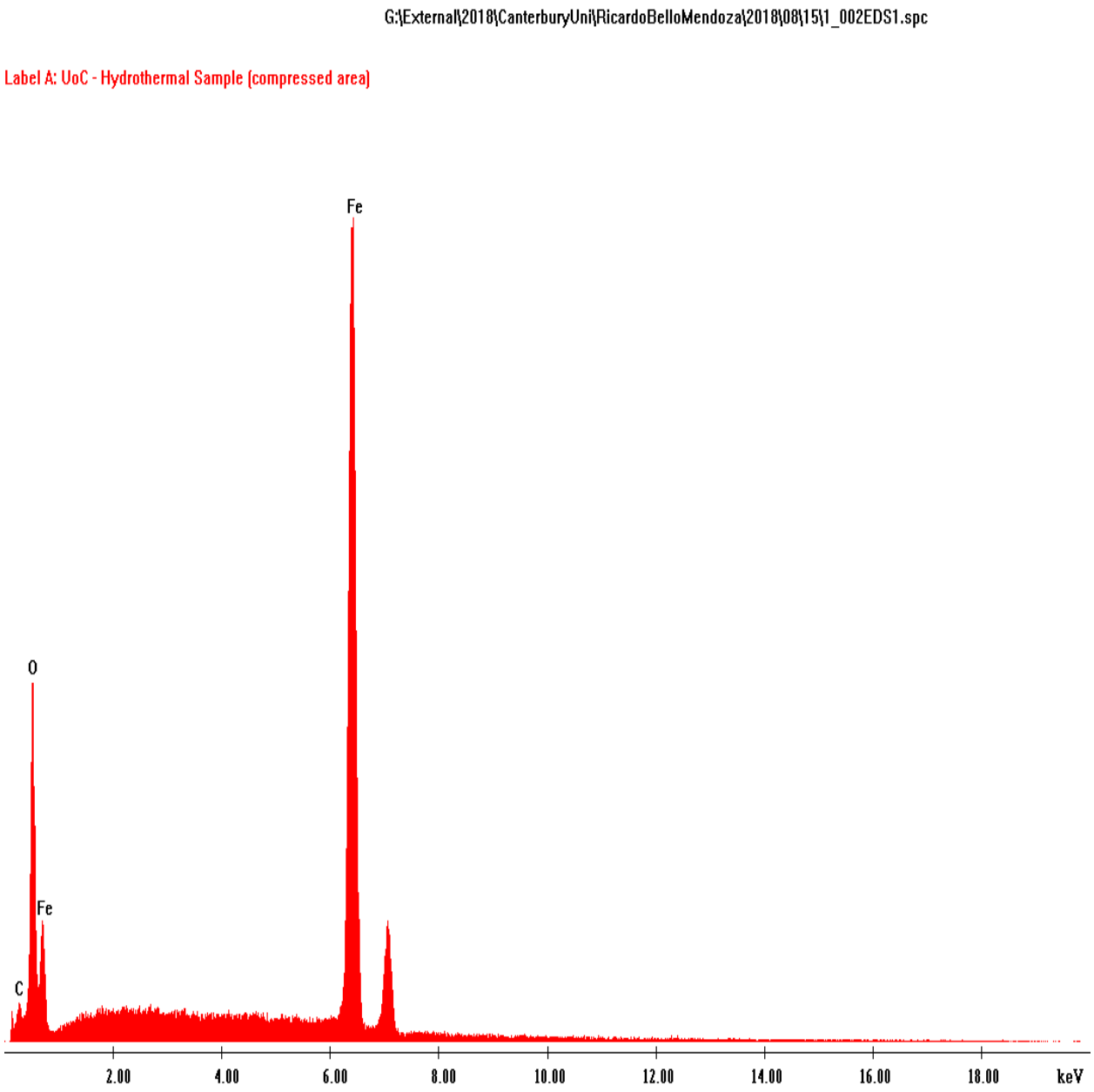

Figure A.5. EDS results for medium-sized of magnetite.

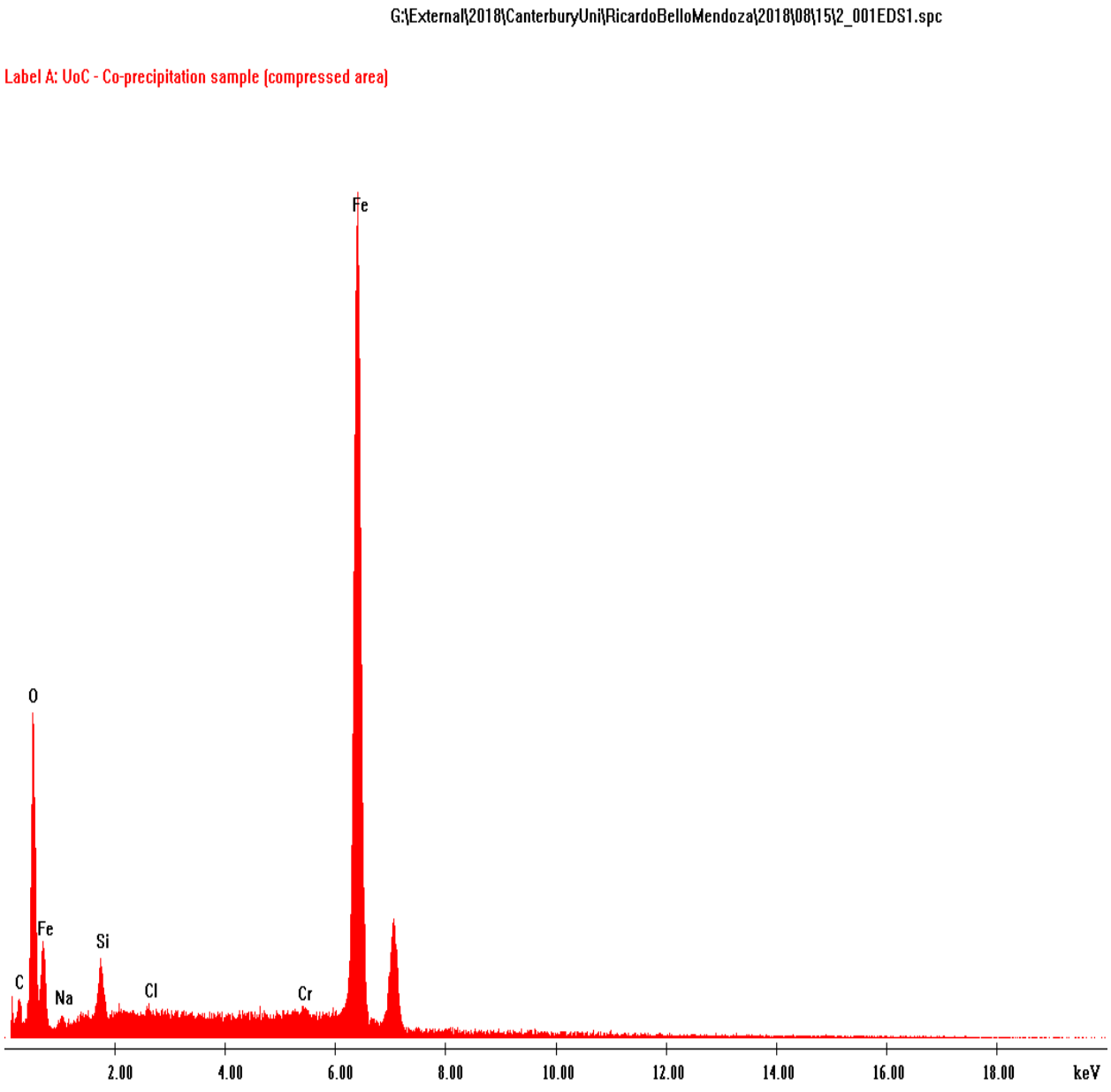

Figure A.6. EDS results of large sized of magnetite.

Appendix B. Physico-Chemical Characterisation

All TS and VS analyzes were completed within 48 hours where calculated as follows:

$$TS\ (mg/l) = \frac{[Mass_{(solids+dish)}]_{\ At\ 105℃} - Mass_{(dish)}}{volume\ of\ sample} \quad (1)$$

$$TS\ \% = \frac{[Mass_{(solids+dish)}]_{\ At\ 105℃} - Mass_{(dish)}}{[Mass_{(wet+dish)}] - Mass_{(dish)}} * 100\% \quad (2)$$

$$VS\ (mg/l) = \frac{[Mass_{(solids+dish)}]_{\ At\ 105℃} - [Mass_{(solids+dish)}]_{\ At\ 550℃}}{volume\ of\ sample} \quad (3)$$

$$VS\ \% = \frac{[Mass_{(solids+dish)}]_{\ At\ 105℃} - [Mass_{(solids+dish)}]_{\ At\ 550℃}}{[Mass_{(solids+dish)}]_{\ At\ 105℃} - Mass_{(dish)}} * 100\% \quad (4)$$

Figure B. 1. Titration procedure to adjust pH of propionic acid by adding NaOH.

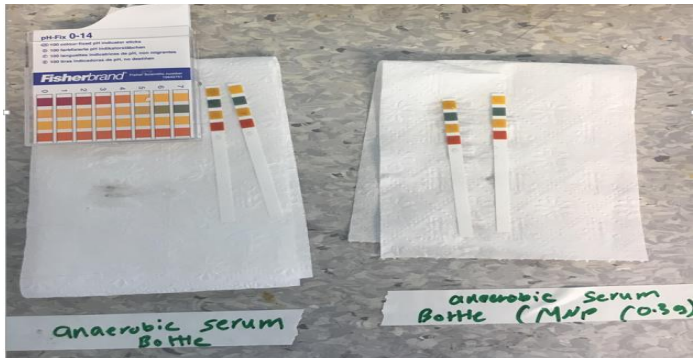

Figure B. 2. Check the pH after the incubation

Appendix C. Biogas Calibration Curves

Table C. 1. The Calibration curves for both carbon dioxide and methane gases

samples					GC reading; Peak area	
Sample #	% CH_4	% CO_2	Volume of standard gas (mL)	Volume of air gas (mL)	CH_4	CO_2
1	15	7.5	2.5	7.5	10.55	10.2
2	30	15	5	5	514.28	399.69
3	45	22.5	7.5	2.5	954.49	718.36

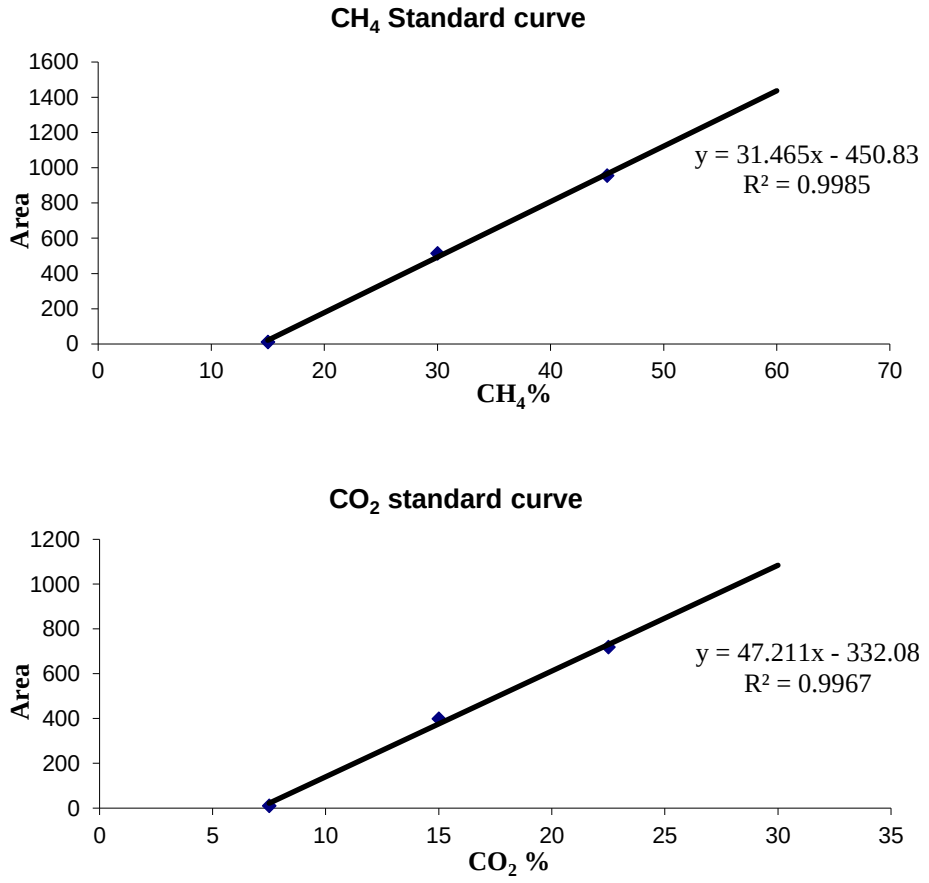

Figure C.1. The calibration curves for individual biogas composition.

Appendix D. Example of Methane Calculation as mmole/g VS

Table D.1. Sample of methane calculation as mmole/g VS.

Measured values							Calculated values						
Time (d)	**Mass media (g)**	**Mass Inoculum (g)**	**Headspace volume (ml)**	**Gas sample(ml)**	**Over pressure (ml)**	**Methane (%)**	**Gas removed**	**Headspace volume at RTP (ml)**	**Headspace methane (ml) RTP**	**Methane removed in sample (ml)**	**Cumulative methane removed (ml)**	**cumulative methane produced (ml)**	**Methane mmole/g VS**
0	100	20	45	4	0	0	0	0	0	0	0	0	0
1	100	20	45	4	0.3	3.89	4.3	2.05	0.17	0.17	2.05	2.05	0.47
2	100	20	45	4	0.2	6.90	4.2	3.55	0.29	0.46	3.72	3.55	0.86

Gas removed (Gas sample (ml) + Over pressure (ml))

Headspace volume at RTP= (Gas removed / Gas sample (ml))* (Headspace volume (ml) + Gas sample (ml))

Headspace methane (ml) RTP = (Headspace volume at RTP* Methane (%))/ 100

Methane removed in sample (ml) = (Gas removed* Methane (%) /100)

Cumulative methane removed (ml) at day N = (Cumulative methane removed (ml) at day (N-1) + (Methane removed in sample (ml))

Cumulative methane produced (ml) at day N = ((Headspace methane (ml) RTP+ Cumulative methane removed (ml) at day (N-1))

Methane mmole/ L = ((1* cumulative methane produced ml /1000))/ (0.0821*293.15)/ ((**Mass** media (g) + Mass Inoculum (g)))*1000000

Methane mmole/g VS = [methane mmole /L] / [(Mass media (g) / ((Mass media (g) + Mass Inoculum (g))]

Appendix E. Evaluation of the Experimental Methane Production and the Predict Value (Modified Gompertz Model)

1. Import the experiment data into the SPSS sheet

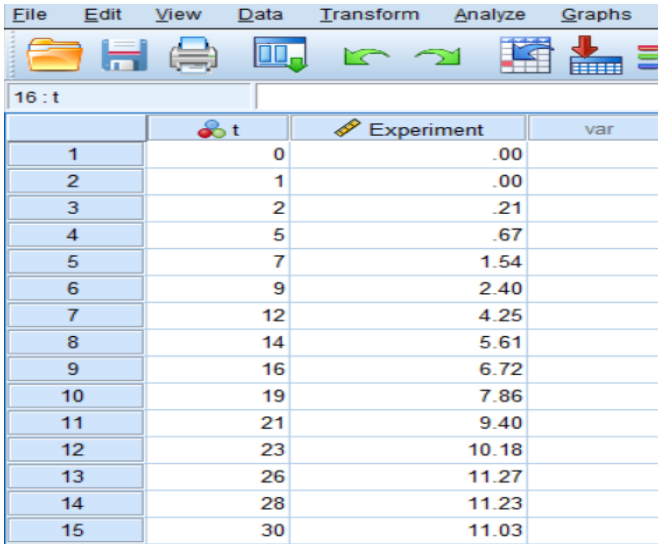

	t	Experiment	var
1	0	.00	
2	1	.00	
3	2	.21	
4	5	.67	
5	7	1.54	
6	9	2.40	
7	12	4.25	
8	14	5.61	
9	16	6.72	
10	19	7.86	
11	21	9.40	
12	23	10.18	
13	26	11.27	
14	28	11.23	
15	30	11.03	

2. Choose analyze, nonlinear regression

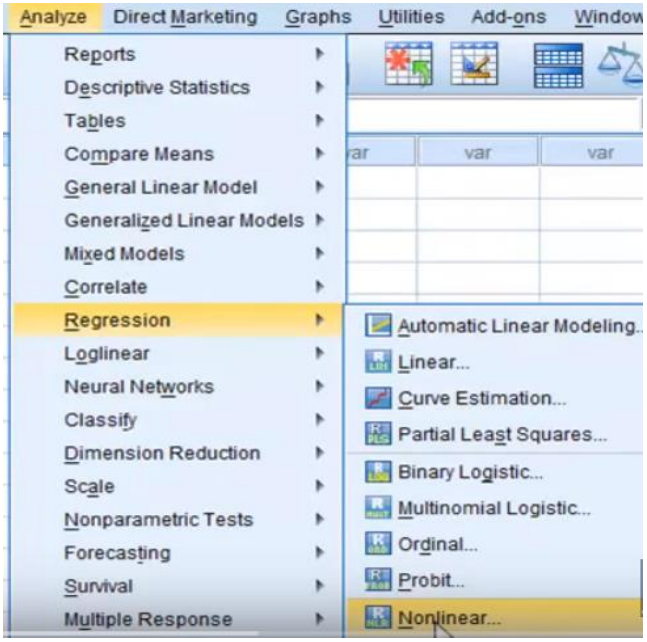

3. Insert the Gompertz equation and estimate initial parameters of R (rate) and L (lag phase), press continue and then OK

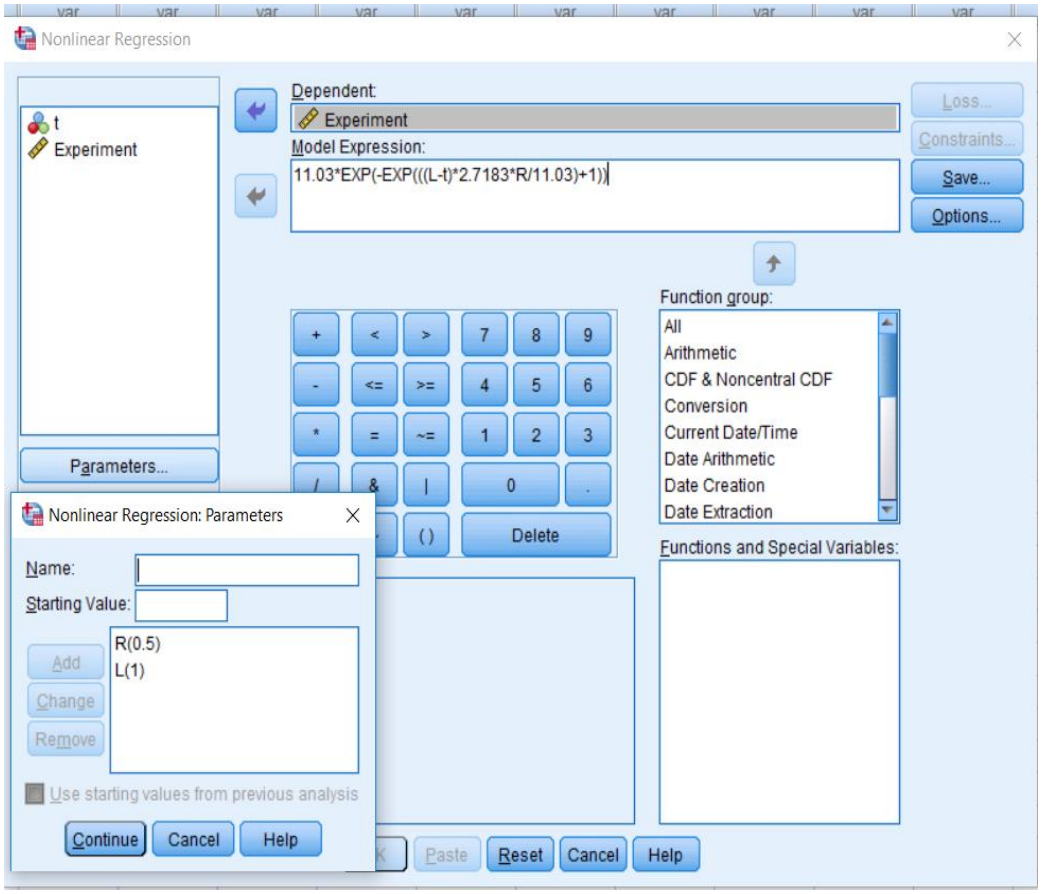

4. Obtain the predicted values of R and L

Parameter Estimates

Parameter	Estimate	Std. Error	95% Confidence Interval	
			Lower Bound	Upper Bound
R	.743	.052	.631	.855
L	6.082	.571	4.849	7.314

5. To predict the value of methane, choose Transform then choose the compute value.

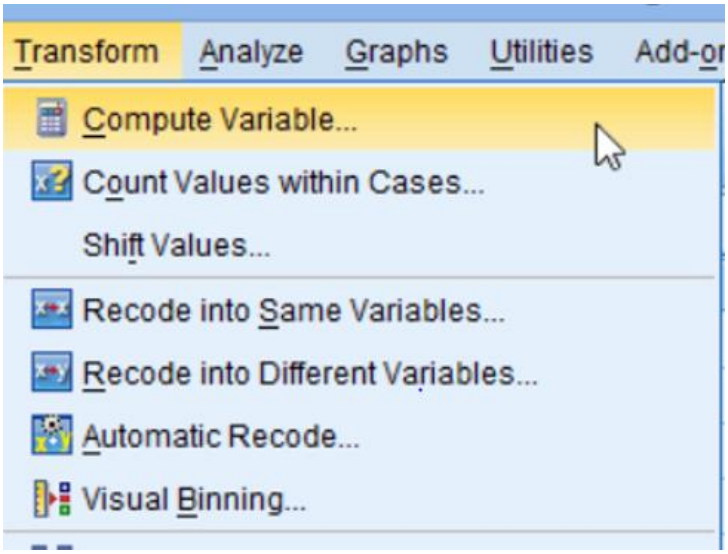

Then dialog box will appear:

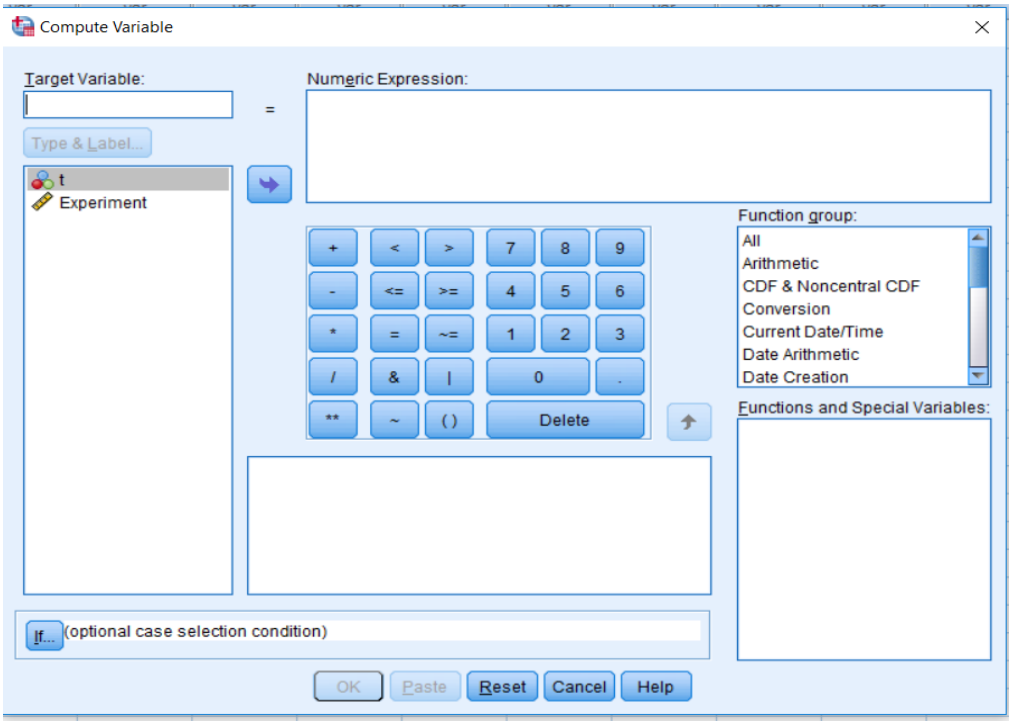

6. Apply the estimated values of R and L in Gompertz equation, then press ok

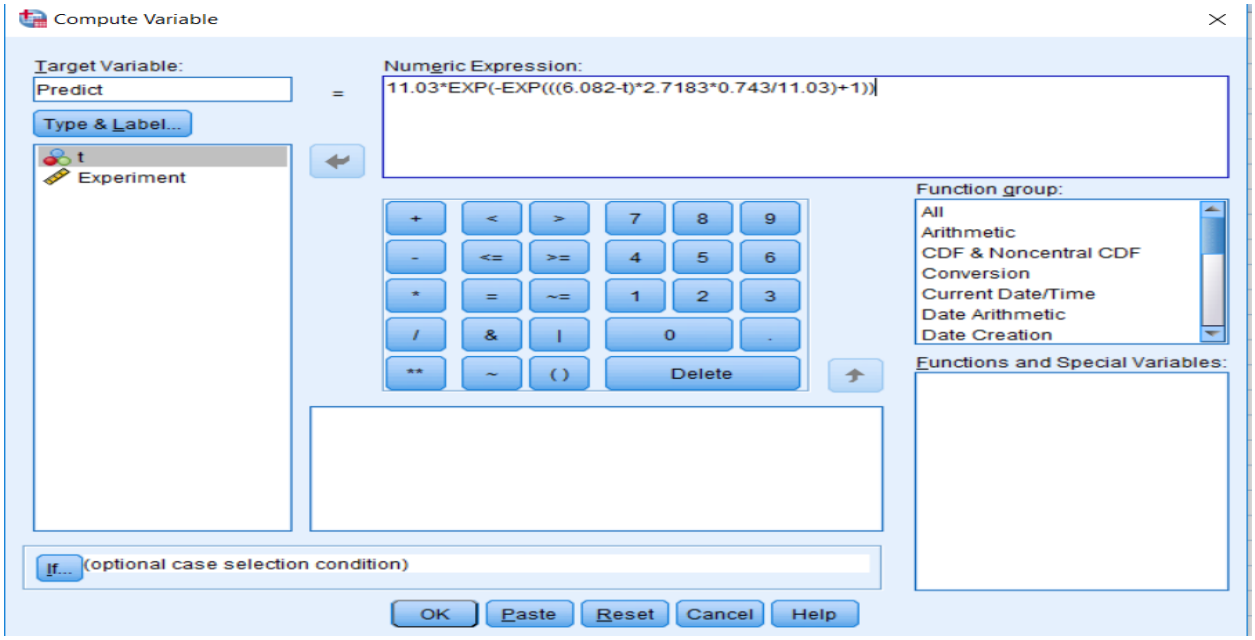

7. Finally, the predict value of methane will be calculated as shown below

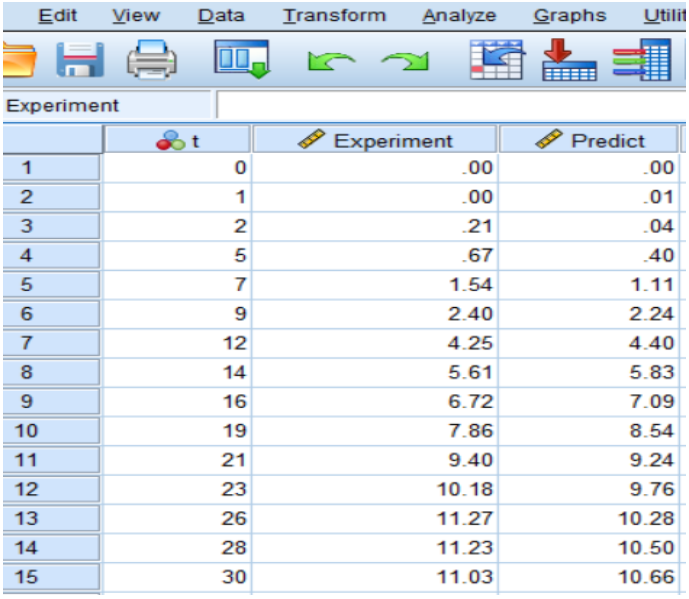

	t	Experiment	Predict
1	0	.00	.00
2	1	.00	.01
3	2	.21	.04
4	5	.67	.40
5	7	1.54	1.11
6	9	2.40	2.24
7	12	4.25	4.40
8	14	5.61	5.83
9	16	6.72	7.09
10	19	7.86	8.54
11	21	9.40	9.24
12	23	10.18	9.76
13	26	11.27	10.28
14	28	11.23	10.50
15	30	11.03	10.66

Appendix F. COD Equivalent Calculation's Sample

As the chemical formula for all carbon sources that were used as microorganisms' food is known ($\mathbf{C_n H_a O_b}$), the COD equivalent was calculated by the following stoichiometry of complete oxidation:

$$\mathbf{C_n H_a O_b} + \left(\mathbf{n} + {}^{\mathbf{a}}/_{\mathbf{4}} - {}^{\mathbf{b}}/_{\mathbf{2}}\right)\mathbf{O_2} \rightarrow \mathbf{n CO_2} + {}^{\mathbf{a}}/_{\mathbf{2}}\ \mathbf{H_2O} \qquad (1)$$

Where $\text{COD}_{\text{equivalent}}$ is a measurement of the oxygen equivalent of the organic matter content. The next example shows a sample of the COD calculation:

In the preliminarily experiment, acetate (CH_3COOH) was used, $\text{COD}_{\text{equivalent}}$ was calculated by the following stoichiometry of complete oxidation as follows:

$$\boldsymbol{C_2H_4O_2}_{\left(1\ \text{mole}*60.05\frac{\text{g}}{\text{mole}}\right)} + \mathbf{2}\boldsymbol{O_2}_{\left(2\ \text{mole}*32\frac{\text{g}}{\text{mole}}\right)} \rightarrow \mathbf{2}\boldsymbol{CO_2}_{\left(2\ \text{mole}*56\frac{\text{g}}{\text{mole}}\right)} + \mathbf{2}\boldsymbol{H_2O}_{\left(2\ \text{mole}*18\frac{\text{g}}{\text{mole}}\right)}$$

According to this stoichiometry and by relative molecular mass, each 60.05 g of acetate requires 64 g of O_2 to be completely oxidized. Therefore, for (X) g/L of acetate, the COD is

$$COD_{equivalent} = \frac{64_{\ g-O2}\ *\ (X)_{\ g-acetate/l}}{60.05_{g-acetate}} \qquad (2)$$

Appendix G. Theoretical Calculation of Interspecies Electron Transfer via H_2 Diffusion and via Magnetite-DIET

In the present study, acetate and propionate were investigated for establishing DIET via magnetite in AD. For the calculations using acetate as a substrate, calculations used the following reactions (Fotidis et al., 2014):

$$\text{Acetate}^- + 4H_2O \rightarrow 2HCO_3^- + 9\,H^+ + 8\,e^- \qquad \Delta G'_O = +104.6\ kJ$$

$$8\,e^- + HCO_3^- + 9\,H^+ \rightarrow CH_4 + 3H_2O \qquad \Delta G'_O = -135.6\ kJ$$

The concentration of acetate, methane and bicarbonate were assumed to be 0.0005 M, 2.04 x 10^{-5} M and 0.03 M respectively (note that 9 H^+ = 4 H_2 + H^+).

Using propionate as a substrate, the following reactions apply:

$$4\ \text{Propionate}^- + 12H_2O \rightarrow 4\ \text{Acetate}^- + 4\ HCO_3^- + 24e^- + 28\ H^+ \qquad \Delta Go' = +304.4\ kJ$$

$$27\ H^+ + 3\ HCO_3^- + 24e^- \rightarrow 3\ CH_4 + 9\ H_2O \qquad \Delta Go' = -408\ kJ$$

The concentration of propionate, acetate, methane and bicarbonate were assumed to be 0.005 M, 0.0005 M, 2.04 x 10^{-5} M, and 0.03 M respectively (note that 28 H^+ = 12 H_2 + 4H^+ and 27 H^+ = 12 H_2 + 3 H^+).

Table 6.5 shows the values of theoretical calculation of interspecies electron transfer via H_2 diffusion and via Magnetite-DIET based on Fick's diffusion law and the Nernst equation as reported by Cruz Viggi et al. (2014) and Lin et al. (2018). These calculations were done under several assumptions (i.e. interbacterial distance, the average diameter and the spherical shape of both acetogen and methanogen, the electrons released are transferred to a methanogen via an electron conduit consisting of magnetite particles, and the electrical conduit was assumed to be a wire).

The maximum electron transfer via H_2 was calculated based on Fick's diffusion law

$$i = D_f * \frac{S_{cell}}{d} * \left([H_2]_{Highest} - [H_2]_{Lowest}\right) * n * F$$

where D_f : Diffusion coefficient of H_2 in water; 4.5 x10^{-9} m^2/s, S_{cell} : Surface area of the cell; (spherical with diameter of 2 x 10^{-6} m) 1.268 x10^{-11} m^2, d : Distance between cells; 5 x10^{-7} m, n : Mol of electron per mole of H_2, F : Faraday's constant; 96485 s*A/mol, $\Delta G^{ó}$: Standard Gibbs free energy change per reaction, R: 0.00831451 kJ/mol/K, and T: 308.15 K.

The maximum electron transfer via magnetite - DIET was calculated based on the Nernst equation;

$$i = \sigma * \frac{S_{conduit}}{d} * (E_{met} - E_{ace})$$

$$(E_{met} - E_{ace}) = {}^{-\Delta G'}/_{n * F}$$

where σ : Electrical conductivity of magnetite; 2.5 x 10^6 **Ω**/m^2, $S_{conduit}$: Cross-sectional area of the conductive material; (a wire with diameter of 168 – 490 x10^{-9} m), d : Distance between cells; 5 x10^{-7} m, n : mol of electron per reaction, F : Faraday's constant ; 96.485 kJ/mol.V, $\Delta G^{ó}$: Standard Gibbs free energy change per reaction, R: 0.00831451 kJ/mol/K, and T: 308.15 K.

As an example, for propionate degradation, the highest H_2 concentration produced by acetogens and the lowest H_2 concentration reached by methanogens would be:

$$\Delta G' = zero = \Delta G^{O\prime} + RTln\left(\frac{[Products]^m}{[Reactants]^n}\right)$$

The Highest H_2 concentration (1.0067 mol/m^3) was calculated as follows

$$zero = +304.4 + RTln\left(\frac{[acetate]^4[HCO_3^-]^4\,[Highest\ H_2]^{12}}{[Propionate]^4}\right)$$

and the lowest H_2 concentration (0.00289 mol/m^3) was calculated as follows

$$\text{zero} = -408 + \text{RTln}\left(\frac{[\text{CH}_4]^3}{[HCO_3^-]^3\,[Lowest\ H_2]^{12}}\right)$$

So, the maximum electron transfer via H_2 was 2.21 x 10^{-8} A.

To calculate the maximum electron transfer via magnetite-DIET, assuming that the electrons are transferred through the overall reaction ($4\text{Propionate}^- + 3\text{H}_2\text{O} \rightarrow 4\,\text{Acetate}^- + 3\text{CH}_4 + \text{HCO}_3^- + \text{H}^+$; $\Delta Go' = -103.6\ kJ$). The value $\Delta G' = -103.6 + RTln\left(\frac{[acetate]^4[HCO_3^-]^1\,[CH_4]^3}{[Propionate]^4}\right)$ and so $\Delta E_{Over\ all\ reaction} = 0.08$ V, the flux via magnetite = 7.16 x 10^{-4} A.

Appendix H. Experimental and Predicted Methane Production by Modified Gompertz Model

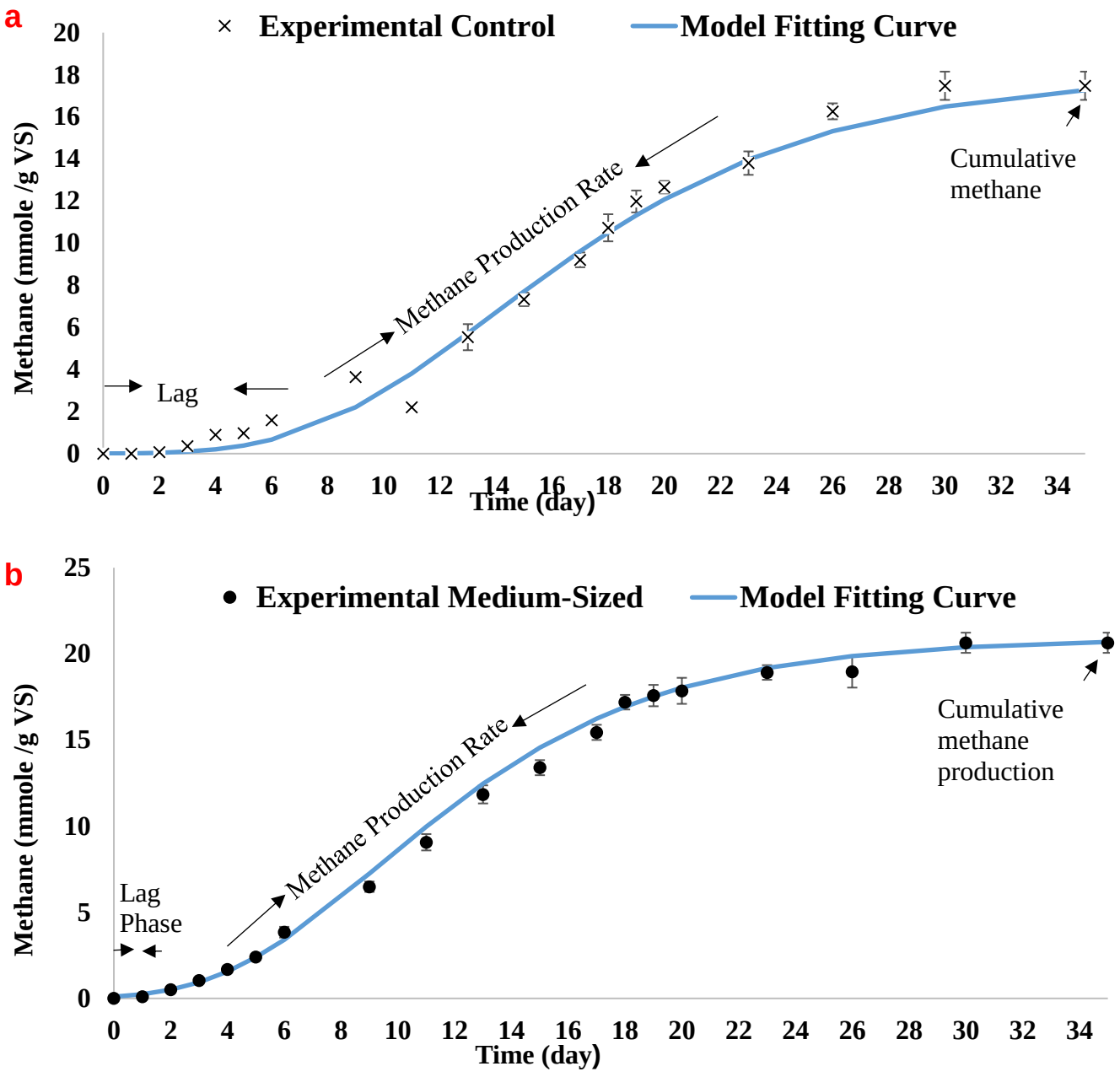

Figure H.1. Examples of evolution of experimental and predicted methane production by modified Gompertz model (a) for control and (b) for medium- sized magnetite.

Appendix I. Microbial Community Compositions

Archaeal community structure (A) and bacterial community structure (B) at specious level associated with different conditions as follows:

Sample ID	Treatment
UC.1.1	Initial sludge
UC.2.1	Control (3 COD:1 VS) at 2 weeks,
UC.6.1	Control (3 COD:1 VS) at 8 weeks,
UC.4.1	Magnetite (3 COD:1 VS) at 2 weeks
UC.8.1	Magnetite (3 COD:1 VS) at 8 weeks
UC.3.1	Control (6 COD:1 VS) at 2 weeks,
UC.7.1	Control (6 COD:1 VS) at 8 weeks,
UC.5.1	Magnetite (6 COD:1 VS) at 2 weeks
UC.9.1	Magnetite (6 COD:1 VS) at 8 weeks

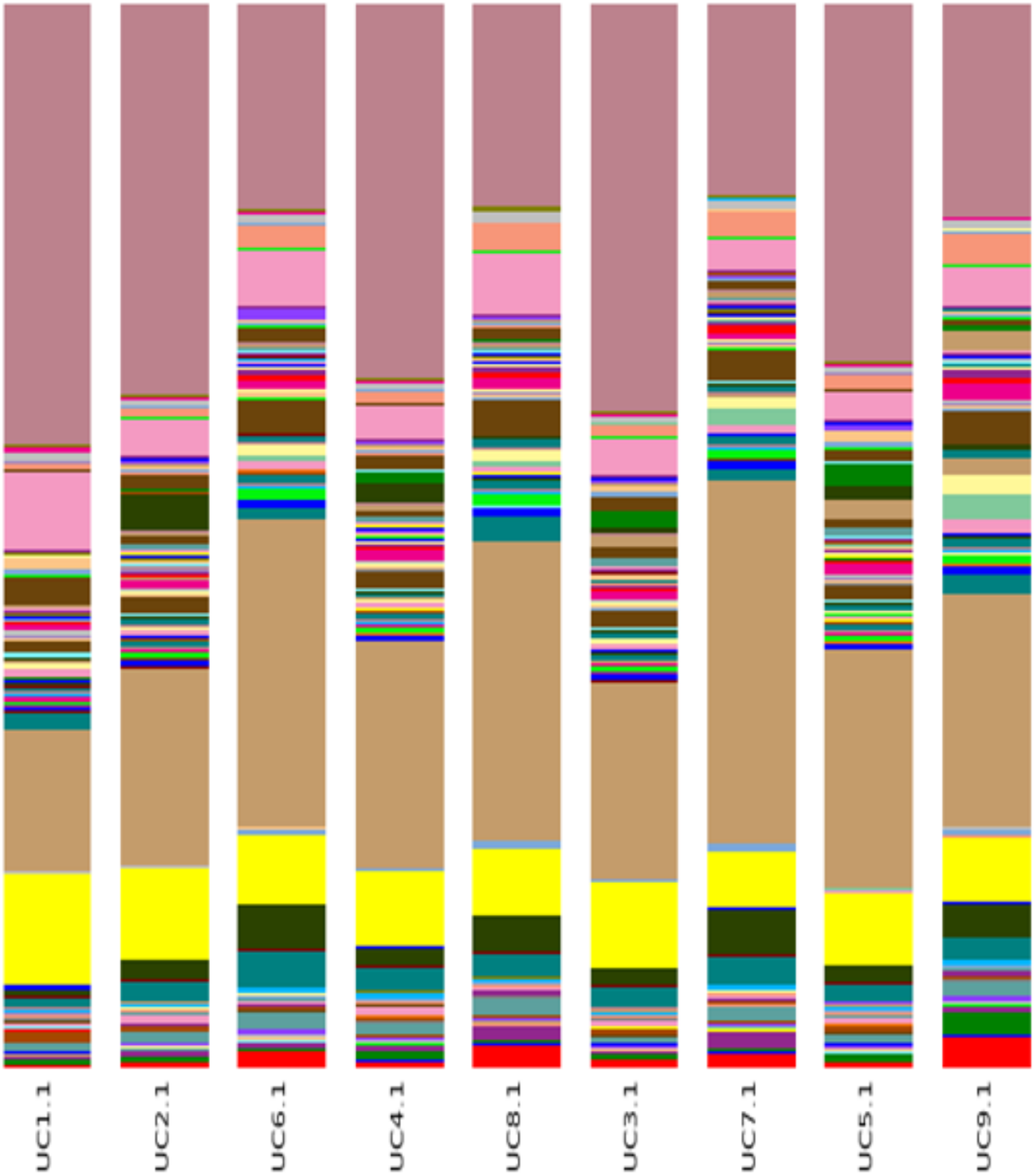

Figure I.1. Archaeal community structure (A) and bacterial community structure (B) at as specious level associated with different conditions.

Table I.1 Microbial community structure at genus level associated with different conditions.

Genus Community Structure	**Initial Sludge**	**Control, 3 COD:1VS after 2 weeks**	**Control, 3 COD:1VS after 8 weeks**	**Magnetite, 3 COD:1VS after 2 weeks**	**Magnetite, 3 COD:1VS after 8 weeks**	**Control, 6 COD:1VS after 2 weeks**	**Control, 6 COD:1VS after 8 weeks**	**Magnetite, 6 COD:1VS after 2 weeks**	**Magnetite, 6 COD:1VS after 8 weeks**
Archaea									
Methanothermobacter	0.4%	0.6%	1.6%	0.7%	2.3%	0.9%	1.5%	0.6%	3.0%
Methanosarcina	0.5%	0.4%	0.1%	0.8%	0.3%	0.4%	0.2%	0.6%	2.1%
Methanothrix	0.1%	0.6%	0.7%	0.5%	1.2%	0.2%	1.6%	0.2%	0.5%
Methanospirillum	0.0%	0.0%	0.1%	0.0%	0.0%	0.00%	0.1%	0.0%	0.0%
Bacteria									
Coprothermobacter	13.4%	18.7%	29.0%	21.3%	28.1%	18.6%	34.0%	22.4%	21.9%
Lutaonella	10.4%	8.4%	6.4%	7.1%	6.3%	8.1%	5.2%	6.8%	6.1%
Rectinema	7.4%	3.4%	5.2%	3.0%	5.8%	3.3%	3.0%	2.7%	3.7%
Tangfeifania		1.9%	4.2%	1.7%	3.4%	1.6%	4.1%	1.5%	3.0%
Gelria	1.1%	1.5%	3.0%	1.6%	3.3%	1.6%	3.0%	1.4%	3.0%
Sunxiuqinia	1.0%	2.0%	3.7%	2.3%	2.3%	2.1%	2.9%	1.9%	2.1%
Smithella	2.6%	1.1%	1.3%	1.2%	1.0%	1.2%		1.3%	
Leucobacter	0.8%	0.9%	1.6%	1.2%	1.7%		1.3%	0.9%	1.5%
Sporosarcina	1.5%		0.9%		2.2%		0.9%		1.9%
Bacteroides	1.2%								
Defluviitoga	1.0%								1.0%
Acetomicrobium		0.9%	2.4%	1.2%	2.7%	1.1%	2.4%	1.2%	3.0%
Desulfobulbus		3.5%		1.9%				1.3%	
Sedimentibacter		0.9%		0.9%	1.0%	0.9%		0.9%	1.5%
Clostridium			0.9%		1.1%		0.9%		0.9%
Desulfofundulus			0.9%		1.1%		0.9%		1.7%
Desulfovibrio				0.9%		1.6%		2.0%	
Cryptanaerobacter							1.6%		2.4%
Thermoclostridium									1.1%
Pelotomaculum									1.7%
Janthinobacterium						1.1%		0.9%	
Thauera						1.0%		1.6%	1.7%
Pseudomonas			1.0%						
Others (all ≤ 0.8%)	57.9%	55.2%	37.0%	53.7%	36.2%	56.3%	36.4%	51.8%	37.1%

Legend	Taxonomy	Total %	UC 1.1 %	UC 2.1 %	UC 6.1 %	UC 4.1 %	UC 8.1 %	UC 3.1 %	UC 7.1 %	UC 5.1 %	UC 9.1 %
	Archaea;__Euryarchaeota;__Methanobacteria;__Methanobacteriales;__Methanobacteriaceae;__Methanothermobacter;__Methanothermobacter tenebrarum	1.2 %	0.3 %	0.6 %	1.4 %	0.6 %	2.1 %	0.8 %	1.4 %	0.5 %	2.9 %
	Archaea;__Euryarchaeota;__Methanobacteria;__Methanobacteriales;__Methanobacteriaceae;__Methanothermobacter;__Methanothermobacter thermautotrophicus	0.1 %	0.1 %	0.0 %	0.2 %	0.1 %	0.2 %	0.1 %	0.1 %	0.1 %	0.1 %
	Archaea;__Euryarchaeota;__Methanomicrobia;__Methanomicrobiales;__Methanospirillaceae;__Methanospirillum;__Methanospirillum hungatei	0.0 %	0.0 %	0.0 %	0.1 %	0.0 %	0.0 %	0.0 %	0.1 %	0.0 %	0.0 %
	Archaea;__Euryarchaeota;__Methanomicrobia;__Methanosarcinales;__Methanosarcinaceae;__Methanosarcina;__Methanosarcina thermophila	0.6 %	0.5 %	0.4 %	0.1 %	0.8 %	0.3 %	0.4 %	0.2 %	0.6 %	2.1 %
	Archaea;__Euryarchaeota;__Methanomicrobia;__Methanosarcinales;__Methanotrichaceae;__Methanothrix;__Methanothrix soehngenii	0.6 %	0.1 %	0.6 %	0.7 %	0.5 %	1.2 %	0.2 %	1.6 %	0.2 %	0.5 %
	Archaea;__Euryarchaeota;__Thermoplasmata;__Methanomassiliicoccales;__Methanomassiliicoccaceae;__Methanomassiliicoccus;__Methanomassiliicoccus luminyensis	0.0 %	0.0 %	0.0 %	0.0 %	0.0 %	0.0 %	0.0 %	0.0 %	0.0 %	0.0 %
	Bacteria;__Acidobacteria;__Acidobacteriia;__Bryobacterales;__Bryobacteraceae;__Paludibaculum;__Paludibaculum fermentans	0.0 %	0.0 %	0.0 %	0.0 %	0.0 %	0.0 %	0.0 %	0.0 %	0.0 %	0.0 %
	Bacteria;__Acidobacteria;__Vicinamibacteria;__;__Vicinamibacteraceae;__Vicinamibacter;__Vicinamibacter silvestris	0.0 %	0.0 %	0.0 %	0.0 %	0.0 %	0.0 %	0.0 %	0.0 %	0.0 %	0.0 %
	Bacteria;__Actinobacteria;__Acidimicrobiia;__Acidimicrobiales;__Acidimicrobiaceae;__Aciditerrimonas;__Aciditerrimonas ferrireducens	0.0 %	0.0 %	0.0 %	0.0 %	0.0 %	0.0 %	0.1 %	0.0 %	0.0 %	0.0 %
	Bacteria;__Actinobacteria;__Acidimicrobiia;__Acidimicrobiales;__Ilumatobacteraceae;__Ilumatobacter;__Ilumatobacter fluminis	0.0 %	0.0 %	0.0 %	0.0 %	0.0 %	0.0 %	0.0 %	0.0 %	0.0 %	0.0 %
	Bacteria;__Actinobacteria;__Actinobacteria;__Actinomycetales;__Actinomycetaceae;__Actinomyces;__Actinomyces polynesiensis	0.0 %	0.0 %	0.0 %	0.0 %	0.0 %	0.0 %	0.0 %	0.0 %	0.0 %	0.0 %
	Bacteria;__Actinobacteria;__Actinobacteria;__Actinomycetales;__Actinomycetaceae;__Actinotignum;__Actinotignum schaalii	0.1 %	0.1 %	0.1 %	0.1 %	0.1 %	0.1 %	0.1 %	0.1 %	0.1 %	0.1 %
	Bacteria;__Actinobacteria;__Actinobacteria;__Actinomycetales;__Actinomycetaceae;__Schaalia;__Schaalia canis	0.1 %	0.0 %	0.0 %	0.1 %	0.1 %	0.1 %	0.0 %	0.1 %	0.1 %	0.1 %
	Bacteria;__Actinobacteria;__Actinobacteria;__Actinomycetales;__Actinomycetaceae;__Schaalia;__Schaalia cardiffensis	0.0 %	0.0 %	0.0 %	0.0 %	0.0 %	0.0 %	0.0 %	0.0 %	0.0 %	0.0 %
	Bacteria;__Actinobacteria;__Actinobacteria;__Bifidobacteriales;__Bifidobacteriaceae;__Bifidobacterium;__Bifidobacterium adolescentis	0.0 %	0.0 %	0.0 %	0.0 %	0.0 %	0.0 %	0.0 %	0.0 %	0.0 %	0.0 %
	Bacteria;__Actinobacteria;__Actinobacteria;__Corynebacteriales;__Corynebacteriaceae;__Corynebacterium;__Corynebacterium terpenotabidum	0.0 %	0.0 %	0.0 %	0.1 %	0.0 %	0.0 %	0.0 %	0.0 %	0.1 %	0.0 %
	Bacteria;__Actinobacteria;__Actinobacteria;__Corynebacteriales;__Corynebacteriaceae;__Corynebacterium;__Corynebacterium xerosis	0.0 %	0.0 %	0.0 %	0.0 %	0.0 %	0.0 %	0.0 %	0.0 %	0.0 %	0.0 %
	Bacteria;__Actinobacteria;__Actinobacteria;__Corynebacteriales;__Dietziaceae;__Dietzia;__Dietzia lutea	0.0 %	0.0 %	0.0 %	0.1 %	0.0 %	0.0 %	0.0 %	0.1 %	0.0 %	0.1 %
	Bacteria;__Actinobacteria;__Actinobacteria;__Corynebacteriales;__Gordoniaceae;__Gordonia;__Gordonia phthalatica	0.1 %	0.0 %	0.1 %	0.1 %	0.1 %	0.1 %	0.1 %	0.1 %	0.1 %	0.1 %
	Bacteria;__Actinobacteria;__Actinobacteria;__Corynebacteriales;__Gordoniaceae;__Gordonia;__Gordonia sinesedis	0.0 %	0.0 %	0.0 %	0.0 %	0.0 %	0.0 %	0.0 %	0.0 %	0.0 %	0.0 %
	Bacteria;__Actinobacteria;__Actinobacteria;__Corynebacteriales;__Mycobacteriaceae;__Mycobacterium;__Mycobacterium lehmannii	0.0 %	0.0 %	0.0 %	0.0 %	0.0 %	0.0 %	0.0 %	0.0 %	0.0 %	0.0 %
	Bacteria;__Actinobacteria;__Actinobacteria;__Corynebacteriales;__Mycobacteriaceae;__Mycolicibacter;__Mycolicibacter minnesotensis	0.1 %	0.0 %	0.1 %	0.1 %	0.1 %	0.1 %	0.1 %	0.1 %	0.1 %	0.1 %
	Bacteria;__Actinobacteria;__Actinobacteria;__Corynebacteriales;__Mycobacteriaceae;__Mycolicibacter;__Mycolicibacter nonchromogenicus	0.0 %	0.0 %	0.0 %	0.0 %	0.0 %	0.0 %	0.0 %	0.0 %	0.0 %	0.0 %
	Bacteria;__Actinobacteria;__Actinobacteria;__Corynebacteriales;__Mycobacteriaceae;__Mycolicibacterium;__Mycolicibacterium arcueilense	0.3 %	0.1 %	0.2 %	0.5 %	0.4 %	0.4 %	0.2 %	0.3 %	0.3 %	0.4 %
	Bacteria;__Actinobacteria;__Actinobacteria;__Corynebacteriales;__Nocardiaceae;__Nocardia;__Nocardia coeliaca	0.0 %	0.0 %	0.0 %	0.0 %	0.0 %	0.0 %	0.0 %	0.0 %	0.0 %	0.0 %
	Bacteria;__Actinobacteria;__Actinobacteria;__Corynebacteriales;__Nocardiaceae;__Williamsia;__Williamsia spongiae	0.0 %	0.0 %	0.0 %	0.0 %	0.0 %	0.0 %	0.0 %	0.0 %	0.0 %	0.0 %
	Bacteria;__Actinobacteria;__Actinobacteria;__Corynebacteriales;__Tsukamurellaceae;__Tsukamurella;__Tsukamurella ocularis	0.0 %	0.0 %	0.0 %	0.0 %	0.0 %	0.0 %	0.0 %	0.0 %	0.0 %	0.0 %
	Bacteria;__Actinobacteria;__Actinobacteria;__Geodermatophilales;__Geodermatophilaceae;__Geodermatophilus;__Geodermatophilus pulveris	0.0 %	0.0 %	0.0 %	0.0 %	0.0 %	0.0 %	0.0 %	0.0 %	0.0 %	0.0 %
	Bacteria;__Actinobacteria;__Actinobacteria;__Geodermatophilales;__Geodermatophilaceae;__Klenkia;__Klenkia marina	0.0 %	0.0 %	0.0 %	0.0 %	0.0 %	0.0 %	0.0 %	0.0 %	0.0 %	0.0 %
	Bacteria;__Actinobacteria;__Actinobacteria;__Glycomycetales;__Glycomycetaceae;__Stackebrandtia;__Stackebrandtia endophytica	0.0 %	0.0 %	0.0 %	0.0 %	0.0 %	0.0 %	0.0 %	0.0 %	0.0 %	0.0 %

Bacteria;__Actinobacteria;__Actinobacteria;__Kineosporiales;__Kineosporiaceae;__Kineosporia;__Kineosporia rhamnosa	0.1 %	0.2 %	0.1 %	0.0 %	0.0 %	0.0 %	0.1 %	0.0 %	0.1 %	0.0 %
Bacteria;__Actinobacteria;__Actinobacteria;__Micrococcales;__Bogoriellaceae;__Georgenia;__Georgenia deserti	0.0 %	0.0 %	0.0 %	0.0 %	0.0 %	0.0 %	0.0 %	0.0 %	0.0 %	0.0 %
Bacteria;__Actinobacteria;__Actinobacteria;__Micrococcales;__Cellulomonadaceae;__Cellulomonas;__Cellulomonas hominis	0.0 %	0.0 %	0.0 %	0.0 %	0.0 %	0.0 %	0.0 %	0.0 %	0.0 %	0.0 %
Bacteria;__Actinobacteria;__Actinobacteria;__Micrococcales;__Cellulomonadaceae;__Oerskovia;__Oerskovia enterophila	0.0 %	0.0 %	0.0 %	0.0 %	0.0 %	0.0 %	0.0 %	0.0 %	0.0 %	0.0 %
Bacteria;__Actinobacteria;__Actinobacteria;__Micrococcales;__Dermatophilaceae;__Kineosphaera;__Kineosphaera nakaumiensis	0.0 %	0.0 %	0.0 %	0.0 %	0.0 %	0.0 %	0.0 %	0.0 %	0.0 %	0.0 %
Bacteria;__Actinobacteria;__Actinobacteria;__Micrococcales;__Dermatophilaceae;__Piscicoccus;__Piscicoccus intestinalis	0.0 %	0.0 %	0.0 %	0.0 %	0.0 %	0.0 %	0.0 %	0.0 %	0.0 %	0.0 %
Bacteria;__Actinobacteria;__Actinobacteria;__Micrococcales;__Microbacteriaceae;__Leucobacter;__Leucobacter aerolatus	0.0 %	0.0 %	0.0 %	0.0 %	0.0 %	0.0 %	0.0 %	0.0 %	0.0 %	0.0 %
Bacteria;__Actinobacteria;__Actinobacteria;__Micrococcales;__Microbacteriaceae;__Leucobacter;__Leucobacter komagatae	1.1 %	0.8 %	0.9 %	1.6 %	1.1 %	1.6 %	0.7 %	1.3 %	0.9 %	1.4 %
Bacteria;__Actinobacteria;__Actinobacteria;__Micrococcales;__Microbacteriaceae;__Leucobacter;__Leucobacter musarum	0.0 %	0.0 %	0.0 %	0.0 %	0.0 %	0.0 %	0.0 %	0.0 %	0.0 %	0.0 %
Bacteria;__Actinobacteria;__Actinobacteria;__Micrococcales;__Microbacteriaceae;__Microbacterium;__Microbacterium flavescens	0.1 %	0.1 %	0.1 %	0.1 %	0.1 %	0.1 %	0.1 %	0.1 %	0.1 %	0.1 %
Bacteria;__Actinobacteria;__Actinobacteria;__Nakamurellales;__Nakamurellaceae;__Nakamurella;__Nakamurella multipartita	0.0 %	0.0 %	0.0 %	0.0 %	0.0 %	0.0 %	0.0 %	0.0 %	0.0 %	0.0 %
Bacteria;__Actinobacteria;__Actinobacteria;__Propionibacteriales;__Nocardioidaceae;__Aeromicrobium;__Aeromicrobium ginsengisoli	0.0 %	0.0 %	0.0 %	0.0 %	0.0 %	0.0 %	0.0 %	0.0 %	0.0 %	0.0 %
Bacteria;__Actinobacteria;__Actinobacteria;__Propionibacteriales;__Nocardioidaceae;__Marmoricola;__Marmoricola pocheonensis	0.0 %	0.0 %	0.0 %	0.0 %	0.0 %	0.0 %	0.0 %	0.0 %	0.0 %	0.0 %
Bacteria;__Actinobacteria;__Actinobacteria;__Propionibacteriales;__Nocardioidaceae;__Marmoricola;__Marmoricola terrae	0.0 %	0.0 %	0.0 %	0.0 %	0.0 %	0.0 %	0.0 %	0.0 %	0.0 %	0.0 %
Bacteria;__Actinobacteria;__Actinobacteria;__Propionibacteriales;__Nocardioidaceae;__Micropruina;__Micropruina glycogenica	0.0 %	0.0 %	0.0 %	0.0 %	0.0 %	0.0 %	0.0 %	0.0 %	0.0 %	0.0 %
Bacteria;__Actinobacteria;__Actinobacteria;__Propionibacteriales;__Nocardioidaceae;__Nocardioides;__Nocardioides caricicola	0.0 %	0.0 %	0.0 %	0.0 %	0.0 %	0.0 %	0.0 %	0.0 %	0.0 %	0.0 %
Bacteria;__Actinobacteria;__Actinobacteria;__Propionibacteriales;__Nocardioidaceae;__Nocardioides;__Nocardioides exalbidus	0.0 %	0.0 %	0.0 %	0.0 %	0.0 %	0.0 %	0.0 %	0.0 %	0.0 %	0.0 %
Bacteria;__Actinobacteria;__Actinobacteria;__Propionibacteriales;__Propionibacteriaceae;__Propioniciclava;__Propioniciclava tarda	0.0 %	0.0 %	0.0 %	0.0 %	0.0 %	0.0 %	0.0 %	0.0 %	0.0 %	0.0 %
Bacteria;__Actinobacteria;__Actinobacteria;__Pseudonocardiales;__Pseudonocardiaceae;__Pseudonocardia;__Pseudonocardia profundimaris	0.0 %	0.0 %	0.0 %	0.0 %	0.0 %	0.0 %	0.0 %	0.0 %	0.0 %	0.0 %
Bacteria;__Actinobacteria;__Actinobacteria;__Sporichthyales;__Sporichthyaceae;__Longivirga;__Longivirga aurantiaca	0.0 %	0.0 %	0.0 %	0.0 %	0.0 %	0.0 %	0.0 %	0.0 %	0.0 %	0.0 %
Bacteria;__Actinobacteria;__Actinobacteria;__Streptomycetales;__Streptomycetaceae;__Streptomyces;__Streptomyces albus	0.0 %	0.0 %	0.0 %	0.0 %	0.0 %	0.0 %	0.0 %	0.0 %	0.0 %	0.0 %
Bacteria;__Actinobacteria;__Actinobacteria;__Streptosporangiales;__Thermomonosporaceae;__Actinomadura;__Actinomadura oligospora	0.0 %	0.0 %	0.0 %	0.0 %	0.0 %	0.0 %	0.0 %	0.0 %	0.0 %	0.0 %
Bacteria;__Actinobacteria;__Coriobacteriia;__Coriobacteriales;__Atopobiaceae;__Atopobium;__Atopobium parvulum	0.0 %	0.0 %	0.0 %	0.0 %	0.0 %	0.0 %	0.0 %	0.0 %	0.0 %	0.0 %
Bacteria;__Actinobacteria;__Rubrobacteria;__Gaiellales;__Gaiellaceae;__Gaiella;__Gaiella occulta	0.0 %	0.0 %	0.0 %	0.0 %	0.0 %	0.0 %	0.0 %	0.0 %	0.0 %	0.0 %
Bacteria;__Actinobacteria;__Rubrobacteria;__Rubrobacterales;__Rubrobacteraceae;__Rubrobacter;__Rubrobacter taiwanensis	0.0 %	0.0 %	0.0 %	0.0 %	0.0 %	0.0 %	0.0 %	0.0 %	0.0 %	0.0 %
Bacteria;__Actinobacteria;__Thermoleophilia;__Solirubrobacterales;__Patulibacteraceae;__Patulibacter;__Patulibacter brassicae	0.0 %	0.0 %	0.0 %	0.0 %	0.0 %	0.0 %	0.0 %	0.0 %	0.0 %	0.0 %
Bacteria;__Actinobacteria;__Thermoleophilia;__Solirubrobacterales;__Solirubrobacteraceae;__Solirubrobacter;__Solirubrobacter ginsenosidimutans	0.0 %	0.0 %	0.0 %	0.0 %	0.0 %	0.0 %	0.0 %	0.0 %	0.0 %	0.0 %
Bacteria;__Bacteroidetes;__Bacteroidia;__Bacteroidales;__Bacteroidaceae;__Bacteroides;__Bacteroides gallinarum	0.4 %	1.1 %	0.5 %	0.2 %	0.4 %	0.1 %	0.5 %	0.1 %	0.6 %	0.1 %
Bacteria;__Bacteroidetes;__Bacteroidia;__Bacteroidales;__Bacteroidaceae;__Bacteroides;__Bacteroides luti	0.0 %	0.0 %	0.0 %	0.0 %	0.0 %	0.0 %	0.0 %	0.0 %	0.0 %	0.0 %
Bacteria;__Bacteroidetes;__Bacteroidia;__Bacteroidales;__Bacteroidaceae;__Bacteroides;__Bacteroides propionicifaciens	0.0 %	0.0 %	0.0 %	0.0 %	0.0 %	0.0 %	0.0 %	0.0 %	0.0 %	0.0 %
Bacteria;__Bacteroidetes;__Bacteroidia;__Bacteroidales;__Bacteroidaceae;__Bacteroides;__Bacteroides timonensis	0.1 %	0.1 %	0.0 %	0.0 %	0.1 %	0.0 %	0.1 %	0.0 %	0.1 %	0.0 %
Bacteria;__Bacteroidetes;__Bacteroidia;__Bacteroidales;__Dysgonamonadaceae;__Proteiniphilum;__Proteiniphilum saccharofermentans	0.0 %	0.0 %	0.0 %	0.0 %	0.0 %	0.0 %	0.0 %	0.0 %	0.0 %	0.0 %
Bacteria;__Bacteroidetes;__Bacteroidia;__Bacteroidales;__Lentimicrobiaceae;__Lentimicrobium;__Lentimicrobium saccharophilum	0.2 %	0.1 %	0.1 %	0.3 %	0.1 %	0.3 %	0.1 %	0.3 %	0.1 %	0.4 %

Bacteria;__Bacteroidetes;__Bacteroidia;__Bacteroidales;__Paludibacteraceae;__Paludibacter;__Paludibacter propionicigenes	0.0 %	0.0 %	0.0 %	0.0 %	0.0 %	0.0 %	0.1 %	0.0 %	0.0 %	0.0 %
Bacteria;__Bacteroidetes;__Bacteroidia;__Bacteroidales;__Porphyromonadaceae;__Macellibacteroides;__Macellibacteroides fermentans	0.0 %	0.0 %	0.0 %	0.0 %	0.0 %	0.0 %	0.0 %	0.0 %	0.0 %	0.0 %
Bacteria;__Bacteroidetes;__Bacteroidia;__Bacteroidales;__Porphyromonadaceae;__Microbacter;__Microbacter margulisiae	0.4 %	0.4 %	0.9 %	0.3 %	0.7 %	0.3 %	0.5 %	0.3 %	0.5 %	0.1 %
Bacteria;__Bacteroidetes;__Bacteroidia;__Bacteroidales;__Porphyromonadaceae;__Petrimonas;__Petrimonas sulfuriphila	0.1 %	0.1 %	0.1 %	0.1 %	0.1 %	0.0 %	0.1 %	0.0 %	0.1 %	0.1 %
Bacteria;__Bacteroidetes;__Bacteroidia;__Bacteroidales;__Tannerellaceae;__Parabacteroides;__Parabacteroides chartae	0.1 %	0.1 %	0.1 %	0.0 %	0.1 %	0.0 %	0.1 %	0.0 %	0.1 %	0.0 %
Bacteria;__Bacteroidetes;__Bacteroidia;__Bacteroidales;__Tannerellaceae;__Parabacteroides;__Parabacteroides gordonii	0.1 %	0.3 %	0.1 %	0.1 %	0.2 %	0.1 %	0.1 %	0.0 %	0.1 %	0.0 %
Bacteria;__Bacteroidetes;__Bacteroidia;__Bacteroidales;__Tannerellaceae;__Tannerella;__Tannerella forsythia	0.0 %	0.0 %	0.0 %	0.0 %	0.0 %	0.0 %	0.0 %	0.0 %	0.0 %	0.0 %
Bacteria;__Bacteroidetes;__Bacteroidia;__Bacteroidales;__Williamwhitmaniaceae;__Williamwhitmania;__Williamwhitmania taraxaci	0.2 %	0.3 %	0.1 %	0.2 %	0.2 %	0.1 %	0.2 %	0.1 %	0.2 %	0.1 %
Bacteria;__Bacteroidetes;__Bacteroidia;__Marinilabiliales;__Marinilabiliaceae;__Alkalitalea;__Alkalitalea saponilacus	0.1 %	0.1 %	0.1 %	0.2 %	0.2 %	0.2 %	0.1 %	0.2 %	0.1 %	0.2 %
Bacteria;__Bacteroidetes;__Bacteroidia;__Marinilabiliales;__Marinilabiliaceae;__Carboxylicivirga;__Carboxylicivirga flava	0.0 %	0.0 %	0.0 %	0.0 %	0.0 %	0.0 %	0.0 %	0.0 %	0.0 %	0.0 %
Bacteria;__Bacteroidetes;__Bacteroidia;__Marinilabiliales;__Marinilabiliaceae;__Carboxylicivirga;__Carboxylicivirga mesophila	0.0 %	0.0 %	0.0 %	0.0 %	0.0 %	0.0 %	0.0 %	0.0 %	0.0 %	0.0 %
Bacteria;__Bacteroidetes;__Bacteroidia;__Marinilabiliales;__Marinilabiliaceae;__Carboxylicivirga;__Carboxylicivirga taeanensis	0.0 %	0.0 %	0.0 %	0.0 %	0.0 %	0.0 %	0.0 %	0.0 %	0.1 %	0.1 %
Bacteria;__Bacteroidetes;__Bacteroidia;__Marinilabiliales;__Marinilabiliaceae;__Geofilum;__Geofilum rhodophaeum	0.0 %	0.1 %	0.1 %	0.0 %	0.1 %	0.0 %	0.0 %	0.0 %	0.0 %	0.0 %
Bacteria;__Bacteroidetes;__Bacteroidia;__Marinilabiliales;__Marinilabiliaceae;__Labilibacter;__Labilibacter aurantiacus	0.0 %	0.0 %	0.0 %	0.0 %	0.0 %	0.0 %	0.0 %	0.1 %	0.0 %	0.0 %
Bacteria;__Bacteroidetes;__Bacteroidia;__Marinilabiliales;__Marinilabiliaceae;__Labilibacter;__Labilibacter marinus	0.0 %	0.0 %	0.0 %	0.0 %	0.0 %	0.0 %	0.0 %	0.0 %	0.0 %	0.0 %
Bacteria;__Bacteroidetes;__Bacteroidia;__Marinilabiliales;__Marinilabiliaceae;__Natronoflexus;__Natronoflexus pectinivorans	0.4 %	0.2 %	0.4 %	0.5 %	0.5 %	0.4 %	0.3 %	0.5 %	0.3 %	0.4 %
Bacteria;__Bacteroidetes;__Bacteroidia;__Marinilabiliales;__Marinilabiliaceae;__Saccharicrinis;__Saccharicrinis carchari	0.1 %	0.1 %	0.1 %	0.0 %	0.1 %	0.0 %	0.2 %	0.0 %	0.2 %	0.0 %
Bacteria;__Bacteroidetes;__Bacteroidia;__Marinilabiliales;__Prolixibacteraceae;__Mariniphaga;__Mariniphaga anaerophila	0.1 %	0.1 %	0.1 %	0.1 %	0.1 %	0.1 %	0.1 %	0.1 %	0.1 %	0.1 %
Bacteria;__Bacteroidetes;__Bacteroidia;__Marinilabiliales;__Prolixibacteraceae;__Mariniphaga;__Mariniphaga sediminis	0.0 %	0.0 %	0.0 %	0.0 %	0.0 %	0.0 %	0.0 %	0.0 %	0.0 %	0.0 %
Bacteria;__Bacteroidetes;__Bacteroidia;__Marinilabiliales;__Prolixibacteraceae;__Prolixibacter;__Prolixibacter denitrificans	0.0 %	0.1 %	0.0 %	0.0 %	0.0 %	0.0 %	0.1 %	0.0 %	0.1 %	0.0 %
Bacteria;__Bacteroidetes;__Bacteroidia;__Marinilabiliales;__Prolixibacteraceae;__Sunxiuqinia;__Sunxiuqinia faeciviva	2.0 %	0.9 %	1.8 %	3.4 %	2.0 %	2.1 %	1.8 %	2.7 %	1.7 %	1.9 %
Bacteria;__Bacteroidetes;__Bacteroidia;__Marinilabiliales;__Prolixibacteraceae;__Sunxiuqinia;__Sunxiuqinia rutila	0.2 %	0.2 %	0.2 %	0.2 %	0.3 %	0.2 %	0.3 %	0.2 %	0.3 %	0.2 %
Bacteria;__Bacteroidetes;__Bacteroidia;__Marinilabiliales;__Prolixibacteraceae;__Tangfeifania;__Tangfeifania diversioriginum	2.5 %	0.7 %	1.9 %	4.2 %	1.7 %	3.4 %	1.6 %	4.1 %	1.5 %	3.0 %
Bacteria;__Bacteroidetes;__Chitinophagia;__Chitinophagales;__Chitinophagaceae;__Flavitalea;__Flavitalea antarctica	0.0 %	0.0 %	0.0 %	0.0 %	0.0 %	0.0 %	0.0 %	0.0 %	0.0 %	0.0 %
Bacteria;__Bacteroidetes;__Chitinophagia;__Chitinophagales;__Chitinophagaceae;__Niabella;__Niabella pedocola	0.0 %	0.0 %	0.0 %	0.0 %	0.0 %	0.0 %	0.0 %	0.0 %	0.0 %	0.0 %
Bacteria;__Bacteroidetes;__Flavobacteriia;__Flavobacteriales;__Flavobacteriaceae;__Capnocytophaga;__Capnocytophaga canimorsus	0.1 %	0.3 %	0.1 %	0.0 %	0.1 %	0.1 %	0.1 %	0.2 %	0.1 %	0.2 %
Bacteria;__Bacteroidetes;__Flavobacteriia;__Flavobacteriales;__Flavobacteriaceae;__Capnocytophaga;__Capnocytophaga cynodegmi	0.0 %	0.0 %	0.0 %	0.0 %	0.0 %	0.0 %	0.0 %	0.0 %	0.0 %	0.0 %
Bacteria;__Bacteroidetes;__Flavobacteriia;__Flavobacteriales;__Flavobacteriaceae;__Cellulophaga;__Cellulophaga tyrosinoxydans	0.0 %	0.0 %	0.0 %	0.0 %	0.0 %	0.0 %	0.0 %	0.0 %	0.0 %	0.0 %
Bacteria;__Bacteroidetes;__Flavobacteriia;__Flavobacteriales;__Flavobacteriaceae;__Galbibacter;__Galbibacter marinus	0.0 %	0.0 %	0.0 %	0.0 %	0.0 %	0.0 %	0.0 %	0.0 %	0.0 %	0.0 %
Bacteria;__Bacteroidetes;__Flavobacteriia;__Flavobacteriales;__Flavobacteriaceae;__Lutaonella;__Lutaonella thermophila	7.2 %	10.4%	8.4 %	6.4 %	7.1 %	6.3 %	8.1 %	5.2 %	6.8 %	6.1 %
Bacteria;__Bacteroidetes;__Flavobacteriia;__Flavobacteriales;__Flavobacteriaceae;__Maribacter;__Maribacter arenosus	0.0 %	0.0 %	0.0 %	0.0 %	0.0 %	0.0 %	0.0 %	0.0 %	0.0 %	0.0 %
Bacteria;__Bacteroidetes;__Sphingobacteriia;__Sphingobacteriales;__Sphingobacteriaceae;__Mucilaginibacter;__Mucilaginibacter roseus	0.0 %	0.0 %	0.0 %	0.0 %	0.0 %	0.0 %	0.0 %	0.0 %	0.0 %	0.0 %
Bacteria;__Bacteroidetes;__Sphingobacteriia;__Sphingobacteriales;__Sphingobacteriaceae;__Pedobacter;__Pedobacter luteus	0.0 %	0.0 %	0.0 %	0.0 %	0.0 %	0.0 %	0.0 %	0.0 %	0.0 %	0.0 %

Bacteria;__Chloroflexi;__Anaerolineae;__Anaerolineales;__Anaerolineaceae;__Anaerolinea;__Anaerolinea thermolimosa	0.0%	0.0%	0.0%	0.0%	0.0%	0.0%	0.0%	0.0%	0.0%	0.0%
Bacteria;__Chloroflexi;__Anaerolineae;__Anaerolineales;__Anaerolineaceae;__Anaerolinea;__Anaerolinea thermophila	0.0%	0.0%	0.0%	0.0%	0.0%	0.0%	0.0%	0.0%	0.0%	0.0%
Bacteria;__Chloroflexi;__Anaerolineae;__Anaerolineales;__Anaerolineaceae;__Bellilinea;__Bellilinea caldifistulae	0.0%	0.0%	0.0%	0.0%	0.0%	0.0%	0.0%	0.0%	0.0%	0.0%
Bacteria;__Chloroflexi;__Anaerolineae;__Anaerolineales;__Anaerolineaceae;__Flexilinea;__Flexilinea flocculi	0.0%	0.0%	0.0%	0.0%	0.0%	0.0%	0.0%	0.0%	0.0%	0.0%
Bacteria;__Chloroflexi;__Anaerolineae;__Anaerolineales;__Anaerolineaceae;__Levilinea;__Leviline a saccharolytica	0.4%	0.1%	0.2%	0.5%	0.1%	0.6%	0.2%	0.7%	0.2%	0.6%
Bacteria;__Chloroflexi;__Anaerolineae;__Anaerolineales;__Anaerolineaceae;__Longilinea;__Longilinea arvoryzae	0.1%	0.0%	0.0%	0.1%	0.0%	0.1%	0.0%	0.1%	0.0%	0.1%
Bacteria;__Chloroflexi;__Anaerolineae;__Anaerolineales;__Anaerolineaceae;__Ornatilinea;__Ornatilinea apprima	0.0%	0.0%	0.0%	0.0%	0.0%	0.0%	0.0%	0.0%	0.0%	0.0%
Bacteria;__Chloroflexi;__Anaerolineae;__Anaerolineales;__Anaerolineaceae;__Pelolinea;__Peloline a submarina	0.0%	0.0%	0.0%	0.0%	0.0%	0.0%	0.0%	0.0%	0.0%	0.0%
Bacteria;__Chloroflexi;__Anaerolineae;__Anaerolineales;__Anaerolineaceae;__Thermanaerothrix;__Thermanaerothrix daxensis	0.0%	0.0%	0.0%	0.0%	0.0%	0.0%	0.0%	0.0%	0.0%	0.0%
Bacteria;__Chloroflexi;__Anaerolineae;__Anaerolineales;__Anaerolineaceae;__Thermomarinilinea;__Thermomarinilinea lacunifontana	0.0%	0.0%	0.0%	0.0%	0.0%	0.0%	0.0%	0.0%	0.0%	0.0%
Bacteria;__Chloroflexi;__Caldilineae;__Caldilineales;__Caldilineaceae;__Caldilinea;__Caldilinea aerophila	0.0%	0.0%	0.0%	0.0%	0.0%	0.0%	0.0%	0.0%	0.0%	0.0%
Bacteria;__Chloroflexi;__Dehalococcoidia;__;__;__Dehalogenimonas;__Dehalogenimonas formicexedens	0.0%	0.0%	0.0%	0.0%	0.0%	0.0%	0.0%	0.0%	0.0%	0.0%
Bacteria;__Coprothermobacterota;__Coprothermobacteria;__Coprothermobacterales;__Coprothermobacteraceae;__Coprothermobacter;__Coprothermobacter proteolyticus	23.0%	13.4%	18.7%	29.0%	21.3%	28.1%	18.6%	34.0%	22.4%	21.9%
Bacteria;__Fibrobacteres;__Chitinispirillia;__Chitinispirillales;__Chitinispirillaceae;__Chitinispirillum;__Chitinispirillum alkaliphilum	0.0%	0.0%	0.0%	0.0%	0.0%	0.0%	0.0%	0.0%	0.0%	0.0%
Bacteria;__Firmicutes;__Bacilli;__Bacillales;__Bacillaceae;__Bacillus;__Bacillus cucumis	0.0%	0.0%	0.0%	0.0%	0.0%	0.0%	0.0%	0.0%	0.0%	0.0%
Bacteria;__Firmicutes;__Bacilli;__Bacillales;__Bacillaceae;__Bacillus;__Bacillus niacini	0.0%	0.0%	0.0%	0.0%	0.0%	0.0%	0.0%	0.0%	0.0%	0.0%
Bacteria;__Firmicutes;__Bacilli;__Bacillales;__Planococcaceae;__Sporosarcina;__Sporosarcina globispora	0.8%	1.5%	0.0%	0.9%	0.0%	2.2%	0.0%	0.9%	0.0%	1.9%
Bacteria;__Firmicutes;__Clostridia;__Clostridiales;__;__Flintibacter;__Flintibacter butyricus	0.2%	0.2%	0.2%	0.1%	0.2%	0.1%	0.1%	0.1%	0.2%	0.1%
Bacteria;__Firmicutes;__Clostridia;__Clostridiales;__;__Intestinimonas;__Intestinimonas butyriciproducens	0.0%	0.0%	0.0%	0.0%	0.0%	0.0%	0.0%	0.0%	0.0%	0.0%
Bacteria;__Firmicutes;__Clostridia;__Clostridiales;__;__Monoglobus;__Monoglobus pectinilyticus	0.0%	0.0%	0.0%	0.0%	0.0%	0.0%	0.0%	0.0%	0.0%	0.0%
Bacteria;__Firmicutes;__Clostridia;__Clostridiales;__;__Proteiniborus;__Proteiniborus ethanoligenes	0.0%	0.0%	0.0%	0.0%	0.0%	0.0%	0.0%	0.0%	0.0%	0.0%
Bacteria;__Firmicutes;__Clostridia;__Clostridiales;__Caldicoprobacteraceae;__Caldicoprobacter;__Caldicoprobacter algeriensis	0.6%	0.4%	0.5%	0.6%	0.5%	0.7%	0.5%	0.7%	0.5%	0.7%
Bacteria;__Firmicutes;__Clostridia;__Clostridiales;__Caldicoprobacteraceae;__Caldicoprobacter;__Caldicoprobacter guelmensis	0.1%	0.0%	0.1%	0.1%	0.1%	0.1%	0.1%	0.1%	0.1%	0.1%
Bacteria;__Firmicutes;__Clostridia;__Clostridiales;__Christensenellaceae;__Christensenella;__Christensenella massiliensis	0.0%	0.0%	0.0%	0.0%	0.0%	0.0%	0.0%	0.0%	0.0%	0.0%
Bacteria;__Firmicutes;__Clostridia;__Clostridiales;__Christensenellaceae;__Christensenella;__Christensenella minuta	0.0%	0.0%	0.0%	0.0%	0.0%	0.0%	0.0%	0.0%	0.0%	0.0%
Bacteria;__Firmicutes;__Clostridia;__Clostridiales;__Clostridiaceae;__Anoxynatronum;__Anoxynatronum buryatiense	0.0%	0.0%	0.0%	0.0%	0.0%	0.0%	0.0%	0.0%	0.0%	0.0%
Bacteria;__Firmicutes;__Clostridia;__Clostridiales;__Clostridiaceae;__Caloramator;__Caloramator proteoclasticus	0.0%	0.0%	0.0%	0.0%	0.0%	0.0%	0.0%	0.0%	0.0%	0.0%
Bacteria;__Firmicutes;__Clostridia;__Clostridiales;__Clostridiaceae;__Caloranaerobacter;__Caloranaerobacter azorensis	0.0%	0.0%	0.0%	0.0%	0.0%	0.0%	0.0%	0.0%	0.0%	0.0%
Bacteria;__Firmicutes;__Clostridia;__Clostridiales;__Clostridiaceae;__Clostridium;__Clostridium acetireducens	0.0%	0.0%	0.0%	0.0%	0.0%	0.0%	0.0%	0.0%	0.0%	0.0%
Bacteria;__Firmicutes;__Clostridia;__Clostridiales;__Clostridiaceae;__Clostridium;__Clostridium akagii	0.1%	0.2%	0.1%	0.1%	0.1%	0.1%	0.0%	0.1%	0.1%	0.0%
Bacteria;__Firmicutes;__Clostridia;__Clostridiales;__Clostridiaceae;__Clostridium;__Clostridium chromiireducens	0.0%	0.0%	0.0%	0.0%	0.0%	0.0%	0.0%	0.0%	0.0%	0.0%
Bacteria;__Firmicutes;__Clostridia;__Clostridiales;__Clostridiaceae;__Clostridium;__Clostridium saudiense	0.6%	0.2%	0.5%	0.8%	0.5%	1.0%	0.5%	0.8%	0.4%	0.8%
Bacteria;__Firmicutes;__Clostridia;__Clostridiales;__Clostridiaceae;__Clostridium;__Clostridium ventriculi	0.0%	0.0%	0.0%	0.0%	0.0%	0.0%	0.0%	0.0%	0.0%	0.1%

Bacteria;__Firmicutes;__Clostridia;__Clostridiales;__Clostridiaceae;__Lutispora;__Lutispora thermophila	0.0 %	0.0 %	0.0 %	0.0 %	0.0 %	0.0 %	0.0 %	0.0 %	0.0 %	0.0 %
Bacteria;__Firmicutes;__Clostridia;__Clostridiales;__Clostridiaceae;__Maledivibacter;__Maledivibacter halophilus	0.0 %	0.0 %	0.0 %	0.0 %	0.0 %	0.0 %	0.0 %	0.0 %	0.0 %	0.0 %
Bacteria;__Firmicutes;__Clostridia;__Clostridiales;__Clostridiaceae;__Thermotalea;__Thermotalea metallivorans	0.0 %	0.0 %	0.0 %	0.0 %	0.0 %	0.0 %	0.0 %	0.0 %	0.0 %	0.0 %
Bacteria;__Firmicutes;__Clostridia;__Clostridiales;__Clostridiaceae;__Youngiibacter;__Youngiibacter fragilis	0.0 %	0.0 %	0.0 %	0.0 %	0.0 %	0.0 %	0.0 %	0.0 %	0.0 %	0.0 %
Bacteria;__Firmicutes;__Clostridia;__Clostridiales;__Clostridiales Family XIII. Incertae Sedis;__Aminipila;__Aminipila butyrica	0.0 %	0.0 %	0.0 %	0.0 %	0.0 %	0.0 %	0.0 %	0.0 %	0.0 %	0.0 %
Bacteria;__Firmicutes;__Clostridia;__Clostridiales;__Clostridiales Family XIII. Incertae Sedis;__Emergencia;__Emergencia timonensis	0.0 %	0.0 %	0.0 %	0.0 %	0.0 %	0.0 %	0.0 %	0.0 %	0.0 %	0.0 %
Bacteria;__Firmicutes;__Clostridia;__Clostridiales;__Eubacteriaceae;__Eubacterium;__Eubacterium coprostanoligenes	0.2 %	0.5 %	0.2 %	0.1 %	0.3 %	0.1 %	0.2 %	0.1 %	0.2 %	0.0 %
Bacteria;__Firmicutes;__Clostridia;__Clostridiales;__Eubacteriaceae;__Garciella;__Garciella nitratireducens	0.2 %	0.1 %	0.1 %	0.2 %	0.1 %	0.2 %	0.1 %	0.2 %	0.1 %	0.3 %
Bacteria;__Firmicutes;__Clostridia;__Clostridiales;__Eubacteriaceae;__Irregularibacter;__Irregularibacter muris	0.0 %	0.0 %	0.0 %	0.0 %	0.0 %	0.1 %	0.1 %	0.0 %	0.0 %	0.1 %
Bacteria;__Firmicutes;__Clostridia;__Clostridiales;__Eubacteriaceae;__Rhabdanaerobium;__Rhabdanaerobium thermarum	0.0 %	0.0 %	0.0 %	0.0 %	0.0 %	0.0 %	0.0 %	0.0 %	0.0 %	0.0 %
Bacteria;__Firmicutes;__Clostridia;__Clostridiales;__Gracilibacteraceae;__Gracilibacter;__Gracilibacter thermotolerans	0.0 %	0.0 %	0.0 %	0.0 %	0.0 %	0.0 %	0.0 %	0.0 %	0.0 %	0.0 %
Bacteria;__Firmicutes;__Clostridia;__Clostridiales;__Hungateiclostridiaceae;__Anaerobacterium;__Anaerobacterium chartisolvens	0.2 %	0.3 %	0.1 %	0.1 %	0.2 %	0.1 %	0.2 %	0.1 %	0.2 %	0.1 %
Bacteria;__Firmicutes;__Clostridia;__Clostridiales;__Hungateiclostridiaceae;__Ercella;__Ercella succinigenes	0.6 %	0.2 %	0.5 %	0.7 %	0.6 %	0.9 %	0.5 %	0.8 %	0.4 %	0.9 %
Bacteria;__Firmicutes;__Clostridia;__Clostridiales;__Hungateiclostridiaceae;__Hungateiclostridium;__Hungateiclostridium alkalicellulosi	0.1 %	0.3 %	0.0 %	0.0 %	0.1 %	0.0 %	0.1 %	0.0 %	0.1 %	0.0 %
Bacteria;__Firmicutes;__Clostridia;__Clostridiales;__Hungateiclostridiaceae;__Hungateiclostridium;__Hungateiclostridium cellulolyticum	0.1 %	0.2 %	0.1 %	0.2 %	0.1 %	0.2 %	0.1 %	0.1 %	0.1 %	0.2 %
Bacteria;__Firmicutes;__Clostridia;__Clostridiales;__Hungateiclostridiaceae;__Hungateiclostridium;__Hungateiclostridium clariflavum	0.1 %	0.2 %	0.1 %	0.1 %	0.1 %	0.1 %	0.1 %	0.1 %	0.1 %	0.1 %
Bacteria;__Firmicutes;__Clostridia;__Clostridiales;__Hungateiclostridiaceae;__Hungateiclostridium;__Hungateiclostridium straminisolvens	0.0 %	0.0 %	0.0 %	0.0 %	0.0 %	0.0 %	0.0 %	0.0 %	0.0 %	0.0 %
Bacteria;__Firmicutes;__Clostridia;__Clostridiales;__Hungateiclostridiaceae;__Hungateiclostridium;__Hungateiclostridium thermocellum	0.2 %	0.3 %	0.2 %	0.2 %	0.2 %	0.2 %	0.2 %	0.1 %	0.2 %	0.1 %
Bacteria;__Firmicutes;__Clostridia;__Clostridiales;__Hungateiclostridiaceae;__Pseudoclostridium;__Pseudoclostridium thermosuccinogenes	0.1 %	0.0 %	0.0 %	0.1 %	0.0 %	0.1 %	0.0 %	0.2 %	0.0 %	0.1 %
Bacteria;__Firmicutes;__Clostridia;__Clostridiales;__Hungateiclostridiaceae;__Ruminiclostridium;__Ruminiclostridium cellobioparum	0.0 %	0.0 %	0.0 %	0.0 %	0.0 %	0.0 %	0.0 %	0.0 %	0.0 %	0.0 %
Bacteria;__Firmicutes;__Clostridia;__Clostridiales;__Hungateiclostridiaceae;__Ruminiclostridium;__Ruminiclostridium hungatei	0.0 %	0.0 %	0.0 %	0.0 %	0.0 %	0.0 %	0.0 %	0.0 %	0.0 %	0.0 %
Bacteria;__Firmicutes;__Clostridia;__Clostridiales;__Hungateiclostridiaceae;__Ruminiclostridium;__Ruminiclostridium sufflavum	0.0 %	0.1 %	0.0 %	0.0 %	0.1 %	0.0 %	0.0 %	0.0 %	0.0 %	0.0 %
Bacteria;__Firmicutes;__Clostridia;__Clostridiales;__Hungateiclostridiaceae;__Saccharofermentans;__Saccharofermentans acetigenes	0.0 %	0.0 %	0.0 %	0.0 %	0.0 %	0.0 %	0.0 %	0.0 %	0.0 %	0.0 %
Bacteria;__Firmicutes;__Clostridia;__Clostridiales;__Hungateiclostridiaceae;__Thermoclostridium;__Thermoclostridium caenicola	0.6 %	0.7 %	0.5 %	0.7 %	0.5 %	0.6 %	0.5 %	0.6 %	0.5 %	1.1 %
Bacteria;__Firmicutes;__Clostridia;__Clostridiales;__Hungateiclostridiaceae;__Thermoclostridium;__Thermoclostridium stercorarium	0.0 %	0.0 %	0.0 %	0.0 %	0.0 %	0.0 %	0.0 %	0.0 %	0.0 %	0.0 %
Bacteria;__Firmicutes;__Clostridia;__Clostridiales;__Lachnospiraceae;__Blautia;__[Ruminococcus] gnavus	0.0 %	0.0 %	0.0 %	0.0 %	0.0 %	0.0 %	0.0 %	0.0 %	0.0 %	0.0 %
Bacteria;__Firmicutes;__Clostridia;__Clostridiales;__Lachnospiraceae;__Fusicatenibacter;__Fusicatenibacter saccharivorans	0.0 %	0.0 %	0.0 %	0.0 %	0.0 %	0.0 %	0.0 %	0.0 %	0.0 %	0.0 %
Bacteria;__Firmicutes;__Clostridia;__Clostridiales;__Lachnospiraceae;__Herbinix;__Herbinix luporum	0.0 %	0.0 %	0.0 %	0.0 %	0.0 %	0.0 %	0.0 %	0.0 %	0.0 %	0.0 %
Bacteria;__Firmicutes;__Clostridia;__Clostridiales;__Lachnospiraceae;__Lachnoclostridium;__[Clostridium] populeti	0.0 %	0.0 %	0.0 %	0.0 %	0.0 %	0.0 %	0.0 %	0.0 %	0.0 %	0.0 %
Bacteria;__Firmicutes;__Clostridia;__Clostridiales;__Lachnospiraceae;__Roseburia;__Roseburia intestinalis	0.0 %	0.0 %	0.0 %	0.0 %	0.0 %	0.0 %	0.0 %	0.0 %	0.0 %	0.0 %
Bacteria;__Firmicutes;__Clostridia;__Clostridiales;__Lachnospiraceae;__Stomatobaculum;__Stomatobaculum longum	0.0 %	0.0 %	0.0 %	0.0 %	0.0 %	0.0 %	0.0 %	0.0 %	0.0 %	0.0 %
Bacteria;__Firmicutes;__Clostridia;__Clostridiales;__Peptococcaceae;__Cryptanaerobacter;__Cryptanaerobacter phenolicus	0.6 %	0.0 %	0.0 %	0.7 %	0.0 %	0.5 %	0.0 %	1.6 %	0.0 %	2.4 %
Bacteria;__Firmicutes;__Clostridia;__Clostridiales;__Peptococcaceae;__Desulfocucumis;__Desulfocucumis palustris	0.0 %	0.0 %	0.0 %	0.0 %	0.0 %	0.0 %	0.0 %	0.0 %	0.0 %	0.0 %

	Bacteria;__Firmicutes;__Clostridia;__Clostridiales;__Peptococcaceae;__Desulfofundulus;__Desulfofundulus thermoacetoxidans	0.7 %	0.7 %	0.3 %	0.9 %	0.3 %	1.1 %	0.4 %	0.9 %	0.3 %	1.7 %
	Bacteria;__Firmicutes;__Clostridia;__Clostridiales;__Peptococcaceae;__Desulfofundulus;__Desulfofundulus thermosubterraneus	0.0 %	0.0 %	0.0 %	0.0 %	0.0 %	0.0 %	0.0 %	0.0 %	0.0 %	0.0 %
	Bacteria;__Firmicutes;__Clostridia;__Clostridiales;__Peptococcaceae;__Desulfohalotomaculum;__Desulfohalotomaculum halophilum	0.0 %	0.0 %	0.0 %	0.0 %	0.0 %	0.0 %	0.0 %	0.0 %	0.0 %	0.0 %
	Bacteria;__Firmicutes;__Clostridia;__Clostridiales;__Peptococcaceae;__Desulfonispora;__Desulfonispora thiosulfatigenes	0.0 %	0.0 %	0.0 %	0.0 %	0.0 %	0.0 %	0.0 %	0.0 %	0.0 %	0.0 %
	Bacteria;__Firmicutes;__Clostridia;__Clostridiales;__Peptococcaceae;__Pelotomaculum;__Pelotomaculum isophthalicicum	0.2 %	0.0 %	0.0 %	0.1 %	0.0 %	0.1 %	0.0 %	0.3 %	0.0 %	1.7 %
	Bacteria;__Firmicutes;__Clostridia;__Clostridiales;__Peptococcaceae;__Pelotomaculum;__Pelotomaculum propionicicum	0.0 %	0.0 %	0.0 %	0.0 %	0.0 %	0.0 %	0.0 %	0.0 %	0.0 %	0.0 %
	Bacteria;__Firmicutes;__Clostridia;__Clostridiales;__Peptostreptococcaceae;__Acetoanaerobium;__Acetoanaerobium sticklandii	0.0 %	0.0 %	0.0 %	0.0 %	0.0 %	0.0 %	0.0 %	0.0 %	0.0 %	0.0 %
	Bacteria;__Firmicutes;__Clostridia;__Clostridiales;__Peptostreptococcaceae;__Intestinibacter;__Intestinibacter bartlettii	0.1 %	0.0 %	0.1 %	0.1 %	0.1 %	0.2 %	0.1 %	0.1 %	0.1 %	0.1 %
	Bacteria;__Firmicutes;__Clostridia;__Clostridiales;__Peptostreptococcaceae;__Romboutsia;__Romboutsia timonensis	0.5 %	0.1 %	0.5 %	0.8 %	0.4 %	0.8 %	0.4 %	0.7 %	0.4 %	0.7 %
	Bacteria;__Firmicutes;__Clostridia;__Clostridiales;__Ruminococcaceae;__Anaerotruncus;__Anaerotruncus colihominis	0.0 %	0.0 %	0.0 %	0.0 %	0.0 %	0.0 %	0.0 %	0.0 %	0.0 %	0.0 %
	Bacteria;__Firmicutes;__Clostridia;__Clostridiales;__Ruminococcaceae;__Caproiciproducens;__Caproiciproducens galactitolivorans	0.2 %	0.2 %	0.3 %	0.2 %	0.2 %	0.2 %	0.2 %	0.3 %	0.2 %	0.4 %
	Bacteria;__Firmicutes;__Clostridia;__Clostridiales;__Ruminococcaceae;__Flavonifractor;__Flavonifractor plautii	0.0 %	0.0 %	0.0 %	0.0 %	0.0 %	0.0 %	0.0 %	0.0 %	0.0 %	0.0 %
	Bacteria;__Firmicutes;__Clostridia;__Clostridiales;__Ruminococcaceae;__Phocea;__Phocea massiliensis	0.0 %	0.0 %	0.0 %	0.0 %	0.0 %	0.0 %	0.0 %	0.0 %	0.0 %	0.0 %
	Bacteria;__Firmicutes;__Clostridia;__Clostridiales;__Ruminococcaceae;__Pseudoflavonifractor;__Pseudoflavonifractor phocaeensis	0.0 %	0.0 %	0.0 %	0.0 %	0.0 %	0.0 %	0.0 %	0.0 %	0.0 %	0.0 %
	Bacteria;__Firmicutes;__Clostridia;__Clostridiales;__Ruminococcaceae;__Ruminococcus;__Ruminococcus albus	0.0 %	0.0 %	0.0 %	0.0 %	0.0 %	0.0 %	0.0 %	0.0 %	0.0 %	0.0 %
	Bacteria;__Firmicutes;__Clostridia;__Clostridiales;__Ruminococcaceae;__Ruminococcus;__Ruminococcus bromii	0.0 %	0.0 %	0.0 %	0.0 %	0.0 %	0.0 %	0.0 %	0.0 %	0.0 %	0.0 %
	Bacteria;__Firmicutes;__Clostridia;__Clostridiales;__Syntrophomonadaceae;__Syntrophomonas;__Syntrophomonas bryantii	0.0 %	0.0 %	0.0 %	0.0 %	0.0 %	0.0 %	0.0 %	0.0 %	0.0 %	0.0 %
	Bacteria;__Firmicutes;__Clostridia;__Clostridiales;__Syntrophomonadaceae;__Syntrophomonas;__Syntrophomonas sapovorans	0.0 %	0.0 %	0.0 %	0.0 %	0.0 %	0.0 %	0.0 %	0.0 %	0.0 %	0.0 %
	Bacteria;__Firmicutes;__Clostridia;__Clostridiales;__Syntrophomonadaceae;__Syntrophomonas;__Syntrophomonas wolfei	0.2 %	0.4 %	0.3 %	0.0 %	0.2 %	0.0 %	0.3 %	0.1 %	0.4 %	0.0 %
	Bacteria;__Firmicutes;__Clostridia;__Clostridiales;__Syntrophomonadaceae;__Syntrophomonas;__Syntrophomonas zehnderi	0.0 %	0.0 %	0.0 %	0.0 %	0.0 %	0.0 %	0.0 %	0.0 %	0.0 %	0.0 %
	Bacteria;__Firmicutes;__Clostridia;__Thermoanaerobacterales;__Thermoanaerobacteraceae;__Desulfovirgula;__Desulfovirgula thermocuniculi	0.0 %	0.0 %	0.0 %	0.0 %	0.0 %	0.0 %	0.0 %	0.0 %	0.0 %	0.0 %
	Bacteria;__Firmicutes;__Clostridia;__Thermoanaerobacterales;__Thermoanaerobacteraceae;__Gelria;__Gelria glutamica	2.2 %	1.1 %	1.5 %	3.0 %	1.6 %	3.3 %	1.6 %	3.0 %	1.4 %	3.0 %
	Bacteria;__Firmicutes;__Clostridia;__Thermoanaerobacterales;__Thermoanaerobacteraceae;__Moorella;__Moorella glycerini	0.1 %	0.1 %	0.1 %	0.1 %	0.1 %	0.2 %	0.1 %	0.1 %	0.1 %	0.1 %
	Bacteria;__Firmicutes;__Clostridia;__Thermoanaerobacterales;__Thermoanaerobacteraceae;__Moorella;__Moorella humiferrea	0.0 %	0.0 %	0.0 %	0.0 %	0.0 %	0.0 %	0.0 %	0.0 %	0.0 %	0.0 %
	Bacteria;__Firmicutes;__Clostridia;__Thermoanaerobacterales;__Thermoanaerobacteraceae;__Tepidanaerobacter;__Tepidanaerobacter syntrophicus	0.0 %	0.0 %	0.0 %	0.0 %	0.0 %	0.0 %	0.0 %	0.0 %	0.0 %	0.0 %
	Bacteria;__Firmicutes;__Clostridia;__Thermoanaerobacterales;__Thermoanaerobacteraceae;__Thermacetogenium;__Thermacetogenium phaeum	0.1 %	0.0 %	0.1 %	0.2 %	0.1 %	0.1 %	0.1 %	0.1 %	0.1 %	0.1 %
	Bacteria;__Firmicutes;__Clostridia;__Thermoanaerobacterales;__Thermoanaerobacteraceae;__Thermoanaerobacter;__Thermoanaerobacter brockii	0.3 %	0.2 %	0.3 %	0.4 %	0.3 %	0.4 %	0.3 %	0.3 %	0.3 %	0.3 %
	Bacteria;__Firmicutes;__Clostridia;__Thermoanaerobacterales;__Thermoanaerobacterales Family III. Incertae Sedis;__Thermosediminibacter;__Thermosediminibacter oceani	0.0 %	0.0 %	0.0 %	0.0 %	0.0 %	0.0 %	0.0 %	0.0 %	0.0 %	0.0 %
	Bacteria;__Firmicutes;__Clostridia;__Thermoanaerobacterales;__Thermoanaerobacterales Family III. Incertae Sedis;__Thermovenabulum;__Thermovenabulum ferriorganovorum	0.1 %	0.1 %	0.1 %	0.2 %	0.1 %	0.2 %	0.1 %	0.2 %	0.1 %	0.2 %
	Bacteria;__Firmicutes;__Erysipelotrichia;__Erysipelotrichales;__Erysipelotrichaceae;__Turicibacter;__Turicibacter sanguinis	0.1 %	0.1 %	0.1 %	0.2 %	0.1 %	0.2 %	0.1 %	0.1 %	0.1 %	0.1 %
	Bacteria;__Firmicutes;__Limnochordia;__Limnochordales;__Limnochordaceae;__Limnochorda;__Limnochorda pilosa	0.3 %	0.7 %	0.3 %	0.1 %	0.3 %	0.1 %	0.3 %	0.1 %	0.4 %	0.3 %
	Bacteria;__Firmicutes;__Tissierellia;__;__;__Sedimentibacter;__Sedimentibacter hydroxybenzoicus	0.8 %	0.3 %	0.9 %	0.6 %	0.9 %	1.0 %	0.9 %	0.6 %	0.9 %	1.5 %
	Bacteria;__Firmicutes;__Tissierellia;__Tissierellales;__Tissierellaceae;__Tepidimicrobium;__Tepidimicrobium ferriphilum	0.0 %	0.1 %	0.1 %	0.0 %	0.0 %	0.0 %	0.1 %	0.0 %	0.0 %	0.0 %

Bacteria;__Fusobacteria;__Fusobacteriia;__Fusobacteriales;__Leptotrichiaceae;__Streptobacillus;__Streptobacillus notomytis	0.0 %	0.0 %	0.0 %	0.0 %	0.0 %	0.0 %	0.0 %	0.0 %	0.0 %	0.0 %
Bacteria;__Ignavibacteriae;__Ignavibacteria;__Ignavibacteriales;__Ignavibacteriaceae;__Ignavibacterium;__Ignavibacterium album	0.0 %	0.0 %	0.0 %	0.0 %	0.0 %	0.0 %	0.0 %	0.0 %	0.0 %	0.0 %
Bacteria;__Kiritimatiellaeota;__Kiritimatiellae;__Kiritimatiellales;__Kiritimatiellaceae;__Kiritimatiella;__Kiritimatiella glycovorans	0.0 %	0.0 %	0.0 %	0.0 %	0.0 %	0.0 %	0.0 %	0.0 %	0.0 %	0.0 %
Bacteria;__Lentisphaerae;__Oligosphaeria;__Oligosphaerales;__Oligosphaeraceae;__Oligosphaera;__Oligosphaera ethanolica	0.0 %	0.0 %	0.0 %	0.0 %	0.0 %	0.0 %	0.0 %	0.0 %	0.0 %	0.0 %
Bacteria;__Nitrospirae;__Nitrospira;__Nitrospirales;__Nitrospiraceae;__Thermodesulfovibrio;__Thermodesulfovibrio thiophilus	0.0 %	0.0 %	0.0 %	0.0 %	0.0 %	0.0 %	0.0 %	0.0 %	0.0 %	0.0 %
Bacteria;__Planctomycetes;__Planctomycetia;__Isosphaerales;__Isosphaeraceae;__Aquisphaera;__Aquisphaera giovannonii	0.0 %	0.0 %	0.0 %	0.0 %	0.0 %	0.0 %	0.0 %	0.0 %	0.0 %	0.0 %
Bacteria;__Planctomycetes;__Planctomycetia;__Pirellulales;__Pirellulaceae;__Pirellula;__Pirellula staleyi	0.0 %	0.0 %	0.0 %	0.0 %	0.0 %	0.0 %	0.0 %	0.0 %	0.0 %	0.0 %
Bacteria;__Planctomycetes;__Planctomycetia;__Pirellulales;__Pirellulaceae;__Rhodopirellula;__Rhodopirellula lusitana	0.0 %	0.0 %	0.0 %	0.0 %	0.0 %	0.0 %	0.0 %	0.0 %	0.0 %	0.0 %
Bacteria;__Planctomycetes;__Planctomycetia;__Pirellulales;__Thermoguttaceae;__Thermogutta;__Thermogutta terrifontis	0.4 %	0.3 %	0.3 %	0.5 %	0.3 %	0.4 %	0.3 %	0.6 %	0.3 %	0.4 %
Bacteria;__Planctomycetes;__Planctomycetia;__Planctomycetales;__Planctomycetaceae;__Rubinisphaera;__Rubinisphaera brasiliensis	0.0 %	0.0 %	0.0 %	0.0 %	0.0 %	0.0 %	0.0 %	0.0 %	0.0 %	0.0 %
Bacteria;__Proteobacteria;__Alphaproteobacteria;__;__;__Phreatobacter;__Phreatobacter oligotrophus	0.0 %	0.0 %	0.0 %	0.0 %	0.0 %	0.0 %	0.0 %	0.0 %	0.0 %	0.0 %
Bacteria;__Proteobacteria;__Alphaproteobacteria;__;__;__Phreatobacter;__Phreatobacter stygius	0.0 %	0.0 %	0.0 %	0.1 %	0.1 %	0.0 %	0.0 %	0.0 %	0.0 %	0.0 %
Bacteria;__Proteobacteria;__Alphaproteobacteria;__Caulobacterales;__Caulobacteraceae;__Brevundimonas;__Brevundimonas lenta	0.3 %	0.0 %	0.3 %	0.4 %	0.2 %	0.5 %	0.2 %	0.5 %	0.2 %	0.7 %
Bacteria;__Proteobacteria;__Alphaproteobacteria;__Caulobacterales;__Caulobacteraceae;__Brevundimonas;__Brevundimonas terrae	0.0 %	0.0 %	0.0 %	0.0 %	0.0 %	0.0 %	0.0 %	0.0 %	0.0 %	0.0 %
Bacteria;__Proteobacteria;__Alphaproteobacteria;__Caulobacterales;__Caulobacteraceae;__Brevundimonas;__Brevundimonas viscosa	0.0 %	0.0 %	0.0 %	0.0 %	0.0 %	0.0 %	0.0 %	0.0 %	0.0 %	0.0 %
Bacteria;__Proteobacteria;__Alphaproteobacteria;__Caulobacterales;__Caulobacteraceae;__Phenylobacterium;__Phenylobacterium haematophilum	0.0 %	0.0 %	0.0 %	0.0 %	0.0 %	0.0 %	0.0 %	0.0 %	0.0 %	0.0 %
Bacteria;__Proteobacteria;__Alphaproteobacteria;__Rhizobiales;__;__Nordella;__Nordella oligomobilis	0.0 %	0.0 %	0.0 %	0.0 %	0.0 %	0.0 %	0.0 %	0.0 %	0.0 %	0.0 %
Bacteria;__Proteobacteria;__Alphaproteobacteria;__Rhizobiales;__;__Pseudorhodoplanes;__Pseudorhodoplanes sinuspersici	0.0 %	0.0 %	0.0 %	0.0 %	0.0 %	0.0 %	0.0 %	0.0 %	0.0 %	0.0 %
Bacteria;__Proteobacteria;__Alphaproteobacteria;__Rhizobiales;__Ancalomicrobiaceae;__Ancalomicrobium;__Ancalomicrobium adetum	0.0 %	0.0 %	0.0 %	0.0 %	0.0 %	0.0 %	0.0 %	0.0 %	0.0 %	0.0 %
Bacteria;__Proteobacteria;__Alphaproteobacteria;__Rhizobiales;__Beijerinckiaceae;__Methylocapsa;__Methylocapsa acidiphila	0.0 %	0.0 %	0.0 %	0.0 %	0.0 %	0.0 %	0.0 %	0.0 %	0.0 %	0.0 %
Bacteria;__Proteobacteria;__Alphaproteobacteria;__Rhizobiales;__Beijerinckiaceae;__Methylocella;__Methylocella silvestris	0.0 %	0.0 %	0.0 %	0.0 %	0.0 %	0.0 %	0.0 %	0.0 %	0.0 %	0.0 %
Bacteria;__Proteobacteria;__Alphaproteobacteria;__Rhizobiales;__Bradyrhizobiaceae;__Afipia;__Afipia felis	0.0 %	0.0 %	0.0 %	0.0 %	0.0 %	0.0 %	0.0 %	0.0 %	0.0 %	0.0 %
Bacteria;__Proteobacteria;__Alphaproteobacteria;__Rhizobiales;__Bradyrhizobiaceae;__Bosea;__Bosea lathyri	0.0 %	0.0 %	0.0 %	0.0 %	0.0 %	0.0 %	0.0 %	0.0 %	0.0 %	0.0 %
Bacteria;__Proteobacteria;__Alphaproteobacteria;__Rhizobiales;__Brucellaceae;__Brucella;__Brucella papionis	0.0 %	0.0 %	0.0 %	0.0 %	0.0 %	0.0 %	0.0 %	0.0 %	0.0 %	0.0 %
Bacteria;__Proteobacteria;__Alphaproteobacteria;__Rhizobiales;__Brucellaceae;__Ochrobactrum;__Ochrobactrum rhizosphaerae	0.0 %	0.0 %	0.0 %	0.0 %	0.0 %	0.0 %	0.0 %	0.0 %	0.0 %	0.0 %
Bacteria;__Proteobacteria;__Alphaproteobacteria;__Rhizobiales;__Hyphomicrobiaceae;__Devosia;__Devosia insulae	0.2 %	0.1 %	0.1 %	0.2 %	0.2 %	0.1 %	0.2 %	0.2 %	0.2 %	0.2 %
Bacteria;__Proteobacteria;__Alphaproteobacteria;__Rhizobiales;__Hyphomicrobiaceae;__Hyphomicrobium;__Hyphomicrobium facile	0.0 %	0.0 %	0.0 %	0.0 %	0.0 %	0.0 %	0.0 %	0.0 %	0.0 %	0.0 %
Bacteria;__Proteobacteria;__Alphaproteobacteria;__Rhizobiales;__Hyphomicrobiaceae;__Hyphomicrobium;__Hyphomicrobium hollandicum	0.0 %	0.0 %	0.0 %	0.0 %	0.0 %	0.0 %	0.0 %	0.0 %	0.0 %	0.0 %
Bacteria;__Proteobacteria;__Alphaproteobacteria;__Rhizobiales;__Methylobacteriaceae;__Microvirga;__Microvirga guangxiensis	0.0 %	0.0 %	0.0 %	0.0 %	0.0 %	0.0 %	0.0 %	0.0 %	0.0 %	0.0 %
Bacteria;__Proteobacteria;__Alphaproteobacteria;__Rhizobiales;__Methylocystaceae;__Methylocystis;__Methylocystis heyeri	0.0 %	0.0 %	0.1 %	0.0 %	0.0 %	0.0 %	0.0 %	0.0 %	0.0 %	0.0 %
Bacteria;__Proteobacteria;__Alphaproteobacteria;__Rhizobiales;__Phyllobacteriaceae;__Mesorhizobium;__Mesorhizobium delmotii	0.0 %	0.0 %	0.0 %	0.0 %	0.0 %	0.0 %	0.0 %	0.0 %	0.0 %	0.0 %
Bacteria;__Proteobacteria;__Alphaproteobacteria;__Rhizobiales;__Phyllobacteriaceae;__Mesorhizobium;__Mesorhizobium denitrificans	0.0 %	0.0 %	0.0 %	0.0 %	0.0 %	0.0 %	0.0 %	0.0 %	0.0 %	0.0 %
Bacteria;__Proteobacteria;__Alphaproteobacteria;__Rhizobiales;__Phyllobacteriaceae;__Nitratireductor;__Nitratireductor soli	0.0 %	0.0 %	0.0 %	0.0 %	0.0 %	0.0 %	0.0 %	0.0 %	0.0 %	0.0 %

Bacteria;__Proteobacteria;__Alphaproteobacteria;__Rhizobiales;__Rhizobiaceae;__Agrobacterium;__Agrobacterium tumefaciens	0.0 %	0.0 %	0.0 %	0.1 %	0.0 %	0.0 %	0.0 %	0.0 %	0.0 %	0.1 %
Bacteria;__Proteobacteria;__Alphaproteobacteria;__Rhizobiales;__Rhizobiaceae;__Rhizobium;__Rhizobium gei	0.0 %	0.0 %	0.0 %	0.0 %	0.0 %	0.0 %	0.0 %	0.0 %	0.0 %	0.0 %
Bacteria;__Proteobacteria;__Alphaproteobacteria;__Rhizobiales;__Xanthobacteraceae;__Pseudolabrys;__Pseudolabrys taiwanensis	0.0 %	0.0 %	0.0 %	0.0 %	0.0 %	0.0 %	0.0 %	0.0 %	0.0 %	0.0 %
Bacteria;__Proteobacteria;__Alphaproteobacteria;__Rhodobacterales;__Rhodobacteraceae;__Defluviimonas;__Defluviimonas aestuarii	0.0 %	0.0 %	0.0 %	0.0 %	0.0 %	0.0 %	0.0 %	0.0 %	0.0 %	0.0 %
Bacteria;__Proteobacteria;__Alphaproteobacteria;__Rhodobacterales;__Rhodobacteraceae;__Gemmobacter;__Gemmobacter nectariphilus	0.0 %	0.0 %	0.0 %	0.0 %	0.0 %	0.0 %	0.0 %	0.0 %	0.0 %	0.0 %
Bacteria;__Proteobacteria;__Alphaproteobacteria;__Rhodobacterales;__Rhodobacteraceae;__Gemmobacter;__Gemmobacter tilapiae	0.1 %	0.1 %	0.1 %	0.1 %	0.1 %	0.1 %	0.1 %	0.1 %	0.1 %	0.1 %
Bacteria;__Proteobacteria;__Alphaproteobacteria;__Rhodobacterales;__Rhodobacteraceae;__Paracoccus;__Paracoccus limosus	0.0 %	0.0 %	0.0 %	0.0 %	0.0 %	0.0 %	0.0 %	0.0 %	0.0 %	0.0 %
Bacteria;__Proteobacteria;__Alphaproteobacteria;__Rhodobacterales;__Rhodobacteraceae;__Rhodobacter;__Rhodobacter blasticus	0.0 %	0.0 %	0.0 %	0.0 %	0.0 %	0.0 %	0.0 %	0.0 %	0.0 %	0.0 %
Bacteria;__Proteobacteria;__Alphaproteobacteria;__Rhodobacterales;__Rhodobacteraceae;__Rhodovulum;__Rhodovulum kholense	0.0 %	0.0 %	0.0 %	0.0 %	0.0 %	0.0 %	0.0 %	0.0 %	0.0 %	0.0 %
Bacteria;__Proteobacteria;__Alphaproteobacteria;__Rhodobacterales;__Rhodobacteraceae;__Rubellimicrobium;__Rubellimicrobium rubrum	0.0 %	0.0 %	0.0 %	0.0 %	0.0 %	0.0 %	0.0 %	0.0 %	0.0 %	0.0 %
Bacteria;__Proteobacteria;__Alphaproteobacteria;__Rhodobacterales;__Rhodobacteraceae;__Tabrizicola;__Tabrizicola aquatica	0.1 %	0.1 %	0.1 %	0.1 %	0.1 %	0.1 %	0.1 %	0.1 %	0.2 %	0.1 %
Bacteria;__Proteobacteria;__Alphaproteobacteria;__Rhodospirillales;__Acetobacteraceae;__Roseomonas;__Roseomonas lacus	0.0 %	0.0 %	0.0 %	0.1 %	0.0 %	0.1 %	0.0 %	0.0 %	0.0 %	0.0 %
Bacteria;__Proteobacteria;__Alphaproteobacteria;__Sphingomonadales;__Sphingomonadaceae;__Novosphingobium;__Novosphingobium ginsenosidimutans	0.0 %	0.0 %	0.0 %	0.0 %	0.0 %	0.0 %	0.0 %	0.0 %	0.0 %	0.0 %
Bacteria;__Proteobacteria;__Alphaproteobacteria;__Sphingomonadales;__Sphingomonadaceae;__Sphingopyxis;__Sphingopyxis fribergensis	0.0 %	0.0 %	0.0 %	0.0 %	0.0 %	0.0 %	0.0 %	0.0 %	0.0 %	0.0 %
Bacteria;__Proteobacteria;__Betaproteobacteria;__Burkholderiales;__;__Aquabacterium;__Aquabacterium citratiphilum	0.0 %	0.0 %	0.0 %	0.0 %	0.0 %	0.0 %	0.0 %	0.0 %	0.0 %	0.0 %
Bacteria;__Proteobacteria;__Betaproteobacteria;__Burkholderiales;__;__Rivibacter;__Rivibacter subsaxonicus	0.0 %	0.0 %	0.0 %	0.0 %	0.0 %	0.0 %	0.0 %	0.0 %	0.0 %	0.0 %
Bacteria;__Proteobacteria;__Betaproteobacteria;__Burkholderiales;__;__Thiobacter;__Thiobacter subterraneus	0.0 %	0.0 %	0.0 %	0.0 %	0.0 %	0.0 %	0.0 %	0.0 %	0.0 %	0.0 %
Bacteria;__Proteobacteria;__Betaproteobacteria;__Burkholderiales;__Alcaligenaceae;__Achromobacter;__Achromobacter aegrifaciens	0.0 %	0.0 %	0.0 %	0.0 %	0.0 %	0.0 %	0.0 %	0.0 %	0.0 %	0.0 %
Bacteria;__Proteobacteria;__Betaproteobacteria;__Burkholderiales;__Alcaligenaceae;__Eoetvoesia;__Eoetvoesia caeni	0.2 %	0.0 %	0.3 %	0.2 %	0.3 %	0.1 %	0.3 %	0.2 %	0.3 %	0.2 %
Bacteria;__Proteobacteria;__Betaproteobacteria;__Burkholderiales;__Alcaligenaceae;__Pusillimonas;__Pusillimonas ginsengisoli	0.0 %	0.0 %	0.0 %	0.0 %	0.0 %	0.0 %	0.0 %	0.0 %	0.0 %	0.0 %
Bacteria;__Proteobacteria;__Betaproteobacteria;__Burkholderiales;__Burkholderiaceae;__Cupriavidus;__Cupriavidus metallidurans	0.0 %	0.0 %	0.0 %	0.0 %	0.0 %	0.0 %	0.0 %	0.0 %	0.0 %	0.0 %
Bacteria;__Proteobacteria;__Betaproteobacteria;__Burkholderiales;__Burkholderiaceae;__Hydromonas;__Hydromonas duriensis	0.0 %	0.0 %	0.0 %	0.0 %	0.0 %	0.0 %	0.0 %	0.0 %	0.0 %	0.0 %
Bacteria;__Proteobacteria;__Betaproteobacteria;__Burkholderiales;__Burkholderiaceae;__Quisquiliibacterium;__Quisquiliibacterium transsilvanicum	0.0 %	0.0 %	0.0 %	0.0 %	0.0 %	0.0 %	0.0 %	0.0 %	0.0 %	0.0 %
Bacteria;__Proteobacteria;__Betaproteobacteria;__Burkholderiales;__Comamonadaceae;__'Geomonas' Khan et al. 2020;__Geomonas soli	0.0 %	0.0 %	0.0 %	0.0 %	0.0 %	0.0 %	0.0 %	0.0 %	0.0 %	0.0 %
Bacteria;__Proteobacteria;__Betaproteobacteria;__Burkholderiales;__Comamonadaceae;__Acidovorax;__Acidovorax defluvii	0.0 %	0.0 %	0.0 %	0.1 %	0.1 %	0.0 %	0.1 %	0.0 %	0.0 %	0.0 %
Bacteria;__Proteobacteria;__Betaproteobacteria;__Burkholderiales;__Comamonadaceae;__Acidovorax;__Acidovorax monticola	0.0 %	0.0 %	0.0 %	0.0 %	0.0 %	0.0 %	0.0 %	0.0 %	0.0 %	0.0 %
Bacteria;__Proteobacteria;__Betaproteobacteria;__Burkholderiales;__Comamonadaceae;__Acidovorax;__Acidovorax radicis	0.1 %	0.1 %	0.1 %	0.2 %	0.1 %	0.1 %	0.1 %	0.1 %	0.1 %	0.1 %
Bacteria;__Proteobacteria;__Betaproteobacteria;__Burkholderiales;__Comamonadaceae;__Alicycliphilus;__Alicycliphilus denitrificans	0.0 %	0.0 %	0.1 %	0.1 %	0.1 %	0.0 %	0.0 %	0.0 %	0.0 %	0.0 %
Bacteria;__Proteobacteria;__Betaproteobacteria;__Burkholderiales;__Comamonadaceae;__Caldimonas;__Caldimonas hydrothermale	0.0 %	0.0 %	0.0 %	0.0 %	0.0 %	0.0 %	0.0 %	0.0 %	0.0 %	0.0 %
Bacteria;__Proteobacteria;__Betaproteobacteria;__Burkholderiales;__Comamonadaceae;__Comamonas;__Comamonas nitrativorans	0.0 %	0.0 %	0.0 %	0.0 %	0.0 %	0.0 %	0.0 %	0.0 %	0.0 %	0.0 %
Bacteria;__Proteobacteria;__Betaproteobacteria;__Burkholderiales;__Comamonadaceae;__Comamonas;__Comamonas phosphati	0.0 %	0.0 %	0.0 %	0.0 %	0.0 %	0.0 %	0.0 %	0.0 %	0.0 %	0.0 %
Bacteria;__Proteobacteria;__Betaproteobacteria;__Burkholderiales;__Comamonadaceae;__Comamonas;__Comamonas piscis	0.0 %	0.0 %	0.0 %	0.0 %	0.0 %	0.0 %	0.0 %	0.0 %	0.0 %	0.0 %
Bacteria;__Proteobacteria;__Betaproteobacteria;__Burkholderiales;__Comamonadaceae;__Comamonas;__Comamonas zonglianii	0.0 %	0.0 %	0.0 %	0.0 %	0.0 %	0.0 %	0.0 %	0.0 %	0.0 %	0.0 %

Bacteria;__Proteobacteria;__Betaproteobacteria;__Burkholderiales;__Comamonadaceae;__Diaphorobacter;__Diaphorobacter aerolatus	0.0 %	0.0 %	0.0 %	0.0 %	0.0 %	0.0 %	0.0 %	0.0 %	0.0 %	0.0 %
Bacteria;__Proteobacteria;__Betaproteobacteria;__Burkholderiales;__Comamonadaceae;__Limnohabitans;__Limnohabitans curvus	0.1 %	0.1 %	0.1 %	0.1 %	0.2 %	0.2 %	0.1 %	0.1 %	0.1 %	0.1 %
Bacteria;__Proteobacteria;__Betaproteobacteria;__Burkholderiales;__Comamonadaceae;__Ottowia;__Ottowia shaoguanensis	0.0 %	0.0 %	0.0 %	0.0 %	0.0 %	0.0 %	0.0 %	0.0 %	0.0 %	0.0 %
Bacteria;__Proteobacteria;__Betaproteobacteria;__Burkholderiales;__Comamonadaceae;__Rhodoferax;__Rhodoferax ferrireducens	0.0 %	0.0 %	0.0 %	0.0 %	0.0 %	0.0 %	0.0 %	0.0 %	0.0 %	0.0 %
Bacteria;__Proteobacteria;__Betaproteobacteria;__Burkholderiales;__Comamonadaceae;__Rhodoferax;__Rhodoferax saidenbachensis	0.2 %	0.1 %	0.2 %	0.2 %	0.2 %	0.1 %	0.2 %	0.3 %	0.2 %	0.2 %
Bacteria;__Proteobacteria;__Betaproteobacteria;__Burkholderiales;__Comamonadaceae;__Simplicispira;__Simplicispira metamorpha	0.0 %	0.0 %	0.0 %	0.0 %	0.0 %	0.0 %	0.0 %	0.0 %	0.1 %	0.0 %
Bacteria;__Proteobacteria;__Betaproteobacteria;__Burkholderiales;__Comamonadaceae;__Xenophilus;__Xenophilus arseniciresistens	0.1 %	0.1 %	0.1 %	0.1 %	0.1 %	0.1 %	0.1 %	0.1 %	0.1 %	0.1 %
Bacteria;__Proteobacteria;__Betaproteobacteria;__Burkholderiales;__Oxalobacteraceae;__Glaciimonas;__Glaciimonas singularis	0.2 %	0.2 %	0.2 %	0.2 %	0.2 %	0.2 %	0.2 %	0.3 %	0.2 %	0.2 %
Bacteria;__Proteobacteria;__Betaproteobacteria;__Burkholderiales;__Oxalobacteraceae;__Herminiimonas;__Herminiimonas glaciei	0.3 %	0.0 %	0.7 %	0.0 %	0.5 %	0.1 %	0.8 %	0.1 %	0.7 %	0.0 %
Bacteria;__Proteobacteria;__Betaproteobacteria;__Burkholderiales;__Oxalobacteraceae;__Janthinobacterium;__Janthinobacterium lividum	0.4 %	0.0 %	0.7 %	0.1 %	0.7 %	0.1 %	1.1 %	0.1 %	0.9 %	0.1 %
Bacteria;__Proteobacteria;__Betaproteobacteria;__Burkholderiales;__Oxalobacteraceae;__Janthinobacterium;__Janthinobacterium svalbardensis	0.0 %	0.0 %	0.0 %	0.0 %	0.0 %	0.0 %	0.0 %	0.0 %	0.0 %	0.0 %
Bacteria;__Proteobacteria;__Betaproteobacteria;__Burkholderiales;__Oxalobacteraceae;__Undibacterium;__Undibacterium jejuense	0.0 %	0.0 %	0.0 %	0.0 %	0.0 %	0.0 %	0.0 %	0.0 %	0.0 %	0.0 %
Bacteria;__Proteobacteria;__Betaproteobacteria;__Nitrosomonadales;__Methylophilaceae;__Methylotenera;__Methylotenera mobilis	0.0 %	0.0 %	0.0 %	0.0 %	0.0 %	0.0 %	0.0 %	0.0 %	0.0 %	0.0 %
Bacteria;__Proteobacteria;__Betaproteobacteria;__Rhodocyclales;__Azonexaceae;__Azonexus;__Azonexus caeni	0.0 %	0.1 %	0.0 %	0.0 %	0.0 %	0.0 %	0.0 %	0.0 %	0.0 %	0.0 %
Bacteria;__Proteobacteria;__Betaproteobacteria;__Rhodocyclales;__Azonexaceae;__Dechloromonas;__Dechloromonas hortensis	0.0 %	0.0 %	0.0 %	0.0 %	0.0 %	0.0 %	0.0 %	0.0 %	0.0 %	0.0 %
Bacteria;__Proteobacteria;__Betaproteobacteria;__Rhodocyclales;__Rhodocyclaceae;__Azospira;__Azospira restricta	0.0 %	0.0 %	0.0 %	0.0 %	0.0 %	0.0 %	0.0 %	0.0 %	0.0 %	0.0 %
Bacteria;__Proteobacteria;__Betaproteobacteria;__Rhodocyclales;__Rhodocyclaceae;__Azovibrio;__Azovibrio restrictus	0.0 %	0.0 %	0.0 %	0.0 %	0.0 %	0.0 %	0.0 %	0.0 %	0.0 %	0.0 %
Bacteria;__Proteobacteria;__Betaproteobacteria;__Rhodocyclales;__Rhodocyclaceae;__Propionivibrio;__Propionivibrio dicarboxylicus	0.0 %	0.0 %	0.0 %	0.0 %	0.0 %	0.0 %	0.0 %	0.0 %	0.0 %	0.0 %
Bacteria;__Proteobacteria;__Betaproteobacteria;__Rhodocyclales;__Rhodocyclaceae;__Propionivibrio;__Propionivibrio limicola	0.0 %	0.0 %	0.0 %	0.0 %	0.0 %	0.0 %	0.0 %	0.0 %	0.0 %	0.0 %
Bacteria;__Proteobacteria;__Betaproteobacteria;__Rhodocyclales;__Rhodocyclaceae;__Propionivibrio;__Propionivibrio pelophilus	0.0 %	0.0 %	0.0 %	0.0 %	0.0 %	0.0 %	0.0 %	0.0 %	0.0 %	0.0 %
Bacteria;__Proteobacteria;__Betaproteobacteria;__Rhodocyclales;__Zoogloeaceae;__Azoarcus;__Azoarcus communis	0.0 %	0.0 %	0.0 %	0.0 %	0.0 %	0.0 %	0.0 %	0.0 %	0.0 %	0.0 %
Bacteria;__Proteobacteria;__Betaproteobacteria;__Rhodocyclales;__Zoogloeaceae;__Thauera;__Thauera humireducens	0.7 %	0.1 %	0.4 %	0.2 %	0.4 %	0.3 %	1.0 %	0.6 %	1.6 %	1.6 %
Bacteria;__Proteobacteria;__Betaproteobacteria;__Rhodocyclales;__Zoogloeaceae;__Thauera;__Thauera terpenica	0.0 %	0.0 %	0.0 %	0.0 %	0.0 %	0.0 %	0.0 %	0.0 %	0.0 %	0.0 %
Bacteria;__Proteobacteria;__Betaproteobacteria;__Rhodocyclales;__Zoogloeaceae;__Zoogloea;__Zoogloea ramigera	0.0 %	0.0 %	0.0 %	0.0 %	0.0 %	0.0 %	0.0 %	0.0 %	0.0 %	0.0 %
Bacteria;__Proteobacteria;__Deltaproteobacteria;__Desulfobacterales;__Desulfobacteraceae;__Desulfofaba;__Desulfofaba fastidiosa	0.1 %	0.1 %	0.1 %	0.2 %	0.2 %	0.2 %	0.1 %	0.1 %	0.1 %	0.1 %
Bacteria;__Proteobacteria;__Deltaproteobacteria;__Desulfobacterales;__Desulfobacteraceae;__Desulfonema;__Desulfonema magnum	0.0 %	0.0 %	0.0 %	0.0 %	0.0 %	0.0 %	0.0 %	0.0 %	0.0 %	0.0 %
Bacteria;__Proteobacteria;__Deltaproteobacteria;__Desulfobacterales;__Desulfobacteraceae;__Desulfosarcina;__Desulfosarcina widdelii	0.0 %	0.0 %	0.0 %	0.0 %	0.0 %	0.0 %	0.0 %	0.0 %	0.0 %	0.0 %
Bacteria;__Proteobacteria;__Deltaproteobacteria;__Desulfobacterales;__Desulfobulbaceae;__Desulfobulbus;__Desulfobulbus propionicus	0.8 %	0.0 %	3.5 %	0.0 %	1.9 %	0.0 %	0.5 %	0.0 %	1.3 %	0.0 %
Bacteria;__Proteobacteria;__Deltaproteobacteria;__Desulfobacterales;__Desulfobulbaceae;__Desulfocapsa;__Desulfocapsa thiozymogenes	0.0 %	0.0 %	0.0 %	0.0 %	0.0 %	0.0 %	0.0 %	0.0 %	0.0 %	0.0 %
Bacteria;__Proteobacteria;__Deltaproteobacteria;__Desulfovibrionales;__Desulfomicrobiaceae;__Desulfomicrobium;__Desulfomicrobium aestuarii	0.0 %	0.0 %	0.0 %	0.0 %	0.0 %	0.0 %	0.0 %	0.0 %	0.0 %	0.0 %
Bacteria;__Proteobacteria;__Deltaproteobacteria;__Desulfovibrionales;__Desulfovibrionaceae;__Desulfovibrio;__Desulfovibrio aminophilus	0.0 %	0.0 %	0.0 %	0.0 %	0.0 %	0.0 %	0.0 %	0.0 %	0.0 %	0.0 %
Bacteria;__Proteobacteria;__Deltaproteobacteria;__Desulfovibrionales;__Desulfovibrionaceae;__Desulfovibrio;__Desulfovibrio gigas	0.0 %	0.0 %	0.0 %	0.0 %	0.0 %	0.0 %	0.0 %	0.0 %	0.0 %	0.0 %
Bacteria;__Proteobacteria;__Deltaproteobacteria;__Desulfovibrionales;__Desulfovibrionaceae;__Desulfovibrio;__Desulfovibrio oxamicus	0.6 %	0.0 %	0.4 %	0.1 %	0.9 %	0.2 %	1.6 %	0.1 %	2.0 %	0.4 %

Bacteria;__Proteobacteria;__Deltaproteobacteria;__Desulfovibrionales;__Desulfovibrionaceae;__Desulfovibrio;__Desulfovibrio vulgaris	0.0 %	0.0 %	0.0 %	0.0 %	0.0 %	0.0 %	0.0 %	0.0 %	0.0 %	0.0 %
Bacteria;__Proteobacteria;__Deltaproteobacteria;__Desulfuromonadales;__Desulfuromonadaceae;__Pelobacter;__Pelobacter carbinolicus	0.0 %	0.0 %	0.0 %	0.0 %	0.0 %	0.1 %	0.0 %	0.0 %	0.0 %	0.0 %
Bacteria;__Proteobacteria;__Deltaproteobacteria;__Desulfuromonadales;__Geobacteraceae;__Geobacter;__Geobacter anodireducens	0.0 %	0.0 %	0.0 %	0.0 %	0.2 %	0.0 %	0.0 %	0.0 %	0.2 %	0.0 %
Bacteria;__Proteobacteria;__Deltaproteobacteria;__Myxococcales;__Kofleriaceae;__Haliangium;__Haliangium ochraceum	0.0 %	0.0 %	0.0 %	0.0 %	0.0 %	0.0 %	0.0 %	0.0 %	0.0 %	0.0 %
Bacteria;__Proteobacteria;__Deltaproteobacteria;__Myxococcales;__Sandaracinaceae;__Sandaracinus;__Sandaracinus amylolyticus	0.0 %	0.0 %	0.0 %	0.0 %	0.0 %	0.0 %	0.0 %	0.0 %	0.0 %	0.0 %
Bacteria;__Proteobacteria;__Deltaproteobacteria;__Syntrophobacterales;__Syntrophaceae;__Smithella;__Smithella propionica	1.2 %	2.6 %	1.1 %	1.3 %	1.2 %	1.0 %	1.2 %	0.6 %	1.3 %	0.7 %
Bacteria;__Proteobacteria;__Deltaproteobacteria;__Syntrophobacterales;__Syntrophaceae;__Syntrophus;__Syntrophus aciditrophicus	0.0 %	0.0 %	0.0 %	0.0 %	0.0 %	0.0 %	0.0 %	0.0 %	0.0 %	0.0 %
Bacteria;__Proteobacteria;__Deltaproteobacteria;__Syntrophobacterales;__Syntrophaceae;__Syntrophus;__Syntrophus gentianae	0.1 %	0.1 %	0.1 %	0.1 %	0.1 %	0.1 %	0.1 %	0.0 %	0.1 %	0.0 %
Bacteria;__Proteobacteria;__Deltaproteobacteria;__Syntrophobacterales;__Syntrophobacteraceae;__Syntrophobacter;__Syntrophobacter sulfatireducens	0.1 %	0.0 %	0.1 %	0.1 %	0.2 %	0.1 %	0.1 %	0.0 %	0.1 %	0.0 %
Bacteria;__Proteobacteria;__Deltaproteobacteria;__Syntrophobacterales;__Syntrophorhabdaceae;__Syntrophorhabdus;__Syntrophorhabdus aromaticivorans	0.4 %	0.7 %	0.3 %	0.3 %	0.4 %	0.4 %	0.4 %	0.2 %	0.5 %	0.4 %
Bacteria;__Proteobacteria;__Epsilonproteobacteria;__Campylobacterales;__Campylobacteraceae;__Arcobacter;__Arcobacter cryaerophilus	0.3 %	0.8 %	0.3 %	0.1 %	0.2 %	0.0 %	0.6 %	0.1 %	0.9 %	0.1 %
Bacteria;__Proteobacteria;__Epsilonproteobacteria;__Campylobacterales;__Helicobacteraceae;__Sulfuricurvum;__Sulfuricurvum kujiense	0.0 %	0.0 %	0.0 %	0.0 %	0.0 %	0.0 %	0.0 %	0.0 %	0.0 %	0.0 %
Bacteria;__Proteobacteria;__Gammaproteobacteria;__Cellvibrionales;__Cellvibrionaceae;__Marinimicrobium;__Marinimicrobium koreense	0.0 %	0.0 %	0.0 %	0.0 %	0.0 %	0.0 %	0.0 %	0.0 %	0.0 %	0.0 %
Bacteria;__Proteobacteria;__Gammaproteobacteria;__Chromatiales;__Chromatiaceae;__Marichromatium;__Marichromatium purpuratum	0.0 %	0.2 %	0.0 %	0.0 %	0.0 %	0.0 %	0.0 %	0.0 %	0.0 %	0.0 %
Bacteria;__Proteobacteria;__Gammaproteobacteria;__Chromatiales;__Wenzhouxiangellaceae;__Wenzhouxiangella;__Wenzhouxiangella sediminis	0.0 %	0.0 %	0.0 %	0.0 %	0.0 %	0.0 %	0.0 %	0.0 %	0.0 %	0.0 %
Bacteria;__Proteobacteria;__Gammaproteobacteria;__Pseudomonadales;__Moraxellaceae;__Acinetobacter;__Acinetobacter johnsonii	0.0 %	0.0 %	0.0 %	0.0 %	0.0 %	0.0 %	0.0 %	0.0 %	0.0 %	0.0 %
Bacteria;__Proteobacteria;__Gammaproteobacteria;__Pseudomonadales;__Pseudomonadaceae;__Pseudomonas;__Pseudomonas caeni	0.0 %	0.1 %	0.0 %	0.0 %	0.0 %	0.0 %	0.0 %	0.0 %	0.0 %	0.0 %
Bacteria;__Proteobacteria;__Gammaproteobacteria;__Pseudomonadales;__Pseudomonadaceae;__Pseudomonas;__Pseudomonas coleopterorum	0.1 %	0.0 %	0.1 %	0.1 %	0.1 %	0.0 %	0.1 %	0.1 %	0.1 %	0.0 %
Bacteria;__Proteobacteria;__Gammaproteobacteria;__Pseudomonadales;__Pseudomonadaceae;__Pseudomonas;__Pseudomonas guangdongensis	0.0 %	0.3 %	0.0 %	0.0 %	0.0 %	0.0 %	0.0 %	0.0 %	0.0 %	0.0 %
Bacteria;__Proteobacteria;__Gammaproteobacteria;__Pseudomonadales;__Pseudomonadaceae;__Pseudomonas;__Pseudomonas knackmussii	0.3 %	0.0 %	0.3 %	0.9 %	0.3 %	0.3 %	0.4 %	0.3 %	0.5 %	0.2 %
Bacteria;__Proteobacteria;__Gammaproteobacteria;__Pseudomonadales;__Pseudomonadaceae;__Pseudomonas;__Pseudomonas pohangensis	0.0 %	0.0 %	0.0 %	0.0 %	0.0 %	0.0 %	0.0 %	0.0 %	0.0 %	0.0 %
Bacteria;__Proteobacteria;__Gammaproteobacteria;__Thiotrichales;__Thiotrichaceae;__Thiothrix;__Thiothrix caldifontis	0.0 %	0.0 %	0.0 %	0.0 %	0.0 %	0.0 %	0.0 %	0.0 %	0.0 %	0.0 %
Bacteria;__Proteobacteria;__Gammaproteobacteria;__Xanthomonadales;__Rhodanobacteraceae;__Aquimonas;__Aquimonas voraii	0.0 %	0.0 %	0.0 %	0.0 %	0.0 %	0.0 %	0.0 %	0.0 %	0.0 %	0.0 %
Bacteria;__Proteobacteria;__Gammaproteobacteria;__Xanthomonadales;__Xanthomonadaceae;__Arenimonas;__Arenimonas donghaensis	0.0 %	0.0 %	0.0 %	0.0 %	0.0 %	0.0 %	0.0 %	0.0 %	0.0 %	0.0 %
Bacteria;__Proteobacteria;__Gammaproteobacteria;__Xanthomonadales;__Xanthomonadaceae;__Lysobacter;__Lysobacter xinjiangensis	0.0 %	0.0 %	0.0 %	0.0 %	0.0 %	0.0 %	0.0 %	0.0 %	0.0 %	0.0 %
Bacteria;__Proteobacteria;__Gammaproteobacteria;__Xanthomonadales;__Xanthomonadaceae;__Stenotrophomonas;__Stenotrophomonas acidaminiphila	0.0 %	0.0 %	0.0 %	0.0 %	0.0 %	0.0 %	0.0 %	0.0 %	0.0 %	0.0 %
Bacteria;__Proteobacteria;__Gammaproteobacteria;__Xanthomonadales;__Xanthomonadaceae;__Stenotrophomonas;__Stenotrophomonas rhizophila	0.1 %	0.0 %	0.3 %	0.1 %	0.1 %	0.1 %	0.2 %	0.0 %	0.2 %	0.0 %
Bacteria;__Proteobacteria;__Gammaproteobacteria;__Xanthomonadales;__Xanthomonadaceae;__Stenotrophomonas;__Stenotrophomonas tumulicola	0.0 %	0.0 %	0.0 %	0.0 %	0.0 %	0.0 %	0.0 %	0.0 %	0.0 %	0.0 %
Bacteria;__Proteobacteria;__Gammaproteobacteria;__Xanthomonadales;__Xanthomonadaceae;__Thermomonas;__Thermomonas carbonis	0.0 %	0.0 %	0.0 %	0.0 %	0.0 %	0.0 %	0.0 %	0.0 %	0.0 %	0.0 %
Bacteria;__Proteobacteria;__Gammaproteobacteria;__Xanthomonadales;__Xanthomonadaceae;__Thermomonas;__Thermomonas fusca	0.2 %	0.2 %	0.2 %	0.2 %	0.2 %	0.2 %	0.3 %	0.2 %	0.3 %	0.2 %
Bacteria;__Proteobacteria;__Oligoflexia;__Bdellovibrionales;__Bdellovibrionaceae;__Bdellovibrio;__Bdellovibrio bacteriovorus	0.0 %	0.0 %	0.0 %	0.0 %	0.0 %	0.0 %	0.0 %	0.0 %	0.0 %	0.0 %
Bacteria;__Proteobacteria;__Oligoflexia;__Bdellovibrionales;__Bdellovibrionaceae;__Bdellovibrio;__Bdellovibrio exovorus	0.0 %	0.0 %	0.0 %	0.0 %	0.0 %	0.0 %	0.0 %	0.0 %	0.0 %	0.0 %
Bacteria;__Spirochaetes;__Spirochaetia;__Spirochaetales;__Spirochaetaceae;__Rectinema;__Rectinema cohabitans	4.2 %	7.4 %	3.4 %	5.2 %	3.0 %	5.8 %	3.3 %	3.0 %	2.7 %	3.7 %

Bacteria;__Spirochaetes;__Spirochaetia;__Spirochaetales;__Spirochaetaceae;__Sphaerochaeta;__Sphaerochaeta pleomorpha	0.0 %	0.0 %	0.0 %	0.0 %	0.0 %	0.0 %	0.0 %	0.0 %	0.0 %	0.0 %
Bacteria;__Spirochaetes;__Spirochaetia;__Spirochaetales;__Spirochaetaceae;__Treponema;__Treponema brennaborense	0.1 %	0.1 %	0.1 %	0.0 %	0.1 %	0.0 %	0.1 %	0.1 %	0.1 %	0.1 %
Bacteria;__Spirochaetes;__Spirochaetia;__Spirochaetales;__Spirochaetaceae;__Treponema;__Treponema zuelzerae	0.0 %	0.1 %	0.0 %	0.1 %	0.0 %	0.0 %	0.0 %	0.0 %	0.0 %	0.0 %
Bacteria;__Synergistetes;__Synergistia;__Synergistales;__Synergistaceae;__Acetomicrobium;__Acetomicrobium hydrogeniformans	0.1 %	0.0 %	0.1 %	0.2 %	0.1 %	0.2 %	0.1 %	0.1 %	0.1 %	0.2 %
Bacteria;__Synergistetes;__Synergistia;__Synergistales;__Synergistaceae;__Acetomicrobium;__Acetomicrobium mobile	1.6 %	0.4 %	0.9 %	2.3 %	1.1 %	2.5 %	1.0 %	2.3 %	1.1 %	2.8 %
Bacteria;__Synergistetes;__Synergistia;__Synergistales;__Synergistaceae;__Aminivibrio;__Aminivibrio pyruvatiphilus	0.2 %	0.1 %	0.2 %	0.2 %	0.2 %	0.1 %	0.2 %	0.2 %	0.2 %	0.2 %
Bacteria;__Synergistetes;__Synergistia;__Synergistales;__Synergistaceae;__Aminobacterium;__Aminobacterium colombiense	0.0 %	0.0 %	0.0 %	0.0 %	0.0 %	0.0 %	0.0 %	0.1 %	0.0 %	0.1 %
Bacteria;__Synergistetes;__Synergistia;__Synergistales;__Synergistaceae;__Cloacibacillus;__Cloacibacillus evryensis	0.0 %	0.1 %	0.0 %	0.0 %	0.0 %	0.0 %	0.0 %	0.0 %	0.0 %	0.0 %
Bacteria;__Synergistetes;__Synergistia;__Synergistales;__Synergistaceae;__Cloacibacillus;__Cloacibacillus porcorum	0.0 %	0.0 %	0.0 %	0.0 %	0.0 %	0.0 %	0.0 %	0.0 %	0.0 %	0.0 %
Bacteria;__Synergistetes;__Synergistia;__Synergistales;__Synergistaceae;__Thermovirga;__Thermovirga lienii	0.0 %	0.0 %	0.0 %	0.0 %	0.0 %	0.1 %	0.0 %	0.1 %	0.0 %	0.1 %
Bacteria;__Thermotogae;__Thermotogae;__Petrotogales;__Petrotogaceae;__Defluviitoga;__Defluviitoga tunisiensis	0.7 %	1.0 %	0.6 %	0.8 %	0.5 %	0.9 %	0.6 %	0.7 %	0.7 %	1.0 %
Bacteria;__Thermotogae;__Thermotogae;__Thermotogales;__Fervidobacteriaceae;__Fervidobacterium;__Fervidobacterium riparium	0.2 %	0.4 %	0.2 %	0.1 %	0.1 %	0.2 %	0.2 %	0.1 %	0.2 %	0.1 %
Bacteria;__Verrucomicrobia;__Opitutae;__Opitutales;__Opitutaceae;__Cephaloticoccus;__Cephaloticoccus primus	0.0 %	0.0 %	0.0 %	0.0 %	0.0 %	0.0 %	0.0 %	0.0 %	0.0 %	0.0 %
Bacteria;__Verrucomicrobia;__Opitutae;__Puniceicoccales;__Puniceicoccaceae;__Ruficoccus;__Ruficoccus amylovorans	0.0 %	0.0 %	0.0 %	0.0 %	0.0 %	0.0 %	0.0 %	0.0 %	0.0 %	0.0 %
Bacteria;__Verrucomicrobia;__Verrucomicrobiae;__Verrucomicrobiales;__Verrucomicrobia subdivision 3;__Limisphaera;__Limisphaera ngatamarikiensis	0.3 %	0.2 %	0.4 %	0.4 %	0.3 %	0.3 %	0.3 %	0.3 %	0.3 %	0.2 %
Bacteria;__Verrucomicrobia;__Verrucomicrobiae;__Verrucomicrobiales;__Verrucomicrobiaceae;__Roseimicrobium;__Roseimicrobium gellanilyticum	0.0 %	0.0 %	0.0 %	0.0 %	0.0 %	0.0 %	0.0 %	0.0 %	0.0 %	0.0 %
__;__;__;__;__;__;__;Other	29.1%	41.5%	36.7%	19.2%	35.2%	19.1%	38.3%	18.0%	33.6%	19.9%

REFERENCES

Abdelsalam, E., Samer, M., Attia, Y., Abdel-Hadi, M., Hassan, H. and Badr, Y. (2017) Influence of zero valent iron nanoparticles and magnetic iron oxide nanoparticles on biogas and methane production from anaerobic digestion of manure. Energy 120, 842-853.

Achinas, S., Achinas, V. and Euverink, G.J.W. (2017) A technological overview of biogas production from biowaste. Engineering 3(3), 299-307.

Ağdağ, O.N. and Sponza, D.T. (2005) Effect of alkalinity on the performance of a simulated landfill bioreactor digesting organic solid wastes. Chemosphere 59(6), 871-879.

Ahring, B.K., Sandberg, M. and Angelidaki, I. (1995) Volatile fatty acids as indicators of process imbalance in anaerobic digestors. Applied microbiology and biotechnology 43(3), 559-565.

Albalasmeh, A.A., Berhe, A.A. and Ghezzehei, T.A. (2013) A new method for rapid determination of carbohydrate and total carbon concentrations using UV spectrophotometry. Carbohydrate polymers 97(2), 253-261.

Ali, A., Hira Zafar, M.Z., ul Haq, I., Phull, A.R., Ali, J.S. and Hussain, A. (2016) Synthesis, characterization, applications, and challenges of iron oxide nanoparticles. Nanotechnology, science and applications 9, 49.

Amann, R.I., Ludwig, W. and Schleifer, K.-H. (1995) Phylogenetic identification and in situ detection of individual microbial cells without cultivation. Microbiology and Molecular Biology Reviews 59(1), 143-169.

Angelidaki, I. and Ahring, B. (1994) Anaerobic thermophilic digestion of manure at different ammonia loads: effect of temperature. Water research 28(3), 727-731.

Angelidaki, I., Alves, M., Bolzonella, D., Borzacconi, L., Campos, J., Guwy, A., Kalyuzhnyi, S., Jenicek, P. and Van Lier, J. (2009) Defining the biomethane potential (BMP) of solid organic wastes and energy crops: a proposed protocol for batch assays. Water science and technology 59(5), 927-934.

Angelidaki, I., Karakashev, D., Batstone, D.J., Plugge, C.M. and Stams, A.J. (2011) Methods in enzymology, pp. 327-351, Elsevier.

Angelidaki, I. and Sanders, W. (2004) Assessment of the anaerobic biodegradability of macropollutants. Re/Views in Environmental Science & Bio/Technology 3(2), 117-129.

Ariunbaatar, J., Panico, A., Esposito, G., Pirozzi, F. and Lens, P.N. (2014) Pretreatment methods to enhance anaerobic digestion of organic solid waste. Applied energy 123, 143-156.

Aslanzadeh, S., Rajendran, K., Jeihanipour, A. and Taherzadeh, M.J. (2013) The effect of effluent recirculation in a semi-continuous two-stage anaerobic digestion system. Energies 6(6), 2966-2981.

Association, A.-A.P.H. (2005) Standard methods for the examination of water and wasterwater. Sprimgfield: Byrd Prepress.

Aulenta, F., Rossetti, S., Amalfitano, S., Majone, M. and Tandoi, V. (2013) Conductive Magnetite Nanoparticles Accelerate the Microbial Reductive Dechlorination of Trichloroethene by Promoting Interspecies Electron Transfer Processes. Chemsuschem 6(3), 433-436.

Baalousha, M. (2009) Aggregation and Disaggregation of Iron Oxide Nanoparticles: Influence of Particle Concentration, Ph and Natural Organic Matter. Science of the Total Environment 407(6), 2093-2101.

Baek, G., Kim, J., Kim, J. and Lee, C. (2018) Role and potential of direct interspecies electron transfer in anaerobic digestion. Energies 11(1), 107.

Baek, G., Kim, J. and Lee, C. (2016) A long-term study on the effect of magnetite supplementation in continuous anaerobic digestion of dairy effluent–Enhancement in process performance and stability. Bioresource technology 222, 344-354.

BANZ (2011) Biogas Strategy, New Zealand.

BANZ (2019) Biogas - a Bioenergy Association site, New Zealand.

Barua, S. and Dhar, B.R. (2017) Advances towards understanding and engineering direct interspecies electron transfer in anaerobic digestion. Bioresource technology 244, 698-707.

Beiki, H. and Keramati, M. (2019) Improvement of methane production from sugar beet wastes using TiO 2 and Fe 3 O 4 nanoparticles and chitosan micropowder additives. Applied biochemistry and biotechnology, 1-13.

Bolzonella, D., Pavan, P., Battistoni, P. and Cecchi, F. (2005) Mesophilic anaerobic digestion of waste activated sludge: influence of the solid retention time in the wastewater treatment process. Process Biochemistry 40(3-4), 1453-1460.

Boone, D.R. and Bryant, M.P. (1980) Propionate-degrading bacterium, Syntrophobacter wolinii sp. nov. gen. nov., from methanogenic ecosystems. Applied and Environmental Microbiology 40(3), 626-632.

Bowen, E.J., Dolfing, J., Davenport, R.J., Read, F.L. and Curtis, T.P. (2014) Low-temperature limitation of bioreactor sludge in anaerobic treatment of domestic wastewater. Water science and technology 69(5), 1004-1013.

Bryant, M., Campbell, L.L., Reddy, C. and Crabill, M. (1977) Growth of Desulfovibrio in lactate or ethanol media low in sulfate in association with H2-utilizing methanogenic bacteria. Applied and Environmental Microbiology 33(5), 1162-1169.

Carlos, L., Einschlag, F.S.G., González, M.C. and Mártire, D.O. (2013) Applications of magnetite nanoparticles for heavy metal removal from wastewater. Waste water-treatment technologies and recent analytical developments, 63-77.

Carpenter, A.W., Laughton, S.N. and Wiesner, M.R. (2015) Enhanced Biogas Production from Nanoscale Zero Valent Iron-Amended Anaerobic Bioreactors. Environmental Engineering Science 32(8), 647-655.

Casals, E., Barrena, R., García, A., González, E., Delgado, L., Busquets-Fité, M., Font, X., Arbiol, J., Glatzel, P. and Kvashnina, K. (2014) Programmed iron oxide nanoparticles disintegration in anaerobic digesters boosts biogas production. Small 10(14), 2801-2808.

Chae, K., Jang, A., Yim, S. and Kim, I.S. (2008) The effects of digestion temperature and temperature shock on the biogas yields from the mesophilic anaerobic digestion of swine manure. Bioresource technology 99(1), 1-6.

Chen, S., Rotaru, A.-E., Liu, F., Philips, J., Woodard, T.L., Nevin, K.P. and Lovley, D.R. (2014) Carbon cloth stimulates direct interspecies electron transfer in syntrophic co-cultures. Bioresource technology 173, 82-86.

Cruz Viggi, C., Rossetti, S., Fazi, S., Paiano, P., Majone, M. and Aulenta, F. (2014) Magnetite particles triggering a faster and more robust syntrophic pathway of methanogenic propionate degradation. Environmental Science and Technology 48(13), 7536-7543.

Dalla Vecchiaa, C., Mattiolia, A., Bolzonellaa, D., Palmab, E., Viggib, C.C. and Aulenta, F. (2016) Impact of Magnetite Nanoparticles Supplementation on the Anaerobic Digestion of Food Wastes: Batch and Continuous-Flow Investigations. Chemical Engineering Journal 49.

Dang, Y., Holmes, D.E., Zhao, Z., Woodard, T.L., Zhang, Y., Sun, D., Wang, L.-Y., Nevin, K.P. and Lovley, D.R. (2016) Enhancing anaerobic digestion of complex organic waste with carbon-based conductive materials. Bioresource technology 220, 516-522.

de Lemos Chernicharo, C.A. (2007) Anaerobic reactors. Water Intelligence Online 6, 9781780402116.

De Vrieze, J., Raport, L., Willems, B., Verbrugge, S., Volcke, E., Meers, E., Angenent, L.T. and Boon, N. (2015) Inoculum selection influences the biochemical methane potential of agro-industrial substrates. Microbial biotechnology 8(5), 776-786.

Dinamarca, S., Aroca, G., Chamy, R. and Guerrero, L. (2003) The influence of pH in the hydrolytic stage of anaerobic digestion of the organic fraction of urban solid waste. Water science and technology 48(6), 249-254.

Du, X., He, J., Zhu, J., Sun, L. and An, S. (2012) Ag-deposited silica-coated Fe3O4 magnetic nanoparticles catalyzed reduction of p-nitrophenol. Applied Surface Science 258(7), 2717-2723.

Dubois, M., Gilles, K.A., Hamilton, J.K., Rebers, P.t. and Smith, F. (1956) Colorimetric method for determination of sugars and related substances. Analytical chemistry 28(3), 350-356.

El-Mashad, H.M. and Zhang, R. (2010) Biogas production from co-digestion of dairy manure and food waste. Bioresource technology 101(11), 4021-4028.

Faisal, S., Yusuf Hafeez, F., Zafar, Y., Majeed, S., Leng, X., Zhao, S., Saif, I., Malik, K. and Li, X. (2019) A review on nanoparticles as boon for biogas producers—nano fuels and biosensing monitoring. Applied Sciences 9(1), 59.

Fallde, M. and Eklund, M. (2015) Towards a sustainable socio-technical system of biogas for transport: the case of the city of Linköping in Sweden. Journal of Cleaner production 98, 17-28.

Fang, H.H. and Liu, H. (2002) Effect of pH on hydrogen production from glucose by a mixed culture. Bioresource technology 82(1), 87-93.

Fotidis, I., Karakashev, D. and Angelidaki, I. (2014) The dominant acetate degradation pathway/methanogenic composition in full-scale anaerobic digesters operating under different ammonia levels. International Journal of Environmental Science and Technology 11(7), 2087-2094.

Gagliano, M., Braguglia, C., Petruccioli, M. and Rossetti, S. (2015) Ecology and biotechnological potential of the thermophilic fermentative Coprothermobacter spp. FEMS microbiology ecology 91(5).

George, T., Franklin, L. and Stensel, H.D. (2003) Wastewater engineering: treatment and reuse. Metcalf & Eddy, Inc., New York.

Gou, C., Yang, Z., Huang, J., Wang, H., Xu, H. and Wang, L. (2014) Effects of temperature and organic loading rate on the performance and microbial community of anaerobic co-digestion of waste activated sludge and food waste. Chemosphere 105, 146-151.

Grant, W.D. and Long, P.E. (1985) The natural environment and the biogeochemical cycles, pp. 125-237, Springer.

Guo-Qin, X., Fang, Y., ZHANG, W.-D. and Jing, L. (2016) The Effects of Different Concentration Glucose on Methane Fermentation. DEStech Transactions on Environment, Energy and Earth Sciences (edep).

Hadiyarto, A., Budiyono, B., Djohari, S., Hutama, I. and Hasyim, W. (2015) The Effect of F/M Ratio to the Anaerobic Decomposition of Biogas Production from Fish Offal Waste. Waste Technology 3(2), 58-61.

Hakawati, R., Smyth, B.M., McCullough, G., De Rosa, F. and Rooney, D. (2017) What is the most energy efficient route for biogas utilization: Heat, electricity or transport? Applied energy 206, 1076-1087.

Hanaki, K., Matsuo, T. and Nagase, M. (1981) Mechanism of inhibition caused by long-chain fatty acids in anaerobic digestion process. Biotechnology and bioengineering 23(7), 1591-1610.

Hansen, K.H., Angelidaki, I. and Ahring, B.K. (1999) Improving thermophilic anaerobic digestion of swine manure. Water research 33(8), 1805-1810.

Haveman, S.A., Holmes, D.E., Ding, Y.H.R., Ward, J.E., DiDonato, R.J. and Lovley, D.R. (2006) C-Type Cytochromes in Pelobacter carbinolicus. . Applied Environmental Microbiology 72(11), 6980−6985.

Holm-Nielsen, J.B. and Esbensen, K.H. (2011) Monitoring of biogas test plants—a process analytical technology approach. Journal of Chemometrics 25(7), 357-365.

Hussain, A. and Dubey, S.K. (2017) Specific methanogenic activity test for anaerobic degradation of influents. Applied Water Science 7(2), 535-542.

Jiang, J., Zhang, Y., Li, K., Wang, Q., Gong, C. and Li, M. (2013) Volatile fatty acids production from food waste: effects of pH, temperature, and organic loading rate. Bioresource technology 143, 525-530.

Jiang, W., Kim, B.Y., Rutka, J.T. and Chan, W.C. (2008) Nanoparticle-mediated cellular response is size-dependent. Nature Nanotechnology 3(3), 145.

Jiang, Y., Heaven, S. and Banks, C. (2012) Strategies for stable anaerobic digestion of vegetable waste. Renewable energy 44, 206-214.

Jing, Y., Wan, J., Angelidaki, I., Zhang, S. and Luo, G. (2017) iTRAQ quantitative proteomic analysis reveals the pathways for methanation of propionate facilitated by magnetite. Water research 108, 212-221.

Kang, Y.S., Risbud, S., Rabolt, J.F. and Stroeve, P. (1996) Synthesis and characterization of nanometer-size Fe3O4 and γ-Fe2O3 particles. Chemistry of Materials 8(9), 2209-2211.

Kassab, G., Khater, D., Odeh, F., Shatanawi, K., Halalsheh, M., Arafah, M. and Lier, J.B.v. (2020) Impact of Nanoscale Magnetite and Zero Valent Iron on the Batch-Wise Anaerobic Co-Digestion of Food Waste and Waste-Activated Sludge. Water 12(5), 1283.

Kato, S., Hashimoto, K. and Watanabe, K. (2012a) Methanogenesis facilitated by electric syntrophy via (semi) conductive iron-oxide minerals. Environmental Microbiology 14(7), 1646-1654.

Kato, S., Hashimoto, K. and Watanabe, K. (2012b) Microbial Interspecies Electron Transfer Via Electric Currents through Conductive Minerals. Proceedings of the National Academy of Sciences 109(25), 10042-10046.

Kato, S., Nakamura, R., Kai, F., Watanabe, K. and Hashimoto, K. (2010) Respiratory Interactions of Soil Bacteria with (Semi) Conductive Iron-Oxide Minerals. Environmental Microbiology 12(12), 3114-3123.

Kelly, G. (2007) Renewable energy strategies in England, Australia and New Zealand. Geoforum 38(2), 326-338.

Kelly, G. (2011) History and potential of renewable energy development in New Zealand. Renewable and Sustainable Energy Reviews 15(5), 2501-2509.

Keyhanian, F., Shariati, S., Faraji, M. and Hesabi, M. (2011) Magnetite Nanoparticles with Surface Modification for Removal of Methyl Violet from Aqueous Solutions. Arabian Journal of Chemistry.

Khanal, S.K. (2008) Anaerobic biotechnology for bioenergy production. Principles and Application Willey and Blackwell, 161-186.

Kim, D., Zhang, Y., Voit, W., Rao, K. and Muhammed, M. (2001) Synthesis and characterization of surfactant-coated superparamagnetic monodispersed iron oxide nanoparticles. Journal of Magnetism and Magnetic Materials 225(1-2), 30-36.

Kim, J.K., Oh, B.R., Chun, Y.N. and Kim, S.W. (2006) Effects of temperature and hydraulic retention time on anaerobic digestion of food waste. Journal of Bioscience and Bioengineering 102(4), 328-332.

Kleinstreuer, C. and Poweigha, T. (1982) Dynamic simulator for anaerobic digestion processes. Biotechnology and bioengineering 24(9), 1941-1951.

Kwietniewska, E. and Tys, J. (2014) Process characteristics, inhibition factors and methane yields of anaerobic digestion process, with particular focus on microalgal biomass fermentation. Renewable and Sustainable Energy Reviews 34, 491-500.

Lee, D.H., Behera, S.K., Kim, J.W. and Park, H.-S. (2009) Methane production potential of leachate generated from Korean food waste recycling facilities: a lab-scale study. Waste Management 29(2), 876-882.

Lee, J.-Y., Lee, S.-H. and Park, H.-D. (2016) Enrichment of specific electro-active microorganisms and enhancement of methane production by adding granular activated carbon in anaerobic reactors. Bioresource technology 205, 205-212.

Li, H., Chang, J., Liu, P., Fu, L., Ding, D. and Lu, Y. (2015) Direct Interspecies Electron Transfer Accelerates Syntrophic Oxidation of Butyrate in Paddy Soil Enrichments. Environmental Microbiology 17(5), 1533-1547.

Li, X.-q., Brown, D.G. and Zhang, W.-x. (2007) Stabilization of biosolids with nanoscale zero-valent iron (nZVI). Journal of nanoparticle research 9(2), 233-243.

Lin, R., Deng, C., Cheng, J., Xia, A., Lens, P.N., Jackson, S.A., Dobson, A.D. and Murphy, J.D. (2018) Graphene Facilitates Biomethane Production from Protein-Derived Glycine in Anaerobic Digestion. iScience 10, 158-170.

Liu, C., Li, H., Zhang, Y. and Chen, Q. (2016) Characterization of methanogenic activity during high-solids anaerobic digestion of sewage sludge. Biochemical Engineering Journal 109, 96-100.

Liu, F., Rotaru, A.-E., Shrestha, P.M., Malvankar, N.S., Nevin, K.P. and Lovley, D.R. (2012a) Promoting Direct Interspecies Electron Transfer with Activated Carbon. Energy & Environmental Science 5(10), 8982-8989.

Liu, Y., Zhang, Y., Quan, X., Li, Y., Zhao, Z., Meng, X. and Chen, S. (2012b) Optimization of anaerobic acidogenesis by adding Fe0 powder to enhance anaerobic wastewater treatment. Chemical Engineering Journal 192, 179-185.

Lovley, D.R. (2011) Live Wires: Direct Extracellular Electron Exchange for Bioenergy and the Bioremediation of Energy-Related Contamination. Energy & Environmental Science 4(12), 4896-4906.

Lovley, D.R. (2017) Happy Together: Microbial Communities That

Hook up to Swap Electrons. The ISME journal 11, 327−336.

Lu, A.H., Salabas, E.e.L. and Schüth, F. (2007) Magnetic nanoparticles: synthesis, protection, functionalization, and application. Angewandte Chemie International Edition 46(8), 1222-1244.

Luo, C., Lü, F., Shao, L. and He, P. (2015) Application of eco-compatible biochar in anaerobic digestion to relieve acid stress and promote the selective colonization of functional microbes. Water research 68, 710-718.

Luste, S. and Luostarinen, S. (2010) Anaerobic co-digestion of meat-processing by-products and sewage sludge–Effect of hygienization and organic loading rate. Bioresource technology 101(8), 2657-2664.

M.B.I.E. (2018) Energy in New Zealand. Ministry of Business, Innovation & Employment

New Zealand.

Ma, M., Zhang, Y., Guo, Z. and Gu, N. (2013) Facile synthesis of ultrathin magnetic iron oxide nanoplates by Schikorr reaction. Nanoscale Research Letters 8(1), 16.

Madigan, M.T., Martinko, J.M., Dunlap, P.V. and Clark, D.P. (2008) Brock biology of microorganisms 12th edn. International Microbiology 11, 65-73.

Manure, F.D. (2001) Dairy Waste Anaerobic Digestion Handbook.

Mao, C., Feng, Y., Wang, X. and Ren, G. (2015) Review on research achievements of biogas from anaerobic digestion. Renewable and Sustainable Energy Reviews 45, 540-555.

Marchaim, U. and Krause, C. (1993) Propionic to acetic acid ratios in overloaded anaerobic digestion. Bioresource technology 43(3), 195-203.

Marini, R.P. (2003) Approaches to analyzing experiments with factorial arrangements of treatments plus other treatments. HortScience 38(1), 117-120.

Martins, G., Salvador, A.F., Pereira, L. and Alves, M.M. (2018) Methane production and conductive materials: a critical review. Environmental science & technology 52(18), 10241-10253.

Mascolo, M.C., Pei, Y. and Ring, T.A. (2013) Room temperature co-precipitation synthesis of magnetite nanoparticles in a large pH window with different bases. Materials 6(12), 5549-5567.

Mawson, A.J., Earle, R.L. and Larsen, V. (1991) Degradation of acetic and propionic acids in the methane fermentation. Water research 25(12), 1549-1554.

Maximova, N. and Dahl, O. (2006) Environmental Implications of Aggregation Phenomena: Current Understanding. Current Opinion in Colloid & Interface Science 11(4), 246-266.

McDonald, H.B. (2007) The effect of sulfide inhibition and organic shock loading on anaerobic biofilm reactors treating a low-temperature, high-sulfate wastewater, ProQuest.

McMahon, K.D., Zheng, D., Stams, A.J., Mackie, R.I. and Raskin, L. (2004) Microbial population dynamics during start-up and overload conditions of anaerobic digesters treating municipal solid waste and sewage sludge. Biotechnology and bioengineering 87(7), 823-834.

Morita, M., Malvankar, N.S., Franks, A.E., Summers, Z.M., Giloteaux, L., Rotaru, A.E., Rotaru, C. and Lovley, D.R. (2011) Potential for Direct Interspecies Electron Transfer in Methanogenic Wastewater Digester Aggregates. Mbio 2(4), e00159-00111.

Müller, N., Worm, P., Schink, B., Stams, A.J. and Plugge, C.M. (2010) Syntrophic butyrate and propionate oxidation processes: from genomes to reaction mechanisms. Environmental Microbiology Reports 2(4), 489-499.

Nagamani, B. and Ramasamy, K. (1999) Biogas production technology: an Indian perspective. Current Science, 44-55.

Nagao, N., Tajima, N., Kawai, M., Niwa, C., Kurosawa, N., Matsuyama, T., Yusoff, F.M. and Toda, T. (2012) Maximum organic loading rate for the single-stage wet anaerobic digestion of food waste. Bioresource technology 118, 210-218.

Nakamura, R., Kai, F., Okamoto, A., Newton, G.J. and Hashimoto, K. (2009) Self-Constructed Electrically Conductive Bacterial Networks. Angewandte Chemie International Edition 48(3), 508-511.

Nakano, M.M. and Zuber, P. (2004) Strict and facultative anaerobes: medical and environmental aspects, CRC Press.

Namal, O. (2019) Investigation of the effects of different conductive materials on the anaerobic digestion. International Journal of Environmental Science and Technology, 1-10.

Nasir, I.M., Ghazi, T.I.M. and Omar, R. (2012) Anaerobic digestion technology in livestock manure treatment for biogas production: a review. Engineering in Life Sciences 12(3), 258-269.

Nges, I.A. and Liu, J. (2010) Effects of solid retention time on anaerobic digestion of dewatered-sewage sludge in mesophilic and thermophilic conditions. Renewable energy 35(10), 2200-2206.

Nguyen, P., Kuruparan, P. and Visvanathan, C. (2007) Anaerobic digestion of municipal solid waste as a treatment prior to landfill. Bioresource technology 98(2), 380-387.

Nielfa, A., Cano, R. and Fdz-Polanco, M. (2015) Theoretical methane production generated by the co-digestion of organic fraction municipal solid waste and biological sludge. Biotechnology Reports 5, 14-21.

Ogejo, J.A., Wen, Z., Ignosh, J., Bendfeldt, E.S. and Collins, E. (2009) Biomethane technology.

Ozkaya, T., Toprak, M.S., Baykal, A., Kavas, H., Köseoğlu, Y. and Aktaş, B. (2009) Synthesis of Fe3O4 nanoparticles at 100 C and its magnetic characterization. Journal of Alloys and Compounds 472(1-2), 18-23.

Park, J.-H., Kang, H.-J., Park, K.-H. and Park, H.-D. (2018) Direct interspecies electron transfer via conductive materials: a perspective for anaerobic digestion applications. Bioresource technology 254, 300-311.

Parkin, G.F. and Owen, W.F. (1986) Fundamentals of anaerobic digestion of wastewater sludges. Journal of Environmental Engineering 112(5), 867-920.

Phelps, T., Conrad, R. and Zeikus, J. (1985) Sulfate-dependent interspecies H2 transfer between Methanosarcina barkeri and Desulfovibrio vulgaris during coculture metabolism of acetate or methanol. Applied and Environmental Microbiology 50(3), 589-594.

Procházka, J., Mrázek, J., Štrosová, L., Fliegerová, K., Zábranská, J. and Dohányos, M. (2012) Enhanced biogas yield from energy crops with rumen anaerobic fungi. Engineering in Life Sciences 12(3), 343-351.

Punal, A., Trevisan, M., Rozzi, A. and Lema, J. (2000) Influence of C: N ratio on the start-up of up-flow anaerobic filter reactors. Water research 34(9), 2614-2619.

Regueiro, L., Veiga, P., Figueroa, M., Alonso-Gutierrez, J., Stams, A.J., Lema, J.M. and Carballa, M. (2012) Relationship between microbial activity and microbial community structure in six full-scale anaerobic digesters. Microbiological research 167(10), 581-589.

Rolfe, M.D., Rice, C.J., Lucchini, S., Pin, C., Thompson, A., Cameron, A.D., Alston, M., Stringer, M.F., Betts, R.P. and Baranyi, J. (2012) Lag phase is a distinct growth phase that prepares bacteria for exponential growth and involves transient metal accumulation. Journal of Bacteriology 194(3), 686-701.

Rotaru, A.-E., Shrestha, P.M., Liu, F., Markovaite, B., Chen, S., Nevin, K.P. and Lovley, D.R. (2014a) Direct Interspecies Electron Transfer between Geobacter Metallireducens and Methanosarcina Barkeri. Applied and Environmental Microbiology 80(15), 4599-4605.

Rotaru, A.E., Shrestha, P.M., Liu, F., Shrestha, M., Shrestha, D., Embree, M., Zengler, K., Wardman, C., Nevin, K.P. and Lovley, D.R. (2014b) A New Model for Electron Flow During Anaerobic Digestion: Direct Interspecies Electron Transfer to Methanosaeta for the Reduction of Carbon Dioxide to Methane. Energy & Environmental Science 7(1), 408-415.

Rotaru, A.E., Shrestha, P.M., Liu, F., Ueki, T., Nevin, K., Summers, Z.M. and Lovley, D.R. (2012) Interspecies Electron Transfer via Hydrogen and Formate Rather than Direct Electrical Connections in Cocultures of Pelobacter carbinolicus and Geobacter sulfurreducens.

. Applied Environmental Microbiology 78(21), 7645−7651.

Rozzi, A. and Remigi, E. (2004) Methods of assessing microbial activity and inhibition under anaerobic conditions: a literature review. Re/Views in Environmental Science & Bio/Technology 3(2), 93-115.

Sanchez, E., Borja, R., Weiland, P., Travieso, L. and Martın, A. (2001) Effect of substrate concentration and temperature on the anaerobic digestion of piggery waste in a tropical climate. Process Biochemistry 37(5), 483-489.

Shrestha, P.M., Rotaru, A.E., Aklujkar, M., Liu, F., Shrestha, M., Summers, Z.M., Malvankar, N., Flores, D.C. and Lovley, D.R. (2013) Syntrophic Growth with Direct Interspecies Electron Transfer as the Primary Mechanism for Energy Exchange. Environmental Microbiology Reports 5(6), 904-910.

Sieber, J.R., Le, H.M. and Mcinerney, M.J. (2014) The Importance of Hydrogen and Formate Transfer for Syntrophic Fatty, Aromatic and Alicyclic Metabolism. . Environmental Microbiology 16 (1), 177−188.

Siegert, I. and Banks, C. (2005) The effect of volatile fatty acid additions on the anaerobic digestion of cellulose and glucose in batch reactors. Process Biochemistry 40(11), 3412-3418.

Speece, R.E. (1983) Anaerobic biotechnology for industrial wastewater treatment. Environmental science & technology 17(9), 416A-427A.

Speece, R.E. (1996) Anaerobic biotechnology for industrial wastewaters.

Stams, A.J., De Bok, F.A., Plugge, C.M., Eekert, V., Miriam, H., Dolfing, J. and Schraa, G. (2006) Exocellular electron transfer in anaerobic microbial communities. Environmental Microbiology 8(3), 371-382.

Stams, A.J. and Plugge, C.M. (2009) Electron transfer in syntrophic communities of anaerobic bacteria and archaea. Nature Reviews Microbiology 7(8), 568-577.

Stanley, A., Stanley, D., Dadu, D. and Abah, A. (2013) Appraising the combustion of biogas for sustainable rural energy needs. African Journal of Environmental Science and Technology 7(6), 350-357.

Storck, T., Virdis, B. and Batstone, D.J. (2016) Modelling extracellular limitations for mediated versus direct interspecies electron transfer. The ISME journal 10(3), 621.

Su, L., Shi, X., Guo, G., Zhao, A. and Zhao, Y. (2013) Stabilization of sewage sludge in the presence of nanoscale zero-valent iron (nZVI): abatement of odor and improvement of biogas production. Journal of Material Cycles and Waste Management 15(4), 461-468.

Suanon, F., Sun, Q., Mama, D., Li, J., Dimon, B. and Yu, C.-P. (2016) Effect of nanoscale zero-valent iron and magnetite (Fe 3 O 4) on the fate of metals during anaerobic digestion of sludge. Water research 88, 897-903.

Summers, Z.M., Fogarty, H.E., Leang, C., Franks, A.E., Malvankar, N.S. and Lovley, D.R. (2010) Direct Exchange of Electrons within Aggregates of an Evolved Syntrophic Coculture of Anaerobic Bacteria. Science 330(6009), 1413-1415.

Tang, S.C. and Lo, I.M. (2013) Magnetic Nanoparticles: Essential Factors for Sustainable Environmental Applications. Water research 47(8), 2613-2632.

Tanimu, M.I., Ghazi, T.I.M., Harun, M.R. and Idris, A. (2014) Effect of feed loading on biogas methane production in batch mesophilic anaerobic digesters treating food waste. International Journal 5(1).

Teng, X., Black, D., Watkins, N.J., Gao, Y. and Yang, H. (2003) Platinum-maghemite core− shell nanoparticles using a sequential synthesis. Nano Letters 3(2), 261-264.

Thauer, R.K., Kaster, A.-K., Seedorf, H., Buckel, W. and Hedderich, R. (2008) Methanogenic archaea: ecologically relevant differences in energy conservation. Nature Reviews Microbiology 6(8), 579-591.

Thiele, J.H. and Mayes, J. (2008) An overview of New Zealand's biogas potential.

Tian, T., Qiao, S., Li, X., Zhang, M. and Zhou, J. (2017) Nano-graphene induced positive effects on methanogenesis in anaerobic digestion. Bioresource technology 224, 41-47.

Van Lier, J.B., Grolle, K., Frijters, C., Stams, A. and Lettinga, G. (1993) Effects of acetate, propionate, and butyrate on the thermophilic anaerobic degradation of propionate by methanogenic sludge and defined cultures. Applied and Environmental Microbiology 59(4), 1003-1011.

Van Loosdrecht, M.C. and Henze, M. (1999) Maintenance, endogeneous respiration, lysis, decay and predation. Water science and technology 39(1), 107-117.

Verma, A. and Stellacci, F. (2010) Effect of surface properties on nanoparticle–cell interactions. Small 6(1), 12-21.

Villain, M. and Marrot, B. (2013) Influence of sludge retention time at constant food to microorganisms ratio on membrane bioreactor performances under stable and unstable state conditions. Bioresource technology 128, 134-144.

Wang, T., Zhang, D., Dai, L., Chen, Y. and Dai, X. (2016) Effects of metal nanoparticles on methane production from waste-activated sludge and microorganism community shift in anaerobic granular sludge. Scientific Reports 6, 25857.

Wang, X., Lu, X., Li, F. and Yang, G. (2014) Effects of temperature and carbon-nitrogen (C/N) ratio on the performance of anaerobic co-digestion of dairy manure, chicken manure and rice straw: focusing on ammonia inhibition. PloS one 9(5), e97265.

Wang, X., Yang, G., Feng, Y., Ren, G. and Han, X. (2012) Optimizing feeding composition and carbon–nitrogen ratios for improved methane yield during anaerobic co-digestion of dairy, chicken manure and wheat straw. Bioresource technology 120, 78-83.

Whitman, W., Bowen, T., Boone, D., Balows, A., Truper, H., Dworkin, M., Harder, W. and Schleifer, K. (1992) The methanogenic bacteria. The prokaryotes: a handbook on the biology of bacteria: ecophysiology, isolation, identification, applications, vol. I. (Ed. 2), 719-767.

Wong, Y.-S., Teng, T.T., Ong, S.-A., Norhashimah, M., Rafatullah, M. and Lee, H.-C. (2013) Anaerobic acidogenesis biodegradation of palm oil mill effluent using suspended closed anaerobic bioreactor (SCABR) at mesophilic temperature. Procedia Environmental Sciences 18, 433-441.

Wu, W.-M., Hickey, R.F., Jain, M.K. and Zeikus, J.G. (1993) Energetics and regulations of formate and hydrogen metabolism by Methanobacterium formicicum. Archives of Microbiology 159(1), 57-65.

Wu, X., Yao, W., Zhu, J. and Miller, C. (2010) Biogas and CH 4 productivity by co-digesting swine manure with three crop residues as an external carbon source. Bioresource technology 101(11), 4042-4047.

Yamada, C., Kato, S., Ueno, Y., Ishii, M. and Igarashi, Y. (2015) Conductive iron oxides accelerate thermophilic methanogenesis from acetate and propionate. Journal of Bioscience and Bioengineering 119(6), 678-682.

Yan, W., Shen, N., Xiao, Y., Chen, Y., Sun, F., Tyagi, V.K. and Zhou, Y. (2017) The role of conductive materials in the start-up period of thermophilic anaerobic system. Bioresource technology 239, 336-344.

Yang, Z., Guo, R., Shi, X., Wang, C., Wang, L. and Dai, M. (2016) Magnetite Nanoparticles Enable a Rapid Conversion of Volatile Fatty Acids to Methane. Rsc Advances 6(31), 25662-25668.

Yang, Z., Shi, X., Wang, C., Wang, L. and Guo, R. (2015a) Magnetite nanoparticles facilitate methane production from ethanol via acting as electron acceptors. Scientific Reports 5.

Yang, Z., Xu, X., Guo, R., Fan, X. and Zhao, X. (2015b) Accelerated methanogenesis from effluents of hydrogen-producing stage in anaerobic digestion by mixed cultures enriched with acetate and nano-sized magnetite particles. Bioresource technology 190, 132-139.

Yates, G.T. and Smotzer, T. (2007) On the lag phase and initial decline of microbial growth curves. Journal of Theoretical Biology 244(3), 511-517.

Yin, Q., Miao, J., Li, B. and Wu, G. (2017) Enhancing electron transfer by ferroferric oxide during the anaerobic treatment of synthetic wastewater with mixed organic carbon. International Biodeterioration & Biodegradation 119, 104-110.

Zhang, P., Chen, Y. and Zhou, Q. (2009) Waste activated sludge hydrolysis and short-chain fatty acids accumulation under mesophilic and thermophilic conditions: effect of pH. Water research 43(15), 3735-3742.

Zhang, T., Liu, L., Song, Z., Ren, G., Feng, Y., Han, X. and Yang, G. (2013) Biogas production by co-digestion of goat manure with three crop residues. PloS one 8(6), e66845.

Zhang, W., Lang, Q., Wu, S., Li, W., Bah, H. and Dong, R. (2014) Anaerobic digestion characteristics of pig manures depending on various growth stages and initial substrate concentrations in a scaled pig farm in Southern China. Bioresource technology 156, 63-69.

Zhao, Z., Zhang, Y., Li, Y., Dang, Y., Zhu, T. and Quan, X. (2017) Potentially shifting from interspecies hydrogen transfer to direct interspecies electron transfer for syntrophic metabolism to resist acidic impact with conductive carbon cloth. Chemical Engineering Journal 313, 10-18.

Zhao, Z., Zhang, Y., Woodard, T., Nevin, K. and Lovley, D. (2015) Enhancing Syntrophic Metabolism in up-Flow Anaerobic Sludge Blanket Reactors with Conductive Carbon Materials. Bioresource technology 191, 140-145.

Zhou, S., Xu, J., Yang, G. and Zhuang, L. (2014) Methanogenesis Affected by the Co-Occurrence of Iron (Iii) Oxides and Humic Substances. FEMS microbiology ecology 88(1), 107-120.

Zhu, M.-Y., Peng, S.-C., Tao, W., Wang, J., Tang, T., Chen, T.-H. and Yue, Z.-B. (2017) Response of methane production and microbial community to the enrichment of soluble microbial products in goethite-dosed anaerobic reactors. Fuel 191, 495-499.

Zhuang, L., Ma, J., Yu, Z., Wang, Y. and Tang, J. (2018) Magnetite accelerates syntrophic acetate oxidation in methanogenic systems with high ammonia concentrations. Microbial biotechnology 11(4), 710-720.

Zhuang, L., Tang, J., Wang, Y., Hu, M. and Zhou, S. (2015a) Conductive Iron Oxide Minerals Accelerate Syntrophic Cooperation in Methanogenic Benzoate Degradation. Journal of Hazardous Materials 293, 37-45.

Zhuang, L., Xu, J., Tang, J. and Zhou, S. (2015b) Effect of ferrihydrite biomineralization on methanogenesis in an anaerobic incubation from paddy soil. Journal of Geophysical Research: Biogeosciences 120(5), 876-886.